

Application of Pseudo-Analysis in the Synchronization of Container Terminal Equipment Operation

Endre Pap^{1,2}, Vladimir Bojanić³, Milosav Georgijević³, Goran Bojanić³

¹ Department of Mathematics and Informatics, University of Novi Sad
Trg Dositeja Obradovića 4, 21000 Novi Sad, Serbia

² Óbuda University, Bécsi út 96/B, H-1034 Budapest, Hungary
E-mail: pape@eunet.rs; pap@dmi.uns.ac.rs

³ Faculty of Technical Sciences, University of Novi Sad
Trg Dositeja Obradovića 6, 21000 Novi Sad, Serbia
E-mail: ydad@uns.ac.rs; georgije@uns.ac.rs; gbojanic@uns.ac.rs

Abstract: Based on the global increase in the volume of containerized goods, there is an emerging need for analysis and improvement in all aspects of the logistic chain of container transport. Mathematical description of equipment operation in container terminal is of key importance for understanding complex container terminals. This paper presents an innovative concept in the modeling of a container reloading operation inside a container terminal and its equipment based on pseudo-analysis in the form of max-plus semiring. The presented synchronization of the equipment operation (quay container cranes and automated guided vehicles, shortly AGV) during container unloading leads to minimization of the required number of automated guided vehicles. The presented method is demonstrated in a numerical example.

Keywords: container terminal; automated guided vehicles (AGV); max-plus semiring; pseudo-analysis; synchronization of equipment

1 Introduction

Operation studies and description of container terminals, as elements of large logistic networks and therefore the key factor within their parent system of SCM (Supply Chain Management), represent a complex problem (see papers: [4], [11], [12], [33]). In addition, with the aim of increasing the accuracy of results, each part of the system should be analyzed separately, paying attention to the preservation of the general approach of the study.

The economic effects of improvements in container terminal equipment operation can be recognized by the transshipment price, which amounts to approximately 50 € per TEU. If one observes a smaller seaport or average size riverport with 100,000 TEUs, increasing the effect with the organization by only 2% brings 100,000 € more, which is not negligible. The monograph [12] presents a number of papers that deal with the subject of container terminal organization as a whole, as well as separate subsystems within these terminals. Also, several examples analyze the problem of creating the terminal concept presented on an actual example of a new terminal within ECT (Europe Container Terminal, Rotterdam). A mathematical description of the equipment operation in the container terminal is of key importance for understanding complex container terminals. However, not one paper (to the author's knowledge) has analyzed the reduction of the number of automated guided vehicles (AGVs) on the basis of the relation between the manner the container quay crane unloads containers and the distance of storage area parts where unloaded containers should be stored.

Based on the semiring structure (see [14]) developed in [21], [23], the so-called pseudo-analysis in an analogous way as classical analysis introduced \oplus measure, pseudo integral, pseudo-convolution, pseudo-Laplace transform, etc. The pseudo-linear superposition principle resulted from the pseudo-analysis [13], [16], [21], where, roughly speaking, instead of the field of real numbers a semiring on the real interval is taken $[a, b] \subset [-\infty, +\infty]$, denoting the corresponding operations as \oplus (pseudo-addition) and \odot (pseudo-multiplication). It is successfully applied as a universal mathematical method in many fields, e.g., fuzzy systems, decision making, optimization theory, differential equations, etc.

The change in the classical linear system can often be shown in the following way:

$$x(t+1) = Ax(t), \quad t = 0, 1, 2, \dots,$$

where the vector x represents the state of a model, and this state evolves in time according to this equation; and $x(t)$ denotes the state in time t . The symbol A denotes the real $n \times n$ matrix (system transformation matrix).

The proceeding equation can be written in the following form:

$$x_i(t+1) = \sum_{j=1}^n A_{ij} x_j(t), \quad i = 1, 2, \dots, n, \quad t = 0, 1, \dots$$

Depending on the technical performances of equipment in the terminal, different transformation matrices A can be determined.

Different kinds of nonlinear equations are treated in mathematics with various tools [1], [2], [6], [7], [16], [17], [20], [22], [25], [26], [28]. In the same way, max-

plus algebra found its application in many areas, such as: production, traffic, communication, and image coding (see papers [1], [19]). In analogy with the approach in papers [1], [27] and [28], we shall use the following model. Now, we suppose that multiplication becomes the common addition and addition becomes the maximization. Then the corresponding equation in relation to the preceding equation is given by:

$$x_i(t+1) = \bigoplus_{j=1}^n A_{ij} \odot x_j(t), \quad i=1,2,\dots,n, \quad t=0,1,\dots, \quad (1)$$

where: $\bigoplus = \max$ and $\odot = +$. The preceding equation can be written in the following form:

$$x_i(t+1) = \max_{1 \leq j \leq n} (A_{ij} + x_j(t)), \quad i=1, 2, \dots, n, \quad t=0, 1, \dots \quad .$$

We shall use the following shorter notation for the preceding equation:

$$x(t+1) = A \odot x(t), \quad t=0, 1, 2, \dots \quad (2)$$

In the case when the initial stage x_0 is known, system transformation matrix A preceding equations model deterministic systems.

After the introduction, the second section of the paper presents some necessary notions of pseudo-analysis. The third section provides description of the problem of the minimal number of required AGV. The fourth section gives two theorems related to the unloading of one bay. The fifth section is devoted to a synchronization model and numerical example. The sixth section covers some important related remarks. The main conclusions from this paper are given in the end.

2 Pseudo-Analysis

Pseudo-analysis is a generalization of classical analysis, where instead of the field of real numbers, a semiring is taken on a real interval $[a, b] \subset [-\infty, +\infty]$ endowed with pseudo-addition \bigoplus and with pseudo-multiplication \odot , see [9], [12], [14], [16], [21], [22], [24], [29], [30].

Let $[a, b] \subset [-\infty, +\infty]$.

Pseudo-addition is a function $\bigoplus: [a, b] \times [a, b] \rightarrow [a, b]$ which is commutative, nondecreasing, associative and has a zero element, denoted by $\mathbf{0}$.

Let $[a, b]_+ = \{x : x \in [a, b], x \geq \mathbf{0}\}$.

Pseudo-multiplication is a function $\odot: [a, b] \times [a, b] \rightarrow [a, b]$ which is commutative, positively nondecreasing, i.e. $x \leq y$ implies

$x \odot z \leq y \odot z$, $z \in [a, b]_+$; associative and for which there exists a unit element $\mathbf{1} \in [a, b]$, i.e., for each $x \in [a, b]$; $\mathbf{1} \odot x = x$. We further suppose, that $\mathbf{0} \odot x = \mathbf{0}$ and that \odot is a distributive pseudo-multiplication with respect to \oplus , i.e.,

$$x \odot (y \oplus z) = (x \odot y) \oplus (x \odot z).$$

The structure $([a, b], \oplus, \odot)$ is called a semiring; see [14], [16], [21]. Special cases of real semirings are investigated in papers [7], [16], [27]. In this paper, we shall use the case $\oplus = \max$ and $\odot = +$ on the interval $[-\infty, +\infty]$; see [1], [2], [7], [16], [27]. In usual real algebra we have $\mathbf{1} \cdot x = x$ and $\mathbf{0} + x = x$, but in max-plus algebra we have $\mathbf{0} \odot x = x$ and $-\infty \oplus x = x$, so the neutral elements for pseudo-multiplication and pseudo-addition are $\mathbf{0}$ and $-\infty$, respectively. We will denote $\mathbf{1} = \mathbf{0}$ and $\mathbf{0} = -\infty$. The condition $\mathbf{0} \odot x = \mathbf{0}$ ensures the convention $-\infty + \infty = -\infty$. Several other properties of pseudo-addition and pseudo-multiplication and their consequences are discussed and illustrated in paper [3].

Remark. If we compare the properties of \oplus and \odot with the usual operations of addition and multiplication we see that:

- (i) We have lost the property: for a given a there exists only one element b such that $a + b = \mathbf{0}$, because for $a \neq -\infty$ we have $\max(a, b) \neq -\infty$;
- (ii) We have gained the idempotency of addition;
- (iii) There are no zero divisors in $([-\infty, +\infty], \max, +)$, because

$$a \oplus b = -\infty \implies a = -\infty \text{ and } b = -\infty ;$$
- (iv) The maximum operation is no longer cancellative, because $\max(a, b) = b$ does not imply $a = -\infty$.

3 Description of the Problem

Today, over 60% of the world's deep-sea cargo is transported in containers, while some routes, especially between economically strong and stable countries, are containerized up to 100% (industrial products) [31]. Container applications, or containerization of cargo flows, has required research in the domain of organization, particularly for reloading and storing in terminals.

Container terminals constantly search for new techniques, such as automated transportation systems, and new ways of planning and control. Therefore, new planning and control concepts need to be developed for the various systems in the container terminal [34]; see also traffic models [32]. There are a number of papers that analyze crane scheduling problems and overview of existing literature is presented in paper [4]. However, not one analyzes the influence of crane scheduling on the number of required AGVs necessary for the continual flow of transshipment.

Many papers analyze systems with AGVs. In paper [34], Vis discusses literature related to design and control issues of AGV systems in manufacturing, distribution, transshipment and transportation systems. In paper [36], the authors describe the development of the minimum flow algorithm to determine the number of AGVs required at semi-automated container terminals. The problem the authors analyzed in [5] was to assign each container to a yard location and dispatch vehicles to the containers so as to minimize the time required to unload all the containers from the ship. In paper [8] the goal is to determine the best allocation of resources in the yard with the objective of minimizing the costs of the terminal. The comparison of vehicle types at an automated container terminal is presented in paper [35].

In paper [10], the authors propose a heuristics search algorithm called the greedy randomized adaptive search procedure for constructing a schedule of quay cranes in a way of minimizing the makespan and considering the interference among yard cranes, but without analyzing the number of trailers. In paper [33], the authors model the seaport system with the objective of determining the storage strategy for various containers –the handling schedules. “Multi-crane oriented” is a scheduling method that yard trailers can be shared by different quay cranes. This method is presented in paper [37]. In paper [15], the objective is to minimize the weighted sum of the total delay of requests and the total travel time of yard trucks. The problem of minimizing the time taken to load the containers from the container stack yard onto the ship is presented in paper [18].

Not one paper analyzed the number of minimum required AGVs on the basis of the relation between the manner the container quay crane unloads containers and the distance of different blocks inside the container yard where unloaded containers should be stored. This paper shall deal with synchronization of equipment operation in the container terminal with the help of pseudo-analysis. Similarly, modeling on the basis of stations (in this case, the locations for transshipment of containers), as in papers [1], [27], [28], \oplus (pseudo-addition) and \odot (pseudo-multiplication) shall be used as operators. Containers are unloaded and loaded at locations intended for this purpose, so these locations can be regarded as stations (in analogy with railway stations in [1], [28]).

The basic division of container quay cranes is into:

- Cranes intended for operation in river terminals;
- Cranes intended for operation in sea terminals.

In this paper we analyze cases when container quay cranes do not service the container yard. Such utilization of these cranes is characteristic for all cranes that operate in sea terminals and for some that operate in river terminals. Therefore, in this case, the crane unloads the containers to the shore and further container manipulation is continued with AGVs, straddle carriers, reach stackers and forklifts. As the most expensive and complex equipment in the terminal, container quay cranes determine the operation of other equipment. The price of container quay cranes ranges between 6 and 10 million euros. This paper observes the system of container transshipment by a container quay crane, after which the containers are transferred to the container storage yard by using AGVs. Further manipulation in the container yard is done by yard cranes (This is the most common case in sea terminals). Therefore, AGVs transport containers between the shore and the container yard. One of the automated guided vehicles' characteristics is that other equipment (cranes) is necessary in order to load containers onto or unload containers from AGVs.

Container terminal is shown in Figure 1.

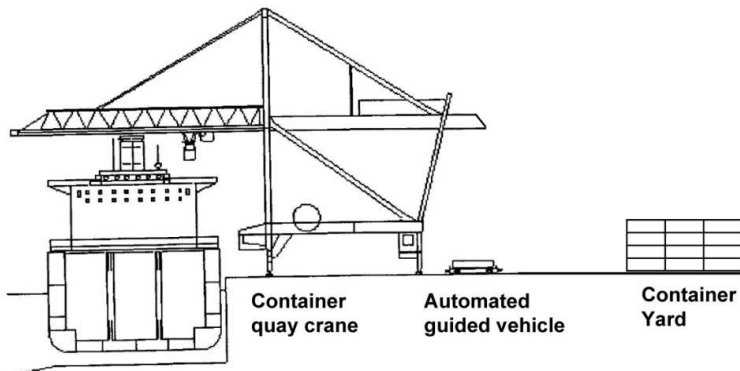


Figure 1
Container terminal

In this paper we shall analyze the relation between the container quay crane and the number of required AGVs depending on the distances of different parts of container yard. The methodology to be shown can lead to a reduction in the necessary number of AGVs for performing the same work. In this paper, it shall be proved that the manner of synchronization of the stated equipment operation shall not affect the time of transshipment and operation of the container quay crane but shall only affect the minimization of the necessary number of AGVs. In order to illustrate the methodology from the next section, a numerical example is given.

4 Unloading of One Bay

The ship has a number of container stacking compartments called bays, and only one crane can work on a bay at the same time (Figure 2). Thus, the crane most often reloads the ship by reloading one bay at a time. In this paper, it is implied that container quay crane first reloads all containers from one bay and then moves to the next bay. On the basis of the aforementioned, unloading of one bay is analyzed.

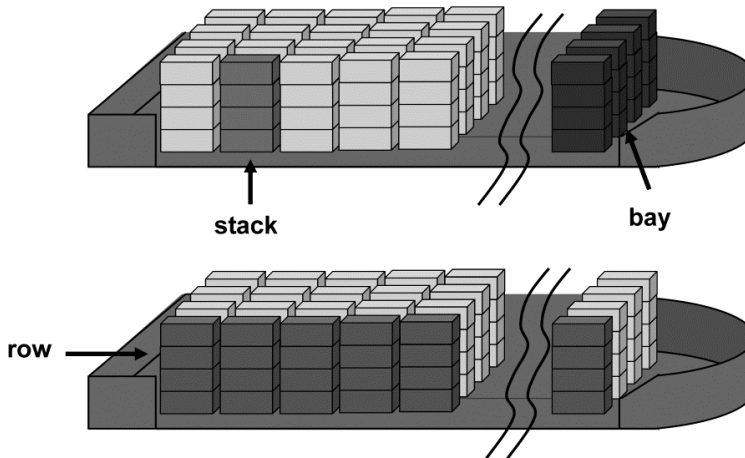


Figure 2
Container ship, bay

We shall prove that there is no difference if a container quay crane unloads containers from a bay “one after the other” or “in any other way”.

Theorem 1: *If a container quay crane unloads containers from a bay “one after the other” and if container quay crane unloads containers from a bay “in any other way”, time of unloading is the same.*

Proof: We stress that “one after the other” implies that all containers from the first stack are unloaded first and then all containers from the second stack, and so on, until the last container from the last stack is unloaded.

We stress that “in any other way” implies ways that do not lead to unnecessary increase of the number of transshipped containers (e.g., second container from the first stack cannot be transshipped if the first container from the first stack is not transshipped. This is presented in Figure 4 in the following manner: u_2 is unloaded, and then u_1 is unloaded – if such thing occurs, it would lead to an unnecessary increase in the number of transshipped containers, i.e., it would lead to an unnecessary increase in rehandled containers because u_1 then behaves as a rehandled container).

If l_i , $i=1,2,3,\dots,n$ denotes the distance of each container (which is to be unloaded) from location S_1 (the location where the container quay crane loads containers onto the AGVs), the sum of all distances remains the same

$$2(l_1 + l_2 + l_3 + \dots + l_n) = l_{uk},$$

until unloading which shall increase the number of traveled distances (i.e., until the unnecessary number of transshipped containers) occurs. This means that the time of unloading shall remain the same until unloading, which will unnecessarily increase the number of transshipped containers occurs. In other words: the time of unloading the ship does not depend on the order of unloading containers.

In the next theorem we stress the connection of the order of unloading containers with the number of AGVs.

Theorem 2: *Order of unloading containers affects currently required number of AGVs.*

Proof: Let us assume that only the order of unloading of containers which shall not unnecessarily increase the number of transshipped containers is analyzed. If r_i , $i=1,2,3,\dots,n$ denotes the distance from location S_1 to the container yard location S_j $j=2,3,4,\dots,m$ the total sum of traveled distances from S_1 to S_j is given by

$$2(r_1 + r_2 + r_3 + \dots + r_n) = r_{uk}.$$

The total amount of traveled distances of containers from their location on a ship to the container yard location is given by

$$2(l_1 + r_1 + l_2 + r_2 + l_3 + r_3 + \dots + l_n + r_n) = l_{uk} + r_{uk}.$$

The way of forming the sum plays a key role. If we specify that

$$2(l_1 + r_1) = c_1; \quad 2(l_2 + r_2) = c_2; \quad 2(l_3 + r_3) = c_3; \quad \dots \quad 2(l_n + r_n) = c_n,$$

the total sum of traveled distances is

$$c_1 + c_2 + c_3 + \dots + c_n = c_{uk}.$$

Since $c_i + c_{i+1}$ does not have to be equal to $c_i + c_{i+2}$, the distances AGVs must travel during these transshipments do not have to be equal. It happens that the AGVs return to station S_1 before schedule, which again makes them ready for transshipment; i.e., the order of unloading containers affects the currently required number of AGVs.

The preceding two theorems indicate that order of unloading containers from the ship directly affects the required number of AGVs without an influence on container quay crane, i.e., on time required for transshipment.

5 A Model of Synchronization

The model in Figure 3 represents the system that consists of the container quay crane, the AGVs and the yard cranes. In this paper, the model of the synchronization of the equipment operation in an example of unloading a ship is presented. S_i , $i=1,2,3,\dots$ are reloading locations, such as: S_1 - location on the shore where the container quay crane loads the containers onto the automated guided vehicles; S_2, S_3, S_4, S_5 - different blocks inside the container terminal.

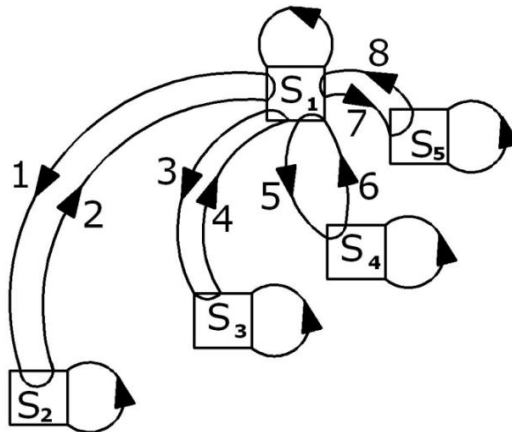


Figure 3

Model with five locations for loading and unloading of containers

Adopted assumptions:

- As aforementioned, container quay cranes are the most expensive and the largest machines in a container terminal and what is to be adopted here is that for each container the crane locations onto the shore there must exist a free AGV onto which the crane loads the container; i.e., the crane must not at any moment wait for the AGV.
- Since it is adopted in the example that only one quay crane transships the containers (in such way that the flow of containers is not large), the yard cranes are always prepared to unload the container from the AGV when it arrives and to transfer the container to container storage yard location.
- The AGV always travel the same distance within the same time.
- Each container on a ship has its pre-specified storage yard location.

A mathematical description of the presented system is given in the following form:

$$x_i(t+1) = \bigoplus_{j=1}^n A_{ij}(t) \odot x_j(t), \quad i = 1, 2, \dots, n, \quad t = 0, 1, \dots \quad (3)$$

We shall use the following shorter notation for the preceding equation:

$$x(t+1) = A(t) \odot x(t), \quad t = 0, 1, 2, \dots \quad (4)$$

Unlike expressions (1) and (2), expressions (3) and (4) have the transformation matrix $A(t)$ which depends on the time interval. If instead of time $t = 0, 1, 2, \dots$, we observe events $k = 0, 1, 2, \dots$ that changed the system, and equation (4) can be written in the following form:

$$x(k+1) = A(k) \odot x(k), \quad k = 0, 1, 2, \dots \quad (5)$$

$x(k)$ - marks the k -th departure time of the AGVs in direction i ,

$A(k)$ - system transformation matrix.

If we adopt that time intervals between locations (for container transshipment) are: $s_{12} = s_{21} = 60$; $s_{13} = s_{31} = 50$; $s_{14} = s_{41} = 20$; $s_{15} = s_{51} = 15$.

Then we can assume that container quay crane should unload the bay as in Fig. 4:

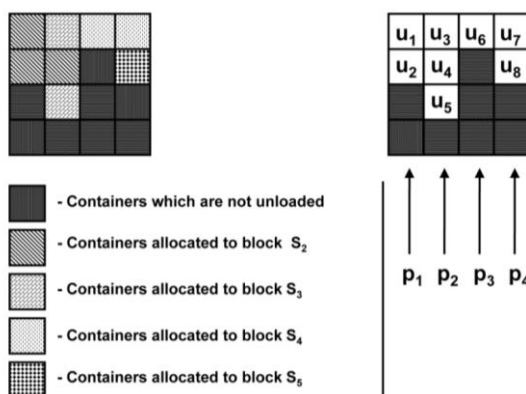


Figure 4

An example of a bay in a ship which is to be unloaded (side view)

Figure 4 displays a bay which is to be unloaded. Let the time units for unloading of containers in the bay be adopted:

$$u_1 = 2; \quad u_2 = 3; \quad u_3 = 4; \quad u_4 = 5;$$

$$u_5 = 6; \quad u_6 = 7; \quad u_7 = 8; \quad u_8 = 9;$$

It is stressed that all adopted values are given as an example only to show the methodology of synchronization.

For a crane to unload the first container (which is on top) from the first stack, $2+2$ time units are required (i.e., 2 time units from location S_1 to first container in the first stack and 2 time units from the first container in the first stack to location S_1). For a crane to unload the second container from the first stack, $3+3$ time units are required (i.e., 3 time units from location S_1 to the second container in the first stack and 3 time units from the second container in the first stack to location S_1).

Case 1 Analyse the unloading of container with the stacks order p1,p2,p3,p4 (Figure 4). This makes it clear that the departure times for containers from station S_1 are: 4,10,18,28,40,54,70,88. **Case 2** (order p4,p1,p2,p3) shows other departure times for containers from station S_1 (see Table 2). In order to obtain integer numbers in matrices, time units are used in this paper.

Let us assume that the bay presented in Figure 4 should be unloaded, with the existence of a system with AGVs and yard cranes (as in Figure 3). The description of the given system can be presented by max-plus equation:

$$\begin{bmatrix} x_1(k+1) \\ x_2(k+1) \\ x_3(k+1) \\ x_4(k+1) \\ x_5(k+1) \\ x_6(k+1) \\ x_7(k+1) \\ x_8(k+1) \end{bmatrix} = \begin{bmatrix} s_{11}(k) & s_{21}(k) & \mathbf{0} & s_{31}(k) & \mathbf{0} & s_{41}(k) & \mathbf{0} & s_{51}(k) \\ s_{12}(k) & \mathbf{1} & \mathbf{0} & \mathbf{0} & \mathbf{0} & \mathbf{0} & \mathbf{0} & \mathbf{0} \\ \mathbf{0} & s_{21}(k) & s_{33}(k) & s_{31}(k) & \mathbf{0} & s_{41}(k) & \mathbf{0} & s_{51}(k) \\ \mathbf{0} & \mathbf{0} & s_{13}(k) & \mathbf{1} & \mathbf{0} & \mathbf{0} & \mathbf{0} & \mathbf{0} \\ \mathbf{0} & s_{21}(k) & \mathbf{0} & s_{31}(k) & s_{55}(k) & s_{41}(k) & \mathbf{0} & s_{51}(k) \\ \mathbf{0} & \mathbf{0} & \mathbf{0} & \mathbf{0} & s_{14}(k) & \mathbf{1} & \mathbf{0} & \mathbf{0} \\ \mathbf{0} & s_{21}(k) & \mathbf{0} & s_{31}(k) & \mathbf{0} & s_{41}(k) & s_{77}(k) & s_{51}(k) \\ \mathbf{0} & \mathbf{0} & \mathbf{0} & \mathbf{0} & \mathbf{0} & \mathbf{0} & s_{15}(k) & \mathbf{1} \end{bmatrix} \odot \begin{bmatrix} x_1(k) \\ x_2(k) \\ x_3(k) \\ x_4(k) \\ x_5(k) \\ x_6(k) \\ x_7(k) \\ x_8(k) \end{bmatrix} \quad (6)$$

In the presented equation, s_{ij} represents the time required for the AGVs to travel from location S_i to location S_j , and in the case when $i=j$, s_{ij} represents activation time of location S_i (this is the connection with transshipment done by container quay crane). The transformation matrix depends directly on the manner of transshipment and the way the locations S_i are connected.

If we observe the first AGV (order (p4, p1, p2, p3)), it can be concluded that the system will change four times.

$$x(1) = A(0) \odot x(0); \quad x(2) = A(1) \odot x(1); \quad x(3) = A(2) \odot x(2);$$

$$x(4) = A(3) \odot x(3); \text{ i.e.,}$$

$$\begin{pmatrix} 1 \\ 1 \\ 1 \\ 1 \\ 16 \\ 1 \\ 1 \\ 1 \end{pmatrix} = \begin{pmatrix} 1 & 0 & 0 & 0 & 0 & 0 & 0 & 0 \\ 0 & 1 & 0 & 0 & 0 & 0 & 0 & 0 \\ 0 & 0 & 1 & 0 & 0 & 0 & 0 & 0 \\ 0 & 0 & 0 & 1 & 0 & 0 & 0 & 0 \\ 0 & 0 & 0 & 0 & 16 & 0 & 0 & 0 \\ 0 & 0 & 0 & 0 & 0 & 1 & 0 & 0 \\ 0 & 0 & 0 & 0 & 0 & 0 & 1 & 0 \\ 0 & 0 & 0 & 0 & 0 & 0 & 0 & 1 \end{pmatrix} \odot \begin{pmatrix} 0 \\ 0 \\ 0 \\ 0 \\ 0 \\ 0 \\ 0 \\ 0 \end{pmatrix}; \quad \begin{pmatrix} 1 \\ 1 \\ 1 \\ 1 \\ 16 \\ 36 \\ 1 \\ 1 \end{pmatrix} = \begin{pmatrix} 1 & 0 & 0 & 0 & 0 & 0 & 0 & 0 \\ 0 & 1 & 0 & 0 & 0 & 0 & 0 & 0 \\ 0 & 0 & 1 & 0 & 0 & 0 & 0 & 0 \\ 0 & 0 & 0 & 1 & 0 & 0 & 0 & 0 \\ 0 & 0 & 0 & 0 & 1 & 0 & 0 & 0 \\ 0 & 0 & 0 & 0 & 20 & 1 & 0 & 0 \\ 0 & 0 & 0 & 0 & 0 & 0 & 1 & 0 \\ 0 & 0 & 0 & 0 & 0 & 0 & 0 & 1 \end{pmatrix} \odot \begin{pmatrix} 1 \\ 1 \\ 1 \\ 1 \\ 16 \\ 36 \\ 1 \\ 1 \end{pmatrix};$$

$$\begin{pmatrix} 1 \\ 1 \\ 1 \\ 1 \\ 56 \\ 36 \\ 1 \\ 1 \end{pmatrix} = \begin{pmatrix} 1 & 0 & 0 & 0 & 0 & 0 & 0 & 0 \\ 0 & 1 & 0 & 0 & 0 & 0 & 0 & 0 \\ 0 & 0 & 1 & 0 & 0 & 0 & 0 & 0 \\ 0 & 0 & 0 & 1 & 0 & 0 & 0 & 0 \\ 0 & 0 & 0 & 0 & 1 & 20 & 0 & 0 \\ 0 & 0 & 0 & 0 & 0 & 1 & 0 & 0 \\ 0 & 0 & 0 & 0 & 0 & 0 & 1 & 0 \\ 0 & 0 & 0 & 0 & 0 & 0 & 0 & 1 \end{pmatrix} \odot \begin{pmatrix} 1 \\ 1 \\ 1 \\ 1 \\ 16 \\ 36 \\ 1 \\ 1 \end{pmatrix}; \quad \begin{pmatrix} 1 \\ 1 \\ 1 \\ 1 \\ 56 \\ 36 \\ 1 \\ 1 \end{pmatrix} = \begin{pmatrix} 62 & 0 & 0 & 0 & 0 & 0 & 0 & 0 \\ 0 & 1 & 0 & 0 & 0 & 0 & 0 & 0 \\ 0 & 0 & 1 & 0 & 0 & 0 & 0 & 0 \\ 0 & 0 & 0 & 1 & 0 & 0 & 0 & 0 \\ 0 & 0 & 0 & 0 & 1 & 0 & 0 & 0 \\ 0 & 0 & 0 & 0 & 0 & 1 & 0 & 0 \\ 0 & 0 & 0 & 0 & 0 & 0 & 1 & 0 \\ 0 & 0 & 0 & 0 & 0 & 0 & 0 & 1 \end{pmatrix} \odot \begin{pmatrix} 1 \\ 1 \\ 1 \\ 1 \\ 56 \\ 36 \\ 1 \\ 1 \end{pmatrix}$$

By the application of the given mathematical model (equation (6)), the following results can be presented:

Due to easier track of changes of system state, the changes are given in tables.

Table 1
Results of numerical example (order p1,p2,p3,p4)

AGV	Order of unloading of stacks (p1, p2, p3, p4)							
	x_1	x_2	x_3	x_4	x_5	x_6	x_7	x_8
1	4	64	-	-	-	-	-	-
2	10	70	-	-	-	-	-	-
3	-	-	18	68	-	-	-	-
4	28	88	-	-	-	-	-	-
5	-	-	40	-	-	-	-	-
6	-	-	-	-	54	74	-	-
7	-	-	-	-	70	-	-	-
8	-	-	-	-	-	-	88	-

Table 2
Results of numerical example (order p4,p1,p2,p3)

AGV	Order of unloading of stacks (p4, p1, p2, p3)							
	x_1	x_2	x_3	x_4	x_5	x_6	x_7	x_8
1	62	-	-	-	16	36	-	-
2	-	-	74	-	-	-	34	49
3	38	-	-	-	-	-	-	-
4	44	-	-	-	-	-	-	-
5	-	-	52	-	-	-	-	-
6	-	-	-	-	88	-	-	-

From Tables 1 and 2 it can be seen that the transfer of the last unloaded container, in both cases, began at station S_1 in the 88th time unit. This means that, as Theorem 1 showed, the time of the ending the unloading, from the aspect of container quay crane, is the same in both cases. As Theorem 2 showed, the number of required AGVs is not the same in both cases (In the first case $AGV=8$, while in the second case $AGV=6$). From the given calculation, it can be seen that in the 36th time unit, one AGV departs from location S_4 towards location S_1 , while it can also be seen that in the 49th time unit, another AGV departs from location S_5 towards S_1 . These two AGVs return to station S_1 in the 56th and 64th time unit. This means that these two AGVs are again used for unloading of containers, and therefore fewer AGVs were required to perform the same work.

As in the numerical example, during transshipment of containers by the container quay crane, it is possible to simultaneously unload several containers that are being transferred (by AGVs) to the most remote storage yard locations; thus AGVs are then busy for a longer period of time.

6 Important Notes

This paper presents the model made on the basis of pseudo-operator (\oplus (pseudo-addition), \odot (pseudo-multiplication)) as a result of already presented models [1], [27], [28]. The presented models can be used for various types of system optimization. However, this paper presents a manner of the synchronization of equipment in a container terminal, where it is possible to optimize the number of AGVs.

We should aim at a constant number of AGVs

During reloading of containers by the quay crane, it has been proved that the order of unloading containers does not affect the time necessary for unloading the ship.

However, it is quite clear, on the basis of the aforementioned, that the number of AGVs during unloading varies at times. By using the given method, the best optimum way of using the AGVs can be achieved by minimizing the oscillations of the number of AGVs. In other words, this would be aimed at achieving a constant number of vehicles.

The effect of rehandled containers

During reloading, there are containers that need to be rehandled. Such containers cause the time of reloading the ship to extend. When a crane takes the container which later needs to be put back onto the ship, it places it on the shore or some other place on the ship. Nevertheless, AGVs are not required during transshipment of such containers.

This implies that while a crane is unloading such containers, AGVs are not needed in the station S_1 .

Even if there are priorities, savings are possible

When unloading large ships, there are containers with priority that need to be unloaded first. Nevertheless, even in such systems, there are containers with the same priority. In such cases, it is possible to apply the stated synchronization and in such manner reduce the required number of AGVs in the process of transshipment.

A larger number of cranes

Unlike the above presented system, it is possible to observe the state in which a large number of cranes unload containers from one ship. Then, the transformation matrix would change the system faster, and the optimization which is possible would be greater. In sea terminals, usually more cranes are used for big ships (2 to 4), which would be appropriate for this system. The matrix would then contain a higher number of changes in the same time moment, i.e., event. It implies that the effects of yard cranes would have to be modeled in the system (i.e., AGVs would at some location have to wait until the yard crane is free to handle them).

Conclusions

This paper presents a possible synchronization of the container quay crane and AGVs' operation on the basis of modeling by using the pseudo-analysis. It was shown that if containers are unloaded in specified order, the number of AGVs can be reduced without any effect on the time necessary to unload the ship. It is possible to track the system and acknowledge whether a required reduction of the number of AGVs is possible for each container terminal (i.e., terminal scheduling) and the frequency of different ships being handled in the terminal. The size of the ship, the number of cranes, the size of the storage yard location and the technical performances of the equipment will affect the possible minimization of the required number of AGVs. It is stressed that this way of synchronization can lead

only to a reduction in the required number of AGVs. To the author's knowledge, no similar research for this kind of equipment synchronization has been conducted so far. Finally, as was stressed at the beginning: resulting from the global increase in the volume of containerized goods, there is an emerging need for analysis and improvement in all aspects of the logistic chain of container transport.

Acknowledgement

Results of this paper were supported by the project: TR-35036 Ministry of Education and Science (Serbia): Application of information technologies in ports of Serbia - from machine monitoring to connected computer network system with EU environment. The first author was supported by the project MPNS 174009 and Provincial Secretariat for Science and Technological Development of Vojvodina.

References

- [1] F. Baccelli, G. Cohen, G. J. Olsder, J. P. Quadrat, Synchronization and Linearity: An Algebra for Discrete Event Systems, Wiley, New York, 1992
- [2] R. E. Bellman, S. E. Dreyfus, Applied Dynamic Programming, Princeton University Press, Princeton, NJ, 1962
- [3] P. Benvenuti, R. Mesiar, Pseudo-Arithmetical Operations as a Basis for the General Measure and Integration Theory, Information Sciences 160 (2004) pp. 1-11
- [4] C. Bierwirth, F. Meisel, A Survey of Berth Allocation and Quay Crane Scheduling Problems in Container Terminals, European Journal of Operational Research 202 (2010) pp.615-627
- [5] E. K. Bish, T. Y. Leong, C. L. Li, J. W. C. Ng, D. Simchi-Levi, Analysis of a New Vehicle Scheduling and Location Problem, Naval Research Logistics 48 (2001) pp. 363-385
- [6] J. G. Braker, Max-Algebra Modelling and Analysis of Time-Table Dependent Networks, Proc. 1st European Control Conf. Grenoble (France), Hermes (1991) pp. 1831-1836
- [7] R. A. Cuninghame-Green, Minimax Algebra, Lecture Notes in Economics and Math. Systems 166, Springer, Berlin, 1979
- [8] L. M. Gambardella, M. Mastrolilli, A. E. Rizzoli, M. Zaffalon, An Optimization Methodology for Intermodal Terminal Management, Journal of Intelligent Manufacturing 12 (2001) pp. 521-534
- [9] M. Grabisch, J. L. Marichal, R. Mesiar, E. Pap, Monograph: Aggregation Functions, Acta Polytechnica Hungarica 6,1 (2009) 79-94
- [10] D. H. Jung, Y. M. Park, B. K. Lee, K. H. Kim, K. R. Ryu, A Quay Crane Scheduling Method Considering Interference of Yard Cranes in Container Terminals, Proc. of the 5th Mexican International Conference on Artificial

- Intelligence (MICAI 2006) Lecture Notes in Computer Science 4293 (2006) pp. 461-471
- [11] K. H. Kim, Y. M. Park, A Crane Scheduling Method for Port Container Terminals, *European Journal of Operational Research* 156 (2004), pp. 752-768
- [12] K. H. Kim, H. O. Günther, *Container Terminals and Cargo Systems Design. Operations Management and Logistics*, Springer-Verlag, Berlin, Heidelberg 2007
- [13] V. N. Kolokoltsov, V. P. Maslov, *Idempotent Analysis and Its Applications*, Kluwer Academic Publishers, Dordrecht, Boston, London 1997
- [14] W. Kuich, *Semirings, Automata, Languages*, Springer-Verlag, Berlin, 1986
- [15] D. H. Lee, J. X. Cao, Q. Shi, J. H. Chen, A Heuristic Algorithm for Yard Truck Scheduling and Storage Allocation Problems, *Transportation Research Part E* 45 (2009) pp. 810-820
- [16] V. P. Maslov, S. N. Samborskij, *Idempotent Analysis, Advances in Soviet Mathematics*, Vol. 13, Amer. Math. Soc., Providence, Rhode Island, 1992
- [17] B. Mihailović, E. Pap, Asymmetric General Choquet Integrals, *Acta Polytechnica Hungarica* 6, 1 (2009) 161-173
- [18] A. Narasimhan, U. S. Palekar, Analysis and Algorithms for the Transtainer Routing Problem in Container Port Operations, *Transportation Science* 36 (2002) pp. 63-78
- [19] H. Nobuhara, D. B. K. Trieu, T. Maruyama, B. Bede, Max-Plus Algebra-based Wavelet Transforms and their FPGA Implementation for Image Coding, *Information Sciences* 180 (2010) pp. 3232-3247
- [20] G. J. Olsder, Applications of the Theory of Stochastic Discrete-Event Systems to Array Processors and Scheduling in Public Transportation, *Proc. 28th Conf. on Decision and Control IEEE*, 1989
- [21] E. Pap, *Null-Additive Set Functions*, Kluwer Academic Publishers, Dordrecht- Boston- London 1995
- [22] E. Pap, Pseudo-Analysis as a Base for Soft Computing, *Soft Computing* 1 (1997) pp. 61-68
- [23] E. Pap, Decomposable Measures and Nonlinear Equations, *Fuzzy Sets and Systems* 92 (1997) pp. 205-222
- [24] E. Pap, Generalized Real Analysis and its Application, *International Journal of Approximate Reasoning* 47 (2008) pp. 368-386
- [25] E. Pap, Pseudo-Analysis in Engineering Decision Making, *Towards Intelligent Engineering and Information Technology* (Eds. Imre J. Rudas,

- János Fodor, Janusz Kacprzyk), *Studies in Computational Intelligence* 243 (2009) pp. 3-16
- [26] E. Pap, Pseudo-Analysis Approach to Nonlinear Partial Differential Equations, *Acta Polytechnica Hungarica* 5 (2008) 31-45
- [27] E. Pap, M. Georgijević, V. Bojanić, G. Bojanić, Pseudo-Analysis Application in Complex Mechanical Systems Modelling of Container Quay Cranes, Proc. 8th IEEE International Symposium on Intelligent Systems and Informatics, 2010, pp. 493-496
- [28] E. Pap, K. Jegdić, Pseudo-Analysis and its Application in Railway Routing, *Fuzzy Sets and Systems* 116 (2000) pp. 103-118, Corrigendum to Pseudo-Analysis and its Application in Railway Routing. *Fuzzy Sets and Systems* 126 (2002) pp. 131-132
- [29] E. Pap, N. Ralević, Pseudo-Laplace Transform, *Nonlinear Analysis* 33 (1998) pp. 553-560
- [30] E. Pap, M. Štrboja, Generalization of the Jensen Inequality for Pseudo-Integral, *Information Sciences* 180 (2010), pp. 543-548
- [31] P. Preston, E. Kozan, An Approach to Determine Storage Locations of Containers at Seaport Terminals, *Computers & Operations Research* 28 (2001) pp.983-995
- [32] E. Schmidt, Elementary Investigation of Transportation Problems, *Acta Polytechnica Hungarica* 6, 2 (2009) 17-40
- [33] D. Steenken, S. Voß, R. Stahlbock, Container Terminal Operation and Operations Research – a Classification and Literature Review, *OR Spectrum*, 26 (2004) pp. 3-49
- [34] I. F. A. Vis, Survey of Research in the Design and Control of Automated Guided Vehicle Systems, *European Journal of Operational Research* 170 (2006) pp. 677-709
- [35] I. F. A. Vis, I. Harika, Comparison of Vehicle Types at an Automated Container Terminal, *OR Spectrum* 26 (2004) pp. 117-143
- [36] I. F. A. Vis, R. Koster, K. J. Roodbergen, L. W. P. Peeters, Determination of the Number of Automated-guided Vehicles Required at a Semi-automated Container Terminal, *Journal of the Operational Research Society* 52 (2001) pp. 409-417
- [37] Q. Zeng, Z. Yang, L. Lai, Models and Algorithms for Multi-Crane-oriented Scheduling Method in Container Terminals, *Transport Policy* 16 (2009) pp. 271-278

Matlab-Simulink Modelling of 6/4 SRM with Static Data Produced Using Finite Element Method

Fevzi Kentli, Hüseyin Çalik

Department of Electrical Education, Faculty of Technical Education, University of Marmara, 34722-Göztepe, Istanbul, Turkey (e-mail: fkentli@marmara.edu.tr)

Electrical Department of Technical Sciences Vocational College, Istanbul University, 34850-Avcılar, Istanbul, Turkey (e-mail: hcalik@istanbul.edu.tr)

Abstract: The static performance of a switched reluctance motor (SRM) is investigated especially by using the finite element method (FEM) in the design and prototype development steps of the SRM in recent years. In order to determine the real working conditions of the motor, the dynamic behaviour of the SRM should be researched. For this purpose, this study has formed a dynamic model of a 6/4 SRM by using the motor's characteristics, such as inductance, flux and torque obtained by FEM, in Matlab-SIMULINK software. In addition, all the characteristics of the motor are obtained and discussed by using this dynamic model.

Keywords: Switched Reluctance Motor (SRM); Torque; Current Controller; Linear Model

1 Introduction

The switched reluctance motor (SRM) has the advantages of a simple and robust structure, high thermal capability and high speed potential [1, 2]. Commercial products based on SRMs are making their way into the market place. The operational principles of the SRM are quite simple and straightforward, but the proper control of the SRM is not sufficiently completed.

The inherent nonlinearity of a SRM makes torque production highly dependent upon the geometry of the poles, which is characterized by the dependence on both stator current and rotor position. In the past, either a linear or nonlinear model [3-5] with predefined parameters of SRM was used for close-loop control. In spite of the nonlinear nature of the SRM, its linear model represents the dynamic behaviour of SRM with very good approximation. Therefore, for the sake of simplicity, this study represents a linear model of SRM.

In order to produce the maximum torque from a motor at a given speed, the combination of motor – converter should be determined. In general, Computer Aided Design (CAD) tools are employed for this purpose. Some researchers have previously studied in various subjects such as different motor shapes, control strategies and converter types [6, 7], but the studies are not completed and they continue to be discussed in the literature [1-3]. On the other hand, very few simulation studies of the SRM have been achieved with circuit-based languages such as Spice, Simulink, Matrix, Tutsim, Vissim and Mathcad [8, 9].

In this study, a linear dynamic model of 6/4 SRM is generated and the following are examined.

- The dynamic torque ripple of the motor; whether it is in accordance with its static torque ripple or not,
- The amplitude of phase currents to be able to design the driver circuit,
- Dynamic torque, current and flux variations are investigated by applying current control to minimize the torque ripple generated by the motor.

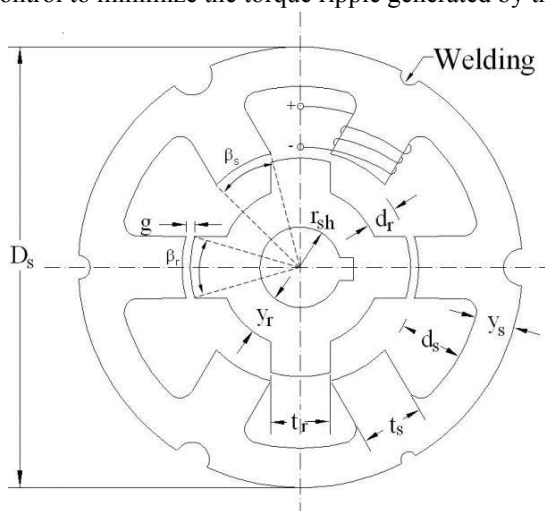


Figure 1
SRM's geometric structure

The geometric structure of the examined motor is given in Fig. 1 and its parameter values are shown in Table I [1]. In dynamic modelling of the 6/4 SRM based on the given specifications, static inductance and torque profiles obtained by the Finite Element Method (FEM) for various current values and 5° rotor angle steps are used [10]. The electrical and mechanical circuit equations are realized by using the Matlab-Simulink program. Mostly, working on a simulink model instead of an actual machine is cheaper, easier and more practical. Also, in some cases, working on a simulink model is a requirement. For example, throughout the manufacturing

of the prototype machine, the machine, just before manufacturing, can be made in the most economic, effective way and with the highest performance by means of changing each parameter on the simulink model in cognizance of machine characteristics such as machine dimensions and the forms of machine parts.

Table I
Motor Parameters [1]

Phase numbers (m) = 3	Shaft radius(r_{sh}) = 0.0087m
Stator pole numbers (N_s) = 6	Rotor pole numbers (N_r) = 4
Stator pole arc (β_s) = 30°	Rotor pole arc (β_r) = 32°
Stator diameter(D_s) = 0.0938 m	Airgap (g) = 0.0002286 m.
Stator pole width(t_s)= 0.0123 m	Rotor pole width(t_r)= 0.0129 m
Stack length (L_{stk}) = 0.047 m	Motor length (L_e) = 0.0762 m
Slot fill factor (k_{sf}) = 33 %	Slot area (A_{slot}) = 0.000309 m ²
Stator slot depth(d_s) = 0.0151m	Rotor slot depth (d_r)= 0.0061m
Stator yoke thickness (y_s) = 0.008178 m.	Rotor yoke thickness (y_r) = 0.008636 m.
$J = 0.000189 \text{ kgm}^2$	$k_t = 0.005 \text{ Nms/rad.}$
$k_f = 0.0001 \text{ Nms/rad.}$	$R = 1.11 \Omega$
$P = 450 \text{ W}$	$V_s = 24 \text{ V}$

In this study, simulink models of a 6/4 SRM, the parameters and geometrical structure of which are given respectively in Table I and Fig. 1, are obtained as shown in the following figures, and the magnitudes such as the current, flux, torque, and speed of motor are provided by making required data input on these obtained models. As is known, these simulink models can be formed simply by means of a computer.

In this context, a PC-based model in electrical machine design is developed.

1.1 SRM's Linear Models

For various rotor angles, the magnetic flux versus current obtained by FEM is given in Fig. 2. In Fig. 2, the slope of the curve in the linear region without saturation represents the value of the related inductance. The value of inductance varies not only with θ rotating angle, but also with the current through winding due to the saturation feature of magnetic material.

Therefore, the inductance equation in general form can be given as $L = L(\theta, i)$ where θ is the rotor position angle and i is the phase current. Thus, the general expression of total linkage fluxes in the motor becomes as follows.

$$\lambda(\theta, i) = L(\theta, i) \cdot i \quad (1)$$

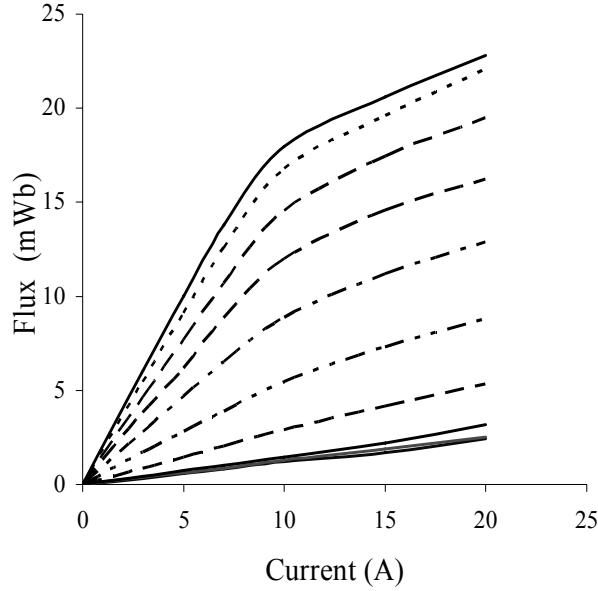


Figure 2

SRM's static flux-current characteristics obtained by using FEM

In this case, if the mutual inductance with short time between the phases is neglected, the winding voltage equation for one phase of SRM can be written as follows.

$$\begin{aligned}
 V_s &= R \cdot i_s + \frac{d\lambda(\theta, i)}{dt} = R \cdot i_s + \frac{dL(\theta, i)}{dt} \cdot i_s + L(\theta, i) \frac{di_s}{dt} \\
 &= R \cdot i_s + \left[L(\theta, i) + \frac{\partial L(\theta, i)}{\partial i} \cdot i_s \right] \frac{di_s}{dt} + \frac{\partial L(\theta, i)}{\partial \theta} \cdot \frac{\partial \theta}{dt} \cdot i_s
 \end{aligned} \quad (2)$$

where V_s is the winding voltage (V), R is the winding resistance (Ω), i is the winding current (A), $\lambda(\theta, i)$ is the total linkage flux (Wb), $L(\theta, i)$ is the winding inductance (H), θ is the rotor position angle, $(\partial L(\theta, i) / \partial \theta) (\partial \theta / \partial t) \cdot i_s = E$ is the counter (reverse) e.m.f.(V), $[L(\theta, i) + \partial L(\theta, i) \cdot i_s / \partial i] = L'(\theta, i)$ and the subscribe s is the phase number (like 1,2,3), respectively. Moreover, R and $L(\theta, i)$ values of each phase winding are equal to each other.

Thus, the equivalent circuit for one phase of the SRM is given in Fig. 3. However, in the case of a constant current in the linear model, the total flux expression is given as follows.

$$\lambda(\theta) = L(\theta) \cdot I \quad (3)$$

So, when the rotor with salient-pole aligns with the stator winding, the related winding inductance reaches its maximum value in accordance with the equation of $L = N^2 \cdot \mu \cdot A / l$, where N is the number of turns on the stator winding, μ is the permeability of the magnetic circuit material (H/m), A is the cross-sectional area of the magnetic path (m²), and l is the average length of the magnetic path (m). L value of the stator winding is only dependent on the rotor angle when the phase current is constant. As seen in Fig. 4, the inductance values are almost constant till 8 A phase current for linear operation in SRM. Thus, it is considered that the winding inductance is only the function of the rotating angle. That is, $L = L(\theta)$. In Fig. 2, the stored energy (W_m) in the magnetic field is represented by the area above the related flux curve and the co-energy (W'_m) is represented by the area below the same magnetization curve. As is known, this co-energy is assumed to be the energy that is converted to mechanical energy. The flux-current characteristics in Fig. 2 show that the motor rotates in the linear region till 8 A. In this case, the co-energy equals to the energy stored in the magnetic field in the linear region.

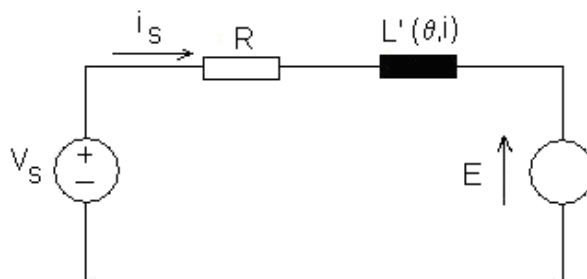


Figure 3

SRM's one phase equivalent circuit

$$W_m = W'_m = \int_0^i \lambda(i, \theta) \cdot di = L(\theta) \cdot i^2 / 2 \quad (4)$$

If the Eq. (4) is rearranged in terms of H and B , Eq. (5) is obtained.

$$W_m = \frac{1}{2} \int H \cdot B \cdot dv \quad (5)$$

where H is the magnetic field intensity (A/m), B is the magnetic flux density (T or Wb/m²).

The torque equation of the motor can be written by using the co-energy equation because of the relationship between energies as follows.

$$T_e = \partial W'_m / \partial \theta = dL(\theta) \cdot i^2 / (2 \cdot d\theta) \quad (6)$$

where T_e is the motor torque (Nm), i is the winding current (A), and $L(\theta)$ is the winding inductance (H), respectively. The torque is obviously a function of the θ

rotor position angle. As seen in (6), the torque equation is proportional to the square of winding current and independent of the phase current direction. In linear operation, the characteristic of the winding inductance and static torque of motor with respect to the rotor position for one phase are given in Figs. 4 and 5, respectively.

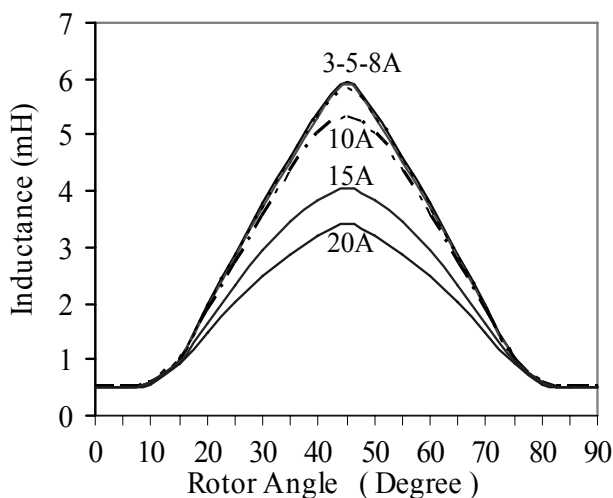


Figure 4

Variation of phase inductance with rotor angle for various phase currents

As shown in Fig. 4, when the angle between the stator pole and rotor pole is at 0° and 90° (unaligned position), the inductance value is at its minimum. In aligned position (at 45°), it has the greatest value. When the rotor pole gets closer to the stator pole, inductance value starts to increase from the minimum value to the maximum, and vice versa.

When in the linear operation, as seen in (6), the produced torque will be constant for the constant current, because the $dL(\theta)/d(\theta)$ ratio is constant. In Fig. 4, the SRM works as a motor by providing positive torque in region (I), and as a generator in region (II) by providing negative torque. In the linear region, however, the inductance slope values remain constant until about 8 A and it decreases for higher current values. Therefore, the motor was assumed to be running within the linear region and the characteristic curve for 8 A was used in obtaining the dynamic model of the SRM.

One of the main purposes of this study is to see the extent to which the static and dynamic characteristic values, such as torques and torque ripples, are in accordance with each other. The static torque characteristic of SRM obtained by using FEM for one phase is presented in Fig. 5. Here, Eqs. (4)-(7) are used to evaluate the values of L and T_e in FEM. The details are given in the appendix.

$$\frac{\partial^2 A}{\partial x^2} + \frac{\partial^2 A}{\partial y^2} = \frac{J_i}{\gamma} = \mathfrak{R} \cdot J_i \quad (7)$$

where \mathfrak{R} is the magnetic resistance (reluctance) ($1/\gamma = \mathfrak{R}$) (1/H or A/Wb), γ is the magnetic conductivity (inverse of \mathfrak{R}), A is the vector magnetic potential (Wb/m) and J_i is the current density (A/m^2).

The static torques versus rotor position angle of SRM for the 10 A phase current and three phases are given in Fig. 6.

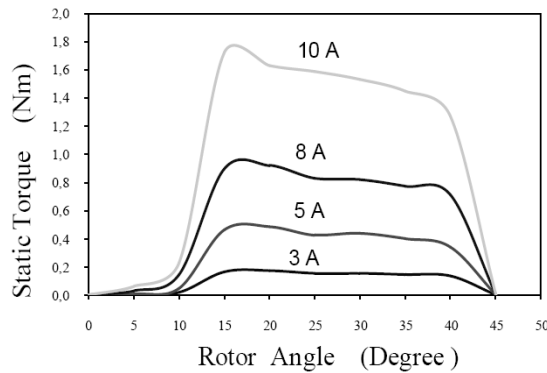


Figure 5

SRM's static torque characteristics obtained by using FEM for one phase and various phase currents

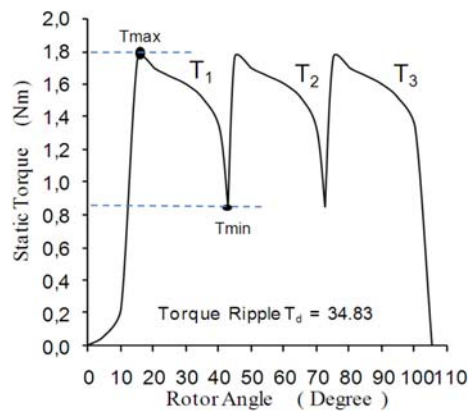


Figure 6

Static torques versus rotor angle (obtained from FEM) for three-phase and 10 A phase current

As is seen from the curve, the torque generated by the motor changes between about 1.8 Nm and 0.87 Nm for the 10 A phase current. In this case, the obtained static torque ripple is 34.83% (In Fig. 6, % torque ripple $T_d = [(T_{max} - T_{min}) / (T_{max} + T_{min})] \times 100\%$).

The L values found by using FEM, as shown in Fig. 4, are used in the drawing of Fig. 5 and Fig. 6. One of the methods used to find the inductance (L) value is to measure it by using an instrument at each step while the rotor is rotating from 0° to 90° by 1° increments. In order to find the L value by means of this method, the motor should be physically manufactured. However, in this study, the motor is at the design stage. Therefore, all motor characteristics (inductance, current, flux, torque and speed, etc.) at the real working conditions of the motor that will be manufactured at given motor power, voltage and size (dimensions) values are found by using its Matlab- Simulink model. The main parameter of this model is the inductance. The L values at certain rotor angles between 0° and 90° (in this study, by 5° increments) should be known to the model in Matlab-Simulink. In this study, the L values are calculated by using FEM for certain rotor angles between 0° and 90° . Equations (4), (5) and (7) are used to calculate the L values.

But, the L values found by using FEM are valid for a certain moment (for example, for 5° rotor angle). In fact, under real working conditions, the parameters such as speed, current and torque values are a function of time and changing continuously. The static analysis that uses FEM cannot show the dynamic working since it only considers a certain moment and uses the values at this moment. In dynamic analysis, the electrical magnitudes of the motor at time varying work can be calculated by using the flux and inductance values obtained using FEM at certain current and position (angle) values. The Flux and inductance values are put into a lookup table whose inputs are I and θ . The interval values are obtained by using interpolation in this table.

2 Modelling of the SRM

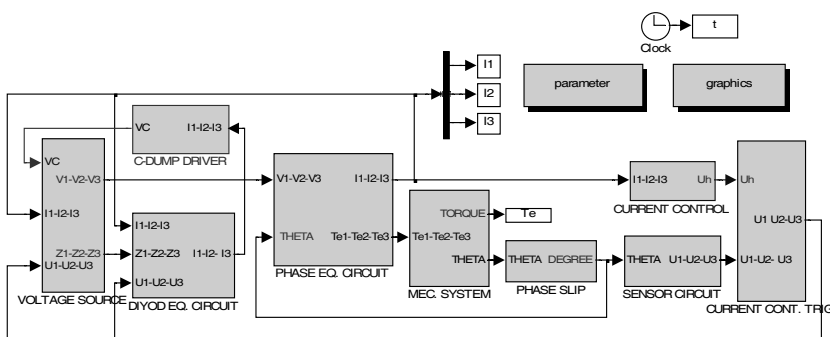


Figure 7

3-Phases SRM's linear model

The block scheme of the linear model generated by the dynamic equations given in Section I is given in Fig. 7. The model is comprised of the induced electrical torque for 3 phases, a C-dump driver circuit, a mechanical system, and a sensor circuit [11]. The block schemes, constituting the whole dynamic model, will be examined in this section.

2.1 One Phase Equivalent Circuit

From (2) and (3),

$$d\lambda/dt = V_s - R \cdot i_s \quad (8)$$

$$i_s = \lambda(\theta)/L(\theta) \quad (9)$$

The block scheme of one phase equivalent circuit obtained by means of (2) and (3) in Section I is given in Fig. 8.

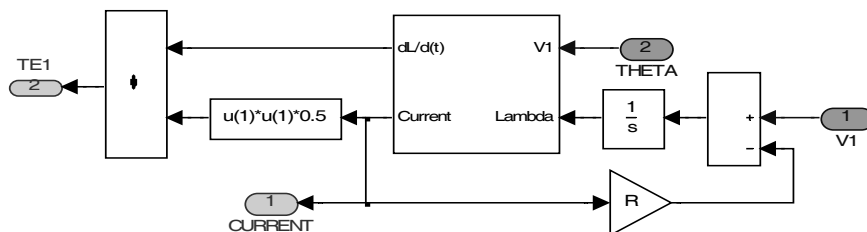


Figure 8

The block scheme of one phase equivalent circuit of SRM

The slope of inductance ($m = dL(\theta)/d\theta$) must be known in order to calculate the electrical torque expression in (6) for a certain phase current. Therefore, the inductance and its slope must be determined with respect to the variation of the rotor angle (θ) for a certain phase current. The inductance equation obtained by using FEM for the one phase and 8 A phase current is given in Table II.

As shown in Table II, the inductance values for the first phase can be divided into four linear regions as constant, increasing, decreasing and again constant region.

The increasing and decreasing regions are described as a line equation such as $L = m \cdot \theta - n_2$ for the increasing region and $L = -m \cdot \theta + n_3$ for the decreasing region.

The slope values are $m = 0$ for L_1 and L_4 , $m = 0.0091149$ in radian and 0.000159 in degree for L_2 and L_3 ; the constant values in radian and in degree are $N_2 = 0.001428$ and $N_3 = 0.012888$ for the 8 a phase current. In practice, the rotation angle is used in degrees. therefore, 0.000159 degree is used instead of 0.0091149 radian in the model since the degree unit is preferred in the matlab-simulink model.

Table II
The linearized equation determined with respect to θ for one phase and 8 A phase current

$L(H)$			θ
$(\theta = \text{Degree})$	$(\theta = \text{Radian})$		
L_1	$L_{min}=0.00056$	$L_{min}=0.00056$	$0.0^\circ \leq \theta \leq 12.5^\circ$ ($0.0 \text{ rad.} \leq \theta \leq 0.2182 \text{ rad.}$)
L_2	$0.000159*\theta - 0.001428$	$0.0091149*\theta - 0.001428$	$12.5^\circ \leq \theta \leq 45.0^\circ$ ($0.2182 \text{ rad.} \leq \theta \leq 0.7854 \text{ rad.}$)
L_3	$-0.000159*\theta + 0.012888$	$-0.0091149*\theta + 0.012888$	$45.0^\circ \leq \theta \leq 77.5^\circ$ ($0.7854 \text{ rad.} \leq \theta \leq 1.3526 \text{ rad.}$)
L_4	$L_{min}=0.00056$	$L_{min}=0.00056$	$77.5^\circ \leq \theta \leq 90.0^\circ$ ($1.3526 \text{ rad.} \leq \theta \leq 1.5708 \text{ rad.}$)

The circuit model identifying the slope and the inductance value for the first phase of the motor is given in Figs. 9 and 10.

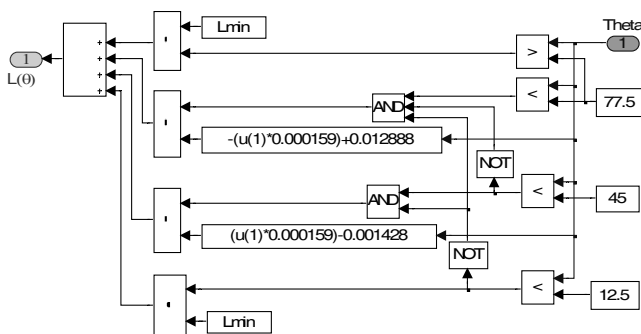


Figure 9

The circuit model identifying the value of the inductance for the first phase of the motor

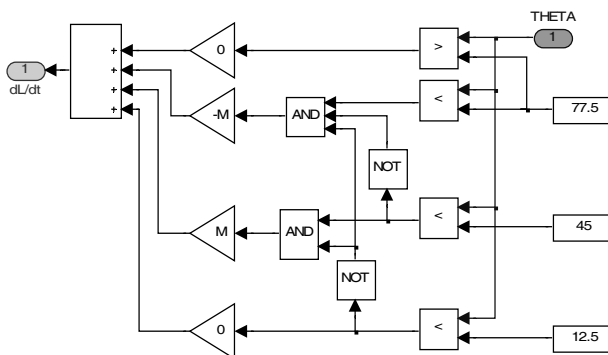


Figure 10

The circuit model identifying the inductance slope ($m=dL(\theta)/d\theta$) for the first phase of the motor

2.2 Mechanical Equivalent Circuit and Determining of the Rotating Angle

One of the expressions linking the electrical and mechanical sides of the motor is the torque expression given in (10), and the other is the acceleration expression of the rotor given in (12).

$$T_e = T_l + T_f + T_j \quad (10)$$

$$T_l = k_l \cdot \omega^2 \quad ; \quad T_f = k_f \cdot \omega \quad ; \quad T_j = J \, d\omega/dt \quad ; \quad \theta = \omega \cdot t \quad (11)$$

where T_e is the electrical motor torque, T_l is the load torque, T_f is the friction or mechanical damping torque, T_j is the inertia torque, k_l is the load constant, k_f is the friction or mechanical damping constant, J is the inertia constant, θ is the rotor position angle, ω is the angular speed and z is the load coefficient, which changes between -1 and 2. The value z is taken as 1 in this study. Thus, the formula for the angular acceleration is derived as

$$d\omega/dt = [T_e - (k_l + k_f) \cdot \omega] / J \quad (12)$$

If the above acceleration expression is successively integrated twice, the rotor position angle can be obtained. This (θ) angle is used to determine the inductance and the slope of inductance and the driving of the SRM phase switches as power electronic components. The equivalent simlink scheme obtained by using (12) is given in Fig. 11.

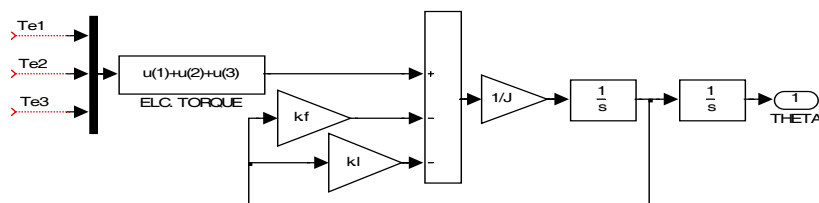


Figure 11

SRM's mechanical equivalent circuit scheme

Each phase winding of the SRM is supplied through power switches so that their conduction (dwell) angles are controlled according to the rotor position of the motor. For this purpose, three sensors are installed on the motor axle to obtain instantaneous (θ) position data, which is calculated as (θ) function by means of the circuit given in Fig. 11. The conduction angles of the semi-conductor switches (for U1, U2, U3) driving the phase windings is respectively shown in Fig. 12. Since the analyzed SRM has three phases, the conduction angle of each phase is 32.5° [4].

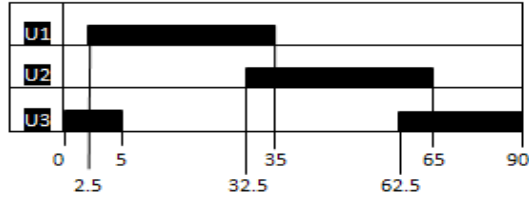


Figure 12
Conduction angles for three phases

2.3 C-Dump Driver Circuit

In the simulation of the SRM, a C-Dump converter is used as a drive circuit. Only one power switch is employed to drive each phase winding of the motor in the C-Dump converter. Since minimum number of switches are needed to supply phase currents in C-Dump converters [12], the C-dump converter is preferred in this study. From the C-Dump driver circuit,

$$dV_c/dt = (I - U_g \cdot I_g) / C_r \tag{13}$$

$$dI_g/dt = (U_g \cdot V_c - V_s - R_g \cdot I_g) / L_g \tag{14}$$

where V_c is the C-Dump voltage (V), V_s is the winding voltage (V), U_g is the constant determined the position of C-dump driver circuit switch (as 1 or 0), I is the total phase current (A), I_g is the C-dump current (A), R_g is the C-dump resistance (Ω) and L_g is the inductance of the C-dump circuit (H). The C-dump driver circuit obtained by means of Eqs. 13 and 14 is shown in Fig. 13. In Fig. 13, Z_g is the impedance of diode used in the C-dump driver circuit (Ω).

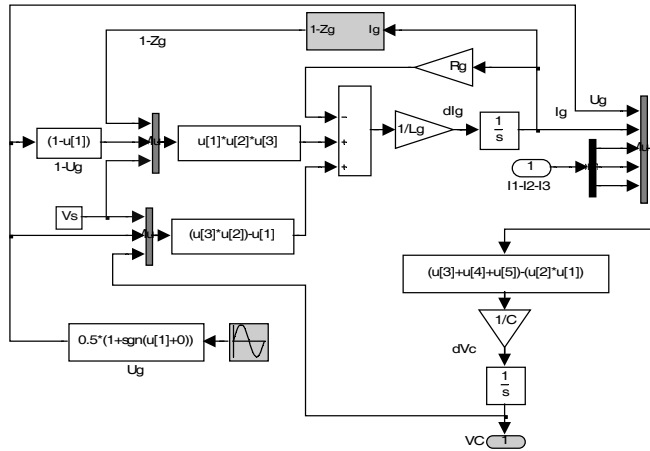


Figure 13
C-Dump driver circuit

3 Simulation Results and Discussions

The characteristic curves of the rotor position, speed, inductance, current, torque and flux obtained by the simulation of the 6/4 SRM's dynamic model given in Fig. 1 are presented in this section. The rotor position angle versus time is given in Fig. 14.

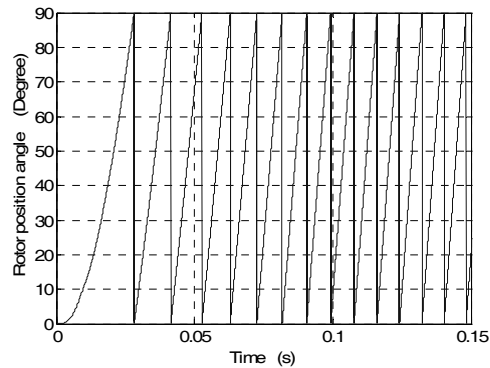


Figure 14

Rotor position angle versus time

As seen from Fig. 14, the period of the rotor position is 90° in 6/4 SRM and the rotor motion from one pole to the other is slow at the beginning, and then it starts to accelerate. The motor speed versus time is given in Fig. 15.

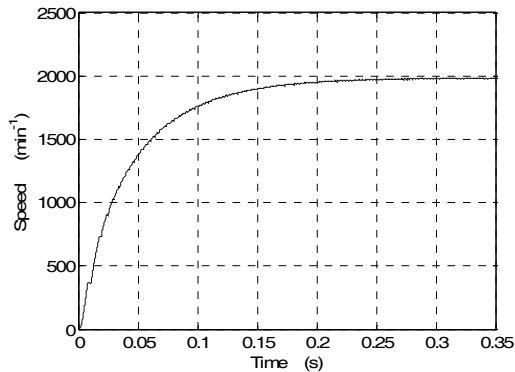


Figure 15

Motor speed versus time

As seen from Fig. 15, the speed of the SRM reaches to the nominal speed of 2000 rpm from 0 within 0.35 seconds after the starting time and comes to a stable condition. The dynamic phase inductances versus time are illustrated in Fig. 16.

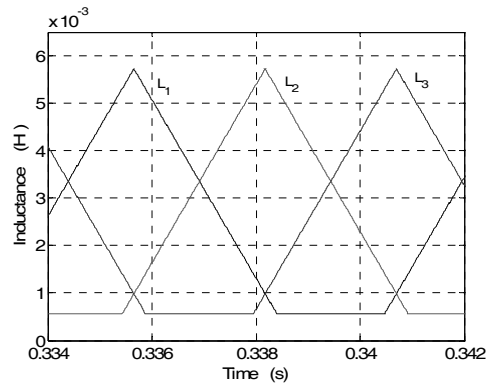


Figure 16

Dynamic phase inductances versus time

As seen from Fig. 16, the value of every phase inductance changes between 5.73 mH and 0.56 mH. These values are equivalent to the static inductance values at about the 8 A phase current. The phase currents versus time are given in Fig. 17. During the conduction angle, the phase currents rise to 17.6 A and finally fall to 8.3 A. If no current limiting protection is applied to the motor, these 17.6 A phase currents may be dangerous for the motor windings. Therefore, these currents must be restricted to a certain level.

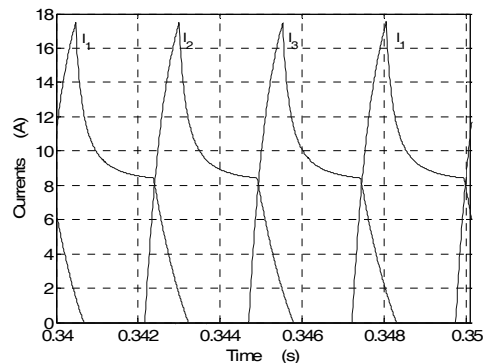


Figure 17

Phase currents versus time

Within the scope of this study, another analysis is also carried out, on in which the phase current is controlled and limited, and the simulation results are compared with those of the unlimited control model. As seen from Fig. 17, the phase currents cross at 8 A, which is the minimum phase current of the SRM. This current value is valuable for designing the driver circuit components since this crossing means that the phase current of the SRM must be 8 A.

When one phase is switched on, the previous phase that is switched off does not immediately show zero current. However, it is desired that it be zero. Therefore, using a C-Dump circuit, this current should be rapidly brought to zero by applying reverse voltage to the phase that is switched off.

The dynamic torque-time characteristics of the SRM are seen in Fig. 18. It is seen that the maximum torque on these curves is 1.33 Nm on this curve and the torque generated by the motor per phase changes between 1.33 Nm and 0.015 Nm periodically. This variation with the sharp wave form shapes in torque causes undesired vibrations and acoustic noise in the motor. The average torque of the SRM is 0.3 Nm.

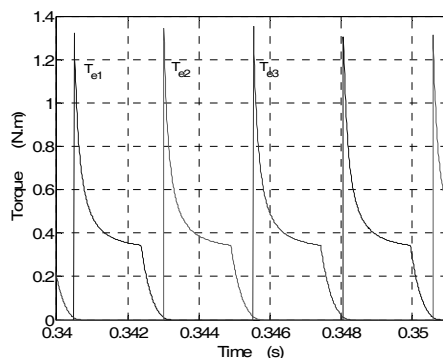


Figure 18

Dynamic torques versus time

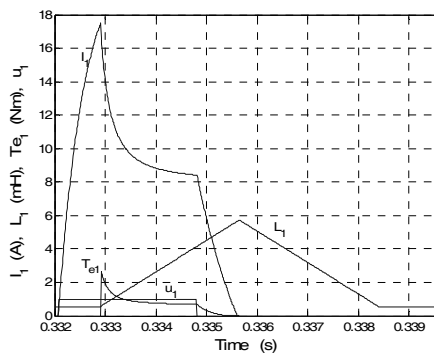


Figure 19

Inductance (L_l), current (I_l), torque (T_{e1}) versus time and conduction times (u_l) for first phase of SRM

To understand the dynamic analysis results better, the inductance, current, torque versus time and conduction times for one phase are illustrated as a whole in Fig. 19. In these curves, the current and inductance values are plotted with their real values, but the torque values are enlarged by 2 to make it clearer.

As can be seen in Fig. 19, the increasing and decreasing of the inductance is symmetric and linear. When the phase winding current is switched off in the increasing region of the inductance, the current rapidly decreases. The current is rapidly brought to zero by applying reverse voltage to the phase winding that is switched off by means of the C-Dump circuit at the end of conduction time. While the motor does not produce the torque in the region where the inductance is constant in Fig. 19, it produces the torque depending on the value of phase current in the increasing region of inductance. On the other hand, the phase flux of the motor increases rapidly in the increasing region of the current. And it continues to increase linearly from the point where the current starts to decrease (the point where the inductance starts to increase) until the end of the conduction time.

At the end of the conduction time, it decreases parallel to the decrease in the current and becomes zero simultaneously with the current. The torque generated by the SRM should remain as stable as possible. Since the torque is proportional to the square of the phase current, the motor current should remain constant at a certain value. In practice, the current control is applied to keep the phase current constant at a certain value in the motor control circuit [13].

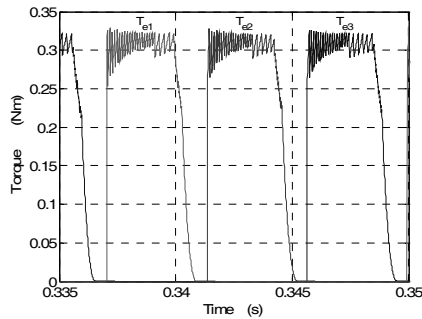


Figure 20

8 A current controlled dynamic torques versus time

The simulated dynamic torques versus time with current control at 8 A are given in Fig. 20. The average torque of the SRM becomes 0.25 Nm and 75% improvement in torque ripple is obtained when the current control is applied to the motor at 8 A, as is shown in Fig. 20. The flux variation versus phase current for one phase of the SRM's dynamic model simulation is given in Fig. 21. When the flux versus current curves (in Figs. 2 and 21) are compared, it is seen that the flux for one phase obtained by dynamic analysis at the 8 A phase current (Fig. 21) is 30.5 mWb, whereas the flux for one phase obtained by using FEM (Fig. 2) is 14.33 mWb for $\theta = 45^\circ$. The curves in Fig. 2 don't exactly conform with the curves in Fig. 21 because of the linearization of the inductance profile. When the motor phase current is controlled at 8 A, the torque and phase currents versus time for the studied SRM are presented in Fig. 22. It is obvious that a 75% improvement is achieved in the torque ripple of the current controlled model.

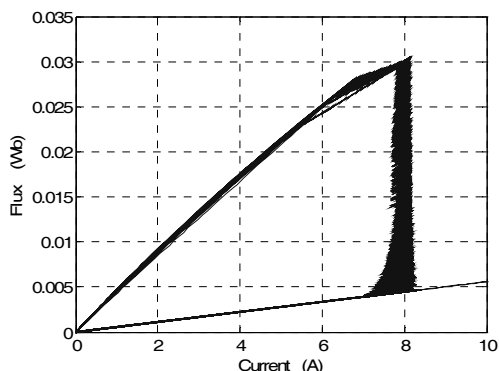


Figure 21

Flux variations versus current for one phase obtained by the result of SRM's dynamic model simulation

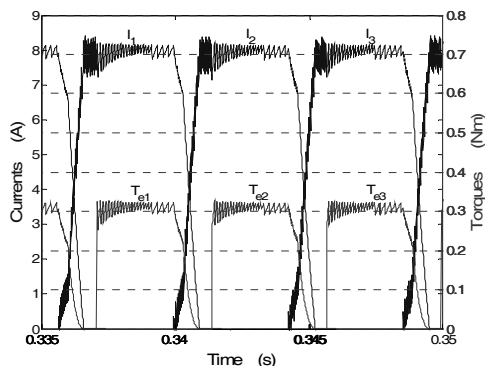


Figure 22

8 A current controlled dynamic torque and phase current versus time

Conclusions

In the article, a computer-based matlab-simulink modelling was presented to supplement the teaching of modelling subjects. The modelling allows learners to see the results of analysis and the possible remedial action. The program provides a better understanding of the SRM's dynamic behaviour and remedial action without the need to perform time consuming hardware experiments, which are also expensive to set-up.

In this study, the results obtained from the linear dynamic analysis of an SRM may be summarized as follows:

- The value of the current through the phase windings and the conduction angles are important criteria for drive design in the linear model of the SRM. Since the phase winding currents are controlled via power electronic switches, the peak

value of the current through the windings must be determined before any control.

- In this study, 97.77% torque ripple is seen in the case of the dynamic analysis without current control, although the static torque ripple for only 10 A is examined and 34.83% torque ripple is achieved in the study of [10]. The reduction in torque ripple is observed when the motor phase current is controlled at 8 A.
- In static analysis, the torque produced by the SRM becomes 1.8 Nm while the current of 10 A flows through the phase windings. On the other side, in dynamic analysis without current control, the produced torque becomes max. 1.33 Nm while the max. 17.6 A current flows through the phase windings and the maximum torque of 0.3 Nm is obtained when the phase current of the motor is controlled at 8 A. Moreover, the linear dynamic analysis determines the torque that will be produced by the motor. That is, it determines the dynamic behaviour of the motor. In order to examine the motor in more detail, a non-linear analysis may be needed.

Appendix

The main definition for inductance is $L = N \cdot \Phi / I$. An equivalent definition for inductance may be made using an energy point of view,

$$L = \frac{2W_m}{I^2} \quad (15)$$

where I is the current flowing in the stator winding and W_m is the energy in the magnetic field produced by the current. If the potential energy W_m is expressed in terms of the magnetic fields,

$$L = \frac{\int_{vol} B \cdot H \cdot dv}{I^2} \quad (16)$$

and replace B by $\nabla x A$

$$L = \frac{1}{I^2} \int_{vol} H \cdot (\nabla x A) \cdot dv \quad (17)$$

The vector identity

$$\nabla \cdot (AxH) \equiv H \cdot (\nabla x A) - A \cdot (\nabla x H) \quad (18)$$

may be proved by expansion in cartesian coordinates. The inductance is then

$$L = \frac{1}{I^2} \left[\int_{vol} \nabla \cdot (AxH) \cdot dv + \int_{vol} A \cdot (\nabla x H) \cdot dv \right] \quad (19)$$

After applying the divergence theorem to the first integral and letting $\nabla \times H = J_i$, we have

$$L = \frac{1}{I^2} \left[\oint_S (AxH) \cdot dS + \int_{vol} A \cdot J_i \cdot dv \right] \quad (20)$$

Since the surface encloses the volume containing all the magnetic energy, the surface integral is zero, which requires that A and H also be zero on the bounding surface. The inductance may therefore be written as

$$L = \frac{1}{I^2} \int_{vol} A \cdot J_i \cdot dv \quad (21)$$

where A is the vector magnetic potential (Wb/m) and J_i is the current density (A/m^2) [14].

References

- [1] T. J. E. Miller: Switched Reluctance Motors and Their Control, Magna Physics Publishing Press, Oxford University, USA, 1993
- [2] P. J. Lawrenson, J. M. Stephenson, P. T. Blenkinsop, J. Korda, N. N. Fulton: Variable-Speed Switched Reluctance Motors, Electric Power Applications (IEE Proceedings B), Vol. 127, Issue 4, July 1980, pp. 253-265
- [3] G. S. Buja, M. I. Valla: Control Characteristics of the SRM Drives-Part I: Operation in the Linear Region, IEEE Trans. Ind. Electron., Vol. 38, 1991, pp. 313-321
- [4] D. A. Torrey, J. H. Lang: Modelling a Nonlinear Variable Reluctance Drive, 5th European Conference on Power Electronics and Applications, Brighton, U.K, 1993
- [5] G. S. Buja, M. I. Valla: Control Characteristics of Switched Reluctance Motor Drive Taking into Account the Motor Saturation, IECON '90, 16th Annual Conference of IEEE, Pacific Grove, California, USA, 1990
- [6] V. F. Ray, P. J. Lawrenson, R. M. Davis, J. M. Stephenson, N. N. Fulton, R. J. Blake: High Performance Switched Reluctance Brushless Drivers, IEEE Trans. Ind. Appl., Vol. 1A-22, No. 4, 1986, pp. 722-729
- [7] M. R. Harris, J. W. Finc, J. A. Mallick, T. J. E. Miller: A Review of the Integral Horsepower Switched Reluctance Drive, IEEE Trans. Ind. Appl., Vol. 1A -22, No. 4, 1986, pp. 716-722
- [8] F. Soares, P. J. C. Branco: Simulation of a 6/4 Switched Reluctance Motor Based on Matlab/Simulink Environment, IEEE Trans. on Aerospace and Electronic Systems, Vol. 37, No. 3, 2001, pp. 989-1009

- [9] S. Sadeghi, M. Mirsalim, A. H. Isfahani: Dynamic Modeling and Simulation of a Switched Reluctance Motor in a Series Hybrid Electric Vehicle, *Acta Polytechnica Hungarica, Journal of Applied Sciences, Hungary*, Vol. 7, Issue 1, 2010, pp. 51-71
- [10] Y. Özođlu: Anahtarlamalı relüktans motorunda kutup başlarına şekil vererek moment dalgalanmasının azaltılması, Ph.D. dissertation, Dept. Electrical Eng., İstanbul Tech. Univ., İstanbul, Turkey, 1999
- [11] H. Çalık: Control of the Switched Reluctance Motor, Ph.D. dissertation, Dept. Electrical Edu., Marmara Univ., İstanbul, Turkey, 2005
- [12] V. Özbülür, M. O. Bilgiç, A. Şabanoviç: Torque Ripple Reduction of Switched Reluctance Motor, *IEEJ-1995 International Power Electronics Conference*, Yokohama, Japan, 1995
- [13] S. Vukosavic, R. Stefanovic: Switched Reluctance Motor Inverter Topologies: a Comparative Evaluation, *IEEE Trans. Ind. App.*, Vol. 27, No. 6, 1991, pp. 1034-1047
- [14] Jr. W. H. Hayt: *Engineering Electromagnetics*, McGraw-Hill Kogakusha Ltd., 3rd Ed., 1974

Historical Origin of the Fine Structure Constant

Part III: Pauli with Jung Retro-Cognizes St. Stephen's Crowning Achievement

Péter Várlaki^{1,2}, Imre J. Rudas³, László T. Kóczy^{1,2}

¹ Széchenyi István University

Egyetem tér 1, H-9026 Győr, Hungary, varlaki@sze.hu, koczy@sze.hu

² Budapest University of Technology and Economics

1111 Műgyetem Rakpart 1-3, Budapest, Hungary

³ Óbuda University

Bécsi út 96/B, H-1034 Budapest, Hungary, rudas@uni-obuda.hu

Abstract: In Part II of the paper we discussed the central role of the number-archetype 137 in some great medieval works related to St Stephen's court. On the basis of the hermeneutical interpretation of certain of Pauli's famous dream series, we intend to show his hypothetical "synchronistic (unconscious) recognition" of the dominant representations and meanings of the medieval works discussed in the earlier parts of this paper, which can be related to his isomorphic mythological and "physical" dream patterns. We can also conclude that Pauli, collaborating with Jung, himself confirms in his consistent "dream-messages" the symbolic meaningful relationship and structural isomorphy between the basic quantum-physical model's features (e.g. the fine structure constant) and their hypothetical primordial images appearing even in the actual medieval works.

Keywords: number-archetype 137; background languages; identification of symbolic systems; hermeneutics

1 Introduction

In the second part of the paper we attempted to show in some great medieval works related to St Stephen's court the central role of the number-archetype 137 organizing "fine structures" together with quaternary and denary proto-Kabbalistic "systems" as a possible primordial image and "model" of the quantum-physical fine structure associated with the four quantum-numbers and the fine structure constant (FSC) concept. On the basis of the hermeneutical interpretation of certain of Pauli's dream series, in this part of the paper, we intend to show his

unconscious recognition of the dominant representations of these medieval works, which can be related to his isomorphic mythological and so called “background physical” dream patterns. Thus, we can conclude that Pauli himself confirms in his consistent “dream-message” the symbolic relationship and isomorphy between the basic quantum-physical model’s features and their hypothetical primordial images with specific synchronicities related to the *Hortus* Incarnation picture, the Hungarian Royal Robe (Casula) and the Holy Crown of Hungary. Finally, in the last dream of his dream-series he “informs” us of his symbolic personal encounter with the possible “author” of the above-mentioned great works. On the basis of his other dominant dream-message, on the disappearing Anima (as Jung’s concept), we may identify the almost complete synchronicity between the disappeared Anima Mundi from the contemporary “physics” (natural philosophy) and the also “disappeared” God’s Mother enamel picture from the Holy Crown of Hungary as an actual “spiritual meaning” of our era as well. But, first we summarize shortly the essential features of the primordial images of the creation and incarnation, as well as the creational “model” of the inverse cosmic tree characterized by the number-archetype of 137.

2 The Short Summary of the “Primordial Images of the Creation and Incarnation with the Number 137

The main “Creation-image” of the Holy Crown and the *Book Bahir*, as we have seen in part two of the paper, originates from the so-called Slavonic Book of Enoch (see footnote 3) in which God, sitting on his throne, is emanating in the primordial light the Aeon of the space-time structure of eternity. Here, as we could observe, the radix of the lights features, in addition to the light of the ancient Sun and the ancient Moon, God’s name with 32, the number of the Creation. God’s name is of course at the same time the symbol of the 10 Sephiroth similarly to the 10 fingers of God. The primordial “fine structure” of the two ancient trees can be given in the composition of 18+6 (the ornamentation of the canopy and the trunk) on both the left and right side too. Thus, using a slightly different numeral interpretation, we get to a 36+12 composition, which is one of the primeval symbols of the space-time structure with the 12 zodiacs (patriarchs, apostles) and the 36 deans [1, 2]. The latter refers also to the space-time structure through $6 \times 6 = 36$, according to the *Bahir* (94 §.) and the Sefer Yetzirah. The $3 \times 12 = 36$ ornaments in the throne, including the 12 tassels, are as if to symbolize the 36 righteous (just men, or 36 pairs of minor apostles). So in this way, with the 2×10 fingers of God, the “fine structure” of the 137 number archetype consists of the 32-type creation of the primordial light, the pleromatic cosmos as well as the space-time world’s order of the 12+36, which is complemented with the psychological symbol of the human world’s 36 righteous men

$(32+(36+12)+36+20+1=137)$ ¹. Even the spectrum (of the “fine structure”) itself can be taken as the schematic drawing of a tree laid on the ground. These allegorical images of the Creation are made complete by the ten each digits of God’s hands and feet. As we have seen, his active 10 fingers symbolize the Creation’s active and fruitful aspect, while his toes refer to the accepting, earthly accommodation of the ten Sephiroth (see Kaplan’s commentary [2]) The unity of these two is embodied in the ancient Aeon between them, in the *Aleph*, in God’s name that also symbolizes the 10 Sephiroth, and the slanted cross that also gives the initial of Christ’s name, which in the Latin interpretation could also mean the number ten. This omphalic symbol originating from the stomach or God’s bosom (lap) is a primordial Aeon, Adoil, (the hypothetical עדיאל) the eternity of God in Hebrew, the numerical value of which is *III*, which in the Hebrew name equals with the numerical value of the Hebrew word *Aleph*. All of these are made current by the Greek interpretation of the slanted cross into the number thousand, which clearly refers to the time of the *resurrectio prima*, the Holy Year of 1032-33. The Holy Crown thus was made for this Holy Year with the images of the Creation, and the number 137 together with the primordial light of the Creation and the

¹ The garment of Christ, on the Pantocrator picture, contains a partly specific and partly symbolic representation of a *tzitzit* (tassel) according to Matthew 9, 20. (“*Just then a woman who had been suffering from chronic bleeding for twelve years (!) came up behind him and touched the tassel of his garment.*”) The 32 structure of the Lord’s tassel (*tzitzit*) can be identified by the $4 \times 3 = 12$ (!) triangles, where each of these four “triangle-groups” indicates five geometrical points. (Fig. 6 of Part II) This can be considered the symbolic representation of the 4×8 ($8 = 3 + 5$) = 32 threads of the *tzitzit*. This “symbolic model” of the 32 structure for the Lord’s *tzitzit* corresponds completely to the *Bahir*’s interpretation of the 32 threads of the *tzitzit*, where the 32 threads correspond to the 32 paths of the Lord’s garden, where the cherubs are watching the Tree of Life (see §.92 and 98). Consequently, above and below the throne the 32 “star-entities” (together with the sun and moon), may represent the “New Testament”, while the above identified 32 entities of the Lord’s *tzitzit* the “Old Testament” 32 “compositions”. Similarly, the two trees of the garden contain 24-24 ornamental entities, together with the 12-12 ornamental elements of the throne on the right and left side, respectively. This ornamental composition can be considered as the 36-36 structures of the “New and Old Testament”, respectively. Thus, it is equivalent to the $2 \times 36 + 2 \times 32$ composition of the frequently discussed white pearls and red gems structure. The other $72 + 1 + 64$ composition of the white pearls and red gems on the Latin crown’s hoops corresponds to the left- and right-hand ornamental $72 + 1 + 64$ compositions of the throne image. The $12 + 12 = 24$ ornamental structure of the throne (Fig. 6 of Part II) corresponds to the 12 white pearls and 12 red gems found on the quadratic frame of the Pantocrator’s picture. In this case the singular entity corresponds to the slanted cross. Thus, we may obtain an equivalent $24 + 1 + 112 = 137$ composition. If we count the above $24 + 1$ entities together with the central singular element of the five star entities under the throne, we can obtain a $111 + 26$ composition as well, similar also to the representational forms found in the Emperor’s enamels picture and the *Hortus* incarnation composition. If we consider the 26 entities of Lord’s name (see Fig. 5 of Part II) together with the five star entities under the throne, we can also get a natural $106 + 31$ composition. Both of these last two compositions can represent, as we have shown, the name of the angel Yophiel. Furthermore, if we consider the $3 \times 24 = 72$ ornamental entities of the two trees and the throne, together with the four symmetric structures of the five star entities under the throne, and considering the upper 27 elements of the sun, moon and star representations and the 32 entities of the Lord’s *tzitzit* (including the two remained singular elements too), we can identify a $76 + 61 = 137$ “incarnational compositions”. This is also similar to the discussed (equivalent) 137 structures of the Emperor and *Hortus* incarnation pictures, showing a fascinating richness of the meaningful “hermeneutical represent-ability” of the number-archetype 137 on the Pantocrator’s enamel picture of the Holy Crown of Hungary.

unfolding of the “fine structure” (based on the symbol of the inverse tree), the inverse of the 137 or the number $1/137$ determine the nature of the original as well as the continuous creation or incarnation of the Messiah.

Based on all of these we can observe that the creation of the world is started with the creation of the ancient Aeon from the ancient chaos, the abyss, which in this interpretation is the number archetype of the 137 or its inverse (since it is about an inverse tree), so it is no other than the primordial image of the “fine structure”. This is that which includes everything, from which everything arises and originates, that which is at the same time, its own first creation. And as it also creates, so it is a Creator, and of course not only in the physical cosmos but, as we have seen, in the human soul too. Since “He” is the incarnational numerical archetype of Christ, the number with which Christ upholds and manages the Church, that is, the world of the souls of all the people believing in him. The creation from the stomach and the abyss can be interpreted as a second creational symbol, since the hand emerging from the abyss of the primordial chaos can symbolize the Torah, the 10 Sephiroth and the Ten Commandments as well. This image, as a primordial model can be found in two forms in the allegorical symbolism of the *Bahir*, the *Holy Crown*, the *Royal Robe (Casula)* and the *Hortus* too. On the one hand, as the verses 3.10, and 11 of Habakkuk, on the other hand as the emergence of the hand of Zara (of Tamar) from the maternal womb’s ancient abyss. The idea of the 137-composite inverse tree (that has 10 Sephiroth - see Fig. 1), as the primordial image of the fine structure in quantum theory carries the organization of the spectrum lines (tree structure) through the inverted number of 137, of course in the decimal system (the Sephirah means “number” in Hebrew).



Figure 1

Inverse tree representations of the Creation and Incarnation (HolyCrown and Hortus)

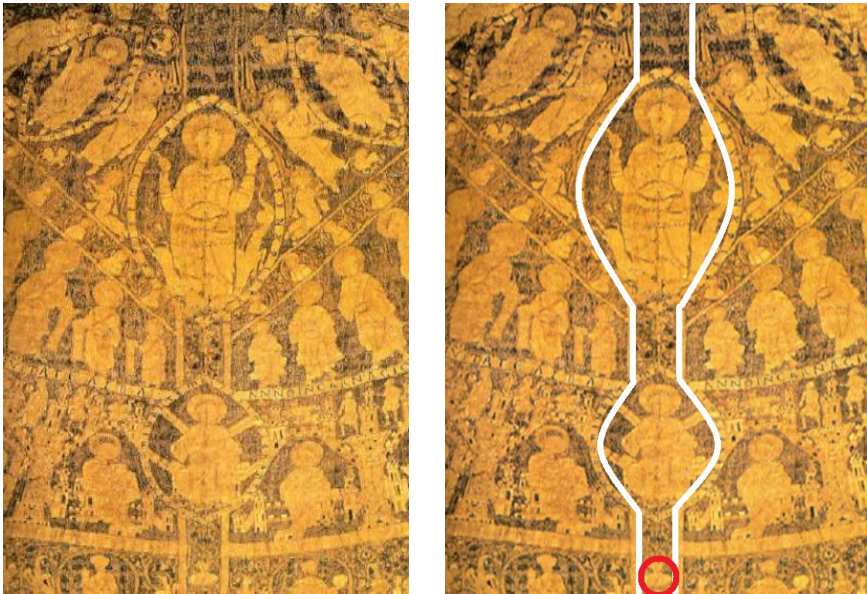


Figure 2

The Casula (Robe) of St. Stephen (1031). The “trunk” of the inverse tree with the “branches”. St. Emeric can be seen in the red circle.

3 The “Creation-Model” of the Inverse World Tree and the Number Archetype of 137. Comprehensive Comparative Analysis

As we discussed previously (in the part two) the whole depiction system of the Coronation Robe can be comprehended also as a so-called inverse tree coming from the sky. The single branches form the hierarchy of the heavenly church, with the apostles, prophets, etc. found there. The comprehension of the “pleromatic cosmic-tree”, characterized with circular branches has been well-known since antiquity. In the same way, this “world tree” on the Casula, with its circle divided into 12, reveals the zodiacal system, and with its 3-3 faces reveals the world-leading spatio-temporal system of the 36 deans (see similar Judaic later representations in [1]). We can find exactly the same world tree interpretation in *Bahir*, where the only inverse pleromatic tree is the Tamaric symbolic date palm tree, which has 12 branches, and the triple division of those branches leads to 36 clerks (officers) or just (true) people. The 95th section of the *Bahir* doubles the 36 officers to 72, and later completes it with the 64 entities of the 4-cherub throne chariot of Ezekiel’s vision, almost exactly in the same system as we see on the

Casula. So the world tree, as a unit, leads to the $72+1+64=137$ system – which is the base scheme of the Holy Crown of Hungary – whose equal division variant was, as we saw, the $68+1+68=137$ structure. We can see this structure exactly on the Robe, where the three faces of the 12 zodiac generates the system of the 36 righteous men or deans (see Fig. 7 in part two). The celestial origin is shown by the fact that the trunk of the tree rises from the cervical part where can be found the two hands of God, who planted the inverse tree. This is followed by the seraphim, the cherubim together with the angels. Then come the prophets, the just men, apostles and saints, who together construct a seven-level hierarchy of the tree. So the tree “continues“ or “develops” towards the earthly existence. Obviously the allegorical system of the tree is compatible with the spinal column in the anthropomorphic description found in the *Bahir*. In the centre of the Casula we can clearly see the upper large mandorla as an expansion of the trunk of the tree, which, based on the principle of the inverse, is followed by a smaller mandorla moving downwards; and at the end, as a closure, a small picture of St. Emeric is in the centre. The trunk of the tree gradually widens above (Fig. 2). The width of the trunk at the lower part is about one third smaller than the width at the upper part. The head of the prince to be crowned, in the anthropomorphic metaphor, represents Christ, while the other parts of the body are the apostles, prophets and the holy Fathers (see also the Admonitions [33]).

In Bahir’s Book, in addition to the interpretation of the inverse tree, the main trunk and the branches of the tree (or rather the spinal column in an anthropomorphic metaphor) are represented by the Casula, which is the symbol of the 6 lower Sephiroth (the six central Sephiroth, between the 3rd and 10th) in the 30th section, with the Hebrew word (שלמה) for King Solomon, which means Robe (see Bahir [2]). In the following three sections (31, 32, 33), the whole Sephirothic system is represented by the author with the crown and the cloak (robe) of the divine king. Thus, (for the careful observer and interpreter) the inverse tree, the body, the crown and the cloak of the king appear as a distinct, but in meaning complementing, representations of the decimal Sephirothic system of the pleroma.

We have also already discussed that we “can interpret” the same inverse tree in the pictures in *Hortus deliciarum* as well (Fol. 80v), where, as we saw, the inverse tree also has the structure 137 (Fig. 1 in part two). This is of course mainly about the incarnation of Christ, but on the branches and on the top flowers of the tree we can get a detailed view of the divided (probably Latin and Greek) Church, while “Israel” can be found in the trunk. The same depiction form can be found in the *Bahir* by interpreting the date palm tree (in Hebrew Tamar) as an inverse tree, where the heart, the trunk of the tree, symbolizes Israel, while its branches and flowers symbolize the people, or the righteous people (sections 98 and 101).

The Tamaric (twin) „metaphor” is here also made complete with the 2×68 interpretation of the *Lulav* ($68=לולב$), which also leads to the number 137. In this picture, because of the manner of depiction, which has multiple explanations, on one hand, God or Abraham plants the tree, whose centre part on top is closed by

Christ as the flower of the flowers (*flos florum*). St. Emeric's picture on the Casula also matches to the Christ picture. On the other hand, the special sitting posture of the Christ-faced divine person – in the context of *Hortus deliciarum* - on the mountain of Pharan hints as if the tree would grow out of the lap or the loins of God himself (or symbolically Abraham). So considering the inscription as well (*Ihesus Xpistus gignit Ecclesiam*) Jesus Christ as the Lord reproduces himself as the flower of the flowers, and also as the unified Church of the Jews and pagans (see the inscription² of the Fol. 199r in [7]). The two inverse trees with the 137 construction, one on the robe, the other from the incarnation picture in *Hortus deliciarum*, show remarkable similarity to each other.

It is particularly interesting that the depiction system of the Casula by itself, and the joint depiction interpretation of the Holy Crown and the Casula, both make possible the interpretation of the 137 inverse tree. We can correlate in the same way the inverse tree in the *Bahir* and the decimal “Sephirotic model” of the Holy Crown and the Casula. This ancient form of the Jewish-Christian interpretation of the inverse tree appears in the Book of Enoch, whose lost Greek version might have been known in the court of Saint Stephen.

Here the main and primary attribute or Aeon of the pleroma grows out of the abdomen or the naval of God, and, as Scholem discerns well, it equals to the inverse tree growing out of the naval or the groin of God³ (Scholem 1990). Because of the original Greek word “Adoil” (obviously Ἀδοίλ) for Aeon's name, many people think of the Hebrew name עדיאל “as original”, since it can mean eternity or the rule in the time of God, so the Hebrew word of עדיאל equals well to the word Aeon. The hypothesis of the Hebrew composition, as a psychic fact of the age, might have been evident for a medieval interpreter knowing both Medieval Greek and Hebrew, in spite of the fact that it is grammatically debatable. So, completely independently from what might have been the original (lost) Hebrew equivalent for the word *Adoil*, in the age of St. Stephen this association might have/had been strengthened by the synchronistic emphasis on the fact that the numerical value of the above-mentioned Hebrew word is 111; in other words, it is identical with the numerical value of the name of the significant Hebrew letter

² “*Petrus et Paulus et ceteri apostoli ducunt utrumque populum, scilicet iudaicum et gentilem in unius ecclesie persona figuratum ad celestem regem Christum*” „*Post coronam regni impugnatur ecclesia* (i.e. the Holy Virgin!) ... *glorificabitur victoria*” [7]

³ “*Using the image of the planting of the cosmic tree (in Book Bahir), this text describes the creation of a primordial aeon. This aeon, it seems to me, not only contains something of the pleroma of the Gnostics but also suggests some relationship to the strange cosmogonic passages in the Slavonic Book of Enoch (from the first century of the Christian era) where mention is made of precisely such a primordial ‘great aeon’. This aeon bears the inexplicable name Adoil; the proposed etymology ‘aeon of God’ would, in any case, be very poor Hebrew. What does the Slavonic Enoch know of this great and enigmatic aeon in the two places that manifestly treat the same motif but partially contradict each other? God, enthroned alone in the primordial light and passing through it, calls forth Adoil from the depths (of nonbeing?). From his stomach is then (chap. 11) ‘born’, as if it were different from Adoil, ‘the great aeon of him who bears all creation’, which should probably be read, ‘the great aeon that bears all creation.’*” (Scholem 1990.[25])

“*Alef*” (and the number thousand). The *Alef*, as we have seen, also means the name of God in the *Bahir*, where the numerical value of $IHVH=IVI$ existing in *Alef* is 26, while the symbolically equivalent *Alef*'s is 111. Their joint interpretation is 137, which expresses the Sephirotic system as decimal, while its unity and its structure is 137 at the same time. So, the great Aeon or the inverse tree growing out of the abdomen or the groin of God was precisely matchable with the name *Adoil* in the given hermeneutical circle, completely independently from its former real Hebrew form, which is unknown even nowadays. As a third inverse tree (or considering *Bahir*) as the fourth inverse tree we can see exactly the same on the upper Pantocrator picture of the Holy Crown, where the inverse tree that equals to *Adoil* is growing out of the abdomen, or groin, of God as a slanting cross (see Fig.6 in part two.). As we have analyzed in detail in several of our studies (e.g. [35]), the slanting cross in its shape perfectly equals to the dual interpretation of *Alef* (111), and $IHVH=IVI$ (26), together with the number 137 of course. Our hypothesis is strongly reinforced by the fact that the determining decorative frame of the slanting cross, which can be found in the centre of the crossbands, is made of 72 white pearls and the 64 red gems. The slanting cross appears in the centre of the pearls and gems as the 137th entity and also as the symbol of the crucifixion, the Hebrew word for which is *celibah* (צליבה), whose number is 137 too. So the main characteristic is that the all is carefully, astonishingly precisely and creatively-designed, and particularly carefully manufactured (see Ferencz 2002 [5]). The Holy Crown aims to emphasize (through the consciously planned completely unique asymmetrical structure⁴) the 137 structure of the inverse tree of the slanting cross growing out of the Lord. Although the slanting cross points upwards because of the evident structural conditions of the crown, in its natural hermeneutical meaning it grows inversely, downwards from God sitting enthroned, and so towards the earth and the very people for whom it mediates (or “interprets”), between themselves and God.

We can as well find a similar depiction method of the inverse tree in the Abraham picture of *Hortus deliciarum* (Fig. 9 in part two). In the picture Abraham is sitting on the throne of God between two palm trees, with a crown above his head. Two

⁴ This characteristic asymmetry of the Holy Crown (as a primordial model of “creation and incarnation”) “synchronistically” can be considered as an anticipation of the crucial quantum-physical phenomena to which Pauli referred, saying “*God is a weak left-hander after all.*” This allegorical image of Pauli was interpreted by Jung as a prevalence of the unconscious [20]). The asymmetric form of the Holy Crown really shows a “*light left-hander construction*” (“ensuring” the slanted cross with its rich interpretational potentiality) according to the view of a proto-Kabbalistic work (pseudo Hai Gaon text [4], “*ומגלגלים מדת הדין למדת הרחמים*”), where the attribute (“energy”) of Judgment (God’s left hand) is continuously transforming into the attribute (“energy”) of Mercy (God’s right hand). In the language of depth psychology, this means that the dominant unconscious contents are transforming into the conscious. In the language of Christian tradition it could mean the continuous incarnation of God into man through the work of the Holy Ghost. Consequently, a perfect symmetrical crown structure with a straight cross would “show only” a static, confirming image without any additional meaning, while the asymmetric crown construction with the slanted cross, in the discussed symbolical theurgical context, ensures a dynamic image with rich meaning capacity as a completely unique and fascinating “poetic-hermeneutic” solution.

similar crowns can be found above the two palm trees (or Tamar), i.e. the Solomonic triple crown (as the “archetypal model” for the Holy Crown), which has been explained in detail along with its meaning construction in our former article. In Abraham’s lap the just (true) men are represented by 14 little boys, among whom the six middle ones are creating the shield or the star of David (Fig. 9 in part two). Here, the “14 construction” consists of two fours and six in the middle, showing the Hebrew name of David in complete agreement with the identical, previously discussed pattern of the Holy Crown [35]. So with the Tamaric allusion, the Messiah grows out of the lap or the groin/loin of Abraham (as an incarnation tree), similarly to the depiction of the inverse tree, already analyzed in detail, emphasizing the Messiah's triple crown system, referring to Solomon, the son of David. So we have been able to show 5 inverse tree depictions, the unique individuality and similarity of which may refer, in our opinion, to the same circle of authors.⁵

4 The Original “clover Archetype” and Its “Unconscious Recognition” by Pauli

As we have shown in other papers [32, 34], Pauli’s introductory dream series [10] is based upon the number archetype motives “1,3,7”, partly to express the Kabbalah’s “(1)3+7” Sefirot structure and dynamics, and partly to hint at the central role of FSC. The (seven-colored) rainbow (the 8th) dream with the double Shekinah dream (Mother as 3. and his sister as 7. in the 15th dream – see still “the seventh!” in the 13th dream); furthermore the famous Ace club and seven card (the 16th) dream can be considered as the main examples [10, 18, 20]. In the succeeding 17th dream, a blue flower is found, which later, in the 23rd dream’s associations, appears as the central four-petalled blue flower [10]. Together with the four “qualities” of the French card it could also be an allusion to the “four worlds” of the Kabbalah. These dreams are associated with the allegorical picture

⁵ It is well known that the inverse tree depictions and the mythologems are widespread among different peoples. Among them, there is one that we would like to call attention to, an archaeological find from Sarkel (a city of the Judaizing Khazaria) from the 9-10th century, where on the “bone-cloak” there is a cross growing out as an inverse tree from the groin of the celestial bird, symbolizing God. Around that celestial bird, both on the left and the right side, there is an inverse palm tree. On the bottom of the “cloak”, from the octal division, there is a straight tree growing out from the ground towards the sky.



Opposite the tree, on the other side of the “cloak”, there is a deer being mounted by a celestial bird perching on his back. We see on the side of the perching bird a phallus, while on the opposite side, on the deer’s side, a receptive (uterus) symbol. The entire picture, together with that written above, and with the Hungarian ancient legend makes such a astonishingly strong connection that we leave the associations and thoughts related to them to the kind reader. (see Flerova V.: Graffiti Khazarii, 1997.)

of Tamar, the Sun-woman and the Holy Virgin (the 6th and 7th dreams). Concerning the dream context, in the 5th dream Pauli is “transformed” into a date palm, whose Hebrew name is Tamar. The tree and flower (plant, see 6th, and 7th dreams) symbols and the clover archetype are dominant patterns, not only in these dreams but in the whole dream series, including the later dreams as well, and as a life-long motif in the central dream [18]⁶. On the Figs. 3, 4 and 5 a comparison is illustrated between Pauli’s clover archetype dreams and the characteristic motifs of the *Hortus* Incarnation picture. The above-mentioned dreams and the Figs. 3, 4 and 5 show a shocking structural and meaning correspondence between the dreams and the meaningful details of the pictorial system and hermeneutical representations of the *Hortus*. The Ace club and seven card dream and the succeeding clover archetype dreams contain the dominant structural system of the Holy Crown of Hungary as well. The interpretation of the elements Ace (As), Club (Treff) and the “7” of the dream is double according to Pauli and Jung: As the Highest, the Ace is Christ, the Club is the Trinity (“3”) with the “7”. From the lowest point of view the Ace is “1” with the (same) “7” and the Club could be the symbol of the cross. Thus we can obtain a “mini-max” interpretation with the structure (I) “3+7” and (II) “8” (“1+7”) as well as Christ with the (III) Cross. It is a perfect isomorphy with the threefold structure of the (“Solomonic”) Holy Crown. Concerning the later discussed “card with 7 diamonds” dream (see later [18, 20]), which is the symbol of Holy Mater and Mary, there is perfect correspondence with the *Hortus* Incarnation picture as well. Later in the dream series the clover archetype is transformed into an eightfold flower archetype with a “strong center” (see the 23rd and 35th dreams). “The final result” of this is the “10+8+1” double crown structure in dream 29: *A bunch of roses, then the sign*  *it should be* . Here, from the denary system only one distinguished pair is dominant with the four other homogenous pairs and the possible “3+7” composition. Furthermore, the 4x2 pairs in the “8” structure with the centre is in full equivalency with the Holy Crown’s structure. This structure  in dream 35

⁶ The texts of the above initial dreams: “1. dream: The dreamer is at social gathering. On leaving, he puts on a stranger’s hat instead of his own. 2. dream: The dreamer going in a railway journey and by standing in front of the window he blocks the view for his fellow passengers. He must get out of their way. 5. dream: A snake describes a circle round the dreamer, who stands rooted to the ground like a tree. 6. dream: (Impression, directly following upon 5:) The veiled figure of a woman seated on a stair. 7. dream: (Visual impression). The veiled woman uncovers her face. It shines like the sun. 8. dream: (Visual impression). A rainbow is to be used as a bridge. But one must go under it and not over it. Whoever goes over it will fail and be killed. 13. dream: The father calls out anxiously, “That is the seventh!” 14. dream: The dreamer is in America looking for an employee with a pointed beard. They say that everybody has such an employee. 15. dream: The dreamer’s mother is pouring water from one basin into another. (In Pauli interpretation the basin belongs to his sister). This action is performed with great solemnity: it is of highest significance for the outside world. Then the dreamer rejected by his father. 16. dream: An ace of clubs lies before the dreamer. A seven appears beside it. 17. dream: The dreamer goes for a long walk, and finds a blue flower on the way”. 18. dream: A man offers some gold coins in his outstretched hand. The dreamer indignantly throws them to the ground...A variety performance then takes place in an enclosed space. 19. dream: A death-head. The dreamer wants to keep it away but cannot. The skull gradually changes into a red ball, then into a woman’s head which emits light. 20. dream: A globe. The unknown woman is standing on it and worshipping the sun.[10]

and 22 appears as a wheel (whose name number is 137 in Hebrew) or as wreath (Stephanus, Στεφάνος in Greek!) or crown⁷. We may mention the hypothetical pre-cognition of the asymmetric (weak left-hander) crown's structure (see dream 29).

It is well known from Pauli's letters that he (together with Jung) thought his dreams could have some cognitive capacity and certain mediumistic abilities [18]. He assumed concerning certain of his dreams that they unconsciously recognized some unknown patterns of documents from antiquity and the middle ages. Both Jung and Pauli meant that in certain cases they can pre-cognize, in a mediumistic way, some important patterns of the preparing "trajectories" of the future too [14, 15, 20]. On the basis of the above comparisons, it seems to us that the Ace Club and Seven Card dream family perhaps may prove Pauli's unique cognitive and mediumistic ability (similarly to the so called "Pauli effect"). This abstract dream and the succeeding sevenfold diamond card dream recognize or retro-cognize the structural characteristic and basic meanings pattern of the *Hortus* Incarnation picture.

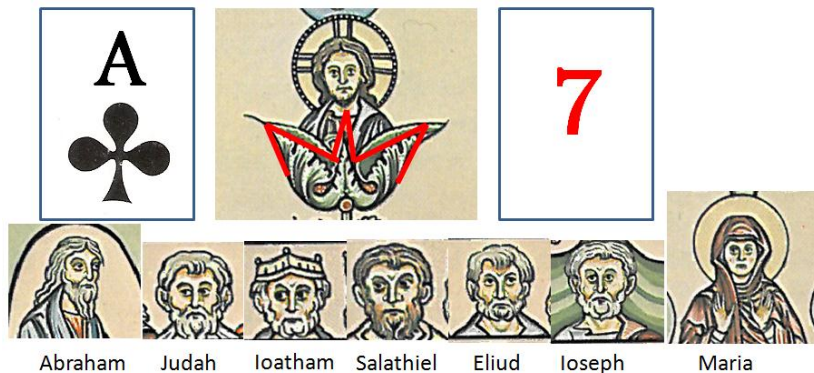


Figure 3

The illustration of the isomorphic pattern for the "Ace club and seven card" dream on the *Hortus* Incarnation picture. On the central vertical axis, under the "clover archetype" with Christ, are six forefathers and as the seventh (!) Virgin Mary

⁷ Concerning the characteristics of the structure and dynamics in the "Ace club seven card" dream series (similarly to the "World Clock" dream family – see in [29,32]) we may use the "4+1" background languages proposed by Pauli. The psychological interpretation, related to the four orientation functions and their personifications, is known through Jung's analysis together with Pauli's important commentaries, while the religious interpretation is self-evidently related to the discussed joint Christian-Judaist proto-cabbalistic system. The physical background language may express the archetypal image of the fine structure associated with the four quantum numbers and the primordial concept of FSC, while the interpretation of the aesthetical (hermeneutical) category can be related to the representations of the Holy Crown and the *Hortus* Incarnation picture etc., which are symbolically isomorphic with the pattern of the dream series. The neutral, number-archetypal interpretation through the quaternary "system-symbolism" may express a rather abstract primordial "system representations".

Beside the psychological and hermeneutical aspects used in the Pauli's and Jung's commentaries, we may identify the mythological and religious background of the dreams as well. Later in 1948 and 1955 these dream patterns appear again in new similar dreams where a background physic language is dominant, related symbolically also to the FSC, fine structure and the quantum numbers. Thus, the Ace Cub or clover archetype dream family can connect the mediumistic recognition of the proto-Kabbalistic system of the *Hortus* picture and the Holy Crown's structure and symbolic with the "allegorical" dream's manifestation of the fine structure, FSC and the four quantum numbers. Consequently, Pauli himself can state and "prove" mainly unconsciously that the "fine structure model" of *Hortus* Incarnation picture⁸ and the similar mentioned representations can be really concerned as the primordial image of the FSC concept, the fine structure with the associated four quantum numbers.

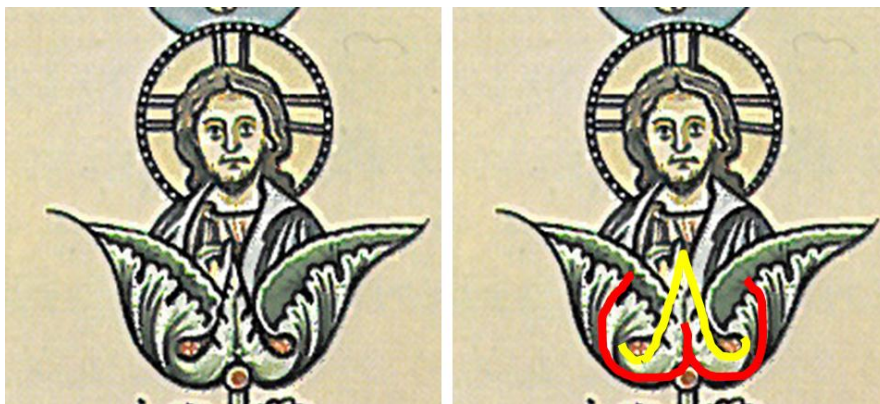


Figure 4

The illustration of the clover (trifolium) archetype with Christ and the sign of "A ω" on the Hortus Incarnation picture

The second significant achievement of Pauli's assumed "historical mediumship" is the identification of the structure and dynamics of the proto-Kabbalah with the great works related somehow to Saint Stephan's court. Probably, these meaningful works could give the spiritual basis, according to the hermeneutical principle of the "creative and productive misunderstanding", for the later purely "Jewish Kabbalah". Finally, Pauli in his two (clover archetype) dreams from 1948 (see [20]) anticipates the basic paradigm and "background model" of Kalman's system and control theory discussed in our earlier papers [30, 32]. These dreams connect the "Ace Cub dream family" with the "World Clock dream family" and their

⁸ But this primordial model contains the all-embracing maternal concept of Anima Mundi through the personification of the Holy Virgin, similar to the much later alchemical interpretations. Thus, because of the hypothetical completeness of the primordial image, the analogous scientific idea –according to Pauli – also demands the revitalized form of Anima Mundi as a possible "answer" to the Einstein-Podolsky-Rosen paradox.

interpretation can be realized by the application of the 4+1 background languages (psychological, religious, hermeneutical, physical and system-control-like) with the consideration of the FSC, the fine structure and its isomorphic crown symbolic. A unique characteristic of the Ace Club dream family is the fading-away and final disappearing of Anima, who is the Mother and the Holy Virgin, partly related to personal and historical events. The “chased Lady” primordial image in Pauli’s dreams is still related to the Demeter-Persephone (Ceres-Libera!) and the double Tamar mythologem (Tamar is both the foremother and daughter of the King David in §.197 of the Bahir) similarly to the double Sophia (Holy Mother-“Ecclesia”) or Shekinah patterns. This image or “pattern” is deeply rooted in the personal unconscious psychology of Pauli. His (“chased”) mother (anima) committed suicide in 1927 due to her husband’s extramarital affairs. “*For the shadow with me was projected onto my father for a long time.*” This personal relation was interpreted “collectively” by Pauli as “*the bond between the light anima and the shadow or Devil*” [20]. It was the “basis” for the archetypal constellation of some important synchronicities.⁹ In the second part of the paper primarily, we will discuss the possible hermeneutical and historical meaning of this important dream pattern.

5 The Synchronistic Constellation and the Dream Series

In the following we would like to show primarily the recognition marked in Pauli’s 14 coherent dream series. 13 dreams of the dream series (which has been analysed by many [18, 21]) were sent to Jung in his letter dated the 23rd of October, 1956. The first dream of the described dream series is dated back to the 15th of July 1954. The dream takes place in Sweden, in the secret laboratory of Gustafson, where a special isotope is being produced.¹⁰ The dream feeds upon the previous visit of Pauli to Lund in Sweden, where he had held a lecture at a spectroscopy conference on the centennial of Rydberg’s birth. (As we have demonstrated in detail in another paper, Rydberg already meant to Pauli the double of 36-32 pair, that is, one of the fundamentally important compositions of the number 137 [20].) Before the conference, as Pauli writes in his commentary on his dreams, he was able to observe a rare solar eclipse in Sweden, which he specifically refers to as the crown of the Sun. As we have already mentioned, in his great dream series, analysed by Jung, the initial dream is connected (symbolically) to a crown (the strange hat) and to the Sun: “*Encircling the head,*

⁹ Pauli was 27 years old when his mother committed suicide and he was “2x27”, in 1954, at the beginning of his discussed dream series!

¹⁰ (15.07.1954.) “*I am in Sweden, where Gustafson (professor of theoretical physics in Lund) is present. He says to me: “This is a secret laboratory in which a radioactive isotope has been isolated. Did you know anything about it?” I reply that I knew nothing about it.*”

the hat is round like the sun disc of a crown...and contains allusion to the mandala” (Jung [10]). In addition to the above, he refers to an important mythological background motif, namely the duplication of the spectrum lines, and he connects the isotope formation with the twin pair, Castor and Pollux [20]:

“Isotope separation is familiar to me as a symbol of the individuation process (doubling motif, cf. the two brothers Castor and Pollux, Christ is God and Man, and so on), which always appears when progress is being made in the development of consciousness and is connected with the “incarnation” of an archetype. The word “radioactive” is used in my dream language to mean the same as C. G. Jung’s term “synchronistic.” The characteristic of radioactivity is always temporary, provisional, an intermediate state, and not a stable final state”.

Here we can see with the coronation, the retro-cognition, the incarnation of Christ as God and Man into “*rex et dux*” according to the “notion of King” (through the twin myth) of St. Stephen [31, 33]. As we have mentioned before in papers, the last dream of the dream series is also related indirectly to a king and the crown, since the king visits him on the day of St. Stephen Protomartyr, on the 26th of December, 1955 [18, 20].

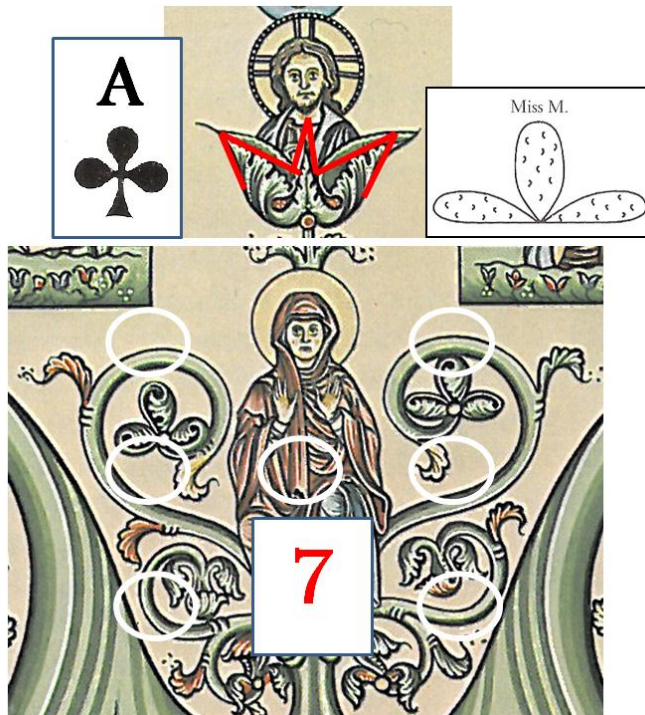


Figure 5

The illustration of the patterns for the “Ace club 7 card”, “Diamond card” and “Einstein” dreams

So indirectly, this is about a king, called St. Stephen, or “Holy Crown” in English, who congratulates Pauli that he can “see” in Danish and in English simultaneously.¹¹ Here Denmark, as Danai (“Dania”), in an archaic, playful composition, could well equal to the Greek language (it is the common name for the Greeks in Homer and other poets. Pauli of course knows very well the common phrase “*timeo danaos et dona ferentes*”). Whilst the world’s new Latin (lingua franca) is the “imperial” English, which, as a Germanic language, having absorbed the Latin into itself, might symbolize the Latin language. (Pauli in his dream comments identified the letter w and the English language with the Latin: “*English words of Latin origin...are written with w at the beginning.*”... “*The English language, incidentally, is itself a synthesis of Latin and German.*” [20]). So we are at the symbolic Latin-Greek crown of St. Stephen, the linguistic crown of which can be found in the Admonitions [33], where it is also the Latin-Greek crown of the Latin and Greek language and traditions. The Hebrew word obedience **גישות** (the main virtue of the 8th chapter) would mean the understanding of languages as well. Thus, obedience, as “translation and interpretation”, binds the flowers of the crown of the kingly interpreter:

“*Spiritus quidem inobedientiae dispergit flores coronae*”¹². “*Mores quidem meos, queos regali vides convenire dignitati, sine vinculo totius ambiguitatis sequere*”. “*Quis Grecus regeret Latinos Grecis moribus aut quis Latinus regeret Grecos Latinis moribus? Nullus.*”

Naturally, at the same time, it is an allusion as well to the Latin-Greek unified crown, i.e. the “Holy Crown” (which means naturally, in English the name of “Sanctus Stephanus”). Thus Pauli’s congratulations are similar to the closing sentence that Stephen addressed to his son: “*Ideirco constitudines sequere meas ut*

¹¹ (26.12.1955) “*There is an official announcement about the visit of a “king.” He actually appears and talks to me with great authority, saying “Professor Pauli, you have an apparatus that enables you to see both Danish and English!”*” (Jung’s spontaneous commentary: *Seeing double: Seeing into one another externally and internally. v = 5. A natural person, who, with perceptive consciousness gets caught in the extension w = 1 the One whole person, sees “double”-namely, the external form and also the inner “meaning” or breadth of meaning.*) Let us see the related dream too: (1.10.1954.) “*Bohr appears and explains to me that the difference between v and w corresponds to the difference between Danish and English. He says I should not just stick with Danish but should move on to English.*”.[20] (From Jung’s dream interpretations) “*With regard to the next dream – that of 1 October 1954 – I would like to add that V is the Roman 5 and that is German the double V = W 2 x 5 = 10, and 10 = 1, so that here the W (double V) is probably the One and the Whole. –Incidentally, I was most impressed by your forays into linguistics”. ... “The important thing about the dream of 26 December 1955 is the double vision. This is a distinctive characteristic of the human being who is at one with himself. He sees the inner and outer oppositeness, not just V = 5, which is a symbol of the natural person who, with his consciousness based on perception, becomes ensnared in the world of sense perception and its vividness. W (double V), by way of contrast, is the One, the whole person who, although himself not split, nevertheless perceives both the external sensory aspect of the world and also its hidden depths of meaning.”.[20]*

¹² Probably planned consciously in order to ensure the anagram (with a mirror-symmetry of the “original” meaning): “*Sed quis regit per Spiritum de obedientia (Is est) Coronans lofiel*”, i.e. (here) the Crown-maker and Crowning Yophiel.(see Yophiel in [3,4])

inter tuos habearis precipius et inter alienos laudabilis."¹³

We can see that the opening and closing dream of both the great dream series that contains 76 units and the dream series that contains 13 (14) units are related to the Holy Crown conception. Now we will briefly touch on the identity of the crown and the window as mandala symbols in Pauli's and Jung's dreams. In order that we examine the closing momentum of the "Danish and English" = "V and W" dream, quoted in footnote 10 along with Pauli's comments: "*I wake up excited and the word vindue immediately comes into my mind, so that I count it as part of the dream*".... "*One example is the word for the German (das) 'Fenster': (from the Latin fenestra): vindue (Danish) – window (English).*" We can see that Pauli identifies the "V/W" letter pair with the idea of the window; furthermore, with the idea of a bilingual window. After the first symbolic crown (a mandala according to Jung) dream in the great dream series, the substitution of the crown (hat) in the second dream is the window. Here the window appears in the same way as in Jung's famous dream of 1927 [35], where the name of the 137 mandala (i.e. as an eternal crown), introduced in part one of the paper, is the "window to eternity". So in the context of the Pauli dream, considering as well Jung's contribution, we can rightfully regard the letter pair as symbolizing the two languages, characterized by the window as a Greek-Latin (137) unified crown or mandala. Considering the dream's imperative to prefer the "w" and on the basis of Pauli's commentary on "das Fenster" and fenestra we may get the anagrams "der S. Stefan I" (if $w=10=1=I$, according to Jung's interpretation), or "Wer? Stefan!" It means both the king's name (in Latin) and the word "crown" (in Greek). It is the case that with the Hebrew interpretation of the name "W. Pauli" (if $w=10=י=I$), we can obtain the Hebrew letters "I P(F)AV L I" (י פאולִי) from which we can easily find the name *IVFIAL* (יִפְיֵאל) i.e. Jophiel, the crown angel. It seems that, according to the Eleasar's fragments, Jofiel would be the representation of the union of the two cherubs. It seems to be the hidden meaning of the Pauli's meeting with "King Stephen" in the role of Jofiel, who is representing both cherubs unifying in itself the two Names of God through the union of the two cherubs [16].¹⁴

¹³ We have shown in our earlier paper [31,33] that the ten chapters of the Royal Mirror of St Stephen correspond to the sephiroth tree of Cabbala. In the centre of the Sephiroth tree we can find the king as interpreter and hermeneutist in Caput VIII. Thus, on the basis of the Hebrew background, in equilibrium between of Latin and Greek, the obedience of the son of king can be understood as the King as Interpreter. In this hermeneutic circle, the "Latin" can as well be interpreted as a symbol of the Roman law, i.e. judgment and the military force. Similarly, the "Greek" can be interpreted as the symbol of vice counsel in "things of life". Consequently, taking into consideration of our analysis in the above paper, the "Latin" and "Greek" are appropriate symbols of the "Judgment" and "Kindness" of the Sephiroth structure, while "Hebrew" could be in this case the harmonizing center personified by the kingly interpreter through the obedience (מִשְׁמָע) which means in Hebrew the "understanding of the language" as well:

¹⁴ The v-w transformation symbol in the dream (Pauli "*should move onto English*" – w, from the Danish - v) would mean symbolically the doubling spectral lines. At the same time it can also be an allusion to the two cherubs systems. Namely, using Jung's interpretation $v=5$ where 5 can be concern as a quincunx which may represents the four cherubs (evangelists) with the God's presence in the

From another point of view, if the window – the mandala – is a Selbst identification according to Jung, the window in the Christian meaning is Jesus Christ himself, and so with the medieval Latin acronym IS XS. Thus, together with the Latin word “FENESTRA” mentioned by Pauli, we get as an anagram, the expression “IS STEFANVS REX”, taking into consideration the letter “V” as well. Therefore - in this circle of interpretation - this mystical window seems as if hiding the name of the king within itself, which obviously means crown, in a strong connection with the second dream of the dream series, where the window is the protagonist. Otherwise here it is about a train window. The train, as a symbol, occurs at one other place in the “great dream series”, namely in the Rubicon dream. In this (14th) dream the train, (“iron foot” – or Rome, in the Christian version of the famous dream interpretation of Daniel) with the window traversing the Rubicon, is the symbol of the Roman (obviously Latin and Greek) crown. On the train, Pauli is with his father, symbolically identified with gens Iulia (Dardania), or considering the whole dream, with the eastern and western gens Dardania [33]. We demonstrated exactly the same genealogical myth in the “king-notion” of St. Stephen.

Remark: Similarly to Pauli’s “vindua” dream the window-symbol plays central role in the hermeneutics of the Hebrew word and letter-symbolic of ZaHaB (zahav=gold) in the Bahir. Here the letter He (ה=5) is the symbol of the higher (3th) and lower (10th) feminine Shekinah in the Sephirothic system. Considering the “inverted” form of the “V and W” we may obtain letter shapes **Λ** and **Μ**, which can be recognized as the Latin-Greek A and M (in the apostolic names of the Holy Crown five letters of the A have the shape **Λ** – see e.g. Fig. 11 in Part I.). As we have seen above these two letters may correspond to the letter A (sign of the **Crown**!) and the number 7 from the “Ace club and seven card dream”, because the letter M consist of 7 points ∷:∷ in another similar (“diamond card”) dream of Pauli (sign of the **Mother** and **Mary**!) discussed later (see page 19 and 20 from the letter of Pauli to Jung–28/2/1936). However the V and W (as 2) letters are interpreted by Jung and Pauli as number 5 and 10(1), respectively. This could lead to the interpretation of the 10 Sephiroth and its unity (1) through the well-known representation of the Sephirothic system realized by the Hebrew word ZaHaB (7+5+2) as well (see the footnote 18 of this Part and page 11 of Part II.). As we discussed earlier, in the Hortus’ Incarnation picture (Fig.1 in Part II.) the 14 Davidian kings, with the golden crowns, constituted the symbol of ZaHaB (7+5+2). Consequently, the above double interpretation of the V and W letters, in the hermeneutical circle of Pauli’s dreams, may represent also the Sephirothic system in the form of a double golden *crown of the kingship*, belonging (in the meaning system of the Bahir) to the

centre. Thus w as a “mirror symmetry” can be considered in this hermeneutical circle as a natural symbol of the two cherubs systems with the masculine and feminine representations of God’s presence in the centers (e. g. in the form of the two names of the God). If we consider Pauli’s hidden hypothetical relationship to the linguist angel-priest Jofiel who is the Atarah, Crown (i. e. in Greek Stephanus) we may conclude that in his final dream his Ego and in the role of his Master (Self, Selbst) King Stephen are together representing the double faced crown-angel (symbol of the union of the two cherubs), the personification of the number archetype 137 and the Acausal Background Creative Intelligence, that concept was assumed by Pauli himself.

queenly bride (the Shekinah) of the Lord as King. At the same time, it is the Crown (A) of Mother or Mary (M) as well (corresponding to the thousand years old Hungarian tradition)! It hints at a symbolic unconscious reconstruction of the original Holy Crown containing the (later disappearing) Holy Mother enamel picture.

From another point of view, the Pauli imagination in the dream is also related to the number 6 and the equation $12=2\times 6$. The latter is the symbol of the seal of the World, the letter of ‘vav’ (which corresponds to the Latin “V” and whose number is 6) in the *Book of Bahir*. Consequently, the letters of V and W in the context of Hebrew can be considered as the letter V (ו) and its word VV (וו) or, in *Bahir*, VAV (וואו), i.e. as double V (ו). If we are spelling, according to its *Bahir* “definition” (using the Aleph), it has the number 137 ($137 = \text{וואו אלה וואו}$). It can be regarded as יי, יופיאל אלה יי, i.e. “Prince Jophiel” as the “Interpreter Archangel,” who is at the same time (as we have seen) the “Atarah” (in Greek, *Stephanos*). Thus, King Stephen also congratulates Pauli on being in the interpreter role of Jophiel as well.¹⁵ So in exactly the same way as we saw in the king concept of St. Stephen [37], in the complete semantic system of the dream series there appears the “House of Joseph” mythical genealogy of the ten lost tribes from the “House of Joseph”, staying in a far-away land (see the Rubicon dream) by means of their father (whose other “Jewish” name is Joseph) [30].

So the dream series written of in the letter starts indirectly with the number 137, with the solar eclipse and the crown of the Sun, and according to our interpretation above, it finishes with the Latin-Greek interpreting crown, with multiple 137 compositions.

6 The “Constellation” of the “Historical” Meaning

The 14th dream, but actually the “opening” dream of Pauli’s dream series, is known from a letter written to Fierz. He dreamed this mysterious dream on the 18th of April, 1954, after returning from the United States, where he met Einstein for the last time. Einstein died exactly one year later on the 18th of April, 1955. This year is certainly the crown of time¹⁶ in the creations of St. Stephen (whose name means crown), and St. Stephen himself is the personification of the year.

¹⁵ In very interesting study, written in a letter to von Franz (about his dreams and active imaginings), Pauli identified himself and the essence of his life symbolically with King David, using in his explanation the double stars (shields) of David. The number of geometrical elements in the star of David is 36 (18 lines, 12 points and 6 triangles with a hexagonal center of unity). This imagination of Pauli is related to the number 6 and number $12=2\times 6$. [18]

¹⁶ The “year” in the *Bahir* (§.72) is as the last Sefhira, the Kingdom or the Crown (Atarah). The World clock dream is compared by Jung with the Church year calendar vision of Guillaume de Digulleville [10]. This one (year) in the *Bahir*’s Biblical interpretation is also the thousand (Aleph in Hebrew) years, so the one year and the thousand years can be naturally interpreted for the “identification” of the hidden meaning of the World clock vision’s symbolism as well.

Because of its significance, we have to emphasize again that the Levite (in Hebrew Levi; LVI (לוי) can be interpreted as a 36×10 composition), St. Stephen Protomartyr (Levita Stephanus [31]) represents the 360th day of the archaic calculated year, so in addition to the “day” of Christ, he can be considered as the representative of the World clock, the circle, the 36 deans and generally the lord of time. This role of his can be established in detail in the analysis of his picture on the Pala d’oro.

A further curiosity of the circumstances of the dream is that Pauli considered himself the crown prince to Einstein’s “kingdom”; he was unconsciously preparing himself to the “succession” of the throne and the crown, anticipating his death one year later.

“Einsteins Tod hat mich auch persönlich erreicht. Ein mir so wohlgesinnter, väterlicher Freund ist nicht mehr. Nie werde ich die Rede vergessen, die er 1945 in Princeton über mich und für mich gehalten, nachdem ich den Nobel-Preis bekommen hatte. Es war wie ein König, der abdankt und mich als seine Art “Wahl-Sohn” zum Nachfolger einsetzt. Leider existieren keine Aufzeichnungen über diese Rede Einsteins (sie war improvisiert und ein Manuskript existiert auch nicht). Letter from Pauli to Max Born, April 24, 1955.”[23]

The “crown prince” is the same in German as well (Kroneprinz). At the same time, in the United States (in Fort Knox), which probably got its name indirectly from St. Stephen’s son Emericus, through the name Americus, there was at that time the real crown, i.e. the Holy Crown of Hungary, namely the crown indicated for Emeric by the king St. Stephen (Corona ‘E(A)merica”). So the “succession” of Einstein’s intellectual crown, indirectly and synchronistically touches upon Emeric (“Americ”!) and the Holy Crown of St Stephen.

The antecedents of the dream are related to the Kepler–Fludd conflict, the famous study Pauli had written about years before [16]. But the dream itself (after the $2 \times 6 = 12$ “number interpretation” which can be related to the important “v/w” dream image discussed above) is directly based on his meditation about Fludd and his radiant Sun child:

“In the 17th century Fludd was archaic, unoriginal, a fossil, and everything seemed to be against him. The situation was dissociative which is also evident in Boehme’s pictures ... (and) ... in More’s dream the split of 12 into 2×6 (!). This split makes the quaternary impossible. The natural division of 12 would have been into 3×4 , this also corresponding to the old division of the zodiac (about which Fludd also never ceases to speak). But the time was not ripe for a quaternary view of the world, and the dark half receded back into the unconscious. We are the first ones to again begin reading under the opaque blue coloring of the covering the features of a writing which again brings us closer to Fludd’s manner of thinking, according to which the “child of the sun” can only arise in the middle sphere”.
[16]

This Sun boy, in this context, is practically identical with the child of the Sun woman from the Revelations, which is the central topic of Jung's famous book, the *Antwort auf Hiob* (1952). The book was greeted with pleasure by Pauli. This radiance of the Sun and the appearance of the Sun woman as the Virgin Mary and Tamar can be connected to his dreams in the 1930s, namely to the Ace of Clubs and the 7-card dream series, among others. Because the dream is hardly understandable by itself, we have to briefly review the text of these dreams and Pauli's and Jung's commentaries on them:

As we have mentioned, Pauli, to the end of his life, was fascinated with the Ace of Clubs and the seven-card dream and in general with the **clover archetype**, which was, in his opinion, the background of his dream, which was followed by other similar dreams. It is also perhaps an interesting synchronicity that the **36**-year-old Pauli reflected in detail on his Ace of Clubs and Seven-card dream motif dreamt at the age of **32**. From the letter of Pauli to Jung (Princeton 28-02-36):

"I was personally amazed to learn how many parallels to the later development are already to be found in these early dreams. And yet I read it as if it mentioned, I would like to mention just one point where I had the feeling that your dream interpretation was not entirely accurate. (As you can see, I still won't be "fobbed off" with just anything.) I am referring to the interpretation of the seven and the ace of clubs in lines 13 and 16. These two dreams have both a retrospective and a futural meaning. In my seventh year, my sister was born. So the 7 is an indication of the birth of the anima. (This appeared again in later dreams.) I can also offer further evidence of the connection for me between the anima and number 7." [20]

It is the "Seven of Diamonds Card" dream: *"In a much later dream, the card with the 7 of diamonds came up, and it looked like this:*

```

*           *
*   *   *
*           *

```

*And then the "wise man" in the dream explained to me that this also meant **M** and referred to Mother and Mary. And he said that the step from the personified Mary to the 7 of diamonds went much further than Catholicism (which fits in beautifully with your interpretation of "expelling" as excommunication). N.B. The diamond card is also a reference to **the color of the sun.**"*[20] Pauli continued his interpretation with the next summary: *"As for the ace of clubs, I am sure you are correct in relating it to the shape of the cross, but for me there does not seem to be such a direct connection to the Christian concept of God as there is for you. In my view, this Ace of Clubs, which comes before the seven, is thus the "Origin of the birth of the anima," an indication of a **Keplerian archetype of power**, which appears much later as "Diocletian," "Dalton" or "the duke who chases the*

maid". (By the way: this interpretation also fits in with the retrospective meaning of the dream – and with the dark color of the club.)¹⁷ [20]

As we have seen, “The Diamond card dream” (1932-1936), to be more exact the 7 card, which contains the 7 diamonds, emphasizes the letter **M**, and refers to the Latin Mater and Maria (Mother and Mary) words. Considering that in Latin M=1000, which in Hebrew is Aleph (elef), in the context of the *Bahir* (where Aleph means 3 letters), this dream’s structure is perfectly isomorphic with the “Ace and seven card” dream. It is interesting also that symbolically the number 7 represents Arcus (pluvius) as the Latin name of rainbow (see his rainbow dream) with its seven colors. Thus, the **M** from 7 diamonds is a connotation for the name “**M**-arcus”, on whose day (25th April, St. Mark’s day) Pauli was born! Since the shape of the M here is equivalent with the capital H and the card 7 at the same time, it is an allusion to A (as the sign of As), and we can get the Latin anagram “*Thamar Mariae*”. The tree is a reference to the meaning of the name *Tamar* (the *date palm*), to the Tree of Life. Therefore, in the given context it is easy to think of Tamar and David together. It is “*verhüllte Frau*” (the veiled woman) in Pauli’s “Sun woman” dreams; “*Thamar verhüllte sich*” in the German Bible. In the first of Pauli’s dreams, the figure of Tamar (without the veil) perfectly illustrates the vision of the Sun Woman who is about to give birth in the Book of Revelations. The word diamond in Latin is *ADAMAS* and contains within itself the words Adam and As (Ace both in Latin and German). Thus the Ace of Clubs, and the cross and the Ace together, could refer to the ancestry of Adam, and the incarnation as well as the delineation process, together with the number 137, which is the number of the “Double Delineation” (from Adam to Christ) according to St. Matthew and St. Luke.

7 The Retro-Cognition of the “Historical” Meaning

It is apparent that it is about the symbolic vision of the Sun woman [33], which with the description of the attack of the red dragon, or the Leviathan (the Ace of clubs/ 7 card dream and its illustration in Jung’s book “Psychology and Alchemy” [10]) represents the four aggravated cases of the persecution of the Church – personified by Tamar too – or the persecution of the Sun woman. The ancient picture is obviously the incarnation as redemption and the deliverance; the second is the persecution of the Church by Diocletian, which finishes with the deliverance

¹⁷ As we can see, the interpretation of Pauli’s dream can be strongly supported by the further dreams which are the continuation or transformation of the Ace of Clubs dream. We could surmise (and taking into consideration his letter from 1939) that the picking of the Leviathan picture and its pairing to the Ace club dream by Jung and Jolanda (Jolán) Jacobi in 1942, is the result of a long-run synchronicity process, in which the dream from 1932 clearly contains the obvious reference to a picture of Hortus deliciarum about the Leviathan. The number 32 and 36 also have a major role in the picture. Therefore, we can also identify a retro-, a pre- and a general cognitive background - like control process, in the exactly 10-year-old synchronistic phenomenon (see in detail [34]).

of the Church; and the third is related through Danton to the persecution of the Church by the 1789 French Revolution. This last one – the date as well – was accurately predicted by Nostradamus in his letter to the king of France. The archetypal and symbolic background of the prophecy was analyzed in detail by Jung in his book titled “Aion” (1950!) [13]. The remaining second one about the persecution of the Church or the virgin by the prince cannot be localized in time or space. We would like to show that this dream of Pauli from around 1934 is completed by the dream from the 18th of April, 1954 through localizing in time and in space this allusion of the persecution of the Catholic Church, in which truly it seemed like a prince was chasing the Virgin Mother, both concretely and symbolically. So let us look through the actual text of the dream:

“(April 18.) Dream: I see an English text in front of me. (I could no longer recall its words when I awoke). Beneath this text there are, however, other words to which special arrows on the paper point. (These arrows were probably supposed to draw my attention away from the English text to that second text). These other words seem “secret” to me. They say: “Today the sun will demonstrate itself to be as effective as it was during Kepler’s time.” Now there is a man with a superior air standing next to me, an “old sage”, a “master”. I ask him if these secret words are those of Newton. But the master answers me with a clear, firm voice: “They are those of Chancellor (Kanzler) Regiomontanus!” Then I awaken. (NB. By “chancellor” I understood in any case a government official.) When I awaken Müller of Königsberg comes to my mind as Regiomontanus. He was surely close to being Newton’s contemporary. I certainly had to find out what he wrote. When dreaming I frequently have such ‘cryptomnesias’.” [16]

There are two languages appearing in the dream, English and an unidentified language consisting of secret words, which we would like to connect with Danish, based on the two dreams of the dream series concerned (in the context of the “English”, the arrows maybe, could refer to the conquering Danish Vikings. This is personified by the “intellectual conquest” of the Danish Bohr in “England”). The dream itself – after the antecedents – refers to the Fludd–Kepler conflict, which in addition to the English obviously represents not the Danish but the German language. Here Latin and Greek, which were well known by both of the authors, appear as a similar language pair. The main issue of the dream is the efficacy of the radiance of the Sun. This might be the precognition of the experience of the solar eclipse in Sweden in June. Based on the solar eclipse, the dream from 1954 and the Sun dreams of the dream series before that, and considering the antecedents and the dreams of the actual dream series, the motif of the efficacy of the Sun’s radiance in the dream is connected to the Virgin Mary as the Sun woman, and to the crown in general¹⁸. Therefore, considering the previous

¹⁸ As we have discussed above in the *Bahir* the mystical linguistic symbol of ZaHab (“Gold” in Hebrew) refers to the Shekinah (the crowned daughter of the king), the ten (3+7) Sephiroth and also indirectly the sun-moon (masculine-feminine) crown symbolism. We have seen that this motif in the *Hortus* incarnation picture is related unambiguously to the Davidian kingship and the crown in the

aspects and also according to the Sun boy associations of Fludd, it is about the crown of St. Stephen and its lost Virgin Mary image (with the Virgin Mary representing the Sun woman - see diamond gold card, i.e. the letter M, Mary — Mother - sun radiance - enamel-card). The disappearance of the enamel picture could be set to the 1619-22 period, when the crown was really in the possession of a prince, who – being a protestant – persecuted the Catholic Church and evidently did not like the Virgin Mary cult. This period of time matches the time period of the highest pitch of the Kepler-Fludd in 1622.¹⁹

The “Regiomontanus dream”, one year before the death of Einstein (after Pauli’s arrival from the USA), synchronistically we may relate to the “Einstein dream” dreamt by Pauli on the 32nd day after the death of Einstein²⁰. In this dream the appearing threefold picture is connected by Pauli to the Ace club seven card dream. As we saw earlier, it is isomorphic to the dream of the seven diamonds constructing a letter M, because in the “Einstein dream”, above the screen is the anima, as Miss M with an allusion to the number seven. This dream symbolizes the radiance of the Sun, while the letter M is referencing the Mother and Virgin Mary, who in the dream’s associations of Pauli is the subject of chasing. In the “Einstein dream” the “anima M” fades away and finally disappears, similarly to the weakening radiance of the sun in the “Regiomontanus dream”. Considering the symbolic play of “Einstein as king and Pauli as crown prince” (and at this time, the American presence of the Holy Crown (in Fort Knox) as well as the number 32’s allusion to the 10th Sefhira, i.e. the Atara-crown in the Bahir in §.134), the “Einstein dream” connects and confirms the powerful relationship between the above dreams on the basis of the central hidden meaning of the dreams upon the disappearing radiance of the Sun and the Sun woman, i.e. the Holy Virgin.

Petrus (Péter) Révay, the lord lieutenant of Turoc county, was one of the Hungarian keepers of the crown elected in 1608, who, despite being relatively old

context of the 137 structure. Jung also deals with the symbol of ZaHaB (זאהב) from the *Bahir* and relates it to the Sun-woman, the sun-moon child and the masculine-feminine Sephirothic double crown as well [11]. Thus, we can see that Pauli’s sun dream images are in full accordance with this symbolism of the *Bahir* (and the *Hortus* picture), whose significance was also recognised by Jung. Furthermore, this “Gold” (ZahaB), according to Jung’s interpretation on Pauli’s 18-20. initial dreams, is also related to the Demeter-Persephone (Ceres-Libera!) double Mother mythologem in the Eleusis mystery (together with the “images” of the Sun-lady and Tamar).

¹⁹ Kepler’s “harmonic theory” was published in 1619, as “*Harmonices Mundi*” (“Harmony of the World”) Kepler was convinced “*that the geometrical things have provided the Creator with the model for decorating the whole world.*” In *Harmony*, he attempted to explain the proportions of the natural world; in fact, soon after publishing *Harmonices Mundi*, Kepler was “engaged” in a wild and deep dispute with Robert Fludd, who had recently published his own harmonic theory. (see in detail M. Caspar: *Johannes Kepler*, London, 1959 and [12])

²⁰ “*Once again I am in the laboratory and this time Einstein is conducting the experiments. All they consist of is intercepting rays on a screen (according to a clover archetype). Above the screen is the “unknown woman” (this time resembling a certain Miss M.) On the screen there now appears an optical diffraction pattern, consisting of one central and two subsidiary maxima...The picture resembles a leaf. Marks now appear on the “leaves,” then the woman fades away and finally disappears...*” [20] The clover drawn by Pauli, see in Fig. 5.

and very sick, held his office until 1622, till the peace of Nikolsburg, and then died next to the crown when he was 54. He published the first book about the Hungarian Holy Crown in 1613. His invaluable work makes him a “crown witness” from multiple perspectives. We know from him that in 1613, instead of the picture of Emperor Michael Doukas, there was a picture of the Holy Mother.

“On the band on the front there is the picture of our Savior holding an apple, and on the opposite side, the picture of the divine Holy Mother.” (Révay, *Commentarius*, 77): *“In ipsa vero circumferentia fronte recta, imago Salvatoris nostri pomum tenentis; ex adverso Divae Mat-ris Virginis.”*²¹ (see the reconstruction of the enamel picture in Fig. 6, in part one of the paper).

Révay’s description of the crown, despite the several minute inaccuracies about details (like about the apple held in the hand) can be considered correct (He had a rank of master in science). If we accept his observations, then after 1622, this brutal mutilation of the Holy Mother picture of the Crown could only have happened under the Habsburg kings. We can exclude among the perpetrators the zealous Catholic Habsburg kings, who carried the name Maria among their names and who deeply respected the Holy Mother. So accepting Révay’s almost certainly authentic observation, the mutilation of the Crown could only have happened between 1619 and 1622. So at the time of the Kepler–Fludd “duel”.

We would like to point out that in this specific hermeneutical circle we do not wish to claim any person responsible (causally) for the mutilation of the Crown and we do not infer any value judgment upon the catholic-protestant conflicts at that time in Hungary; we would only like to show that Pauli’s dream series and the “symbolically modified (distorted)” retro-cognitions of the *synchronicities* related to it unambiguously indicate this time period for the removal of the Sun woman, i.e. the picture of the Virgin Mother from the Crown, or to use Pauli’s expression, to diminish the efficacy of the Sun’s radiance.

In this dream context, the sun’s radiance, the sun-child (with the sun woman), is a natural allusion to the Anima Mundi in natural philosophy, alchemy and “early physics” as well. According to Pauli, the concept of the Anima Mundi disappeared during this time, symbolically even at the peak of the Fludd-Kepler debate, i.e. around 1620-1622:

“The physically unique individual (in the quantum physics) is no longer separable from the observer – and for this reason it goes through the meshes of the net of physics. The individual case is occasio and not causa. I am inclined to see in this occasion which includes within itself the observer and the selection of the experimental procedure which he has hit upon – a revenue of the anima mundi which was pushed aside in the seventeenth century (naturally “in an altered

²¹ Révay P.: *De Sacrae Coronae regni Hungariae ortu, virtute, victoria, fortuna, annos ultra DC clarissimae brevis commentarius*, Augsburg, 1613. *Commentarius Petri de Rewa Comitis Comitatus de Turóc, de Sacra Regni Hungariae Corona ad nostra usque tempora continuatus*, Kolozsvár, 1735. (as Révay, *Commentarius*.)

form"). *La donna e mobile – so are the anima mundi and the occasion. Here something has remained open which previously appeared to be closed, and it is my hope that new concepts, which are uniformly simultaneously physical and "psychological" (concerning the undetached observer), can force themselves through this gap in place of "parallelism."* (Letter to Fierz 1951 [16])

Thus, we can see, on the basis of Pauli's unconscious "undetached observation" in the Regiomontanus dream and his related dream series, that there is a strong synchronicity between the disappearing all-embracing "maternal concept" of Anima Mundi from the contemporary "physics" and the disappearing enamel picture of God's Mother from the Holy Crown. The recognition of this coincidence can be 'explained' by his deep unconscious involvement in the Holy Crown's 137 structure and his permanent dream's motif with the chased and disappearing Anima. Similarly to the recognition of the primordial concept of the FSC related to the Holy Crown and the *Hortus* Incarnation's picture, in the discussed dream series, there is a joint presence of the religious, physical, psychological and hermeneutical aspect of the disappearing Anima as well²².

Incidentally, Gabriel Bethlen (1580-1629) was elected to the throne of Transylvania precisely on the 23rd of October (!) in 1613. He occupied Pressburg (Pozsony) and got hold of the Crown on the 15th of October in 1619; he returned it in the summer of 1622 to the emperor and Hungarian king Ferdinand II, in accordance with the Peace of Nikolsburg. At that time, Révay had been dead for more than a month. Bethlen was elected as a rival king on the 25th of August 1620, but the coronation never happened. Therefore the mysterious statement of Regiomontanus in the dream – "*Today the sun will demonstrate itself to be as effective as it was during Kepler's time*" – may refer to the Crown's Virgin Mary, or Sun woman, picture. The picture (with mirror-symmetrical time-projection) was at its rightful place at the time of Kepler (in our case before 1619-1622), and

²² Concerning the meaning of the "chased and disappearing Anima" in the "Ace club seven card" dream series (which can be identified in the "World Clock dream family" as well, with the promise of her return in solstice time!), we may use the "4+1" background languages proposed by Pauli (see [20,29,31]). The psychological interpretation, related symbolically to the Holy Virgin, is well-known through Jung's analysis together with Pauli's important commentaries, while the religious interpretation is self-evidently related to the chased Holy Virgin as the personification of the Catholic Church. The image of the chased Holy Mother fits to the chased Hungary motif as well, because (according to the thousand years old Hungarian tradition) Hungary is the eternal kingdom of the Holy Mother as "Regina" (After the liberation of Hungary from the Turks, at the end of 17th century, king of Hungary Leopold I reconfirmed the offer of the Holy Crown by St Stephen to the Holy Mother). The physical background language may express the "chased and slowly disappearing "maternal concept" of the Anima Mundi from contemporary physics or natural philosophy, while the interpretation of the aesthetical (hermeneutical) category is the chased and finally disappearing enamel picture of the Holy Virgin from the Holy Crown, which is symbolically isomorphic (beside the *Hortus* Incarnation picture) with the pattern of the dream series. The neutral, number-archetypal interpretation through the quaternary "system symbolism," as a final meaning, may express the unity of the four orientation functions of the consciousness in the central "unprejudiced, objective" transcendent function personified also symbolically by the Holy Virgin with the four cherubs (see e.g. pictures of Hortus' Fols. 150r, 225v and the Holy Mother mandorla on the Coronation Robe (Casula)).

Johannes “*Regiomontanus*”, together with Johannes “*Chancellor*” (*Vitéz*) of Hungary, could have seen it at the court of King Matthias, where he worked and wrote important works for four years. However, it was not there at the time of Newton, i.e. from the second part of the 17th century. Kepler could also have seen it in the treasury of Emperor Rudolph in Prague and at the coronation of the Hungarian king and future emperor, Matthias II (who died on the 21st of March 1619) at Pressburg (Pozsony, now Bratislava) on November 18, 1608.

Even the “improbable” character of “Chancellor (and) Regiomontanus” (as an unconscious “data-compression”) strengthens our hypothesis above, because between 1467 and 1471, in one of the most productive times of his life, he worked at (Pressburg) Pozsony (!), Esztergom and at the court of King Matthias at Buda.²³ He came there at the calling of Chancellor (“*Kanzler*”!) Johannes (János) Vitéz, 1408-1472, archbishop), who took - a couple years earlier in 1463 - the returned crown of St. Stephen from the Roman (German) emperor, after the negotiations handled by him. The crest of Matthias was a raven holding a golden ring in his beak. His dynastic name, Corvinus, means raven, or black bird as well. He governed for exactly 32 years, and in 1485 he conquered Vienna, where he died unexpectedly in 1490. (Obviously Pauli could have known this from his school books. Pauli also must have known that 900 years before his World clock vision dream, in 1031-32, St. Stephen conquered the city of Vienna.). Thus, based on the raven of King Matthias, its golden ring and the number 32, and through the character of Regiomontanus, the World clock dream appears from 1932. But we must also know that one of the leaders of the army conquering Vienna was the future Hungarian king, Samuel (Aba). According to later traditions, on Abas’s coat of arms there is a black eagle, sometimes with a crown on his shoulder or on his head, sometimes with a golden ring in his beak. In this way the World clock dream transforms to a real world clock, since the time period from the birth of St. Stephen till the Hungarian October Revolution in 1956 – the day on which Pauli wrote down his dream series – encompasses almost 1000 years. That can be justified by the fact that the centre of the hidden symbolism of the revolution in 1956 is the dream of the World clock. The base of the civil rebels was at the Corvin cinema, where the first color film was played in Budapest. This is a separate, almost round-shaped building. With the color film, it refers to the (three or) four primary colors, and with its shape to the disc. It was named after Matthias Corvinus, so it carries the black bird with the golden ring in his beak in its symbolism. Near the cinema, on Baross street, in a direct line from the cinema, there is the Square of the 32, which was named after the 32nd cavalry regiment of the Hungarian queen Maria Theresa. Between the Corvin Cinema and Square of the 32, exactly in the middle, from Joseph boulevard starts Paul Street, “*via*

²³ In 1467, Regiomontanus left Rome to work for Chancellor (Kanzler) of the King Matthias Johannes (János) Vitéz, archbishop of Esztergom, at Pozsony, and later at the court of Matthias Corvinus of Hungary. There he calculated extensive astronomical tables and built astronomical instruments. (*Tabulae directionum profectionumque in nativitatibus multum utiles*). *The zodiac decoration of his room is still visible at Esztergom.*

Pauli” in Latin (with the Street of Sun in front!). This short street connects Maria (Mary) Street with Joseph Boulevard, symbolizing by itself – in the specific hermeneutical circle – the complete 137 incarnation. (The military centre was about 50 meters away from Corvin cinema, on the corner of József Boulevard and Üllői Street in the Kilian Barracks.) Thus the black bird with the golden ring, along with the number 32, dates back to St. Stephen and his “sororius” (nephew?), the future king Samuel and the third person of his kingdom, and through the two Kings Matthias goes till the Hungarian revolution in 1956, as a real world calendar, which is fulfilled by Pauli’s letter about his dream series dated October 23, 1956. As we have seen, in the letter the spectral lines, the isotope dating – therefore indirectly the number 137, appears for Pauli in a mythological background language as Castor and Pollux. Nothing suits better to the contemporary and historical Hungary than the prophecy of Nostradamus about the country, where he describes the Hungarians with the special and unique archetypical picture of the conflicting Castor and Pollux (which is a pre-cognition and retro-cognition at the same time, of a primordial image):

“Par vie et mort changé regne d’Ongrie, La loy fera plus aspre que feruice: En grand cité urlemens plains et crys, Castor et Polux ennemis dans la lyce.” (II.90.)²⁴

We have seen that Jung illustrates the World clock vision with a twin black eagle pair and a dual crown, and the number of the footnote (of the dream) in the English edition is 137. The *rex* and the *dux* sovereign pair was instituted in the kingdom by St. Stephen, where he intended his son to be the king and Samuel Aba to be the dux. Here we have the eternal and temporal sovereign pair matching exactly to the Jungian interpretation. But St. Emeric died unexpectedly in 1031, so the sovereign pair was inherited by St. Stephen’s other nephew, the Venetian Peter Orseolo, who originated from the Byzantine royal house on his father’s side. After the death of the Holy King, they (Samuel Aba and Orseolo) truly represented the formula of Nostradamus; they stood as mortal enemies against each other, like Castor and Pollux, which led to the violent death of both. The allegorical picture of the sovereign pair was depicted with the Tamaric messianic twin pair by St. Stephen both on the Casula and the Crown, which – as we wrote in our earlier articles – matches to the Castor and Pollux mythologem and, as the unity of the twin “Lulav” symbolism, carries the number 137 in itself. We can see that the World clock vision (in the context of Pauli’s later dreams, and especially of the dream series written down in 1956, with a review of the Hungarian history, and with special regard to the significance of the Holy Crown and the Coronation Robe) has made the number 137 into a “world number”. In the World clock dream series, first appear four boys with a ring, to whom an unknown woman – the

²⁴ It is almost certain that Pauli did not know the above original version (or its translation) from Nostradamus concerning the “fate of Hungary”. It seems to be an astonishing example of the *conjunctio* (the most important purpose of Pauli’s intellectual and spiritual endeavour) of the pre-cognition and retro-cognition in the synchronistical phenomena.

anima – shows up as the governess of time, referring to the solstice. (According to tradition, the solstice (the turn of the Sun) is the birthday of Christ, the 25th of December, after which comes St. Stephen Protomartyr’s day). In the following dream, from the egg in the middle of the ring, a black eagle or a black bird comes up, then the ring turns to a golden ring and the black bird takes it in its beak. The next dream is the World clock dream itself, where the four “*kabirs*” match to four children, the black bird to the egg, the golden ring to the gray ring, the 32 division and the 36 spatial order to the calendar. This masculine–feminine duality exactly matches to the two cherub system that we can only find on the Coronation Robe, the *Hortus* incarnation picture and on the Venetian Pala d’Oro as the representation of the two cherubs of the Ark of the Covenant and the Temple of Solomon, by the hierogamy of whom the new Messiah king is born. Thus, as we have shown, not only are the Holy Crown’s structure and semantic system isomorphic with the World clock dream, but even more, the Coronation Robe, which bears the 32-structure in focus, is as well. From the perspective of the Coronation Robe, its wearer is the black eagle bird, and the golden ring obviously equals to the golden crown.

Returning to Regiomontanus, it is worth emphasizing again the contraction of his name with the word *Kanzler*, which refers, as a data compression, to his bishop partner, his inviter, (the Chancellor) Johannes Vitéz, according to us. From the onomastic point of view, we have three “Johns”, (Johannes), since in addition to the chancellor and Regiomontanus himself, Kepler is a “John” as well. Just as Regiomontanus knew the Hungarian king Matthias I, Kepler knew the Hungarian king Matthias II, since he almost surely attended his coronation in Pressburg (Pozsony). He was, almost surely, the last Hungarian king who was crowned with the crown that had had the Virgin Mary on it. His successor, Ferdinand II, got back the crown from Gabriel Bethlen in 1622, at the time of the height of the Kepler–Fludd conflict, when almost certainly the crown no longer had the Sun woman, the Virgin Mary, on it. Thus, the radiance of the Sun could not be as effective as it was at the time of Regiomontanus. The dream is the mirror–symmetrical equivalent of that situation. The onomastic potential hides another curiosity in itself. The third character named in the dream is Isaac Newton (as the “Messiah” of new natural philosophy). Isaac, as the son of Abraham, links to Christ, while Abraham matches to the Eternal Father in the famous allegory of St. Paul. His mother Sarah is Libera, the symbol of the Christian Church, which was persecuted until Constantine the Great. If Isaac is Christ, then the unifying name “John”, name of Regiomontanus and Kepler, refers to John the Baptist, reminding us of the couple of God as the Prophet Elias. In the other royal mythologem of St. Stephen, as we showed years ago, the Christ–Elias (John the Baptist) pair represented the dignity of the Holy Roman rex et dux [31, 33]. Returning to the 1930s, to the Sun woman-, Maria-, Tamar-dream, the virgin persecuted by the prince (in addition to the persecution by Diocletian and Danton) synchronistically refers to the successful persecution of the Sun woman picture on the Holy Crown, sharply marking in the dream of April 1954 the date of the “successful

persecution²⁵ (1619-1622). The other curiosity of the dream series is the Wallenstein dream²⁶, which, in addition to the Regiomontanus dream dated to Kepler, refers to the same period of time in that dream series. (Next to Vienna, the armies of Wallenstein as the “general of the Hungarian king” and Gabriel Bethlen – the elected, never crowned Hungarian “rival king”, who was preparing for the coronation – met in 1620; but in the end, the battle did not happen.)

Conclusions

The obsession of Pauli with the fine structure constant and the number 137 has been well known for a long time. In our articles published in 2007 and 2008, we posed first the central significance of the archetype of the number 137 in the common (“conscious and mainly unconscious”) “thinking” and cooperation of Pauli and Jung [30]. This hypothesis of ours was confirmed by several authors in 2009 and 2010 (see e.g. [4, 21]). We could see that the archetype of the fine structure constant and the number archetype 137 – as a background cognitive process – “set off” from the court of St. Stephen primarily with the depiction and semantic system of the Holy Crown and the Royal Casula. The Holy Crown, the crown of the Virgin Mother (on the basis of King Stephen’s double offering to “Regina Caeli”) is the symbol of the Free Church (Libera), universal human rights, in a broadened meaning, and national freedom. This freedom concept, which is related tidily to the “founding events of liberation” and to the “free hermeneutics of the original sacral texts”, was formulated by Ricoeur with the freedom concept of the ancient historical Israel and with its Christian development [24], which in the Kabbalistic meaning obviously matches the concept of the feminine Shekhinah (the manifestation of the Ten Sephiroth at the Reed Sea) and the later very important concept of Anima Mundy in the Alchemy. In the “*world-clock-like*” retro-cognitions Pauli accompanies roughly the “symbolical war of independence of the crown” through the fight for the freedom of Europe and more concretely Hungary. This touches on the battles against the early German hegemony, and later the fights against the Turks for the protection of Europe, primarily from the perspective of Christianity and the Catholic Church. It is well known that, at the same time, the Sun woman was the symbol for defeating the Turks, in the way that she was trampling with her foot on the symbol of the Ottoman Empire, the half moon. (From the subjective perspective of the young Catholic Pauli from the Austro-Hungarian Monarchy, the vassal prince, called Gabriel the Turk by his contemporaries, could be seen as the symbol of the Ottoman conquest). The images of the Holy Virgin can be seen on the military

²⁵ A strong additional synchronicity can be identified according to the above-discussed dream pattern, “the *duke* (Herzog) who chases the *maid*” related to the “Ace club seven card” dream (which was interpreted by us as a dream image of the Holy Crown). It corresponds to the “fact” that the chased maid’s image – i.e. the *Holy Virgin*’s enamel picture – is substituted “aggressively” on the Holy Crown by the “*duke*”, i.e. (Michael) *Doukas*’s picture where the emperor’s name corresponds to the Latin dux and the English *duke*.

²⁶ (2.09.1954.) “A voice says: “At the place where Wallenstein atoned for his sins with his death, a new religion shall arise.””[23]

flags of the Hungarian Revolution and the war of independence in 1848/49 as well. These wars of independence and for the protection of Europe finished with the Hungarian Revolution in 1956, according to Pauli's "unconscious" recognition. In the symbolical background of the historical and cognitive process, the event considered the most tragic is the removal of the Eternal Virgin, who personifies freedom (as "Libera"), from the Holy Crown. (Pauli "recognizes" this in the opening dream of the discussed dream series, while for the "recognition" of the original "complete crown" the creator king himself congratulates Pauli in the closing dream.) The main message of dream series (which occurred a couple years after the proclamation of the dogma *Assumptio Beatae Virginis* of Pius XII, greeted enthusiastically by Jung) is the threat of the strengthening new spiritual and intellectual barbarity and the slowly building new spiritual slavery—felt by both of the geniuses – understood as an important call for the guard of the "Eternal Virgin Mother" (and her "crown of 137", together with Pauli's imperative on the "revitalization" of "physical concept" for the Anima Mundi). Where, according to Jung, the Holy Virgin symbolically is the unbiased, unprejudiced, objective, chaste human sense, where God and the "eternal meaning" (in our case through the mediumship of the number 137) can truly be reborn.

References

- [1] Ameisenowa, Z.: *Animal-headed Gods, Evangelists, Saints and Righteous Men*. Warburg Institute, London, 1948, pp. 21-44
- [2] *The Book Bahir*. (ed. A. Kaplan) Samuel Weiser, INC., York Beach, Maine, 1989
- [3] Dan, J.: 'The Emergence of Mystical Prayer', *Studies in Jewish Mysticism, Proceedings of Regional Conferences held at the University of California, Los Angeles, and McGill University*, eds. Joseph Dan and Frank Talmage, Cambridge Mass: Association for Jewish Studies 1982, pp. 85-120
- [4] Dattoli, G.: *Fine Structure Constant and Numerical Alchemy*, ENEA, Rome, 2010
- [5] Ferencz, Cs.: *The crown of St Stephen of Hungary*, Budapest, Heraldika, 2002 (in Hungarian)
- [6] Gaster, M.: „Hebrew Visions of Hell and Paradise,” in the *Journal of The Royal Asiatic Society*, London, 1893
- [7] Green, R. (ed.): *Herrad of Hohenbourg: Hortus Deliciarum, (Commentary and Reconstruction) I-II*. London, 1979
- [8] Heisenberg, W. „Wolfgang Paulis Philosophische Auffassungen”, in *Ztschr. für Parapsychologie und Grenzgebiete der Psychologie*. III. Nr. 2/3, 1960, p. 127
- [9] Idel, M.: *Kabbalah, New Perspectives*, Yale Univ. Press, 1988
- [10] Jung, C. G.: *Psychologie und Alchemy*. Walter Verlag, Olten (1972)

-
- [11] Jung, C. G.: *Mysterium Conjunctionis*, Princeton Univ. Press, 1977
- [12] Jung, C. G., Pauli, W.: *Naturerklärung und Psyche*. Rascher Verlag, Zürich (1952). In English: *The Interpretation of Nature and the Psyche*, New York, 1955
- [13] Jung, C. G.: *Collected Works*, Bollingen, Vol. 8, 9, 11, 12, 14. Princeton University Press (1973)
- [14] Jung, C. G. (ed. G. Adler, A Jaffe) *Letters I-II*, Princeton Univ. Press (1973)
- [15] Jung C. G. *Speaking* (ed. McGuire and R. F. C. Hull), Princeton Univ. Press, 1993
- [16] Laurikainen, K.: *Beyond the Atom: The Philosophical Thought of Wolfgang Pauli*. Springer Verlag, Berlin (1988)
- [17] Lawrence, R. M. *The Magic of the Horse-Shoe, With Other Folk-Lore Notes* (1898)
- [18] Lindorff, D.: *Pauli and Jung: The Meeting of Two Great Minds*, Quest Books (2004)
- [19] Mac Gregor, Malcolm H., *The Power of Alpha*, World Scientific, Singapore, 2007
- [20] Meier, C. (ed.): *Atom and Archetype: The Pauli/Jung Letters, 1932–1958*. Routledge, London (2002)
- [21] Miller, I. A. *Deciphering the Cosmic Number, The Strange Friendship of W. Pauli and C. G. Jung*, W. W. Norton, New York London, 2009
- [22] Pauli, W.: *Phenomenon and Physical Reality*, *Dialectica* 11, 35-48 (1957), Introduction to a Symposium on the occasion of the International Congress of Philosophers in Zürich, 1954
- [23] Pauli, W. (eds. Enz, C., Meyenn, K. V.): *Writings on Physics and Philosophy*. Springer (1994)
- [24] Ricoeur, P.: *Structure et herméneutique*. In: *Le Conflit des Interprétations*, pp. 31-63, Seuil (1969)
- [25] Scholem, G.: *Origins of the Kabbalah*, Princeton Univ. Press, 1990
- [26] Scholem, G.: *Major Trends in Jewish Mysticism*, Schocken, New York, 1983
- [27] Tóth E., Szelényi K.: *The Holy Crown of Hungary*, Budapest, 2002 (in English)
- [28] Várlaki, P., Kóczy, L.: *A Comparative Study of Pictures from Pala d'oro in St. Mark Cathedral of Venice and from the Holy Crown of Hungary*. In:

- Proc. of Int. Conference on Genealogy and Heraldry, Hungary (2006) pp. 131-171 (In Hungarian)
- [29] Várlaki, P., Nádai, L., Bokor, J.: Number Archetypes and “Background” Control Theory Concerning the Fine Structure Constant. *Acta Polytechnica* 5 pp. 71-104 (2008)
- [30] Várlaki, P., Nádai, L., Background Control and Number Archetype in Perspective of the Pauli–Jung Correspondence, In Proc. of Workshop On System and Control Theory, In Honor of J. Bokor on 60th birthday, Budapest, pp. 195-229, 2009
- [31] Várlaki P., Kóczy L T. Genealogical Myth and Allegory in the Pala d’Oro of Venice and Saint Stephen’s Royal Mirror. *Int. Conf. of the Hungarian Heraldic and Genealogical Society*, pp. 89-124 (In Hungarian)
- [32] Várlaki, P., Rudas, I.: Twin Concept of Fine Structure Constant as the ‘Self Number-Archetype’ in perspective of the Pauli-Jung Correspondence. Part I. Observation, Identification and Interpretation, and Part II, Cognition, Imagination and Background Process, *Acta Polytechnica Hungarica*, 2009, No. 2, pp. 77-108 and pp. 109-137
- [33] Várlaki P, Bokor J Number Archetypes, Symbolic Coding Letters and "Background Communication Theory" in Saint Stephen’s Royal Mirror. In: *IEEE 7th International Conference on Computational Cybernetics*, Palma de Mallorca, 2009, pp. 201-211
- [34] Várlaki, P., Bokor J, Rudas I J "System Identification" and Hermeneutics for Long Run Series of Synchronicities in the Pauli-Jung Relationship, In: *IEEE 7th International Conference on Computational Cybernetics*, Palma de Mallorca, 2009. pp. 129-140
- [35] Várlaki, P., Rudas, I., Kóczy, L.: Historical Origin of the Fine Structure Constant. Part I and Part II, *Acta Polytechnica Hungarica*, Vol. 7, No. 1, pp. 119-157, and Vol. 8, No. 2, pp. 161-196

Appendix: Comparison of the structures of Holy Crown with the Reliquary Crown of King St Ladislaus of Hungary

As we have seen, on the Holy Crown’s Pantocrator picture’s quadratic frame we can find 12 white pearls and 12 red gems around Christ’s monogram **X**. On the four hoops of the crown we can identify a 5+8+10+5 “pearl-gem structure” (15 white pearls, 5 horizontal and 8 vertical posed red gems) for each of them, which could be a map of the Hebrew word of the living creature (5+8+15=החיה) or cherub. It is a unique (pictorial-linguistic) abstract representational form of the Lord’s throne picture, in the style of Ezekiel vision, from the Apocalypse (4,4-6 and 5,6-8.): “*Around the throne are ... twenty-four elders, dressed in white robes,*

with golden crowns on their heads... and on each side of the throne are four living creatures.” Thus the four hoops symbolically represent the four cherubs; that is, the four evangelists. This hypothesis is confirmed by the fact that the on the hoops John, Peter, James and Paul may represent – according to the tradition – John, Mark, Matthew and Luke, respectively.



Figure A1

Top view of the St. Stephen's Holy Crown and the Reliquary Crown of St. Ladislaus. (Photo: A. Murdák with the kind permission of bishop Dr. L. Pápai, diocese of Győr)

Thus the twice four pictures may represent symbolically the two cherub-systems, as well probably ensuring the incarnation of the God through the ten Sephiroth between the two cherub-systems by the $10+8(4+4)+1$ composition (see Jung's recognition of God's incarnation via the Sephiroth system in footnote 13 of Part II)²⁷. This hypothesis may explain the “cosmic significance” of the King's coronation in the early 11th century²⁸. The Reliquary Crown of Saint Ladislaus (probably from the XII century), king of Hungary (1077-1095), shows a complete isomorphic structure with the Holy Crown concerning the four cherub faces with the four names of the four evangelists, which also means a “ $10+8+1$ ” symbolic composition on the Reliquary Crown. It could mean an older tradition which also probably originated from the court of St Stephen of Hungary.

²⁷ It is in “complete” isomorphy with dream 29 and the already mentioned related dreams of Pauli.

²⁸ The two cherubim on the Ark of Testament correspond the two Holy Names. The relationship between the two divine names (Tetragrammaton and Elohim) and their corresponding attributes (Mercy and Judgment), as masculine and feminine, can be found in *Midrash Tadhse*. In the Talmud these cherubim as male and female are sometimes found in sexual embrace, at other times separated from each other. (Yoma, 54a. and Babba Batra, 99a – see the sexual union of the two cherubim in Eleasar's Commentary on Sefer Yetzirah [9]). Thus the manifestation of God between the two cherubim would mean, naturally, in the Christian tradition, the archetypal image of God's incarnation.



Figure A2

The four cherubs representing the four evangelists, together with the inscriptions. (Photo: A. Murdák). Above: S MARCV " S, S MATE " VS (!), below: S IOhAnn " ES, S LVCA " S x

The shape of the two crowns shows an old Hebrew Teth letter, which is the symbol of the womb in the *Bahir* (Section 84). The crown of Solomon according to Saint Great Gregory and the *Hortus*' triple Solomonic crown description is also a symbolic womb of the king Messiah (see [33]).

Let us consider the structural representation of the Reliquary Crown on the basis of the cherubs' names (S MARCV " S, S MATE " VS (!), S IOhAnn " ES, S

LVCA “ S X), fingers and frame decoration entities. The number of the fingers of the hands of Mark, Matthew, John and Luke is $9+7+7+9=32$. The number of the (sign-like) frame-sections is $18+24+22+18=82$ (the 24 frame sections of the unique picture of Matthew could be the number-symbol of the “24 elders”). One of the main features of the number representation is the $4 \times 4=16$ fingers which separate the letters of the names of evangelists into two groups (see Fig. A2). The number of the letters of the “first part” of the names is $6+5+7+5=23$. Thus, we find a composition of 137 i.e. $32+82+23$ or $104+1$ (T from the name of MATE “VS!) $+32 = 137$. In the “second part” of the names are 7 letters (6 separated letters with a sign or letter of X after the name of Luke), and so the total number of the entities is 144. Here the “sign” X could be an allusion to the verse Rev 7, 4 which is confirmed by the number 144 according to the “role of 144” in the Rev 7, 4 („I heard the number of those who were sealed (signed!), 144 thousands, having been sealed”). If we consider the total entities for each cherub (i.e. the number of the sign sections of the frame-decorations, number of the letters in the first parts of the names and fingers of the hands) we have 36-36 entities for Matthew and John and 32+33 entities for Luke and Mark. This could mean the usual $72+65=137$ composition (which can be considered as a representation of the $2 \times 36=72$ minor apostles (the just men) as well). The 7 entities of the “second part” of the names with the 9 fingers of the Lord’s hands and the 10 toes of his feet could give us 26 entities, i.e. the number of Tetragrammaton. With the allusion of the X after the name of Luke, the “26” can be interpreted as Aleph (111) and YHVH (26) according to our discussions related to the Holy Crown’s slanted cross and the interpretation of the Aleph in the *Bahir* (§.70).

In the actual hermeneutical circle of the Reliquary Crown, there is a self-evident meaning of the separated 6 (or 7) letters²⁹ (EV SSSS x) on the basis of the “anagram” ‘EV S S S XS’, i.e. “EV, SANCTVS SANCTVS SANCTVS XPISTVS (Splendid, Holy, holy, holy Christ) according to the Rev 4,8: “*et quattuor animalia ... requiem non habent die et nocte dicentia sanctus sanctus sanctus Dominus Deus...*”. („... the four living creatures ... had no rest day and night, saying, Holy, holy, holy, Lord God, the Almighty, who was and is and is to come”). The triple “Holy” in the *Bahir* is the symbol of the tree sections of the Ten Sephiroth (§.128) and so it is related to the number 137 as the number of the Hebrew word of (“Acceptation”) Kabbalah (which follows from the above discussed composition $105+32=137$, i.e. $\text{קבלה} = \text{לב} \text{קה}$). Consequently and naturally the Reliquary Crown is a crown of the Throne-Chariot (Merkabah) and at the same time the crown of the “Acceptation” (i.e. the “Cabbala”) into the Heavenly Jerusalem.

The following part of the *Bahir* almost entirely corresponds to the above part of Rev 4.8. “... the Living Creatures, i.e. the Cherubs, (holy Chayoth), the Wheels (Ophanim) and all the groups of the Lord...bless, exalt, praise and sanctify the mighty King with the Trisagion (the great Kedushah), ... and they crown Him with

²⁹ It is confirmed by the special shape of the last „letter” „(X)S” in the name of Luke.

three “holies”, ...*God is King, God was King, God will be King forever and ever.*” (Bahir §. 126-7.) In the Bahir the heavenly troops consist of $3 \times 24 = 72$ entities (see §. 94-112) according to the image of 24 thrones, 24 crowned elders and 24 wings of the cherubs from Rev 4.8. Furthermore, the Holy Trinity with the seven spirits of God can be recognized here, by a medieval interpreter, as a symbolic image of the denary Sephirothic system. Consequently, in the Bahir, the cherubs and the Heavenly troops are crowning the Lord with the Trishagion which is the symbol here of the (comprised) treefold (!) crown of the Ten Sephiroth (§. 126-131). We can see that the Holy and the Reliquary Crown have the same representational and meaning system with the number 10 (and 19) as well as with the “number” and shape of the old Hebrew letter of Teth as a symbol of the holy kingly rebirth in the womb of the “*Virgo, Mater Ecclesia*” according to the Hortus’ symbolical context. Therefore, the Bahir, at least partly, seems to be the “theoretical” basis for the “creation” of the representational and hidden meaning system for both crowns too.



Figure A2

The Pantocrator picture of the Reliquary Crown

Sensitivity Analysis of Imperfect Systems Using Almost Orthogonal Filters

Dragan Antić, Saša Nikolić, Marko Milojković, Nikola Danković, Zoran Jovanović, Staniša Perić

Department of Control Systems
Faculty of Electronic Engineering
University of Niš, Serbia

Email: dragan.antic@elfak.ni.ac.rs, sasa.s.nikolic@elfak.ni.ac.rs,
marko.milojkovic@elfak.ni.ac.rs, nikola.dankovic@elfak.ni.ac.rs,
zoran.jovanovic@elfak.ni.ac.rs, stanisa.peric@elfak.ni.ac.rs

Abstract: This paper considers the application of the almost orthogonal filters in the sensitivity analysis of imperfect systems. First, we explain the concepts of dynamical systems sensitivity. Then we design almost orthogonal filters based on almost orthogonal polynomials. These filters are a generalization of the classical orthogonal filters commonly used in circuit theory, control system theory, signal processing, signal approximation and process identification. The advantage of the almost orthogonal filters is that they can be used for the modeling and analysis of systems with imperfections, i.e. imperfect technical systems. In this paper, we use a designed filter to obtain a model of an imperfect system, where the model's parameters have been determined with the help of genetic algorithm. A new approach for determining the sensitivity of imperfect systems is also given and an example of an imperfect system in the form of a hydraulic multitank system is considered.

Keywords: sensitivity analysis; imperfect systems; almost orthogonal polynomials; almost orthogonal filters; multitank system

1 Introduction

Sensitivity analysis considers the impact of parameter or disturbance changes on the change of the systems' state coordinates. In this paper, our focus is on the parametric sensitivity of the imperfect systems. Analysis of the parametric sensitivity is usually performed as a series of tests in which the operator sets different parameter values to see if and how these changes impact the system dynamic behaviour. By showing how the model behaviour responds to changes in the parameter values, sensitivity analysis is a useful tool in model design as well as in model evaluation.

Uncertainty in engineering analysis usually pertains to stochastic uncertainty, i.e., variance in product or process parameters [1-3] characterized by probability. Methods for calculating sensitivity under stochastic uncertainty are well documented. Imprecision, or the concept of uncertainty in choice, is one such form. Recently, systems with imperfections have been intensively studied [4-8]. The components, used for designing any real system, are not perfect and their parameters values are in the range of allowed (or not) tolerance. The reasons can be various: imperfect manufacturing, systems exploitation conditions (environment temperature, pressure, moisture, electromagnetic fields, variations in voltage, etc.). With respect to that fact, every real system in analogue technique is in some way imperfect. Digital systems, on the other hand, are considered to be perfect. Imperfections of their components do not impact system accuracy as a whole.

Therefore, because of the imperfections, parameters are not completely defined, i.e. they can vary in a certain range. In the case of systems modeling by some classical method, we use fixed parameters values, although it is not the case in reality. For the purpose of modeling these systems, it is possible to use orthogonal functions, i.e. orthogonal polynomials [9, 10]. Orthogonal polynomials are already used in approximation theory and numerical integration, and also in other scientific disciplines, e.g. in solving series of limitary problems in mathematics and physics and in solving some quantum mechanics problems. A very important application of orthogonal polynomials is the designing of orthogonal filters [11-15]. These filters are useful for orthogonal signal generators, least square approximations, and the practical realizations of optimal and adaptive systems. However, since the components of these systems cannot be manufactured exactly, filters made with these components are not quite orthogonal, but rather almost orthogonal. The signals obtained by these filters are almost orthogonal as well. The measure of nearness between the obtained and the regular orthogonal signals depends on the exactness of the component manufacturing. Thus, almost orthogonal filters are imperfect filters. Therefore, for designing these filters we cannot use the classical orthogonal polynomials, but rather we must use almost orthogonal [16-18]. In this paper, almost orthogonal filters have been used for the sensitivity analysis of imperfect systems. Theoretical results have been verified with performed experiments on laboratory setup, consisting of a multitank hydraulic system, and compared with similar method for sensitivity analysis.

2 Sensitivity of Dynamical Systems

Consider the linear system described by the transfer function in general form:

$$W(s) = \frac{b_m s^m + b_{m-1} s^{m-1} + \dots + b_1 s + b_0}{a_n s^n + a_{n-1} s^{n-1} + \dots + a_1 s + a_0} \quad (1)$$

with the output:

$$y(s) = W(s)x(s) \quad (2)$$

where $x(s)$ represents the input of the system.

Equation (1) has $(n+m+2)$ parameters a_i ($i=0,1,\dots,n$), b_j ($j=0,1,\dots,m$) [19]. So it is possible to define $(n+m+2)$ sensitivity functions in s -domain as follows:

$$u_{a_i}(s) = \frac{\partial y(s)}{\partial a_i} \quad i = 0, 1, \dots, n \quad (3)$$

$$u_{b_i}(s) = \frac{\partial y(s)}{\partial b_i} \quad i = 0, 1, \dots, m$$

In accordance we have:

$$u_{a_i}(s) = \frac{b_m s^m + b_{m-1} s^{m-1} + \dots + b_1 s + b_0}{(a_n s^n + a_{n-1} s^{n-1} + \dots + a_1 s + a_0)} \frac{s^i}{(a_n s^n + a_{n-1} s^{n-1} + \dots + a_1 s + a_0)} x(s) \quad (4)$$

For parameters b_i , sensitivity functions can be also obtained:

$$u_{b_i}(s) = \frac{s^i}{(a_n s^n + a_{n-1} s^{n-1} + \dots + a_1 s + a_0)} x(s) \quad (5)$$

In the case of the system sensitivity in steady state, we can use [20-24]:

$$y_i(\infty) = \lim_{s \rightarrow 0} s W_s(s) x(s) \quad (6)$$

$$u_{a_i} = \frac{\Delta y_i(\infty)}{\Delta a_i} \quad (7)$$

$$u_{b_i} = \frac{\Delta y_i(\infty)}{\Delta b_i}$$

3 Almost Orthogonal Filters

To analyze the sensitivity of the imperfect systems, we need to have the best possible model of the given system. For that purpose we will use almost orthogonal Legendre type polynomials [1, 4]. It has already been demonstrated how relation (1) can be turned into an orthogonal filter [12-14]. Then this filter can be used for systems modeling. This modeling method achieves greater accuracy with a lesser number of variable parameters used [11, 12].

The filter generates almost orthogonal functions $\varphi_k^{(\varepsilon)}(t)$ [1, 8], which can be used for designing the imperfect systems models and for the least square approximation, using the following relation:

$$y_M(t) \approx \sum_{k=0}^n c_k \varphi_k^{(\varepsilon)}(t) \tag{8}$$

An adjustable model of imperfect system is given in Fig. 1. Labels in the figure have the following meanings: $\delta(t)$ is the Dirac impulse function, $h(t)$ is the Heaviside step function, functions $\varphi_i(t)$ are inverse Laplace transforms of the functions $\Phi_i(s)$, and $\varphi_n^{(\varepsilon)}(t)$ represent Legendre type almost orthogonal functions. This is the sequence of almost orthogonal exponential functions over interval $(0, \infty)$ with weight function $w(t) = e^{-t}$.

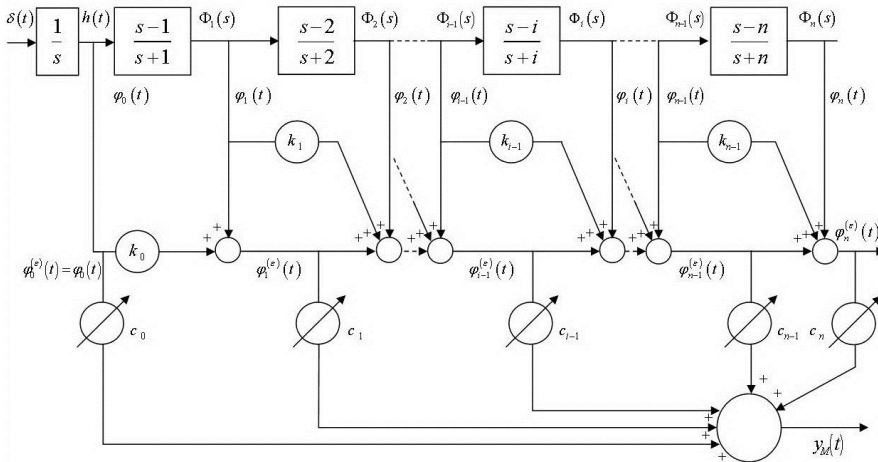


Figure 1
Adjustable model of imperfect system

The transfer function of the system model, described by almost orthogonal filter (see Fig. 1), has the following form [1]:

$$W_n^{(\varepsilon)}(s) = \frac{b_m(\varepsilon)s^m + b_{m-1}(\varepsilon)s^{m-1} + \dots + b_1(\varepsilon)s + b_0(\varepsilon)}{a_n s^n + a_{n-1} s^{n-1} + \dots + a_1 s + a_0}, \quad m < n \quad (9)$$

Coefficients $b_m(\varepsilon)$ have complex dependence on parameter ε , and we can write this in the following way: $b_m(c_n(k_n(r_n(\varepsilon))))$, where $r_n(\varepsilon)$ is coefficient defined in [1]. The coupled transfer function of this system is:

$$W_s^{(\varepsilon)}(s) = \frac{\sum_{j=0}^m b_j(\varepsilon) s^j}{\sum_{i=0}^n a_i s^i + \sum_{j=0}^m b_j(\varepsilon) s^j} \quad (10)$$

Now, sensitivity functions related to parameters a_i and b_i are the following:

$$u_{a_i}(s) = \frac{\sum_{j=0}^m b_j(\varepsilon) s^j}{\left(\sum_{i=0}^n a_i s^i + \sum_{j=0}^m b_j(\varepsilon) s^j \right)^2} s^i x(s) \quad (11)$$

$$u_{b_i}(s) = \frac{\sum_{i=0}^n a_i s^i}{\left(\sum_{i=0}^n a_i s^i + \sum_{j=0}^m b_j(\varepsilon) s^j \right)^2} s^i x(s) \quad (12)$$

4 Case Study – Description

For the purpose of sensitivity analysis of imperfect systems model, we will use a multitank system shown in Fig. 2. The multitank system [25] (Fig. 2) comprises a number of separate tanks fitted with drain valves. The separate tank mounted in the base of the set-up acts as a water reservoir for the system. Some of the tanks have a constant cross section, while others are spherical or conical, and so have a variable cross section. This creates the main nonlinearities of the system. A variable speed pump is used to fill the upper tank. The liquid flows out of the tanks due to gravity. The tank valves act as flow resistors. The area ratio of the valves is controlled and can be used to vary the outflow characteristic. Each tank is equipped with a level sensor based on hydraulic pressure measurement.



Figure 2

The multitank system by Inteco

The multitank system relates to liquid level control problems commonly occurring in industrial storage tanks. For example, steel producing companies around the world have repeatedly confirmed that substantial benefits are gained from accurate mould level control in continuous bloom casting. Mould level oscillations tend to stir foreign particles and flux powder into molten metal, resulting in surface defects in the final product. The multitank system has been designed to operate with an external, PC-based digital controller. The control computer communicates with the level sensors, valves and pump by a dedicated I/O board and the power interface. The I/O board is controlled by the real-time software which operates in MATLAB®/Simulink RTW/RTWT® rapid prototyping environment.

The multitank system given in Fig. 2 can be described using the well-known “mass balance” equations:

$$\begin{aligned}
 \frac{dH_1}{dt} &= \frac{1}{\beta_1(H_1)} q - \frac{1}{\beta_1(H_1)} C_1 H_1^{\alpha_1} \\
 \frac{dH_2}{dt} &= \frac{1}{\beta_2(H_2)} C_1 H_1^{\alpha_1} - \frac{1}{\beta_2(H_2)} C_2 H_2^{\alpha_2} \\
 \frac{dH_3}{dt} &= \frac{1}{\beta_3(H_3)} C_2 H_2^{\alpha_2} - \frac{1}{\beta_3(H_3)} C_3 H_3^{\alpha_3}
 \end{aligned} \tag{13}$$

where q represents the inflow to the upper tank, H_i is the fluid level in the i -th tank ($i=1, 2, 3$), C_i is the resistance of the output orifice of i -th tank, α_i represents the

flow coefficient for the i -th tank. $\beta_1(H_1)$ represents the cross sectional area of i -th tank at the level H_i . These values for the single tanks are the following: $\beta_i(H_i) = aw$ is the constant cross sectional area of the upper tank; $\beta_2(H_2) = cw + \frac{H_2}{H_{2\max}}bw$ is the variable cross sectional area for the middle tank, and $\beta_3(H_3) = w\sqrt{R^2 - (R - H_3)^2}$ is the variable cross sectional area of the lower tank.

The specified parameter values are the following:

$$a = 0.25m, b = 0.345m, c = 0.1m, w = 0.035m, R = 0.364m,$$

$$\text{and } H_{1\max} = H_{2\max} = H_{3\max} = 0.35m.$$

Rewrite the right sides of (13) in the form $F(x, q) = [F_1, F_2, F_3]$, where:

$$\begin{aligned} F_1(q, H_1) &= \frac{1}{\beta_1(H_1)}q - \frac{1}{\beta_1(H_1)}C_1H_1^{\alpha_1} \\ F_2(H_1, H_2) &= \frac{1}{\beta_2(H_2)}C_1H_1^{\alpha_1} - \frac{1}{\beta_2(H_2)}C_2H_2^{\alpha_2} \\ F_3(H_2, H_3) &= \frac{1}{\beta_3(H_3)}C_2H_2^{\alpha_2} - \frac{1}{\beta_3(H_3)}C_3H_3^{\alpha_3} \end{aligned} \quad (14)$$

For the model (13), for fixed $q=q_0$ we can define an equilibrium state (steady-state points) given by $q_0 = C_1H_{10}^{\alpha_1} = C_2H_{20}^{\alpha_2} = C_3H_{30}^{\alpha_3}$.

The linearized model is obtained by the Taylor expansion of (14) around the assumed equilibrium state:

$$\frac{dh}{dt} = J_H h + J_q u \quad (15)$$

where: $h=H-H_0$ is the modified state vector (deviation from the equilibrium state H_0), $u=q-q_0$ is deviation of the control, relative to q_0 , J_p and J_q are Jacobians of the

$$\text{function (14): } J_H = \left[\frac{\partial F(H, q)}{\partial H} \right]_{H=H_0, q=q_0}, \quad J_q = \left[\frac{\partial F(H, q)}{\partial q} \right]_{H=H_0, q=q_0} \quad \text{i.e.:$$

$$\begin{aligned}
J_H &= \begin{bmatrix} \frac{-C_1\alpha_1}{(H_{10})^{1-\alpha_1} \beta_1(H_{10})} & 0 & 0 \\ \frac{C_1\alpha_1}{(H_{10})^{1-\alpha_1} \beta_2(H_{20})} & \frac{-C_2\alpha_2}{(H_{20})^{1-\alpha_2} \beta_2(H_{20})} & 0 \\ 0 & \frac{C_2\alpha_2}{(H_{20})^{1-\alpha_2} \beta_3(H_{30})} & \frac{C_3\alpha_3}{(H_{30})^{1-\alpha_3} \beta_3(H_{30})} \end{bmatrix}, \\
J_q &= \begin{bmatrix} 1 \\ \beta_1(H_{10}) \\ 0 \\ 0 \end{bmatrix}
\end{aligned} \tag{16}$$

This linear model (16) can be used for the sensitivity analysis, for the stability analysis, and for the design of local controllers of the pump-controlled system.

5 Case Study – Almost Orthogonal Modeling

The multitank (imperfect system) model can be obtained in two ways [1]. The first method is to use (8) with direct appliance of genetic algorithm [26, 27] to the adjustment of the parameters c_i with respect to the minimization of the mean squared error:

$$J = \frac{1}{T} \int_0^T (y_S - y_M)^2 dt \tag{17}$$

where y_S is the output of unknown system and y_M is the model output. Genetic algorithm is an optimization technique based on the simulation of the phenomena taking place in the evolution of the species and adapting it to an optimization problem. They have demonstrated very good performances as global optimizers in many types of applications [1, 12, 28-30].

After obtaining the optimal parameters, Laplace transform is applied to the output signal. The model of the imperfect system can be directly obtained by dividing the output $Y(s)$ with the input $X(s)$.

The second method is to assume the form of the transfer function and then to adjust the function parameters in order to minimize the criteria function. In the case of imperfect systems, these coefficients will be dependent on ε . To obtain the model of the multitank system, we will use the almost orthogonal filter in Fig. 1,

which has three sections. The only known data about the system is the measured output - tank liquid level $H_2(t)$ for a given step input, shown in Fig. 3.

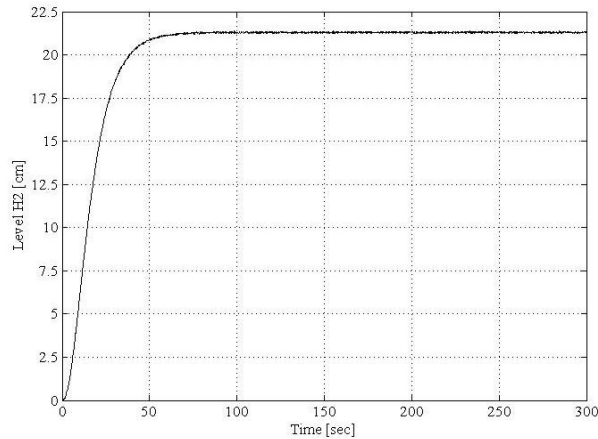


Figure 3

Step response of unknown hydraulic system

The transfer function of unknown imperfect system (the multitank system) can be obtained by applying inverse Laplace transform:

$$W_3^{(\varepsilon)}(s) = \frac{b_3(\varepsilon)s^3 + b_2(\varepsilon)s^2 + b_1(\varepsilon)s + b_0(\varepsilon)}{s^3 + 6s^2 + 11s + 6} \quad (18)$$

with the parameters $b_i(\varepsilon)$, which directly depends on ε i.e., $b_i(\varepsilon) = f(c_i(\varepsilon))$, $i=0,1,2,3$ [1]. $c_i(\varepsilon)$ are coefficients from (8).

The transfer function directly depends on ε . Parameter ε is an uncertain quantity which describes the imperfection of the system. Variations of ε contain cumulative impacts of all imperfect elements, model uncertainties, and measurement noise on the system output. The range of variations can be determined by conducting several experiments. Hence, it is expected that the responses obtained from different experiments are mutually different. The responses are within certain boundaries, which depend on parameter ε i.e., on the real system components quality. So, $W_3^{(\varepsilon)}(s)$ represents the model of imperfect system, obtained by the almost orthogonal polynomials. This general model describes all the possible models whose parameters are in the range $\pm\varepsilon$ relative to the idealized system model. In our case, the experimental value obtained for ε is equal to 0.01.

The optimal values of the adjustable parameters c_0 , c_1 , c_2 and c_3 , needed for the best model of the unknown imperfect system, are determined by using genetic algorithm. Genetic algorithm used in simulation has the following parameters: an

initial population of 150, a number of generations 300, a stochastic uniform selection, reproduction with 12 elite individuals, and Gaussian mutation with shrinking and scattered crossover. The chromosome has a structure which consists of four parameters encoded as real numbers: c_0 , c_1 , c_2 , c_3 . The goal of the simulation was to make a mean squared error as small as possible for a chosen input, i.e., to obtain the best model of the unknown system in the sense of mean squared error. So, relation (17) was used as the fitness function for the genetic algorithm. The experiment time was 300 seconds.

6 Case Study – Sensitivity Analysis

Applying the previously described procedure, the following parameters values are obtained: $c_0=1.14095$, $c_1=-2.08069$, $c_2=1.29674$, and $c_3=-0.2287$. To perform sensitivity analysis of the obtained imperfect systems model, the first parameter c_0 was changed in the limits $\pm 10\%$, $\pm 5\%$ and $\pm 1\%$ from the optimal value obtained by genetic algorithm, while the other parameters kept their values. For each change of parameter c_0 , the output in steady state was measured. Based on the equations given in Section 2, the sensitivity value related to parameter c_0 was calculated.

Table I

$c_1=-2.08069, c_2=1.29674, c_3=-0.2287$			
Tolerance	c_0	$\Delta y(\infty)$	$ u_{c_0} $
+10%	1.255045	-0.004118	0.036094
+5%	1.197997	-0.002041	0.035777
+1%	1.152359	-0.000412	0.036112
-1%	1.129541	0.000413	0.036199
-5%	1.083903	0.002085	0.036549
-10%	1.026855	0.004216	0.036951

Table II

$c_0=1.14095, c_2=1.29674, c_3=-0.2287$			
Tolerance	c_1	$\Delta y(\infty)$	$ u_{c_1} $
+10%	-1.872621	0.007451	0.035814
+5%	-1.976655	0.003382	0.032517
+1%	-2.059883	0.002142	0.020512
-1%	-2.059884	0.002137	0.020464
-5%	-2.184721	-0.003363	0.032327
-10%	-2.288759	-0.006888	0.033104

Table III

$c_0=1.14095, c_1=-2.08069, c_3=-0.2287$			
Tolerance	c_2	$\Delta y(\infty)$	$ u_{c_2} $
+10%	1.426414	-0.003801	0.029312
+5%	1.361577	-0.001772	0.027331
+1%	1.309707	-0.000221	0.017099
-1%	1.283773	0.000202	0.015601
-5%	1.231903	0.001705	0.026309
-10%	1.167066	0.003678	0.028366

Table IV

$c_0=1.14095, c_1=-2.08069, c_2=1.29674$			
Tolerance	c_3	$\Delta y(\infty)$	$ u_{c_3} $
+10%	-0.205831	0.000315	0.027585
+5%	-0.217261	0.000285	0.024962
+1%	-0.226413	0.000026	0.011368
-1%	-0.230987	0.000031	0.013229
-5%	-0.240135	0.000263	0.023025
-10%	-0.251572	0.000683	0.029864

The results are given in Table I, where $\Delta y(\infty)$ represents a deviation of the response in steady state and $|u_{c_0}|$ represents system sensitivity in steady state related to parameter c_0 . We repeat this procedure for the other parameters c_1 , c_2 and c_3 and the results are given in Tables II, III and IV respectively. The results demonstrated that the imperfect systems model is most sensitive to parameter c_0 , and least sensitive to parameter c_3 (see Fig. 4). This result can be used in reality, when it is necessary to parametrically adjust the desired output value. In our case it is the best to use adjustable parameter c_0 , because the output is the most sensitive to this parameter. If it is not possible to adjust the steady state output with only one parameter, it is necessary to make adjustments with two parameters c_0 and c_1 , and so on. This also means that the model is most sensitive to parameter b_0 , and the least sensitive to parameter b_3 with the highest index.

The results obtained by the developed method for sensitivity analysis using the almost orthogonal filter have been compared with those obtained by the nominal range sensitivity method [31], a known method for sensitivity analysis. Nominal range sensitivity analysis evaluates the effect on model outputs exerted by individual inputs, varying only one of the model inputs across its entire range of plausible values, while holding all other inputs at their nominal or base-case values.

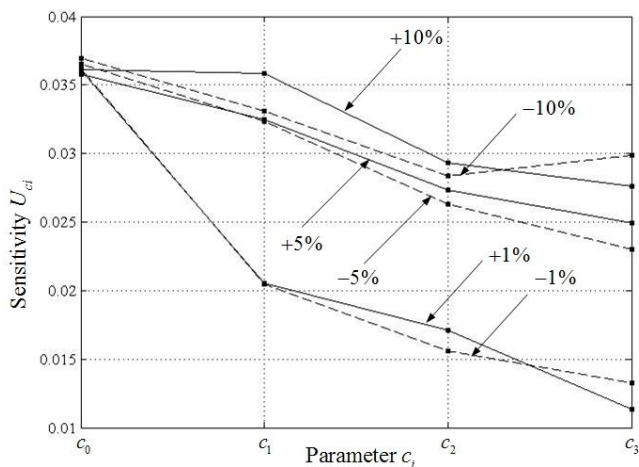


Figure 4

Graphic dependence $|u_{c_i}| = f(c_i)$

The results are given in Table V and Fig. 5. We can see that the results are similar to those shown in Fig. 4, with dependencies moved to the lower sensitivity values. The drawback of this method is that it does not include the effect of interactions or correlated inputs. The method is also time-consuming and demands a nominal range for each input.

Table V

Tolerance	$ u_{c_0} $	$ u_{c_1} $	$ u_{c_2} $	$ u_{c_3} $
+10%	0.033678	0.032718	0.028477	0.026577
+5%	0.031261	0.030171	0.026964	0.022911
+1%	0.030147	0.027221	0.014335	0.011377
-1%	0.028883	0.026508	0.013844	0.012561
-5%	0.031455	0.030054	0.026022	0.024163
-10%	0.032149	0.030115	0.028401	0.027476

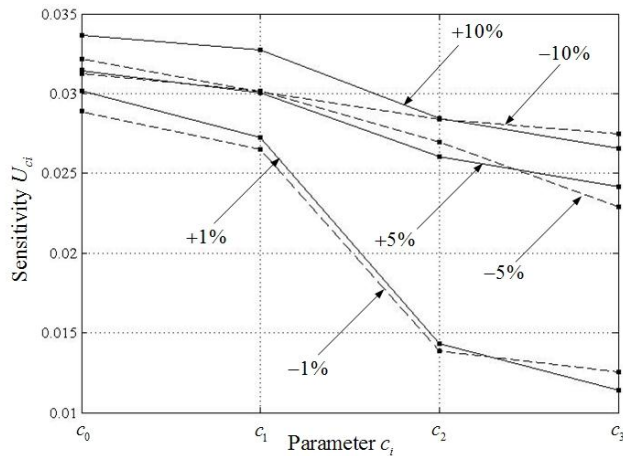


Figure 5

Graphic dependence $|u_{c_i}| = f(c_i)$

Conclusions

In this paper, the concept of the almost orthogonal polynomials is applied in the sensitivity analysis of imperfect systems. First, we designed almost orthogonal filters as generators of almost orthogonal functions. These filters can be used for the modeling, identification, simulation, and analysis of different dynamical systems as well as for the designing of adaptive systems. In this paper, an almost orthogonal filter has been used to obtain a model of an imperfect system, where the models parameters have been determined using genetic algorithm. The necessary mathematical relations for the proposed approach for determining sensitivity of imperfect systems are also given. Experiments with a multitank hydraulic system were performed to validate the theoretical results and to demonstrate that the method described in the paper is suitable for the sensitivity analysis of imperfect systems. The results have been compared with another known method for sensitivity analysis.

Acknowledgement

This paper was realized as a part of the projects “Studying climate change and its influence on the environment: impacts, adaptation and mitigation” (III 43007), “Development of new information and communication technologies, based on advanced mathematical methods, with applications in medicine, telecommunications, power systems, protection of national heritage and education” (III 44006) and “Research and Development of New Generation Wind Turbines of High-energy Efficiency” (TR 35005), financed by the Ministry of Education and Science of the Republic of Serbia within the framework of integrated and interdisciplinary research.

References

- [1] M. Milojković, S. Nikolić, B. Danković, D. Antić, Z. Jovanović: Modelling of Dynamical Systems Based on Almost Orthogonal Polynomials, *Mathematical and Computer Modelling of Dynamical Systems*, Vol. 16, No. 2, pp. 133-144, 2010
- [2] B. Danković, P. Rajković, S. Marinković: On a Class of Almost Orthogonal Polynomials, in *Lecture Notes in Computer Science* 5434, S. Margenov, L. G. Vulkov, and J. Wasniewski, Eds., Springer-Verlag, Berlin, 2009, pp. 241-248
- [3] Y. C. Schorling, T. Most, C. Bucher: Stability Analysis for Imperfect Systems with Random Loading, *Proceedings of the 8th International Conference on Structural Safety and Reliability*, Newport Beach, California, USA, June 17.-22, 2001, pp. 1-9
- [4] B. Danković, S. Nikolić, M. Milojković, Z. Jovanović: A Class of Almost Orthogonal Filters, *Journal of Circuits, Systems, and Computers*, Vol. 18, No. 5, pp. 923-931, 2009
- [5] T. Most, C. Bucher, Y. C. Schorling: Dynamic Stability Analysis of Nonlinear Structures with Geometrical Imperfections under Random Loading, *Journal of Sound and Vibration*, Vol. 276, pp. 381-400, 2004
- [6] H. Chen, L. Li: Semisupervised Multicategory Classification with Imperfect Model, *IEEE Transactions Neural Networks*, Vol. 20, No. 10, pp. 1594-1603, 2009
- [7] G. M. Coghill, A. Srinivasan, R. D. King: Qualitative System Identification from Imperfect Data, *Journal of Artificial Intelligence Research*, Vol. 32, pp. 825-877, 2008
- [8] B. Danković, Z. Jovanović, S. Nikolić, D. Mitić: Modelling of Imperfect System Based on Almost Orthogonal Polynomials, *Proceedings of the 9th International Conference on Telecommunications in Modern Satellite, Cable and Broadcasting Services, TELSIKS 2009*, Niš, Serbia, October 7-9, 2009, Vol. 2, pp. 514-517
- [9] G. Szegő: *Orthogonal Polynomials*, American Mathematical Society, Colloquium Publications, 23, Providence, 1975
- [10] Ya. L. Geronimus: *Polynomials Orthogonal on a Circle and Interval*. Fiz. Mat. Lit., Moscow, 1958
- [11] D. Antić, B. Danković, M. Milojković, S. Nikolić: Dynamical Systems Modeling Based on Legendre Orthogonal Function, *TEHNIKA-Elektrotehnika*, Vol. 58, No. 5, pp. 1-6, 2009
- [12] B. Danković, D. Antić, Z. Jovanović, S. Nikolić, M. Milojković: Systems Modeling Based on Rational Functions, *Scientific Bulletin of UPT*,

- Transactions on Automatic Control and Computer Science, Vol. 54(68), No. 4, pp. 149-154, 2009
- [13] P. Heuberger, P. Van den Hof, B. Wahlberg: Modelling and Identification with Rational Orthogonal Basis Functions. Springer-Verlag, London, 2005
- [14] S. Nikolić, D. Antić, B. Danković, M. Milojković, Z. Jovanović, S. Perić: Orthogonal Functions Applied in Antenna Positioning, Advances in Electrical and Computer Engineering, Vol. 10, No. 4, pp. 35-42, 2010
- [15] P. C. McCarthy, J. E. Sayre, B. L. R. Shawyer: Generalized Legendre Polynomials, Journal of Mathematical Analysis and Applications, Vol. 177, pp. 530-537, 1993
- [16] A. Beny, R. H. Torres: Almost Orthogonality and a Class of Bounded Bilinear Pseudodifferential Operator, Mathematical Research Letters, Vol. 11, pp. 1-11, 2004
- [17] I. Ben-Yaacov, F. Wagner: On Almost Orthogonality in Simple Theories, Journal of Symbolic Logic, Vol. 69, pp. 398-408, 2004
- [18] B. Danković, P. Rajković: On a Class of Almost Orthogonal Polynomials, Proceedings of the 4th International Conference on Numerical Analysis and Application, Lozenetz, Bulgaria, 2008, pp. 241-248
- [19] B. Danković, D. Antić, Z. Jovanović, D. Mitić: On a Correlation between Sensitivity and Identifiability of Dynamical Systems, Proceedings of the IEEE International Joint Conferences on Computational Cybernetics and Technical Informatics, ICC-CONTI 2010, Timisoara, Romania, May 27-29, 2010, pp. 361-366
- [20] L. Breierova, M. Choudhari: An Introduction to Sensitivity Analysis. MIT System Dynamics in Education Project, 1996
- [21] R. Tomović: Sensitivity Analysis of Dynamic Systems. McGraw-Hill, New York, 1983
- [22] R. Gumovski: Sensitivity of the Control Systems. Nauka, Moscow, 1993, (in Russian)
- [23] R. Pintelon, J. Schoukens: System Identification. IEEE Press, New York, 2001
- [24] R. E. Precup, S. Preitl: Stability and Sensitivity Analysis of Fuzzy Control Systems. Mechatronics Applications, Acta Polytechnica Hungarica, Vol. 3, No. 1, pp. 61-76, 2006
- [25] Inteco, Modular Servo System-User's Manual (2008) Available at www.inteco.com.pl
- [26] J. H. Holland: Adaptation in Natural and Artificial Systems. University of Michigan Press, Ann Arbor, 1975

- [27] M. Mitchel: *An Introduction to Genetic Algorithms*. MIT Press, Cambridge, 1996
- [28] D. Mitić, D. Antić, S. Nikolić, M. Milojković: Identification of the Multitank System Using Genetic Algorithm, *Proceedings of the XLV International Scientific Conference on Information, Communication and Energy Systems and Technologies, ICEST 2010, Ohrid, Macedonia, June 23-26, 2010, Vol. 1, pp. 453-456*
- [29] F. Durovsky, L. Zboray, Ž. Ferkova: Computation of Rolling Stand Parameters by Genetic Algorithm, *Acta Polytechnica Hungarica, Vol. 5, No. 2, pp. 59-70, 2008*
- [30] B. Danković, D. Antić, Z. Jovanović, S. Nikolić, M. Milojković: Systems Modeling Based on Legendre Polynomials, *Proceedings of the 5th International Symposium on Applied Computational Intelligence and Informatics, SACI 2009, Timisoara, Romania, May 28.-29, 2009, pp. 241-246*
- [31] A. C. Cullen, H. C. Frey: *Probabilistic Techniques in Exposure Assessment*. Plenum Press, New York, 1999

Real-Time Estimation of Emissions Emerging from Motorways Based on Macroscopic Traffic Data

Alfréd Csikós^a, István Varga^b

^a Budapest University of Technology and Economics, Department of Control and Transport Automation, Bertalan Lajos utca 2, H-1111 Budapest, Hungary
e-mail: csikos.alfred@mail.bme.hu

^b Systems and Control Laboratory, Computer and Automation Research Institute, Hungarian Academy of Sciences, Kende u. 13-17, H-1111 Budapest, Hungary

Abstract: In this paper a complex traffic emission modeling approach is suggested: based on the considerations of macroscopic traffic flow modeling and an average speed emission model, a macroscopic emission model is formed. The proposed methodology leads to two functions to evaluate traffic emission: a model for actually realized emissions and one for the emission level of traffic. The former one is useful for a more exact estimation of emissions relative to inventory methods; the latter one is for the analysis of optimal traffic control objectives. The introduced functions are validated in VISSIM/MatLab environment on a real motorway segment model located in Hungary.

Keywords: traffic emission modeling; macroscopic traffic modeling; freeway traffic flow

1 Introduction

Sustainable development, a catchword of modern times is more relevant than ever. Road traffic provides a variety of fields in which the ideas of sustainable development challenge engineers. As mobility needs of developed countries increase permanently, several issues arise: delays caused by congestions directly effect national economic performance, while excessive fuel consumption aggravates the exhaustion of wastable energy sources and emissions are responsible for global (greenhouse effect) and local damage (air pollution leading to health issues, acid rain, etc). While traffic control strategies have been widely used to moderate delays and prevent traffic congestion, emission and fuel consumption optimization have only entered the limelight in the relatively recent past. The overlapping of the optima of travel times and emission is not straightforward. In order to formulate control objectives for emission optimization, an understanding of the nature of traffic emission is essential. The current paper

aims to achieve this goal via an analytic traffic emission model that uses real time loop detector measurements.

of road traffic in terms of emissions have been analysed by a variety of models and methods. To estimate the evolved emissions on public roads, emission inventories have been carried out using different emission models such as COPERT and Versit+ [1], [12]. The idea expanded to urban networks in [6]. A more sophisticated approach towards emission estimation is introduced in [12] using speed measurements of loop detectors for inventories. However, other traffic variables such as traffic density have not yet been utilized during emission estimation and total emission is based on total vehicle miles travelled only; no real-time emission level is considered. The idea of real-time data use is mentioned in [8] but used only on microscopic level for the evaluation of macroscopic control measures (speed limits). Emission modeling for traffic control purposes has been used [15], [18] – but though these models are based on reasonable theoretic considerations, they have not yet been validated.

In our research, a long-term perspective is to design a control method on freeway traffic that minimizes traffic emission as well as travel times. The main idea of our approach is that the emerging traffic demand must be serviced by an infrastructure having a capacity limit lower than the demand level. This capacity defect leads to a low system performance or, in worst case, congestion. Traffic performance in the conventional manner means travel times, but another performance criterion can be the amount and composition of emitted pollutants. The idea of using real-time macroscopic traffic data presents itself during emission modeling.

The paper presents a complex traffic-emission model. It serves dual purposes: on the one hand, the emission optimum of the traffic is sought; on the other hand, total emission of freeway traffic as a function of real-time traffic data may serve as a more exact approach to emission estimation.

The model is introduced on freeway traffic as motorways turn over a significant transport performance, and loop detector measurements provide fairly exact information on traffic conditions. High emission levels are typical of motorways because of the speed range. In addition, the lack of frequent stops and the range of freeway travelling speeds mean that acceleration can be neglected [3], [4] which justifies the use of average speed models.

The suggested model is presented in four sections. After the introductory section, preliminaries regarding freeway traffic models and emission modeling are summarized. The following section proposes a complex modeling approach for traffic emission. Finally, in Section 0, a simulation is carried out on an existing motorway stretch near Budapest for model validation.

2 Preliminaries

2.1 Macroscopic Freeway Traffic Modeling

Freeway traffic is most commonly described with macroscopic traffic models. This approach considers traffic as compressible fluid, neglecting individual vehicle dynamics, describing it by aggregated variables such as traffic flow – denoted by q [veh/h], traffic density – denoted by ρ [veh/km] and space mean speed – denoted by v [km/h] of traffic. The model was originally derived in continuous-time, whereas the aforementioned variables can only be measured in discrete temporal and spatial intervals. Thus, a temporally and spatially discretized description was formed. First order models characterize flow speed as a static function of traffic density (2), whereas second-order modeling [10] engages a speed momentum equation (3) in addition to the equilibrium relation (2) of traffic mean speed and density. In the proposed complex model, second order modeling is considered.

The equations of the second-order model regarding segment i at discrete time step k are as follows:

$$\rho_i(k+1) = \rho_i(k) + \frac{T}{L_i} [q_{i-1}(k) - q_i(k) + r_i(k) - s_i(k)] \quad (1)$$

$$V_i(\rho_i) = v_{free} \cdot \exp\left(-\frac{1}{a} \left(\frac{\rho_i}{\rho_{cr}}\right)^a\right) \quad (2)$$

$$v_i(k+1) = v_i(k) + \frac{T}{\tau} [V[\rho_i(k)] - v_i(k)] + \frac{T}{L} \cdot v_i(k) \cdot [v_{i-1}(k) - v_i(k)] - \frac{T \cdot \eta}{\tau \cdot L} \cdot \frac{\rho_{i+1}(k) - \rho_i(k)}{\rho_i(k) + \kappa} - \frac{\delta \cdot T}{L} \cdot \frac{r_i(k) v_i(k)}{\rho_i(k) + \kappa} \quad (3)$$

$$q_i(k) = \rho_i(k) \cdot v_i(k) \quad (4)$$

where q_i , ρ_i and v_i denote respectively the flow, traffic density and mean speed of segment i , r_i denotes the flow of an on-ramp, s_i the flow of an off-ramp of segment i , while a , β , ρ_{cr} , κ , τ , δ , v_{free} , and η are additional constant parameters [9].

2.2 Emission Modeling Based on Copert Model

During our analysis the utilized model is COPERT IV for hot running emissions. The model has been extensively used for road traffic emission modeling [2], [17]. COPERT is an average speed model, i.e. emission factors of different pollutants [g/km] are m -order polynomial functions of the average speed devised by certain driving profiles. For vehicle j and pollutant p , see (5). As average speed contains driving pattern data [13], the sole model input variable is average speed. The

emission factor functions are specific for different vehicle classes, fuel types, Euro norms and engine capacities.

$$ef_j^p(t) = \alpha_m^p v_j^m(t) + \alpha_{m-1}^p v_j^{m-1}(t) + \dots + \alpha_0^p = [g / km] \quad (5)$$

Emission factors are most useful in the case of emission inventories: inventories calculate total traffic emission, denoted as te [g] using the following formula (EEA Technical report): $te = al \cdot ef$, where ef denotes the emission factor, al is the activity level – the number of vehicles that completed a certain distance on a roadway [vehkm] (abbreviated as VKT – total vehicle kilometers travelled). These data can be obtained by offline data of traffic surveys, considering O-D demands and assignment information, or loop detector measurements. In our case, a different approach is carried out, as total emission is calculated by using emission rates [g/h] and integrated by temporal and spatial variables. The relationship between emission rate e_j^p and emission factor ef_j^p of vehicle j for pollutant p is straightforward [14]:

$$e_j^p(t) = ef_j^p(t) \cdot v_j(t) \quad (6)$$

where $v_j(t)$ denotes the instantaneous speed of vehicle j . The formula can be generalized for average emission factors and average emission rates for time intervals if instantaneous speed is substituted by trip-based average speed.

Remark on notations: for the aggregated emission factors of the whole traffic on a segment the appellation of emission level [vehg/km], for aggregated emissions rates of the whole traffic on a segment during a discrete sample step the title total emission rate [vehg/sample step] is used.

3 Methodology

In this section the macroscopic modeling method is introduced using the macroscopic description of traffic and average speed emission modeling.

Consider a homogeneous platoon of vehicles (identical vehicle class and engine type). The assumption is only for the sake of notation simplicity, further on heterogeneous traffic is considered as well (in this case coefficients α_i^p are the same for all vehicles). Emission rate for vehicle j of pollutant p :

$$e_j^p(t) = \alpha_m^p v_j^{m+1}(t) + \alpha_{m-1}^p v_j^m(t) + \dots + \alpha_0^p v_j(t) = [g / h] \quad (7)$$

For a vehicle count of N :

$$E^p(t) = \sum_{j=1}^N e_j^p(t) = \sum_{j=1}^N \alpha_m^p v_j^{m+1}(t) + \alpha_{m-1}^p v_j^m(t) + \dots + \alpha_0^p v_j(t) = [vehg / h] \quad (8)$$

Divide the motorway on segments of number n (spatial discretization). L_i denotes the length of segment i , i, j denotes vehicle number j on segment number i . A total of N_i vehicles are present on segment i . Note that $N_i = N_i(t)$, thus the number of vehicles on segment i is a function of time.

$$E_i^p(t) = \sum_{i=1}^n \sum_{j=1}^{N_i} (\alpha_m v_{i,j}^{m+1}(t) + \alpha_{m-1} v_{i,j}^m(t) + \dots + \alpha_0 v_{i,j}(t)) = [\text{veh g / h}] \quad (9)$$

On segment i :

$$E_i^p(t) = \sum_{j=1}^{N_i} (\alpha_m^p v_{i,j}^{m+1}(t) + \alpha_{m-1}^p v_{i,j}^m(t) + \dots + \alpha_0^p v_{i,j}(t)) = [\text{veh g / h}] \quad (10)$$

Assuming that each vehicle dwelling in the same segment is travelling with the same speed:

$$E_i^p(t) = N_i(t) (\alpha_m^p v_i^{m+1}(t) + \alpha_{m-1}^p v_i^m(t) + \dots + \alpha_0^p v_i(t)) = [\text{veh g / h}] \quad (11)$$

Remember, that $N_i = N_i(t)$, which is also $N_i(t) = \rho_i(t) L_i$

$$E_i^p(t) = \rho_i(t) L_i (\alpha_m^p v_i^{m+1}(t) + \alpha_{m-1}^p v_i^m(t) + \dots + \alpha_0^p v_i(t)) = [\text{veh g / h}] \quad (12)$$

For the sake of simplicity, convert emission rate to a dimension of [veh g/s]:

$$E_i^p(t) = \frac{1}{3600} \rho_i(t) L_i (\alpha_m^p v_i^{m+1}(t) + \alpha_{m-1}^p v_i^m(t) + \dots + \alpha_0^p v_i(t)) = [\text{veh g / s}] \quad (13)$$

Consider (13) with temporally discrete variables – on segment i , speed of each i, j vehicle is approximated with the mean speed of segment i ; $\rho_i(k)$ is available from loop detector measurements/calculated using the fundamental equation of macroscopic traffic flow (4): T_s denotes sample time.

$$\begin{aligned} E_i^p(k) &= \frac{T_s}{3600} \rho_i(k) L_i (\alpha_m^p v_i^{m+1}(k) + \alpha_{m-1}^p v_i^m(k) + \dots + \alpha_0^p v_i(k)) \\ &= [\text{veh g / sample step}] \end{aligned} \quad (14)$$

Equation (14) proposes a formula of the emission of traffic emerging on segment i at time step k . The summation by time steps equals to the estimation of the pollution emerged on segment i during the analysed time interval. The summation by length (segments) leads to the emission of the analysed motorway stretch in sample step k (15).

$$\begin{aligned} E^p(t) &= \frac{T_s}{3600} \sum_{i=1}^n \rho_i(k) L_i (\alpha_m^p v_i^{m+1}(k) + \alpha_{m-1}^p v_i^m(k) + \dots + \alpha_0^p v_i(k)) \\ &= [\text{veh g / sample step}] \end{aligned} \quad (15)$$

The relationship between emission rate and emission factor is discussed in Section 2.2. In this case, the speed variable of emission factor is the average speed of segment i at time step k .

Thus, using (12), emission level (aggregated emission factors) of segment i at time step k :

$$EF_i^p(k) = \rho_i(k) L_i (\alpha_m^p v_i^m(k) + \alpha_{m-1}^p v_i^{m-1}(k) + \dots + \alpha_0^p) = [\text{veh g / km}] \quad (16)$$

The point of the formula is straightforward: traffic emission level is obtained by the real-time summation of individual vehicle's emission factors in a spatially and temporally discrete manner.

In case of inhomogeneous traffic composition, the formulas are as in (16) and (17). As single-variable polynomials of order m (in this case the emission factors) constitute an m -dimensional linear space, the total emission rate and emission level functions turn out as linear combinations of total emission rates and levels of traffic fractions containing different vehicle types:

$$E_i^p(k) = \sum_{c=1}^{N_c} \gamma_c(k) E_i^{p,c}(k) = [\text{veh g / sample step}] \quad (17)$$

$$EF_i^p(k) = \sum_{c=1}^{N_c} \gamma_c(k) EF_i^{p,c}(k) = [\text{veh g / km}] \quad (18)$$

In equations (17) and (18) c denotes vehicle type, N_c denotes the number of vehicle types, γ_c denotes the proportion of vehicle class c of whole traffic.

Remark 1: equations (14) and (16) show that real emission and emission levels are both modular – containing emission factors and macroscopic variables. The emission factors can be framed with functions from other average speed emission models. This establishment means a further analysis in future – the comparison of emission models for real-time emission estimation based on macroscopic traffic data.

Remark 2: the emission inventory-based approach (introduced in [12]) can be considered an exaggerated real time emission function – using only one loop detector for a long road stretch.

Remark 3: emission level functions of different pollutants are also applicable as route costs of transportation assignment problems [11], thus taking fuel consumption and environmental impact into account during process design.

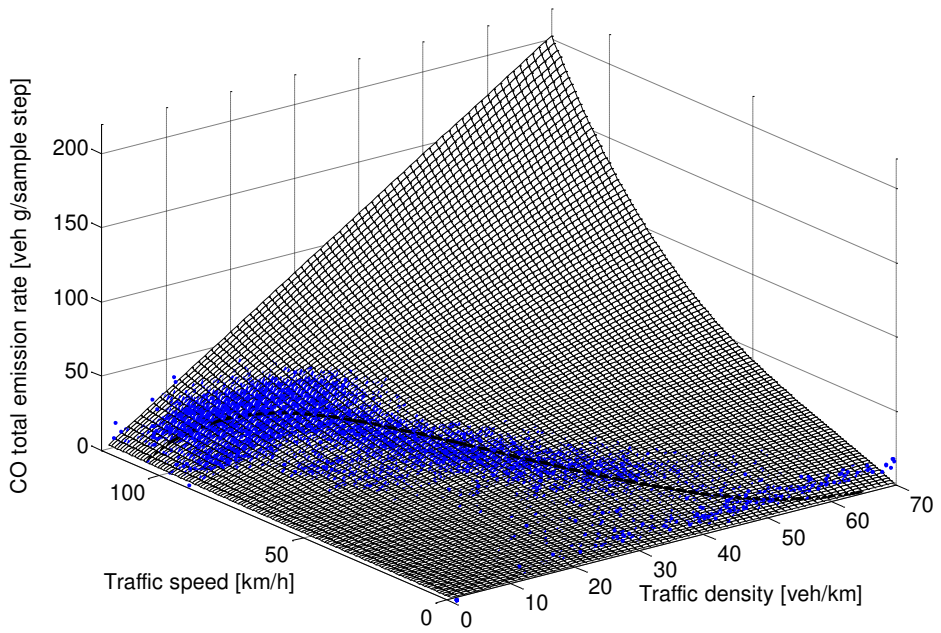


Figure 1
Total emission rate of CO on a 1 km long motorway stretch

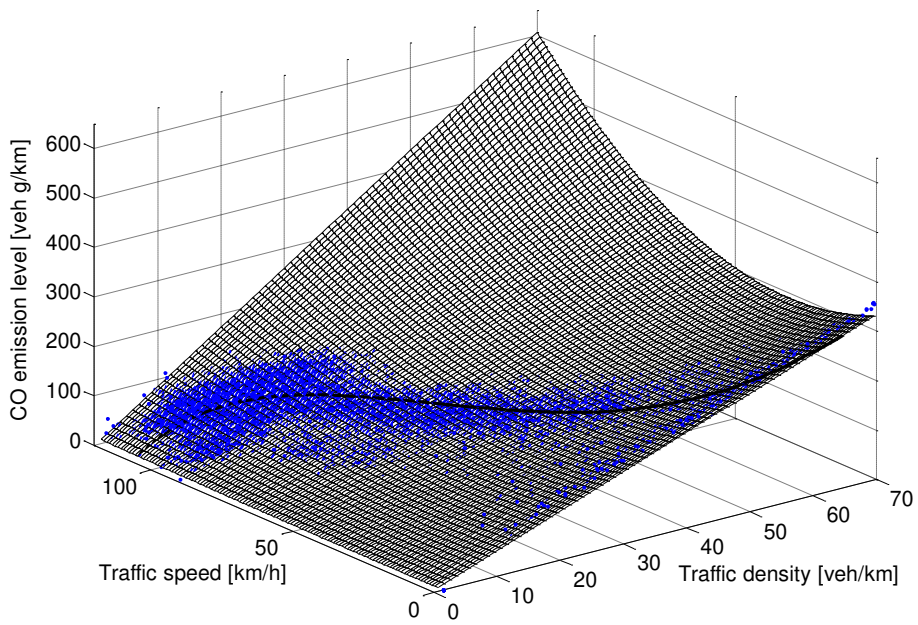


Figure 2
Emission level of CO on a 1 km long motorway stretch

The total emission rate and emission level functions of CO are illustrated in Figs. 1 and 2, using (17) and (18) for a 1 km long motorway stretch, considering the static fleet composition of Hungary from year 2010 (see Table 2) The plot of emission level (Fig. 2) clearly shows that for any traffic density, extremum can be reached by an optimal velocity independent of density, which provides the minimum of the emission factor function – in case of second order traffic modeling. Substituting (2) to (16), a single-variable function arises for the case of first order modeling. (For model parameters of (2) a least-squares fitting of real loop detector measurements of motorway M5 (see Section 0) was carried out.) The function is shown as a curve on the 3D plots. Remember section 2.1- first order traffic modeling means a static relationship between traffic density and traffic speed, while real traffic states and measurements may differ from this curve, and are plotted as dots on both Figs. 1 and 2. The idea of using first order traffic modeling, or at least reducing the range of possible density-speed combinations is another possible research area.

4 Validation

4.1 Simulation Setup

The proposed models were validated on an existing motorway stretch at the border of Budapest: on the M5 motorway from waymark 15 km to 28 km, in both directions. A 30 minute-long period was simulated using VISSIM, and the data were evaluated using MatLab. VISSIM is a microscopic traffic simulation software that is capable of performing loop detector measurements. For the software setup see Fig. 3.

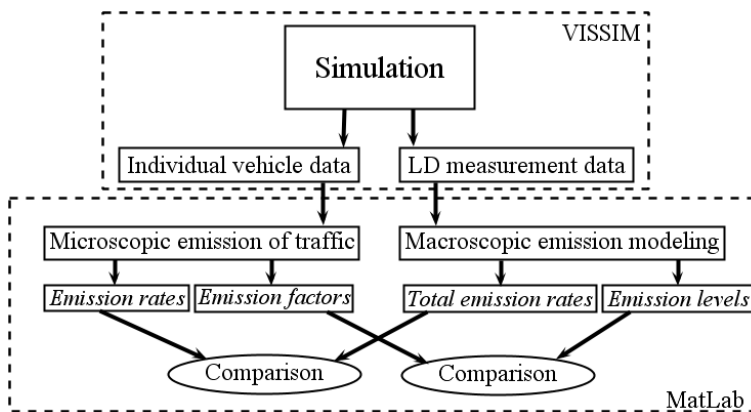


Figure 3
Software environment for model validation

The validation of the macroscopic models was executed in the following way: emission rates and emission factors of each individual vehicle were modeled and aggregated spatially and temporally by segments and time steps. During the microscopic simulation, simulation step was 1 sec, and the average speed model was utilized in a quasi continuous manner, assuming that average speed of each simulation step is the instantaneous speed at that certain moment. This was considered as the reference or real emission of traffic participants (microscopic modeling). At the same time, loop detector measurements were carried out and utilized as discussed in Section 0 (macroscopic modeling). Loop detector measurements are assumed to offer classified average speeds by vehicle classes. Both functions introduced in the previous section (emission levels and total emission rates) were compared to reference emissions. Using the model equations, the following pollutants were analysed: CO₂, CO, HC (VOC), NO_x.

Macroscopic traffic measurements can be realized in a temporally and spatially discrete manner. Measurement sample step size was 10 sec so that the Courant–Friedrichs–Lewy condition is satisfied (i.e. no particle (in this case vehicle) can skip a spatial step during a temporal step). Different loop detector (LD) distances were tested and compared (500 m, 1000 m, 5000 m and an extreme case – only one loop detector in each direction). This was carried out by evaluating only the designated loop detectors. For the loop detector layout see Fig. 5. The evaluated LD measurements for different LD distance cases are summarized in Table 1.

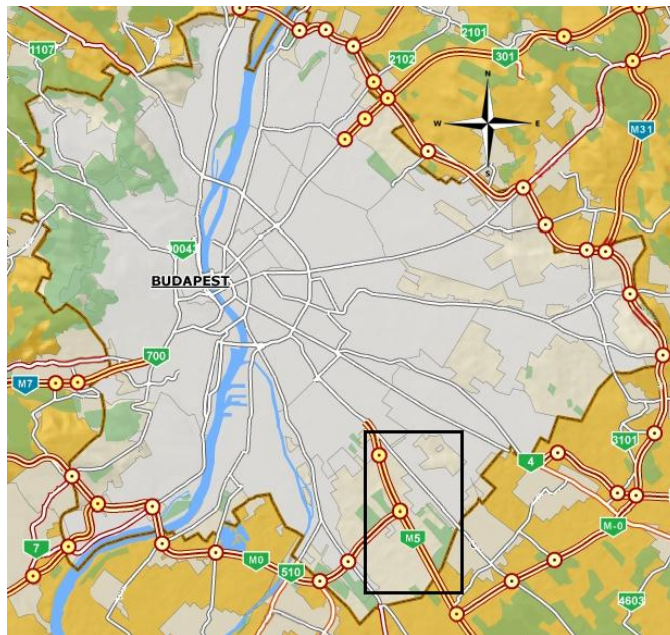


Figure 4

Location of motorway stretch



Figure 5
Loop detector (LD) layout

Table 1
Evaluated loop detector measurements

LD distance	Evaluated LD no.
500 m	all
1000 m	1, 3, 5, 7, 9, 11, 13, 15, 17, 19
5000 m	5, 15
13000 m	9

In the simulations heterogeneous traffic was generated. This heterogeneity was modeled based on the Hungarian static fleet composition of year 2010, the composition of which contains as many as 35 different vehicle classes. In our study, the most frequent vehicle types of each significant vehicle class were considered; this reduced fleet composition made 64.84% of Hungarian static fleet composition of that certain year. For the considered vehicle types see Table 2.

Table 2
Fleet composition of simulation

Vehicle category	Engine type, Euro norm	Fraction [%]	Normed fraction for simulation [%]
PC	Gasoline, Euro1, 1.4-2.0l	12.46	19.22
	Gasoline, Euro3 1.4-2.0l	12.46	19.22
	Diesel, Euro1 <2.0l	9.78	15.08
	Diesel, Euro3 <2.0l	10.13	15.62
LDV (<3.5 t)	Diesel, Euro1	2.91	4.49
	Diesel, Euro2	1.73	2.67
	Diesel, Euro3	2.00	3.08
HDV (Rigid, <7.5 t)	Diesel, Euro1	5.86	9.04
	Diesel, Euro2	3.49	5.38
	Diesel, Euro3	4.02	6.20
Total		64.84	100

During the simulation, different traffic states were generated: free flow conditions (low traffic flow volumes, high traffic speeds), saturated flow (high traffic flow volumes, near critical density), and congested situations (above critical density, and high density situations); these three rather differing situations are the most characteristic and significant states concerning traffic. For the first 15 minutes, free flow and saturating traffic conditions were simulated. From the 16th minute, an accident and then a subsequent 10 minute-interval of slow progression was modeled (from 15 min to 25 min). The transitions among traffic states were realized in all directions (congesting and yielding traffic).

The simulated accident occurs at segment no. 13, north-south direction and since motorway accidents usually lead to bottlenecks, significant changes in traffic density, speed and also in emission can be observed. Therefore, total emission rates and emission levels are illustrated on this particular segment (Figs. 6 and 7). Until the 100th step (1000 sec) free flow traffic is present with no congestion. The accident happens at 1000 sec, and leads to a solid increase in traffic density until 1200 sec, when the congestion is formed. The congestion starts to dissolve at 1600 sec, and the density on segment no 13 starts decreasing.

4.2 Evaluation of Results

This extreme traffic situation is suitable for comparing the accuracy of different LD configurations, measurement points deployed at different distances. Both total emission rates and emission levels are most accurate estimations of reference emission if loop detectors are at 500 m distances, and accuracy declines with increasing loop detector distance. Emission level estimations (Fig. 8) show that a rare ordination of loop detectors leads to delayed measurement of the extreme

traffic state as the effect appears at distant measurement points with delays. For control design purposes, the most dense loop detector layout is advised because the density of loop detectors along a roadway is in direct proportion to the spatial and temporal accuracy of emission levels. In case of distant loop detectors, application of state estimation is advised which has been successfully utilized for traffic variables [16].

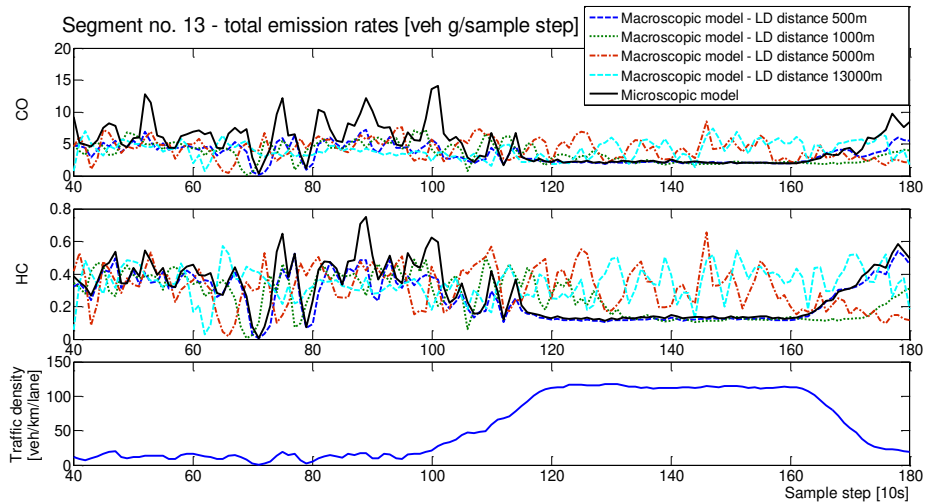


Figure 6

Traffic density, and total CO and HC emission rates of segment 13, north-south direction

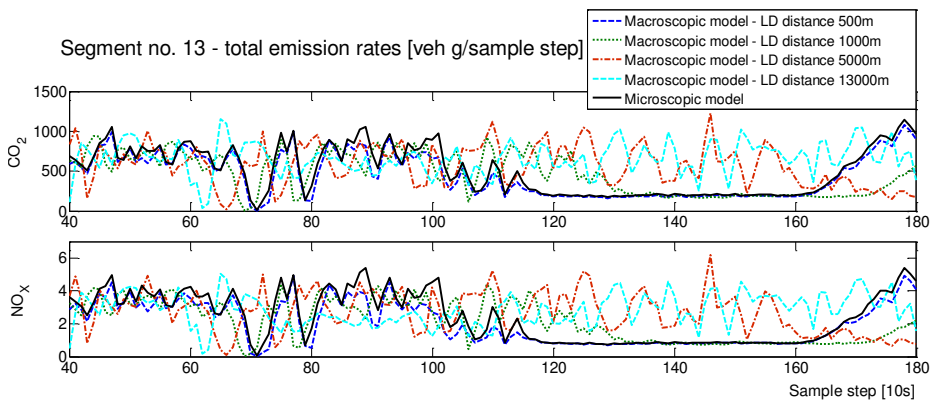


Figure 7

Total CO₂ and NO_x emission rates of segment 13, north-south direction

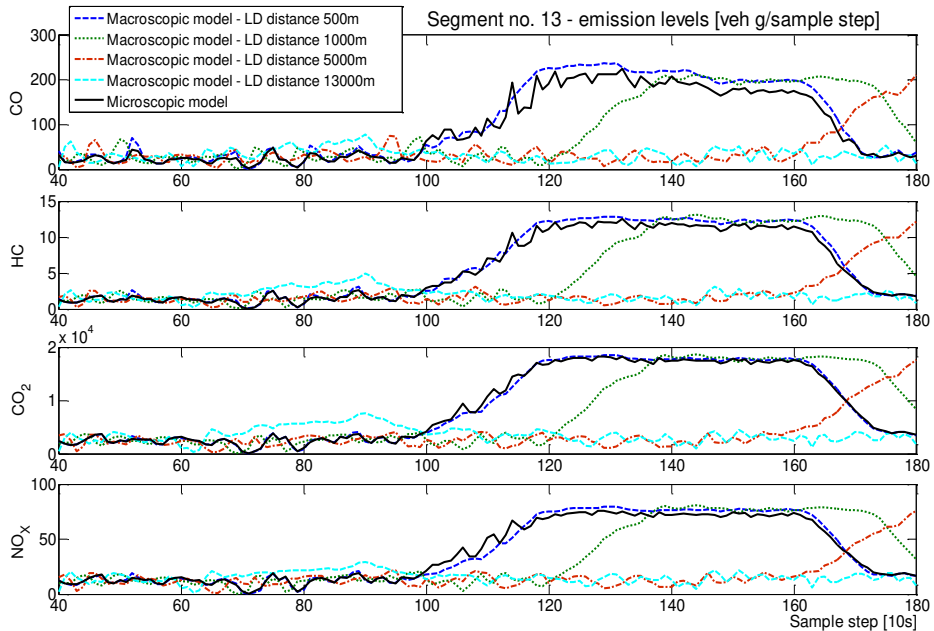


Figure 8

Emission levels of segment 13, north-south direction

Numerical results of simulation for the whole motorway stretch are summarized in Tables 3 to 6, where averages of absolute relative errors (calculated for each discrete step) referred to microscopic modeling are displayed. The most interesting observation of figures is that dense loop detector measurements offer a reasonable estimation of emissions; however, the case of one detector only (LD distance 13000 m) which can be considered as classic inventory calculation may lead to more than 80% of relative errors of real emissions in extreme or changing traffic conditions and relative error is considerable even under free flow conditions (south-north direction). Thus, when considering using real-time data, as many loop detectors is advised for a more accurate emission estimation.

Table 3

Average absolute relative differences of total emission – relative to microscopic modeling

		North-south direction				South-north direction			
LD distance [m]		500	1000	5000	13000	500	1000	5000	13000
Pollutant	CO	0.1314	0.2332	0.3635	0.5776	0.1137	0.1182	0.2510	0.3230
	HC	0.1128	0.1439	0.4119	0.6850	0.1223	0.1510	0.2352	0.4674
	CO ₂	0.0790	0.1094	0.4817	0.8176	0.0868	0.1123	0.3465	0.3952
	NO _x	0.1188	0.1529	0.4246	0.5762	0.1304	0.1543	0.2868	0.2707

Table 4
Average absolute relative differences of emission level – relative to microscopic modeling

		North-south direction				South-north direction			
LD distance [m]		500	1000	5000	13000	500	1000	5000	13000
Pollutant	CO	0.1762	0.1960	0.4222	0.6728	0.1509	0.1607	0.1981	0.3280
	HC	0.0714	0.1764	0.3280	0.5821	0.0789	0.0790	0.1805	0.4084
	CO ₂	0.0331	0.1397	0.2933	0.7604	0.0401	0.0595	0.2983	0.5629
	NO _x	0.0436	0.1519	0.2546	0.5371	0.0518	0.0819	0.1466	0.3093

Table 5
Average absolute relative differences of total emission – segment 13, north-south direction

		Segment 13, north-south direction			
LD distance [m]		500	1000	5000	13000
Pollutant	CO	0.1691	0.1813	0.2179	0.7176
	HC	0.1201	0.1653	0.4823	0.7850
	CO ₂	0.1826	0.2001	0.5256	0.9760
	NO _x	0.1279	0.1713	0.3526	0.4823

Table 6
Average absolute relative differences of emission level – segment 13, north-south direction

		Section 13, north-south direction			
LD distance [m]		500	1000	5000	13000
Pollutant	CO	0.0361	0.1162	0.6237	1.6728
	HC	0.0355	0.0579	0.4126	1.3821
	CO ₂	0.007	0.1241	0.6076	1.3104
	NO _x	0.0126	0.0958	0.6486	1.2970

Summary

In this paper a complex macroscopic approach for motorway traffic emission modeling is suggested. The model is modularly assembled using the second-order macroscopic description of freeway traffic and an average speed model. Emission of traffic is estimated with spatially and temporally discrete variables using loop detector measurements. Two functions are introduced analogous to emission rates and emission factors: total emission rates of traffic and emission level. The former aims at calculating emission using real time traffic data; the latter serves optimization analysis purposes. The control objective is to provide a traffic service for vehicles appearing on the motorway network in a way that they complete their routes with the least time spent in the network and emit a minimal amount of pollutants. A microscopic simulation-based model validation illustrates the viability of the suggested method. Several future research directions arise: a comparison of different average speed emission functions framed to the complex

model, and also an analysis of emission functions using fewer variables can be considered (as second order modeling can be limited to potential traffic states).

Acknowledgments

The work is connected to the scientific program of the “Development of quality-oriented and harmonized R+D+I strategy and functional model at BME” project. This project is supported by the New Széchenyi Plan (Project ID: TÁMOP-4.2.1/B-09/1/KMR-2010-0002), the National Development Agency, the Hungarian National Scientific Research Fund (OTKA CNK 78168) and by János Bolyai Research Scholarship of the Hungarian Academy of Sciences which are gratefully acknowledged.

References

- [1] R. Bellasio, R. Bianconi, G. Corga, P. Cucca: Emission Inventory for the Road Transport Sector in Sardinia (Italy) *Atmospheric Environment* 41 (2007) 677-691
- [2] Corvalán R. M, Osses, M., Irrutia, C. M: Hot Emission Model for Mobile Sources: Application to the Metropolitan Region of the City of Santiago, Chile. *Journal of Air and Waste Management* 52. 2002, 164-174
- [3] Alfréd Csikós, Tamás Luspay, István Varga: Modeling and Optimal Control of Travel Times and Traffic Emission on Freeways. IFAC World Congress 2011, Milan
- [4] Yonglian Ding, Hesham Rakha: Trip-based Explanatory Variables for Estimating Vehicle Fuel Consumption and Emission Rates. *Water, Air and Soil Pollution: Focus* 2: 61-77. 2002
- [5] EEA Technical report No. 9/2009: EMEP/EEA Air Pollutant Emission Inventory Guidebook 2009 Technical Guidance to Prepare National Emission Inventories. ISSN 1725-2237
- [6] Farhad Nejadkoorkia, Ken Nicholsonb, Iain Lakea and Trevor Daviesa: An Approach for Modelling CO₂ Emissions from Road Traffic in Urban Areas. *Science of The Total Environment* Volume 406, Issues 1-2, 15 November 2008, pp. 269-278
- [7] Suresh Pandian, Sharad Gokhale, Alope Kumar Ghoshal: Evaluating Effects of Traffic and Vehicle Characteristics on Vehicular Emissions Near Traffic Intersections. *Transportation Research Part D* 14 (2009) 180-196
- [8] Luc Int Panis, Steven Broekx, Ronghui Liu: Modelling Instantaneous Traffic Emission and the Influence of Traffic Speed Limits. *Science of the Total Environment* 371 (2006) 270-285
- [9] M. Papageorgiou, J.-M. Blosseville and H. Hadj-Salem: Modelling and Real-Time Control of Traffic Flow on the Southern Part of Boulevard

- Peripherique in Paris: Part I Modelling. Part II: Coordinated on Ramp Metering, Transportation Research Part A 24 (5) (1990) pp. 345-370
- [10] H. J. Payne: Models of Freeway Traffic and Control, Simulation Councils Proceedings Series 1 (1971) pp. 51-61
- [11] Edit Schmidt: Elementary Investigation of Transportation Problems. Acta Polytechnica Hungarica Vol. 6, No. 2, 2009
- [12] Robin Smit, Muirel Poelman, Jeroen Schrijver: Improved Road Traffic Emission Inventories by Adding Mean Speed Distributions. Atmospheric Environment 42 (2008) 916-926
- [13] R. Smit, A. L. Brown, Y. C. Chan: Do Air Pollution Emissions and Fuel Consumption Models for Roadways Include the Effects of Congestion in the Roadway Traffic Flow? Environmental Modeling and Software 23 (2008) 1262-1272
- [14] Abhishek Tiwary, Jeremy Colls: Air Pollution. Measurement, Modelling and Mitigation. 3rd edition. Routledge, Taylor and Francis Group, 2010
- [15] Liping Xia, Yaping Shao: Modeling of Traffic Flow and Air Pollution Emission with Application to Hong Kong Island, Environmental Modelling & Software 20 (2005) 1175-1188
- [16] Yibing Wang, Markos Papageorgiou, Albert Messmer, Pierluigi Coppola, Athina Tzimitsi, Agostino Nuzzolo: An Adaptive Freeway Traffic State Estimator. Automatica, Vol. 45, Issue 1, January 2009, pp. 10-24
- [17] Zachariadis, T. I., Samaras, Z. C., (1999) An Integrated Modeling System for the Estimation of Motor Vehicle Emissions. Journal for Air & Waste Management Association 49, 1010-1025
- [18] Solomon Kidane Zegeye, Bart De Schutter, Hans Hellendoorn, and Ewald Breunese: Reduction of Travel Times and Traffic Emissions Using Model Predictive Control, 2009 American Control Conference June 10-12, 2009

A New Approach to Decision Making in Basketball - BBFBR Program

Branko Markoski¹, Predrag Pecev², Laszlo Ratgeber³, Miodrag Ivković⁴, Zdravko Ivanković⁵

¹University of Novi Sad, Technical Faculty "Mihajlo Pupin", Zrenjanin, Serbia, markoni@uns.ac.rs

²University of Novi Sad, Faculty of Sciences / Department of Mathematics and Informatics, Novi Sad, Serbia, predrag.pecev@gmail.com

³University of Pécs, Faculty of Health Sciences, Pécs, Hungary, ratgeber.laszlo@gmail.com

⁴University of Novi Sad, Technical Faculty "Mihajlo Pupin", Zrenjanin, Serbia, misa.ivkovic@gmail.com

⁵University of Novi Sad, Technical Faculty "Mihajlo Pupin", Zrenjanin, Serbia, misa.ivkovic@gmail.com

Abstract: The developed solution is named BBFBR, which stands for Basketball Board for Basketball Referees. The current implementation of the solution is based on drawing the ball's movement on the court, which is the input vector of the neural network, whilst the output vector of the neural network consists of the movement coordinates of the referees. The key segment of this paper describes, in detail, the structure of the input and output vectors of the neural network used in the BBFBR project, as well as the methods, and the advantages and flaws that were noted during the training of the neural network. There are two methods used while training the neural network: the method of sequential repetition. The current solution enables calculating optimal ways of the referee's movement in the case that the movement of the ball in an action consists of not more than 15 key points, e.g. guiding the ball from one point to another, passing the ball to another player, shooting etc. The application value of the current solution bears only educational purpose because it is possible to apply it to training young basketball referees in the terms of their movement, to enable them to be aware of an action and to be able to analyze it. This paper also describes the methods and the developed software which, based on the action and the movement of the ball, using the neural network, determines the movement of a basketball referee on the court, in order to gain the best view of the action. The solution is developed in Microsoft Visual Studio 2010, written in the programming language C# referring to AForge .NET Framework for the support in the aspects of configuring, training and usage of neural networks. AForge .NET Framework is published with LGPL v3 licence.

Keywords: neural networks; basketball; path prediction

1 Introduction

Most solutions that are based on the applications of neural networks in basketball use neural networks to predict the outcome of the game, to analyse the score, to draft score predicting, etc. [2] [3] One of the well-known solutions is called Basketball Predictor and it predicts outcomes of games using neural networks, based on the data on the teams that play, the previous games, teams' selection, etc. The solution covers the American NBA and the WNBA league, and the European leagues: Austria, Czech Republic, France, Germany, Greece, Italy, Poland, Russia, Spain and Sweden.

In the paper [1], it is determined that the most common elements of a basketball game are shots for 2 points under the hoop and the defensive rebound, by analysis of the first B basketball league for men from 2005 and 2010, using a feed forward neural network.

The paper [4] describes how using various neural networks predicts the outcome of a game, emphasizing that the predictions of the trained neural networks were more precise comparing to the basketball experts' predictions. Practically, trained neural networks predicted the outcome of the game correctly in 74.33% cases, while the basketball experts were precise in 68.7% cases. In the paper, the use is presented of feed forward, radial, probabilistic, regressive neural networks, and also the fusion of them.

Based on what has been here mentioned, it can be concluded that the application of neural networks in basketball is a fairly popular field and that the leading trend is predicting the outcome of a game. This goal is also the most profitable considering the gambling industry and the teams' desire to be as high ranked as possible. Using the methods mentioned, it is possible to determine whether a team is able to win another one by simulations based on neural networks. It also enables to turn the game in progress around or find a way to improve the score if losing the game is inevitable.

Various factors influence the outcome of a game: the players' performance, tactics, the time zone, whether the game is played at home or not, etc. However, the impact of the referees who decide on the regularity of the points, and in the end, the final score, is not emphasized enough. It is common that teams lose games because of the referee's wrong decision about a single point. Therefore, the question arises: What can be done to make the basketball referee's work easier?

Watching the basketball game is often disturbed by the crowdedness on the court during an action, so practically nothing can be observed on the referee's part. This can result in referee making a bad decision.

The idea of the BBFBR solution is in fact that some actions can be observed better from certain positions. Therefore, using neural networks it is possible to calculate the ideal path movements of the referees who observe a certain action, regarding

the data on basketball actions. The reason to use neural networks is the fact that basketball actions are prone to variations and improvisations, so, very often, new actions are created. The usage of neural networks in these cases is desired because then, based on experience of the neural network and the similarities with other basketball actions, it is easier to find the optimal path for the referee's movement with prediction in real time. Capabilities and needs mentioned are almost impossible or barely possible to realize via conventional solutions, by writing algorithms.

The use of the solution mentioned has potential wide area of application:

- Great application value in training young basketball referees in the terms of how to move and where to look during the certain actions, in order to observe and make the best decision about the validity of the point, in case of the fault or in other situations.
- Retroactive analysis of the referee's decision, when there is a suspicion that the decision was wrong. For example, could a certain basketball referee have adequately observed the action when it was decided not to take the point into consideration, although it is suspected that there was a fault or any other technical inconsistency previously made? Adding the element of prediction enables one to gain the prediction of the neural network about whether the referee is in the optimal position to observe a certain action in real time, during the action itself. Further development of this application could result in developing a system similar to the HawkEye system, which already exists and is applied in tennis. Applying the idea mentioned, it is possible to minimize the coefficient of human mistake while determining the validity of a point to a certain extent, thereby minimizing unfair game, cheating and favouring certain teams, and it will be very easy to find corrupted referees.
- If it is possible to determine the ideal movement of the referee in a certain action, by implementing predicting neural networks, it is possible to convert the movement of the referee into movement of the cameras, which follow the basketball action in real time. This, in addition to the static cameras that are pointed at players by cameramen during the game, could enable the viewers to see the referee's view, or the first row view. A similar principle is seen in Formula 1, when viewers can see the view that their favourite driver sees from the vehicle.

2 The BBFBR Program - Structure and Class Diagrams

The program BBFBR consists of four parts: BBFBR and NN Trainer developed in one project, nnUtility developed as a separate dll file and AForge .NET framework, which offers support for training realization of the neural network. The structure of the BBFBR program is presented in Figure 1.

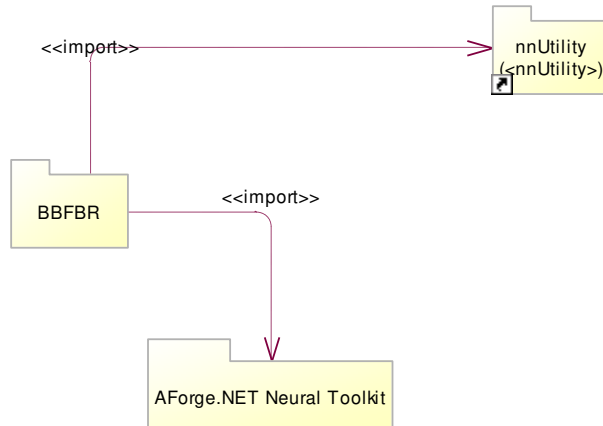


Figure 1

Structure of the BBFBR program

nnUtility package, which offers program's logistics in BBFBR solution and consists of six packages, is presented in Figure 2. Those six packages are:

- BallData – Package contains the structure and logic that is required while describing the movement of the ball in the basketball court.
- RefereeData – Package contains the structure and logic that is required to describe the movement of the referees in the basketball court.
- Calculations – Package contains static methods that are used for detailed calculations of the ball movement during rendering.
- ImageRotation – Package contains useful methods for the rotation of the pictures in the memory.
- nnTrainer – Package contains supporting structures that are used while training the neural network for positioning the basketball referees.
- DoubleBufferPB – Package contains `clsDoubleBufferPB` class, whose instance is the `Display` element which is used for displaying the court, drawing actions and animating and rendering solutions. The functionality of the `Display` element will be described in detail later in the text.

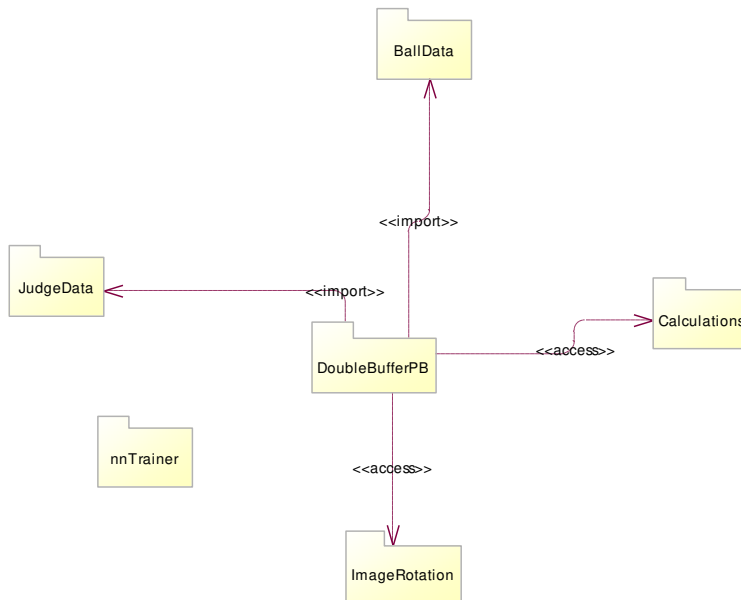


Figure 2

Main diagram of the nnUtility package

2.1 BBFBR Program - Structure and the Contents of the BallData Package

The package BallData, shown in Figure 3, contains the structure and logic classes that are needed for the description of the ball movement on a basketball court. The content of the BallData packages is the following:

- clsGridStructure - Class represents grid model which is applied on a basketball court, and divides it into quadrants and sub-quadrants. [8]
- clsBallPosition - Class defines the position of the ball on a basketball court
- clsBallPath - Class defines movement of the ball on a basketball court
- clsBallMovement - Class defines smooth ball movement on a basketball court for the purpose of animation
- clsAction - Class defines one basketball action
- clsActionDataFile - Class defines a binary file in which actions are stored
- clsActionFileWriter - Class contains a static method for reading and writing binary files in which basketball actions are stored

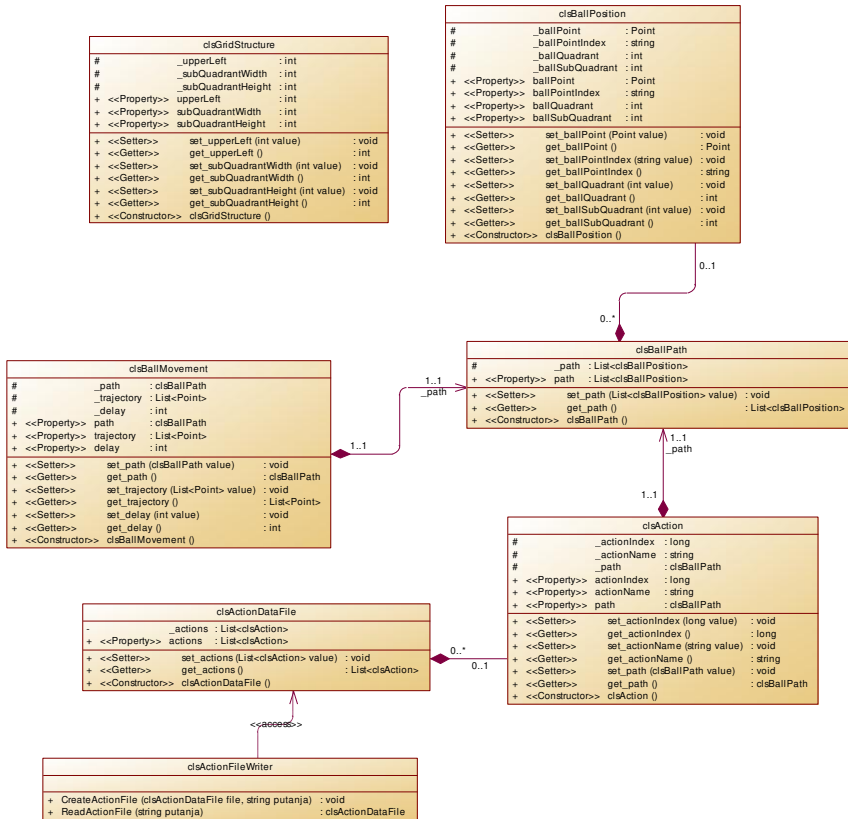


Figure 3
Structure and content of BallData Package

3 BBFBR - Appearance and Usage

In Figure 4, the appearance of the main form of the BBFBR program is presented. The mentioned form consists of three parts:

- Main menu
- Area for displaying, animating and rendering the results of calculated actions (Display Area)
- Area for action management

The main menu contains four submenus: File, Neural Network, Display and Actions.



Figure 3

Appearance of the main form of the BBFBR program

The file submenu contains the following three options:

- *Open Actions File* – This option opens the binary file that contains the defined basketball actions. The file owns *.act extension.
- *Save Actions File* – This option records all changes to previously read *.act file that contains defined actions, or a new one is created if there is no existing *.act file.
- *Exit* – This option closes the program BBFBR.

The Neural Network submenu contains following three options:

- *Load Neural Network* – This option reads the binary file that contains the trained neural network. The extension of the file with the trained neural network is *.ann (Artificial Neural Network)
- *Train Neural Network* – This option calls NN Trainer form, which serves for training and adapting the neural network, for input, which is the movement of the ball in the court during a basketball action, giving as an output the optimal movement of the referees, in order to have the best observance of the current action.
- *Calculate Action* – This option uses the read or just draw new action to determine the optimal movement of the referees by the neural network, in order to gain the best observance of the action.

The Display submenu serves for modifying and managing the Display area of the BBFBR program. The Display area will be explained in detail later in the text. The Display submenu contains the following seven options:

- *Show Grid Lines* – This option displays the scheme that shows how the basketball terrain is divided into quadrants and sub-quadrants.
- *Show Quadrant Numbers* – This option displays the numbers that identify the quadrants of the basketball court.
- *Show SubQuadrant Numbers* – This option displays the numbers that identify the sub-quadrants of the basketball court inside a certain quadrant.
- *Show JMOV Paths* – This option displays the line of movement of the referees around the court.
- *Show Static Referees* – This option restricts the movement of the referees and places them in the predicted positions.
- *Animate* – This option animates the movement of the ball during the action and the referees who observe it.
- *Render* – This option exports the animation into a *.wmv file using the abilities offered by the option Animate.

The Actions submenu, contains following two options:

New Action – This option initialises the creation of a new action.

Reset Court – This option resets the currently chosen action, thereby deleting the path of the ball in the current action. If the path of the ball of a certain action is not recorded after deleting, it will not be removed from the set of actions, regardless of whether it is in the memory, in the stage of creation or in *.act file.

3.1 The BBFBR - Display Area - Area for Displaying, Animating and Rendering the Results of Calculated Actions

The Display area is used for defining an action by drawing the path of the ball, and for displaying and animating the movement of the ball and referees in the court. The appearance of the Display area is shown in Figure 5.

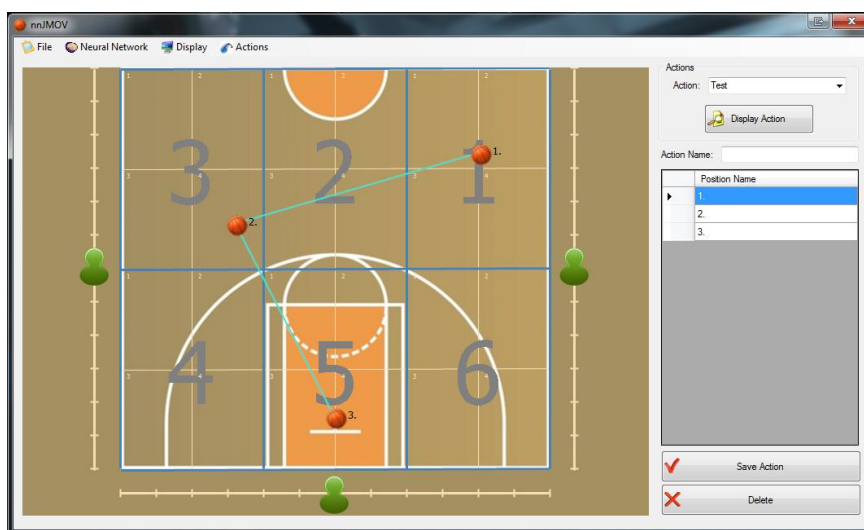


Figure 5
Appearance of the Display area

From Figure 5, it can be concluded:

- The Display area displays a half of the basketball court from the bird's-eye-view perspective.
- The basketball court is divided into six quadrants, and each of these six quadrants has four sub-quadrants [5] [6] [10] [11] [12]
- The quadrants and sub-quadrants mentioned can be marked and mapped differently, leaning on the structure provided by the `clsGridStructure` class. Depending on the values mentioned, the neural network is trained differently, but the input and the output vectors stay in the same format, which means that the results should simply be interpreted differently.
- On the side of the basketball court are three referees, who move according to their defined paths along the court, which is divided in precisely twelve equal distances between positions.
- Clicking on the basketball court, the ball is placed at a point in the action. The point receives the default name depending on the sequence of the numbering. For example, if a point is the first point of the action, it is marked as "1."; the second is marked with "2."; etc. In order to achieve a better and clearer perceptiveness, these points can change their names into any common noun, for instance: dribbling, shooting, etc. An array of the action points represents the path of the ball movement during the action. Those points are matched using a blue line that automatically matches the last, currently added point, with the previous one.

- The appearance of the Display area does not affect the functionality of the Display component, but helps and makes drawing an action easier for a user.
- After loading or drawing an action, it is required to call the option Calculate Action from the menu Neural Network, so that the loaded neural network can calculate the optimal path and positions for the movement of the referees for that action. After executing the option mentioned, using the option Animate from the Display menu, it is enabled to animate the solution for the action drawing. The animation of the solution is presented in Figure 6.



Figure 6

Animation of the solution

By analyzing Figure 6, it can be concluded that:

- During animation, the ball moves following the defined blue path meeting the points that define a basketball action.
- The referees move following the paths that are the result of the neural network calculations and they observe the ball movement.
- Depending on the values of the `clsGridStructure` and the schedule of the quadrants they are responsible for, between the ball and the referees two kinds of lines are drawn. If the ball is in a quadrant that the referee is responsible for, the line between him / her and the ball will be red. Otherwise, it will be green.

The area for the action management is used for displaying, modifying and deleting actions. For the reason the actions are drawn by clicking on the Display area, the area for the action management is basically used for naming the drawn action, renaming the dots of the action and saving in the temporary binary file. The section for the action management is on the right side of the Display area and is shown in Figure 6.

4 Neural Network Training for Analysis and Determination of the Ideal Path for Referees during a Basketball Action

In this paper, the trained neural network is the multilayer neural network, trained by the Back Propagation training algorithm that belongs to the class of controlled training algorithms. The structure of the hidden layers, regarding the number of neurons per layer, is shown in Figure 7, and the number of neurons is 30 in the first, input layer and 45 at the last, output layer. The trained neural network consists of seven layers with 30, 20, 25, 15, 10, 6 and 45 neurons in each layer, respectively. This neural network in hidden layers gradually narrows towards the last layer. All the neurons from a certain layer are connected to all neurons from the adjacent layer.

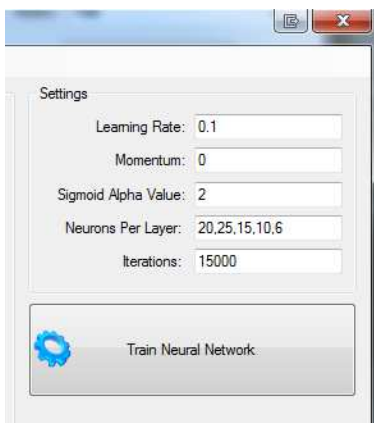


Figure 7

Settings of the neural network

From these facts it is visible that the input vector of neural network has 30 elements, and the output one 45. These elements' values are discrete ones. Depending on the length of a basketball action (no more than 15 key points), the appearance of the input and output vectors may change.

Every key point is determined by the ordered pair: [quadrant, sub-quadrant], while the ideal positions for the basketball referees for such point are determined by ordered three [referee1pos, referee2pos, referee3pos]. The values for the quadrant entity range between 1 and 6, and for the sub-quadrant between 1 and 4. The values for entities referee1pos, referee2pos and referee3pos are between 1 and 12, representing the fixed position from which the certain key point of basketball action may be seen best.

Let us suppose that a basketball action consists of four key points, and that we know the ideal positions for the basketball referees for these four points. Since the maximum length of the input vector of the neural network is 30 elements, or 15 points, noted as $t_1, t_2 \dots t_n$, where $\max(n) = 15$, defined by an ordered pair [quadrant, sub-quadrant], all values of the input vector are set to 0, and are filled, starting from the left-hand side, by ordered pairs, taking care to follow the structure [quadrant- t_1 , subquadrant- t_1 , quadrant- t_2 , subquadrant- $t_2 \dots$] etc. The output vector is formed in a similar way. Since the maximum length of the output vector of the neural network is 45 elements, or 15 points, noted as $t_1, t_2 \dots t_n$, where $\max(n) = 15$, defined by ordered three [referee1pos, referee2pos, referee3pos], all values of the input vector are set to 0 and are filled, starting from the left-hand side, by ordered threes, taking care to follow the structure [referee1pos - t_1 , referee2pos - t_1 , referee3pos - t_1 , referee1pos - t_2 , referee2pos - t_2 , referee3pos - t_2, \dots] etc. Tables 1 and 2 show the basketball action consisting of four key points, described by ordered pairs [quadrant, sub-quadrant] and the ideal positions of the basketball referees for such action, described by ordered threes [referee1pos, referee2pos, referee3pos]. Tables 3 and 4 show the form of the input and output vectors of the neural network for the basketball actions given in Tables 1 and 2.

Table 1
Point coordinates

Point	Quadrant	Subquadrant
t_1	1	4
t_2	6	2
t_3	4	3
t_4	5	1

Table 2
Ideal positions of basketball referees

Point	referee1pos	referee2pos	referee3pos
t_1	4	6	5
t_2	1	8	9
t_3	5	3	1
t_4	10	6	7

Table 3
Input vector of neural network

I.V.E.V.	1	4	6	2	4	3	5	1	0	0	0	...	0
Index	0	1	2	3	4	5	6	7	8	9	10	...	29
Point	t ₁		t ₂		t ₃		t ₄						

Table 4
Output vector of the neural network

O.V.E.V.	4	6	5	1	8	9	5	3	1	10	6	7	0	...	0
Index	0	1	2	3	4	5	6	7	8	9	10	11	12	...	44
Point	t ₁			t ₂			t ₃			t ₄					

I.V.E.V. - Input Vector Element Values O.V.E.V. - Output Vector Element Values

The total set of the training data for this neural network consists of 43 differently defined actions and ideal paths for the referees for each one; for one action, there is only one ideal path. These actions vary in length, based on the previously established rule that they may not be longer than 15 key points. Table 5 shows the relation between the actions' lengths and the number of their instances in the total set of training data.

Table 5
Relation between actions length and number of their instances in a training data set

Action length	No. of instances
3	5
4	4
5	4
6	6
7	4
8	3
9	3
10	6
11	5
12	3
Total	43

The neural network was trained in two ways:

- By sequential repetition
- By sequential repetition with progressive action development

Neural network training by sequential repetition understands the passing of pairs of input and output vectors, one after another, until all 43 pairs are passed as intended to train the neural network. When all pairs (patterns) are passed, this

cycle continues as many times as defined in the Iterations configuration of the neural network. Specifically, regarding settings from Figure 7, 43 pairs of input and output vectors will be passed through neural network 15,000 times, and thus the training will be done.

Neural network training by sequential repetition with progressive action development understands the passing of pairs of input and output vectors, one after another, but this action is treated progressively, i.e. from time aspect. Suppose that an action used for neural network training has four key points. First, the first key point of an action will be passed into the network, namely the ordered pair [quadrant, sub-quadrant] with corresponding output ordered three [referee1pos, referee2pos, referee3pos] as the input and output vector as shown in Tables 3 and 4. After that, in a similar way, the first and second key point will be passed through the neural network; then first, second and third one and so on until the full action length is reached. If this action is four key points long, the whole progressive sequence must be used for this input/output pattern, $[t_1]$, $[t_1, t_2]$, $[t_1, t_2, t_3]$, $[t_1, t_2, t_3, t_4]$, where t_n is the action key point, until there are no new patterns for training. When all pairs (patterns) are passed for training of the neural network, this cycle is repeated as many times as defined in the Iterations settings of the neural network.

Neural network training by the method of Sequential repetition with progressive action development is formed with the aim of minimizing the influence of input nodes on output nodes if those cannot occur within the given task. It has been mentioned that a structure of a formed neural network includes all the neurons from a layer being connected to all the neurons from an adjacent one. By bringing certain input vector into the neural network, all the neurons from the first layer are activated and the further propagation of the signal through the neural network activates all the output neurons of the network. In this way, any value in the output vector sequence depends on the previous values in the input vector sequence. During neural network training by the method of Sequential repetition, with direct training using the input vector comprised of all the points of action, from t_1 to t_n , and the output vector comprised of the complete positions list for the given key points of action, correlation is attained so that the values of the referee positions for point t_k , $k \subseteq n$, are strongly dependent on all previous points, i.e. on point set $S = \{t_1, \dots, t_{k-1}\}$.

The advantages of neural network training using the method of Sequential repetition with progressive action development, in comparison to method of Sequential repetition, are summarized in two points:

- Decreased influence of input node sequence values on certain values of output node sequence values, reflected as solutions produced by thus trained neural network. These solutions are closer to expected, common-sense logical solutions for particular situation than solutions given by the neural network trained by the Sequential repetition method.

- Application of the Sequential repetition method with progressive action development over the same set of patterns for neural network training, quantitatively multiplied number of patterns used for its training. New patterns, formed during neural network training, were formed as subsets of existing patterns.

Now we will consider these theses in more detail, with explanations using data used in tests.

Neural network trained by the method of Sequential repetition gives satisfactory results for actions between 3 and 12 key points long, as defined in training set. Nevertheless, such a neural network could not manage with actions shorter than 3 and longer than 12 key points, which is quite logical. However, if a neural network knows how to find ideal paths for actions longer than 3 key points, why could it not, without any particular training for such cases, find ideal paths for referees in shorter actions?

The answer is given by the method of Sequential repetition with progressive action development. Since for every action defined and its ideal path, through defined points, the neural network is progressively trained, it will be passively trained by subset of actions shorter than the particular action being taught to the neural network. By this method, for action 3 key points long, the neural network will be, in a single pass for this action, also trained for actions that are 1, 2 and 3 key points long. Theoretically, this means that by defining a large number of actions (the currently maximal supported length is 15 key points) such a neural network may be trained in a very short time. Nevertheless, quality training of neural networks is based on the quality, representativeness, variety and validity of the examples used for the neural network training. In this way, neural network training based solely on 15 key points length actions decreases the quality of the neural network, especially bearing in mind that most basketball actions consists of 3 to 8 key points, while longer ones are rarely longer than 12 key points. Tables 6 and 7 show relations between action length and number of their instances in the training data set by using the method of Sequential repetition with progressive action development.

Based on the data from Tables 5 and 7, we may conclude that the method of Sequential repetition with progressive action development considerably increases the data set for training a neural network, in this case about 8 times, from 43 to 317 specimens of training data.

A larger training data set contributes to greater precision of the neural network, which improves its conclusions. In comparative test for actions similar to those used in the training, the output vectors were formed similar to those in similar action from training set. Specifically, the neural network that was trained by the method of Sequential repetition sometimes gave output vectors of position values deviating for +/- 2 to 3 notches (on a fixed scale of referee movement lines) from the common-sense logical expected value.

Table 6

Relation between action length and number of instances in data set for training using method of Sequential repetition with progressive action development

Table 7

Relation between action length and number of their instances in data set for training using method of Sequential repetition with progressive action development – final

Action length	No. of instances	Progressively
3	5	15
4	4	16
5	4	20
6	6	36
7	4	28
8	3	24
9	3	27
10	6	60
11	5	55
12	3	36
Total	43	317

Action length	No, of instance
1	43
2	43
3	43
4	38
5	34
6	30
7	24
8	20
9	17
10	14
11	8
12	3
Total	317

Table 6

Table 7

For actions for which the neural network was trained, independently of the method of training, it gave identical output vectors as attached to such action during the training. An increase or decrease of iteration number, before neural network training by the method of Sequential repetition, influenced the solution quality produced by such a trained neural network. By increasing the iteration number to 30000, such a trained neural network gave results close to results given by the neural network trained by the method of Sequential repetition with progressive action development. Nevertheless, the neural network trained by this method still gave better results. The assumption is that, during progressive action development for the neural network training, paths were shaped for action subsets formed in the course of this development, with strong difficulty coefficients that steered the neural network to a better and more optimal (expected) solution.

The neural networks, trained by these methods, had in all cases correctly established correlation between number of input and output points as input and output vectors. If input action has 4 points, input vector is represented by a sequence of 30 elements, from which the first 8 elements are values for the quadrant and sub-quadrant of points for the key actions formed by previously described rules, while all the other elements of input vector are equal to zero.

Based on this input vector, the output vector is formed as a sequence of 45 elements, from which the first 12 elements are values for referee positions based on the previously described rules, while the other elements of the output vector are equal to zero. For the calculation of ideal paths for animation purpose, zero values of the output vectors are neglected, while calculated values are read and formed based on the previously described rule.

5 NN Trainer - Appearance and Usage

The NN Trainer is called by activating the option Train Neural Network, in the Neural Network submenu of the main form of the BBFBR program. The NN Trainer is used, as the name implies, for training and configuring the neural network. The tool mentioned, which is shown in Figure 8, consists of three segments:

- Main menu
- Area for configuring the input and output data of the neural network
- Area for configuring the neural network

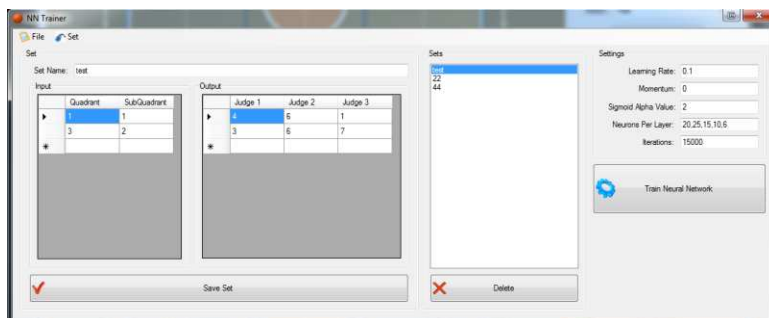


Figure 8
Appearance of the NN Trainer tool

The main menu consists of two submenus: *File* and *Set*.

The file submenu contains four options:

- *Load Neural Network Training Data* – This option reads the *.nnet binary file that contains the actions which will serve for training the neural network
- *Save Neural Network Training Data* – This option creates the *.nnet binary file that contains the actions which will train or have already trained the neural network

- *Train Neural Network* – This option starts the training of the neural network by defined or read input and output data and clearly determined configuration of the neural network, which will be described in more detail later in the text.
- *Save Neural Network As* – This option saves the trained neural network in the binary file with the extension *.ann

The Set submenu has only one option - *New Set*. Activating the New Set option, the control for defining a new set of data for training the neural network, is initialised.

The area for configuring the input and output data of the neural network defines the data for training the neural network leaning on the quadrants and sub-quadrants of the basketball court and twelve fixed positions for each referee.

The section mentioned consists of two parts: The Set and the Sets section. The Set section consists of an input and output table. Rows of the input table are pairs quadrant and sub-quadrant, thereby showing the location of the ball in the court. The rows of the output table are arranged in threes, which, for one position, define the positions of the referees on the fixed scale from 1 to 12. Analysing picture 16, it can be concluded that, for a position of the ball in quadrant 1, sub-quadrant 1, referee 1 should be in position 4, referee 2 in position 6, and referee 3 in position 1. One set for training is one action, which is defined by the path of the ball which consists of the rows of the input table, and the trio from the rows of the output table. Each set of data for training has its own name.

The neural network chosen for solving this problem is a multi-layer neural network with a Sigmoid Bipolar activation function and is trained by the Back Propagation algorithm. In the settings section, all crucial parameters for training the neural network can be found. By analyzing Figure 7, the following parameters can be found:

- *Learning Rate* – This parameter shows the speed of the neural network's learning. The default value is 0.1
- *Momentum* – The momentum of the neural network. The default value is 0.
- *Sigmoid Alpha Value* – The value of the alpha parameter of the Sigmoid bipolar activating function of belonging. The default value is 2. The value of the output values of mentioned function are from -1 to 1.
- *Neurons Per Layer* – The number of neurons per a hidden layer of the neural network. The layers are separated with comma, whilst the numbers show how many neurons there are in each layer. In Figure 7, the value of the box Neurons Per Layer is: 20,25,15,10,6, which means that the neural network has 5 hidden layers. The first hidden layer has 20 neurons, second hidden layer has 25 neurons, etc.
- *Iterations* – The number of iterations required for training the neural network.

The input vector of the neural network has 30 elements, while the output vector has 45 elements, so, in conclusion, the trained neural network in this example has 7 layers in total. This enables the calculation of the ideal position of the referees for actions up to 15 key points, actually the key positions of the ball, although it is statistically shown that the action is usually finished within 6 to 10 key ball points.

Conclusions

Solution BBFBR has shown good results and the solution itself is still in the stage of development. The current realization of the BBFBR solution has implemented only a simple computation of the optimal path for the basketball referees in some actions. Therefore, it currently has only an educational purpose, which means that it can be used for training young basketball referees. During further development of the BBFBR solution, the paths of the basketball players will be implemented, so the percentage of visibility of a certain part of an action from the aspect of a certain referee can be determined. As a next step in the development, the implementation of the retroactive analysis with the research of the percentage of visibility of an action from the aspect of the field of visibility of a referee is planned, and if the results are satisfactory, it will be followed by the use of the adaptive neural networks, so the movement of the referees does not simply depend on the movement of the ball in the court, but on the position and the ability of observing on the part of the other referees as well. Calculating the percentage of visibility will be based on the rules of human visual field, fuzzy controllers and percentage coverage of the visual field. Based on the results mentioned, micro corrections of the referees' positions will be possible, which means that fuzzy controllers will add to the outputs of the neural network. [7]

In addition, further plans for the BBFBR solution include the integration with data mining techniques based on video recording, animations and other techniques. [9]

Acknowledgements

This work was partially supported by the Serbian Ministry of Education and Sciences (Grant No: 171039).

References

- [1] Zdravko Ivankovic, Milos Rackovic, Branko Markoski, Dragica Radosav, Miodrag Ivkovic, "Appliance of Neural Networks in Basketball Scouting", Acta Polytechnica Hungarica, Vol. 7, Issue 4, 2010
- [2] José Manuel Sánchez Santos, Ana Belen Porto Pazos, Alejandro Pazos Sierra, "Team Performance in Professional Basketball: an Approach Based on Neural Networks and Genetic Programming ", XIII IASE and III ESEA Conference of Sports, Prague, May 2011
- [3] Michael E. Young, "Nonlinear Judgment Analysis: Comparing Policy Use by Those Who Draft and Those Who Coach", Psychology of Sport and Exercise, Volume 9, Number 6, November 2008

- [4] Bernard Loeffelholz, Earl Bednar, Kenneth W. Bauer "Predicting NBA Games Using Neural Networks", *Journal of Quantitative Analysis in Sports*: Vol. 5, Issue 1, Article 7, 2009
- [5] Dean Oliver, "Basketball on Paper – Rules and Tools for Performance Analysis", Brassey's, Washington DC, 2004
- [6] Ratgeber, L. Play from a Game: (Head Coach). Mizo Pecs 2010. 2007/2008. Mizo Pecs 2010 vs. Euroleasing Sopron
- [7] Rita Lovassy, László T. Kóczy, László Gál, "Function Approximation Performance of Fuzzy Neural Networks" *Acta Polytechnica Hungarica*, Vol. 7, Issue 4, 2010
- [8] Martin Sarnovský, Peter Butka, Ján Paralič, "Grid-based Support for Different Text Mining Tasks", *Acta Polytechnica Hungarica*, Vol. 6, Issue 4, 2009
- [9] Bojan Kuljić, János Simon, Tibor Szakáll "Pathfinding Based on Edge Detection and Infrared Distance Measuring Sensor" *Acta Polytechnica Hungarica*, Vol. 6, Issue 1, 2009
- [10] Vasiljevic P. Markoski B., Ivankovic Z., Setrajcic J., Milosevic Z., "Basket Supervisor- Collection Statistiacal Data in Basketball and Net Casting" *Technics Technologies Education Management-TTEM*, 169-178, 2011
- [11] FIBA – Basketbal Statisticians Manual (2008)
- [12] FIBA – Basketbal Statisticians Manual (2011)

Similarity Solution to a Thermal Boundary Layer Model of a non-Newtonian Fluid with a Convective Surface Boundary Condition

Gabriella Bognár, Krisztián Hriczó

University of Miskolc, 3515 Miskolc-Egyetemváros Hungary
matvbg@uni-miskolc.hu, krisztian.hriczo@gmail.com

Abstract: The steady laminar boundary layer flow of a non-Newtonian fluid over an impermeable flat plate in a uniform free stream is investigated when the bottom surface of the plate is heated by convection from a hot fluid. We show that similarity solutions to the hydrodynamic and thermal boundary layers are possible if the convective heat transfer associated with the hot fluid on the lower surface of the plate is proportional to a power function of x , where x is the distance from the leading edge of the solid surface. The equations of momentum and energy are transformed into a system of ordinary differential equations. Numerical solutions are provided and the effects of the parameters are examined on the flow and thermal fields.

Keywords: boundary layer; convective boundary condition; heat transfer; similarity solution

1 Introduction

Although the classical problem of a fluid flow along a horizontal, stationary surface located in a uniform free stream was first solved by Blasius [4], it is still a subject of current research (see e.g. [1], [5], [6]-[9]). Convective heat transfer is very important in processes involving high temperature, e.g. gas turbines, nuclear power plants, and thermal energy storage [3]. Recently, the problem of laminar hydrodynamic and thermal boundary layers over a flat plate with convective boundary condition has been examined for a Newtonian fluid, when the bottom surface of the plate is heated by convection from a hot fluid. The similarity solutions to the convective heat transfer problems have been studied by Aziz [2] and Magyari [11] for an impermeable plate, and by Ishak [9] for a permeable plate.

The aim of this paper is to extend the work of Aziz [2] by investigating the hydrodynamic and thermal boundary layers for power-law non-Newtonian fluid on an impermeable plate.

2 Basic Equations

We consider a steady two-dimensional laminar flow of a viscous, incompressible fluid of density ρ and temperature T_∞ over the top surface of a semi-infinite horizontal impermeable stationary flat plate. We assume that the free stream moves on the top of the solid surface with a constant velocity U_∞ . It is assumed that the bottom surface of the plate is heated by convection from a hot fluid of temperature T_f .

Within the framework of the above-noted assumptions, the governing equations of motion and heat transfer for non-Newtonian flow neglecting pressure gradient and body forces can be described by the following equations [13]:

$$\frac{\partial u}{\partial x} + \frac{\partial v}{\partial y} = 0, \quad (1)$$

$$u \frac{\partial u}{\partial x} + v \frac{\partial u}{\partial y} = \frac{1}{\rho} \frac{\partial \tau_{xy}}{\partial y}, \quad (2)$$

$$u \frac{\partial T}{\partial x} + v \frac{\partial T}{\partial y} = \frac{\partial}{\partial y} \left(\alpha_t \frac{\partial T}{\partial y} \right) \quad (3)$$

where u , v are the velocity components along x and y coordinates, respectively, T is the temperature of the fluid in the boundary layer. Furthermore, we apply power-law relation between the shear stress and the shear rate by

$$\tau_{xy} = K \left| \frac{\partial u}{\partial y} \right|^{n-1} \frac{\partial u}{\partial y}, \text{ where } \gamma \left| \frac{\partial u}{\partial y} \right|^{n-1} \text{ denotes the kinematic viscosity, } K \text{ is the}$$

consistency index for non-Newtonian viscosity and α_t is the thermal diffusivity and $\gamma = \frac{K}{\rho}$. Here, n is called the power-law index, that is $n < 1$ for

pseudoplastic, $n = 1$ for Newtonian, and $n > 1$ for dilatant fluids. Then, (2) becomes

$$u \frac{\partial u}{\partial x} + v \frac{\partial u}{\partial y} = \frac{\partial}{\partial y} \left(\gamma \left| \frac{\partial u}{\partial y} \right|^{n-1} \frac{\partial u}{\partial y} \right).$$

The applicable boundary conditions for the present model are

- i. on the plate surface $y = 0$ (no slip, impermeable surface and convective surface heat flux)

$$u(x,0) = 0, \quad (4)$$

$$v(x,0) = 0, \quad (5)$$

$$-k \frac{\partial T}{\partial y} = h_f (T_f - T_w), \quad (6)$$

where h_f is the heat transfer coefficient, and k denotes the thermal conductivity;

ii. matching with the free stream as $y \rightarrow \infty$

$$u(x, \infty) = U_\infty, \quad (7)$$

$$T(x, \infty) = T_\infty. \quad (8)$$

If T_w denotes the uniform temperature over the top surface of the plate we have the relations: $T_f > T_w > T_\infty$.

Introducing the following dimensionless variables

$$\psi = b x^{-\alpha} f(\eta),$$

$$\eta = a \frac{y}{x^\beta},$$

$$w(x, y) = \frac{T - T_\infty}{T_f - T_\infty},$$

for some constants a, b, α, β , where Ψ is the stream function. For $u = \frac{\partial \psi}{\partial y}$,

$v = -\frac{\partial \psi}{\partial x}$, the equation of continuity (1) is satisfied identically. On the other

hand, we have

$$\psi_y \psi_{yx} - \psi_x \psi_{yy} = \gamma (|\psi_{yy}|^{n-1} \psi_{yy})_y \quad (9)$$

and conditions (4), (5), (7) can be written as

$$\psi_y(x,0) = 0, \quad \psi_x(x,0) = 0, \quad \psi_y(x, \infty) = U_\infty. \quad (10)$$

Applying similarity variable η we derive

$$\psi_x = -b x^{-\alpha-1} [\alpha f + \beta \eta f'], \quad \psi_y = a b x^{-\alpha-\beta} f', \quad (11)$$

where a prime denotes differentiation with respect to η . By inserting (10) and (11) into (9) we get

$$\left(|f''|^{n-1} f'' \right)' - \alpha f f'' + (\alpha + \beta) f'^2 = 0 \quad (12)$$

if $(2-n)\alpha + (2n-1)\beta = 1$ and $\gamma a^{2n-1} b^{n-2} = 1$. Taking boundary condition (7) we have $ab = U_\infty$ and $\alpha + \beta = 0$. In order to satisfy conditions in (10), for a, b, α, β one gets

$$\beta = -\alpha = \frac{1}{n+1}, \quad a = \gamma^{-\frac{1}{n+1}} (U_\infty)^{\frac{2-n}{n+1}}, \quad b = \gamma^{\frac{1}{n+1}} (U_\infty)^{\frac{2n-1}{n+1}}$$

and

$$\psi(x, y) = \gamma^{\frac{1}{n+1}} (U_\infty)^{\frac{2n-1}{n+1}} x^{\frac{1}{n+1}} f(\eta), \quad \eta = \gamma^{-\frac{1}{n+1}} (U_\infty)^{\frac{2-n}{n+1}} \frac{y}{x^{\frac{1}{n+1}}}.$$

Equation (12) with the transformed boundary conditions has the form

$$\left(|f''|^{n-1} f'' \right)' + \frac{1}{n+1} f f'' = 0, \quad (13)$$

$$f'(0) = 0, \quad f(0) = 0, \quad f'(\infty) = \lim_{\eta \rightarrow \infty} f'(\eta) = 1. \quad (14)$$

The dimensionless velocity components have the form

$$u(x, y) = U_\infty f'(\eta),$$

$$v(x, y) = \frac{U_\infty}{n+1} Re_x^{-\frac{1}{n+1}} (\eta f'(\eta) - f(\eta)),$$

$$\text{and } \eta = Re_x^{\frac{n+1}{x}} \frac{y}{x}, \text{ where } Re_x = \frac{U_\infty^{2-n} x^n}{\gamma} \text{ is the local Reynolds number.}$$

The thermal diffusivity can be defined as $\alpha_t = \omega \left| \frac{\partial u}{\partial y} \right|^{n-1}$ for $u \neq 0$ (ω positive constant) and $\alpha_t = 0$ for $u = 0$ (see [13]). Hence, from equation (3)

$$u \frac{\partial w}{\partial x} + v \frac{\partial w}{\partial y} = \omega \frac{\partial}{\partial y} \left(\left| \frac{\partial u}{\partial y} \right|^{n-1} \frac{\partial w}{\partial y} \right), \quad (15)$$

Defining the non-dimensional temperature by $\Theta(\eta) = w(x, y)$, i.e. $T = T_\infty + \Theta(\eta)(T_f - T_\infty)$ we get

$$\left(|f''(\eta)|^{n-1} \Theta'(\eta) \right)' + \frac{\text{Pr}}{n+1} f(\eta) \Theta'(\eta) = 0, \quad (16)$$

where $\text{Pr} = \frac{\gamma}{\omega}$ is the Prandtl number. The transformed boundary conditions for the energy equation (16)

$$\Theta'(0) = - \left(\frac{\gamma}{U_\infty^{2-n}} x \right)^{\frac{1}{n+1}} \frac{h_f(x)}{k} (1 - \Theta(0))$$

and substituting $\bar{a} = \frac{c}{k} \left(\frac{\gamma}{U_\infty^{2-n}} \right)^{\frac{1}{n+1}}$ one can obtain

$$\Theta'(0) = -\bar{a}(1 - \Theta(0)) \quad (17)$$

under the assumption that the heat transfer coefficient $h_f = cx^{-1/(n+1)}$. We note that for Newtonian fluids it was shown in [2], [3], [9] that similarity solutions exist if h_f is proportional to $x^{-1/2}$. For a uniform surface temperature $\Theta(0) = 1$ holds and from (17) $\Theta'(0) = 0$. This adiabatic case has been analysed by Magyari [10] for Newtonian fluid.

Boundary condition (8) can be formulated

$$\Theta(\infty) = \lim_{\eta \rightarrow \infty} \Theta(\eta) = 0. \quad (18)$$

According to our knowledge there is no exact solution; therefore one has to use a numerical technique to solve the boundary value problems for the similarity equations (13), (14), (16), (17), (18).

3 Results

The nonlinear ordinary differential equation (13) subject to the boundary conditions in (14) were solved numerically using the symbolic algebra software Maple 12. The boundary value problem has been solved by the Runge-Kutta-Fehlberg fourth-fifth method. Fig. 1 shows the Maple generated numerical solution for the velocity profiles for different values of n .

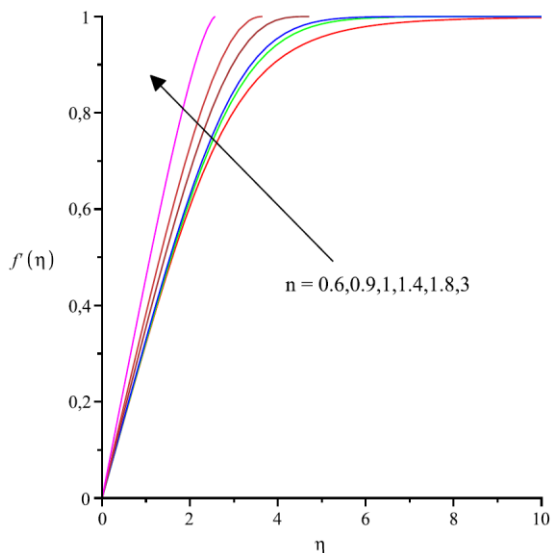


Figure 1

The profiles of $f'(\eta) = u(x, y)/U_\infty$ for different values of n

For fixed Prandtl numbers 0.72 and 10, for selected values of the power index n , for a range of parameters \bar{a} Table 1 and Table 2 provide the numerical data for $-\Theta'(0)$ and $\Theta(0)$, respectively. In the case of $n=1$, the numerical values show a good agreement with those reported by Aziz [2] and Ishak [8].

Figures 2-4 exhibit that the plate surface temperature decreases as either Pr or n increases and also when \bar{a} decreases. The temperature gradient at the surface increases as Pr increases, which implies an increase in the heat transfer rate at the surface. We observe that the thermal boundary layer thickness decreases with an increasing Prandtl number or increasing power index n ; moreover, the hydrodynamic boundary layer thickness decreases as n increases.

Table 1
 Values of $-\Theta'(0)$ for various values of \bar{a} , Pr and n

\bar{a}	$n = 0.5$		$n = 1$		$n = 1.5$	
	$\text{Pr} = 0.72$	$\text{Pr} = 10$	$\text{Pr} = 0.72$	$\text{Pr} = 10$	$\text{Pr} = 0.72$	$\text{Pr} = 10$
0.05	0.043392	0.046625	0.042767	0.046787	0.043390	0.047138
0.10	0.076655	0.087355	0.074724	0.087925	0.076647	0.089174
0.20	0.124294	0.155101	0.119295	0.156903	0.124273	0.160928
0.40	0.180329	0.253329	0.169994	0.258174	0.180285	0.269255
0.60	0.212221	0.321120	0.198051	0.328945	0.212159	0.347148
0.80	0.232808	0.370723	0.215864	0.381191	0.232732	0.405853
1	0.247195	0.408591	0.228178	0.421344	0.247110	0.451682
5	0.308129	0.607006	0.279131	0.635583	0.307997	0.707239
10	0.317925	0.646233	0.287146	0.678721	0.317784	0.761065
20	0.323061	0.667811	0.291328	0.702563	0.322915	0.791172

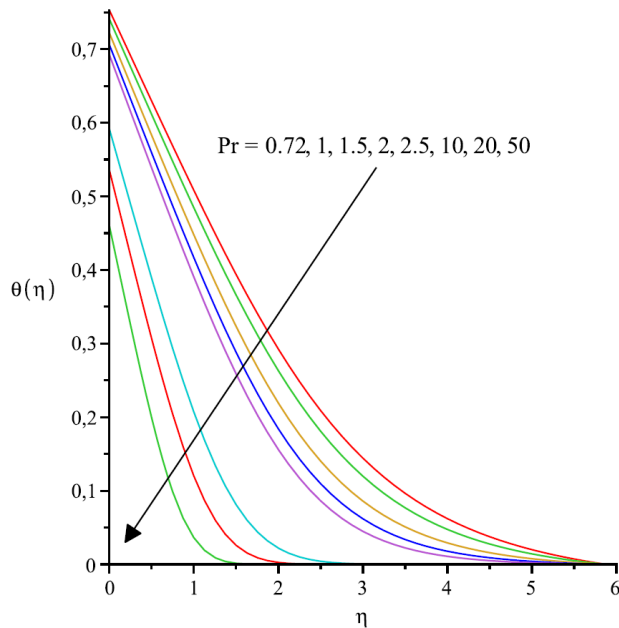


Figure 2
 Temperature profiles for different values of Pr when $n=0.5$ and $\bar{a}=1$

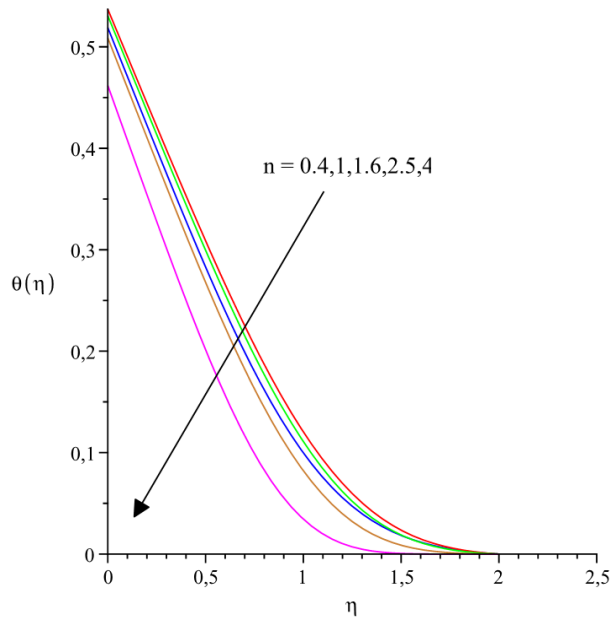


Figure 3

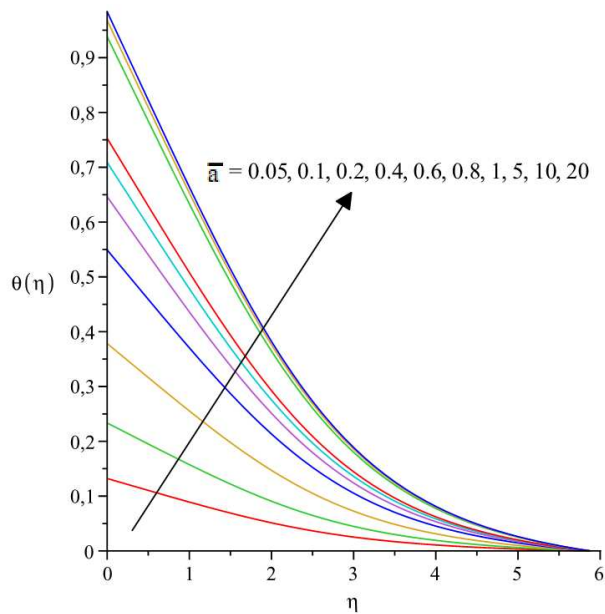
Temperature profiles for different values of n when $Pr=10$ and $\bar{a}=1$ 

Figure 4

Temperature profiles for different values of \bar{a} when $Pr=0.72$ and $n=0.5$

Table 2
Values of $\Theta(0)$ for various values of \bar{a} , Pr and n

\bar{a}	$n = 0.5$		$n = 1$		$n = 1.5$	
	$Pr = 0.72$	$Pr = 10$	$Pr = 0.72$	$Pr = 10$	$Pr = 0.72$	$Pr = 10$
0.05	0.132148	0.067487	0.144661	0.064256	0.132200	0.057224
0.10	0.233446	0.126441	0.252758	0.120752	0.233528	0.108253
0.20	0.378526	0.224497	0.403523	0.215484	0.378634	0.195359
0.40	0.549175	0.366677	0.575014	0.354566	0.549289	0.326862
0.60	0.646298	0.464799	0.669916	0.451759	0.646402	0.421420
0.80	0.708990	0.536596	0.730170	0.523512	0.709085	0.492684
1	0.752805	0.591408	0.771822	0.578656	0.752890	0.548318
5	0.938374	0.878599	0.944173	0.872883	0.938401	0.858552
10	0.968207	0.935377	0.971285	0.932128	0.968222	0.923894
20	0.983847	0.966609	0.985434	0.964872	0.983854	0.960441

Conclusions

In this paper we studied the problem of steady laminar boundary layer flow and heat transfer over a stationary flat surface in a parallel stream with convective boundary condition. Similarity solution to the thermal field is possible when the convective heat transfer from the lower surface varies like $x^{-1/(n+1)}$, where x is the distance from the plate. On the flow and thermal fields, the influence of the governing parameters, the Prandtl number, the power index n and the value of \bar{a} characterizing the hot fluid convection process is discussed.

Acknowledgement

This research was carried out as part of the TAMOP-4.2.1.B-10/2/KONV-2010-0001 project with support by the European Union, co-financed by the European Social Fund.

References

- [1] Ahmad F., Al-Barakati W. H.: An approximate Analytic Solution of the Blasius Problem, *Comm. Nonlinear Sci. Num. Simul.*, **14** (2009), pp. 1021-1024
- [2] Aziz A.: A Similarity Solution for Laminar Thermal Boundary Layer over a Flat Plate with a Convective Surface Boundary Condition, *Comm. Nonlinear Sci. Numer. Simulat.* **14** (2009), pp. 1064-1068
- [3] Bataller R. C.: Radiation Effects for the Blasius and Sakiadis flows with a Convective Surface Boundary Condition, *Appl. Math. Comput.* **206** (2008), pp. 832-840

-
- [4] Blasius H.: Grenzsichten in Flüssigkeiten mit kleiner reibung, *Z. Math. Phys.*, **56** (1908), pp. 1-37
- [5] Cortell R.: Numerical Solutions of the Classical Blasius Flat-Plate Problem, *Appl. Math. Comput.*, **170** (2005), pp. 706–710
- [6] Dénes J, Patkó I.: Computation of Boundary Layers, *Acta Polytechnica Hungarica*, **1** (2004), pp. 79-87
- [7] He J. H.: A Simple Perturbation Approach to Blasius Equation, *Appl. Math. Comput.*, **140** (2003), pp. 217-222
- [8] He J. H.: Approximate Analytical Solution of Blasius Equation, *Comm. Nonlinear Sci. Num. Simul.*, **3** (1998), pp. 260-263
- [9] Ishak A.: Similarity Solution for Flow and Heat Transfer over a Permeable Surface with Convective Boundary Condition, *Appl. Math. Comput.* **217** (2010), pp. 837-842
- [10] Liao S. J.: An Explicit, Totally Analytic Approximate Solution for Blasius Viscous Flow Problems, *Int. J. Non-Linear Mech.*, **34** (1999), pp. 759-778
- [11] Magyari E.: The Moving Plate Thermometer, *Int. J. Therm. Sci.*, **47** (2008), pp. 1436-1441
- [12] Magyari E.: Comment on “A Similarity Solution for Laminar Thermal Boundary Layer Over a Flat Plate with a Convective Surface Boundary Condition” by A. Aziz, *Comm. Nonlinear Sci. Numer. Simul.* 2009; 14:1064-8, *Comm. Nonlinear Sci. Numer. Simulat.* **16** (2011), pp. 599-601
- [13] Zheng L., Zhang X., He J.: Suitable Heat Transfer Model for Self-Similar Laminar Boundary Layer in Power Law Fluids, *J. Thermal Science* **13** (2004), pp. 150-154

Speed Control of Induction Motor Using Genetic Algorithm-based PI Controller

M'hamed Chebre¹, Abdelkader Meroufel², Yessema Bendaha¹

¹Department of Electrical Engineering, University of Sciences and Technology (USTO) BP 1505 EL M'naouer, Oran Algeria, e-mail: chebre_mhamed@yahoo.fr

²Department of Electrical Engineering, Djilala Liabes University, BP 89 Sidi Bel-Abbes, Algeria, e-mail: ameroufel@yahoo.fr

Abstract: In this paper, we present the design of a Proportional Integral (PI) controller using Genetic Algorithm (GA) to control the speed of an induction motor (IM) using indirect field-oriented control method (IFOC). The main advantage of this metaheuristic method (GA) is its simplicity. Based on a criterion defined using an objective function, it helps in the optimal calculation of the PI controller parameters. Several tests of tracking and control by PI-GA are analyzed and compared to the conventional PI controller. The simulation results obtained using Matlab/Simulink showed that the proposed controller had on one hand a good dynamic and static performance and on other hand had a better robustness compared to the conventional PI controller.

Keywords: induction motor; PI controller; IFOC; vector control; genetic algorithm

1 Introduction

Nowadays, as a consequence of the important progress in power electronics and micro-computing, the control of AC electric machines has seen considerable development and the possibility for application [1]. The induction motor, known for its robustness, relatively low cost, reliability and efficiency, is the object of several research works. However its control presents difficulties because of its high non-linearity and its highly coupled structure [2]. The technique known as vector control, first introduced by Blaschke and Hasse, has resulted in a large change in the field of electrical drives. This is because, with this type of control, the robust induction motor can be controlled with high performance. This control strategy can provide the same performance as achieved from a separately excited DC motor [3, 4]. The best known controller used in industry is the proportional-integral (PI) because of its simple structure and its robust performance in a wide range of operating conditions. This linear regulator is based on a very simple structure, whose functioning depends only on two parameters, namely the

proportional gain (kp) and the integral gain (ki). Several methods of tuning a PI controller have been proposed in the literature; the most used are the poles assignment method and the Ziegler-Nichols method [5, 6]. However, the major inconvenience of these two is the necessity of the a priori knowledge of the various parameters of the induction motor. To surmount this inconvenience, we can use a procedure of optimization to better design this type of controller. Genetic Algorithm methods have been widely used in control applications. They are stochastic optimization methods based on the principles of natural biological evolution. The GA methods have been employed successfully to solve complex optimization problems. The use of GA methods in the determination of the different controller parameters is practical due to their fast convergence and reasonable accuracy [7]. The parameters of the PI controller are determined by the minimization of an objective function. The goal of this work is to show that by the optimization of the parameters of the PI controller, an optimization can be achieved. This can be seen by comparing the result of the genetic algorithm based PI controller and the conventional PI controller.

This paper is divided into six sections. The indirect field-oriented control of an induction motor is presented in Section 2, the optimization by GA method is summarized in Section 3, and the optimization of the PI controller parameters by the GA method is developed in Section 4. Simulation results are reported in Section 5. Section 6 concludes the paper.

2 Indirect Field-oriented Control of the IM

The dynamic model of the induction motor can be expressed in the d-q synchronously rotating frame as [8, 9].

$$\left\{ \begin{array}{l} \frac{di_{sd}}{dt} = -\left(\frac{R_s L_r^2 + M^2 R_r}{\sigma L_s L_r^2}\right) i_{sd} + \omega_s i_{sq} + \frac{MR_r}{\sigma L_s L_r^2} \phi_{rd} + \frac{M}{\sigma L_s L_r} \omega \phi_{rq} + \frac{1}{\sigma L_s} v_{sd} \\ \frac{di_{sq}}{dt} = -\left(\frac{R_s L_r^2 + M^2 R_r}{\sigma L_s L_r^2}\right) i_{sq} - \omega_s i_{sd} - \frac{M}{\sigma L_s L_r^2} \omega \phi_{rq} - \frac{M}{\sigma L_s L_r} \omega \phi_{rd} + \frac{1}{\sigma L_s} v_{sq} \\ \frac{d}{dt} \phi_{rd} = -R_r \left(\frac{\phi_{rd}}{L_r} - \frac{M}{L_r} i_{sd}\right) + \phi_{rq} (\omega_s - \omega) \\ \frac{d}{dt} \phi_{rq} = -R_r \left(\frac{\phi_{rq}}{L_r} - \frac{M}{L_r} i_{sq}\right) - \phi_{rd} (\omega_s - \omega) \\ \frac{d\omega}{dt} = \frac{1}{J} \left(\frac{MP^2}{L_r} (\phi_{rd} i_{sq} - \phi_{rq} i_{sd}) - p T_L - f_c \omega\right) \end{array} \right. \quad (1)$$

$$\sigma = 1 - \frac{M^2}{L_s L_r} \quad (2)$$

where i , ϕ , v denote current, flux linkage and voltage, respectively. Subscripts s and r stand for stator and rotor. ω is the rotor speed, d and q denote direct and quadratic components of the vectors with respect to the fixed stator reference frame, L and R are the auto-inductances and resistances, M is the mutual inductance, T_L is the load torque, P is the pole pairs, f_c is the viscous friction coefficient and σ is the coefficient of dispersion.

The vector control of the induction motor is a well-accepted method when high levels of performance of the system response are required. It is based on the decoupling of the magnetizing and torque-producing components of the stator current. Under this condition, the q -axis component of the rotor flux is set to zero, while the d -axis reaches the nominal value of the magnetizing flux, and it follows that [3]:

$$\phi_{rq} = \frac{d\phi_{rq}}{dt} = 0 \quad (3)$$

$$\phi_{rd} = \phi_r \quad (4)$$

Applying the results of (3) and (4), namely the field-oriented control, the torque equation becomes analogous to the DC machine and can be described as follows:

$$T_e = \frac{3 P M}{2 L_r} \phi_r i_{sq} \quad (5)$$

And the slip frequency can be given as follows:

$$\omega_{sl} = \omega_s - \omega = \frac{M R_r}{L_r \phi_{rd}} i_{sq} \quad (6)$$

Consequently, the dynamic equations (1) become [10]:

$$\left\{ \begin{array}{l} \frac{di_{sd}}{dt} = -\left(\frac{R_r L_r^2 + M^2 R_r}{\sigma L_s L_r^2}\right) i_{sd} + \omega_s i_{sq} + \frac{M R_r}{\sigma L_s L_r^2} \phi_r + \frac{1}{\sigma L_s} v_{sd} \\ \frac{di_{sq}}{dt} = -\left(\frac{R_s L_r^2 + M^2 R_r}{\sigma L_s L_r^2}\right) i_{sq} - \omega_s i_{sd} - \frac{M}{\sigma L_s L_r} \omega \phi_r + \frac{1}{\sigma L_s} v_{sq} \\ \frac{d\phi_{rd}}{dt} = \frac{M R_r}{L_r} i_{sd} - \frac{R_r}{L_r} \phi_r \\ \frac{d\omega}{dt} = \frac{P^2 M}{L_r J} i_{sd} \phi_r - \frac{f_c}{J} \omega - \frac{P}{J} T_L \end{array} \right. \quad (7)$$

According to the above analysis, the indirect field-oriented control of the induction motor with a current-regulated PWM drive system, and whose the speed is driven by a PI controller, can be presented by the block diagram shown in Fig. 1.

$$P(s) = s^2 + \frac{f_c + K_p P}{J} s + \frac{K_i P}{J} = 0 \quad (9)$$

By the imposition of two poles complex combined with real part negative, $s_{1,2} = \rho(-1 \pm j)$, we obtain the expression for K_p and K_i of the PI controller.

$$\begin{cases} K_i = \frac{2J\rho^2}{P} \\ K_p = \frac{2\rho J - f_c}{P} \end{cases} \quad (10)$$

where ρ is a positive constant.

PI gain values are given below in Table 1.

Table 1
PI: Controller values

Gain Coeff	K_p	K_i
Values	0.588	11.191

3 Genetic Algorithm

GA is a stochastic global adaptive search optimization technique based on the mechanisms of natural selection [11]. GA was first suggested by John Holland and his colleagues in 1975. GA has been recognized as an effective and efficient technique to solve optimization problems. Compared with other optimization techniques, such as simulating annealing and random search method techniques, GA is superior in avoiding local minima, which is a significant issue in the case of nonlinear systems [12]. GA starts with an initial population containing a number of chromosomes where each one represents a solution of the problem, the performance of which is evaluated by a fitness function. Basically, GA consists of three main stages: Selection, Crossover and Mutation. The application of these three basic operations allows the creation of new individuals, which may be better than their parents. This algorithm is repeated for many generations and finally stops when reaching individuals that represent the optimum solution to the problem. The GA architecture is shown in Fig. 3 [11, 13].

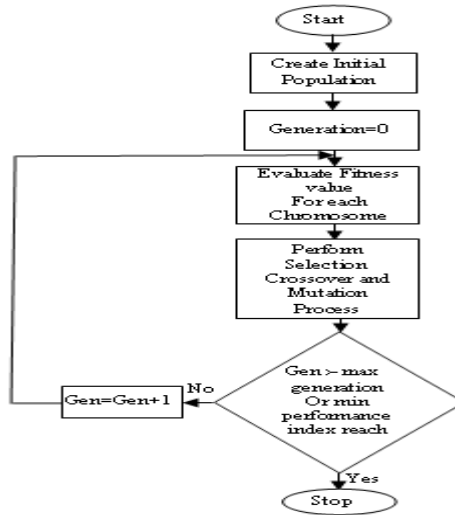


Figure 3
Genetic Algorithm Architecture

3.1 Genetic Operators

In each generation, the genetic operators are applied to selected individuals from the current population in order to create a new population. Generally, the three main genetic operators of reproduction, crossover and mutation are employed. By using different probabilities for applying these operators, the speed of convergence can be controlled. Crossover and mutation operators must be carefully designed, since their choice greatly contributes to the performance of the whole genetic algorithm [14].

3.1.1 Reproduction

A part of the new population can be created by simply copying without change selected individuals from the present population. Also the new population has the possibility of selection by already developed solutions [14].

There are a number of other selection methods available and it is up to the user to select the appropriate one for each process. All selection methods are based on the same principal, i.e. giving fitter chromosomes a larger probability of selection.

Four common methods for selection are:

- 1 Roulette Wheel selection
- 2 Stochastic Universal sampling
- 3 Normalized geometric selection
- 4 Tournament selection

3.1.2 Crossover

The crossover operator is the main operator and is used to produce offspring that are different from their parents but which inherit a portion of their parents' genetic material. Under this operator, a selected chromosome is split into two parts and recombines with another selected chromosome which has been split at the same crossover point. Typically this operator is applied at a rate of 60% to 80% of the population, and the crossover point and each pair is randomly selected [7].

3.1.3 Mutation

The mutation operator plays a secondary role in the evolution. It helps to keep diversity in the population by discovering new or restoring lost genetic materials by searching the neighbourhood solution space. Despite the fact that mutation can serve a vital role in a genetic algorithm, it should be noted that it occurs with a small probability rate of 0.1% to 10% of the entire population [7].

4 Tuning of the PI Speed Controller Using the Genetic Algorithm Approach

GA can be applied in the tuning of the PI speed controller's gains (K_p, K_i) to ensure optimal control performance at nominal condition for the induction motor. The block diagram for the entire system is given below:

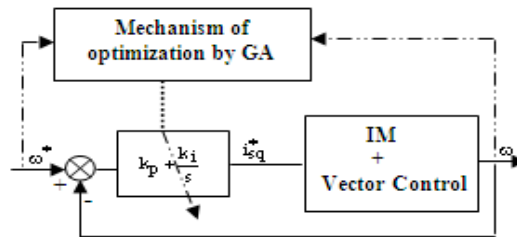


Figure 4

Structure of the technique of optimization of the PI controller by GA

Where:

ω^* is the speed reference

ω is the real speed of the induction motor

The objective function used is the following one [15]:

$$\text{Fitness} = \int_0^{t_{sim}} e^2(t) dt = \int_0^{t_{sim}} (\omega^*(t) - \omega(t))^2 dt \quad (11)$$

In this case, the block of the objective function is used to estimate the performances of the PI controller by minimizing this function.

The genetic algorithm parameters chosen for the tuning purpose are shown below.

Table 2
Parameters of GA

GA property	Value
Population size	60
Maximum number of generations	100
Crossover probability	0.8
Mutation probability	0.1
Tolerance	10^{-6}

After giving the above parameters to GA, the PI controller can be easily tuned and thus system performance can be improved. The parameters of the PI speed controller obtained according to the procedure of optimization by the technique of the GA are given below in Table 3.

Table 3
PI controller gain values

Gain Coeff	K_p	K_i
Values	0.90	9.75

5 Simulation Results and Interpretation

In order to verify the validity of the proposed controller, the computer simulation results for a 1.5 KW induction motor using a PI controller optimized by the GA technique is compared to a conventional PI controller whose parameters are determined by pole assignment method. The parameters of the test motor are given in the appendix.

A simulation program is designed to compare the stable and dynamic performances. Figs. 5 and 6 show the speed curve when the motor speed is at 150 rad/s. Fig. 5 is the result of the conventional PI controller, and Fig. 6 is the speed of the GA-based PI controller.

Fig. 5 shows that the conventional PI control has bigger overshoot. And Fig. 6 shows that the GA based PI controller has less overshoot and more stable performance.

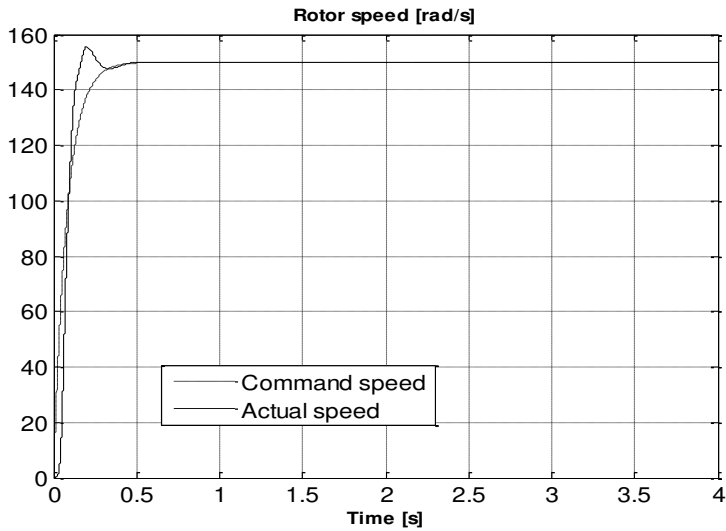


Figure 5

Rotate speed simulation curve when adopting conventional PI regulating strategy

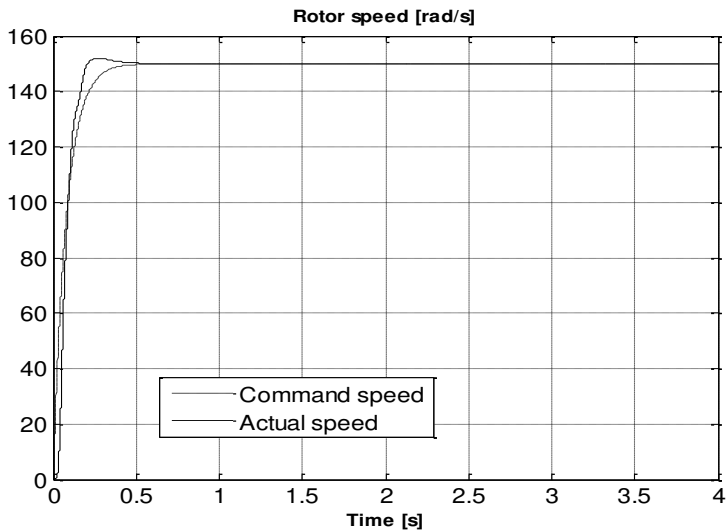


Figure 6

Rotate speed simulation curve when adopting PI controller based on GA

The next simulation, Figs. 7 and 8, were carried out to examine the disturbance rejection of each controller when the motor is fully loaded and operated at 150 rad/s and a load disturbance torque (10 N.m) is suddenly applied first at 1.5 s and at 3s. Figs. 7 and 8 show that the GA-based PI controller rejects the load

disturbance very quickly, while the conventional PI controller takes longer to return to speed command.

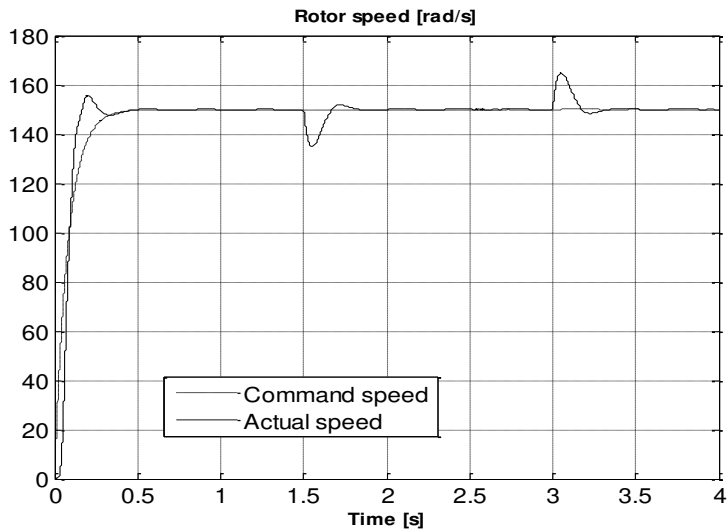


Figure 7

Rotate speed simulation curve using PI controller when load changes

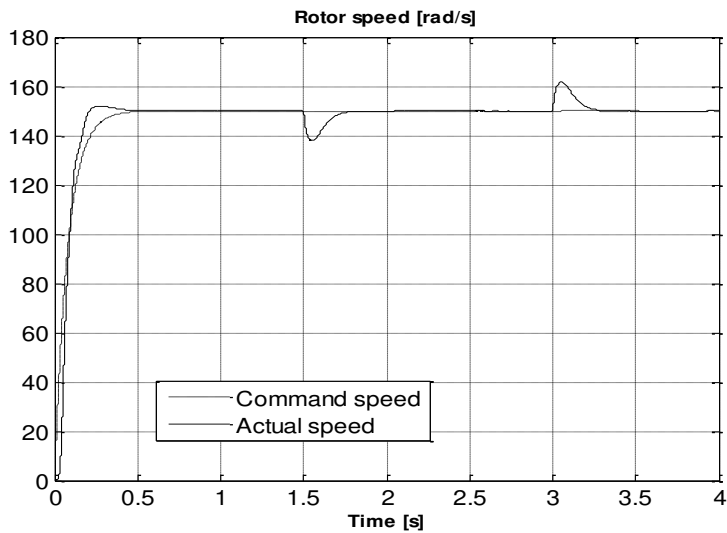


Figure 8

Rotate speed simulation curve using PI controller based on GA when load changes

Figs. 9 and 10 show clearly the comparison of both controllers in the presence of load disturbance. The GA-based PI controller returns the speed to the command speed within 0.37 s with a maximum drop of 12 rad/s. The conventional PI controller takes about 0.49 s to return the speed to 150 rad/s with a maximum drop of 15 rad/s.

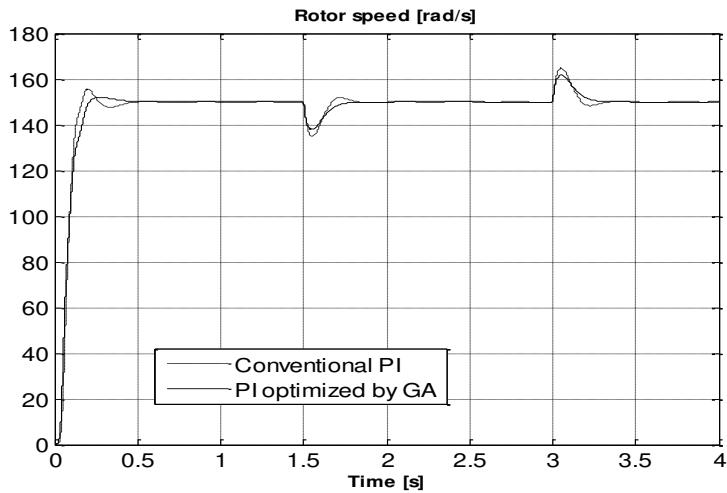


Figure 9

Comparison between the regulation of the IM by conventional PI and a PI optimized by GA when load changes

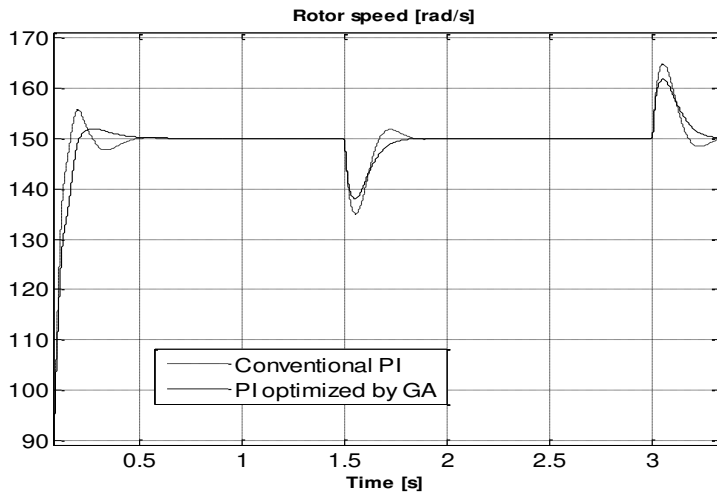


Figure 10

Comparison between the regulation of the IM by conventional PI and a PI optimized by GA when load changes (zoomed response)

Conclusion

The conventional PI controller gave satisfactory results. The major disadvantage of PI controllers resides in the determination of their parameters. Several design techniques of PI controllers were mentioned in literature. The most used are the poles assignment method and the Ziegler-Nichols method, but their disadvantages lie in the required prior knowledge of the various parameters of the IM. In our work we have chosen the GA optimization technique for the determination of the optimal parameters of the used PI controller.

The simulation results showed that the introduction of the GA led to an improvement in the speed regulation of the IM, which leads us to say that optimization by GA gives us the possibility of designing a powerful PI controller by optimizing its parameters.

Appendix

Induction motor parameters:

$P_n [KW]$	1.5	$R_s [\Omega]$	4.85	$f_n [Hz]$	50
$V_n [V]$	220	$R_r [\Omega]$	3.805	$J_n [Kg.m^2]$	0.031
η	0.78	$L_r [H]$	0.274	$f_c [N.m.s / rd]$	0.00114
$\cos \phi_n$	0.8	$L_s [H]$	0.274	P	2
$\omega_n [\min^{-1}]$	1428	$M [H]$	0.258		

References

- [1] A. Hazzab, I. K. Bousserhane, M. Kamli, M. Rahli, 'Design of Fuzzy Sliding Mode Controller by Genetic Algorithms for Induction Machine Speed Control'. Third IEEE International Conference on Systems, Signal & Devices SSD'05, Tunisia, 2005
- [2] A. Mansouri, M. Chenafa, A. Bouhenna, E. Etien 'Power Nonlinear Observer Associated with Field-oriented Control of an Induction Motor'. Int. J. Appl. Math. Comput. Sci., 2004, Vol. 14, No. 2, 209-220
- [3] I. K. Bousserhane, A. Hazzab 'Direct Field-oriented Control Using Backstepping Strategy with Fuzzy Rotor Resistance Estimator for Induction Motor Speed Control' Information Technology And Control, 2006, Vol. 35, No. 4
- [4] S. Meziane, R. Toufouti and H. Benalla, 'Nonlinear Control of Induction Machines Using an Extended Kalman Filter', Acta Polytechnica Hungarica, ISSN 1785-8860, Vol. 5, No. 4, pp. 41-58, 2008
- [5] F. G. Shinskey, Process Control System: Application, Design and Tuning, McGraw-Hill, 4th ed, 1996

-
- [6] M. AOuhrouche, C. Volet, 'Simulation of a Direct Field-oriented Controller for Induction Motor Using Matlab/Simulink Software Package'. Proc. of IASTED Int. Modeling and Simulation (MS'2000), USA
- [7] Wassim. A, Bedwani, and Oussama M. Ismail, 'Genetic Optimization of Variable Structure PID Control Systems', Computer Systems and Applications, ACS/IEEE International conference on 2001
- [8] M. Chebre, M. Zerikat and Y. Bendaha, 'Adaptation des Paramètres d'un Contrôleur PI par un FLC Appliqué à un Moteur Asynchrone', 4th International Conference on Computer Integrated Manufacturing CIP'2007, 03-04 November 2007, Setif, Algeria
- [9] L. Barazane, S. Kharzi, A. Malek and C. Larbés, 'A Sliding Mode Control Associated to the Field-oriented Control of Asynchronous Motor Supplied by Photovoltaic Solar Energy', Revue des Energies Renouvelables, Vol. 11 No. 2 (2008) 317-327
- [10] A. Hazzab, A. Louafi, I. K. Bousserhane and M. Rahli, 'Real Time Implementation of Fuzzy Gain Scheduling of PI Controller for Induction Machine Control', International Journal of Applied Engineering Research, Vol. 1, No. 1 (2006) pp. 51-60
- [11] Shady. M. Gadoue, D. Giaous and J. W. Finch, 'Genetic Algorithm Optimized PI and Fuzzy Mode Speed Control for DTC drives', Proceedings of the World Congress on Engineering 2007, Vol. 1, WCE 2007, July 2-4, 2007, London, U.K.
- [12] R. Anulmozhiyal and Dr. K. Baskarn, 'Speed Control of Induction Motor Using Fuzzy PI and Optimized Using GA', International Journal of Recent Trends in Engineering, Vol. 2, No. 5, November 2009
- [13] Neenu Thomas, Dr. P. Poongodi, 'Position Control of DC Motor Using Genetic Algorithm-based PID Controller', Proceedings of the World Congress on Engineering 2009, Vol. 2, WCE 2009, July 1-3, 2009, London, U.K.
- [14] Jin-Sung Kim, Jin-Hwan Kim, Ji-Mo Park, Sung-Man Park, Won-Yong Choe and Hoon Heo 'Auto Tuning PID Controller Based on Improved Genetic Algorithm for Reverse Osmosis Plant', World Academy of Science, Engineering and Technology 47 2008
- [15] T. O. Mahony, C. J. Dowing and K. Fatla, 'Genetic Algorithm for PID Parameter Optimization: Minimizing Error Criteria', Process Control and Instrumentation, 2000, 26-28 July 2000, University of Strathclyde, pp. 148-153

General Solution for the Self-Organizing, Distributed, Real-Time Scheduling of FMS-Automatic Lot-Streaming Using Hybrid Dynamical Systems

János Somló, Imre J. Rudas

Óbuda University
Bécsi út 96/B, H-1034 Budapest, Hungary
somlo@uni-obuda.hu
rudas@uni-obuda.hu

Abstract: The use of hybrid dynamical systems opens a new horizon for flexible manufacturing systems scheduling. It even makes possible directly connect scheduling and MRP. In the present paper the most important new result is the proposed demand rates determination method for multi-section scheduling problems. Some other important achievements making possible the application of this approach are discussed, too. These are, for example:

- **feedback control law** resulting in stable (implementable with finite buffers) and regular (converging to periodic) processes is described;
- **optimal demand rates determination** for single-section problems is discussed.

In this paper the “buffer principle” of planning is used and a bottleneck scheduling approach is applied. As the result, production times close to the global minimum of net manufacturing time, determined by the loading characteristics of bottleneck machine-groups, may be realized.

*The proposed control is totally self-organizing. No outside control commands are necessary. Every buffer is only connected (in the signal level) with the previous and the next buffer. The actions are real-time controlled. The most important feature of this control is that it significantly improves the efficiency of utilization of system resources. **The generalization for multi-section problems makes it possible to solve the most common application tasks. Ev, the solution of dynamical input problems becomes possible.***

Keywords: Flexible manufacturing systems; Scheduling; Hybrid dynamical systems; Stability; Periodic regimes; Optimal demand rates; Buffers, Bottleneck, Automatic lot-streaming; Overlapping production; Single-sections; Multi-sections; Self-organizing; Distributed; Real-time control; Scheduling and MRP

1 Introduction

In the present paper we extend the development in paper [1] for single-sections hybrid dynamical systems based FMS scheduling method for multi-section scheduling problems. This last is the most common formulation (coming from MRP level) of production tasks. The results may even be used when the tasks (inputs) have a dynamical character.

The good quality of the solution of scheduling problems is a key factor in the effective utilization of flexible manufacturing systems. The value of production of these systems is very high. This is why every improvement in processes quality has a significant economic effect. Classic methods of scheduling manufacturing processes may be used for Flexible Manufacturing Systems (FMS), too. In general, the approaches used for the solution of manufacturing scheduling problems belonged to applied operation research problems. Perkins and Kumar in [4] proposed to use for this goal Hybrid Dynamical Systems (HDS) theory based methods. By this, the scheduling problem became a control theory problem for which the approaches of dynamical systems investigation are suitable.

Concerning manufacturing production planning, problems arise when we want to exploit the advantages and opportunities of these systems, where not only the manufacturing but also the handling processes are automatically realized. As an example of the difficulties, we mention the application of lot-streaming and overlapping production. In systems with high-level computerized control it is trivial to use these methods. But it is not trivial how to realize it. Even with very the powerful technology of computations, similar tasks lead to problems with very high dimensions with no chance of effective solution. Lot-streaming and overlapping production methods can be effectively used in flexible manufacturing systems due to the small values of set-up times. But to plan the processes is extremely difficult because of the increase in dimensions. Exactly this is the field where the application of the methods of hybrid dynamical systems may result in a breakthrough.

The manufacturing scheduling problems are in the centre of attention of the scientific literature. A high number of publications are available. A survey is in [13] and others. From classical works we recall [14, 15].

Hybrid dynamical systems have attracted considerable attention in recent years (see e.g. [2, 3] and references therein). In general, HDS are those that combine continuous and discrete behavior and involve, thereby, both continuous and discrete state variables. In many cases, such systems operate as follows. While the discrete state remains constant, the continuous one obeys a definite dynamical law. Transition to another discrete state implies a change of this law. In its turn, the discrete state evolves as soon as a certain event occurs with both the evolution and the event depending on the continuous state.

The class of HDS we are dealing with in the present paper consists of complex switched server queuing networks. This class of HDS was introduced in [4, 5] to model flexible manufacturing systems. Different aspects of the investigation of the processes in these systems were outlined in [2÷12]. A flexible manufacturing system considered in this paper produces several part-types on a network of machines. Raw parts are the inputs to the network. Parts arriving to a machine are waiting in buffers and are supplied to the machines when required. Each unit of a given part-type requires a predetermined processing time at each of several machines, in a given order. A set-up time is required whenever a machine switches from processing one part-type to another.

The investigation of the fluid analogy of similar systems is a popular research field. Especially the periodic processes in these systems have attracted significant attention (see: [16, 17, 18, 19]).

It should be emphasized here that in FMS the set-up times have small value compared with the manufacturing times. Nevertheless, as is well known from practice, and as is proved by theoretical investigations, their values may not be neglected without serious consequences.

In classic manufacturing scheduling problems, the parts are supposed to be delivered to machines in batches. The batches are properly sized. When hybrid dynamical methods are used, the basic difference in part delivery policy is that the parts are delivered to buffers serving the machines in a continuous flow. More precisely, the part demand is (equally) distributed in time. In the early works (see e.g.: [2÷9]) on HDS theories used for FMS scheduling, the inputs representing the production tasks were introduced as infinite flows without start and end. This representation was suitable for stability problem formulation and for the investigation of periodic motions in such systems. If the systems are stable, the practically interesting regimes of their motion are the periodic ones. Results regarding periodic motions in these systems were published, for example, in [3÷9].

In [10] a new aspect of input flows determination was proposed which reflected the practical requirements of scheduling. Namely, the part demand (part arrival) was determined in a way that it should result in the production of the given part-types in the given number during the given (scheduling) time. Clearly, one of the most important points is that the production time for an order be as low as possible.

The above mentioned method was developed for systems where the tasks (production order) were given for one single (common) scheduling section. **In the present paper we extend the results for cases when multi-section problems are formulated; that is, every series of part-types has its own(individual) scheduling section (interval) but these sections overlap.** This second case, of course, contains the single (common) scheduling section case, too.

In the present paper, as theoretical basis, the results of paper [1] are used. These results concern the solution of manufacturing scheduling problems by the use of hybrid dynamical methods. We remark that throughout the present paper the continuous representation is used. Furthermore, it is supposed that the number of parts is suitably large, and the set-up times are suitably small.

The content of the present paper covers the following:

After this Introduction, in **Section 2** we describe the problem statement for manufacturing scheduling.

In **Section 3** we give a simplified discussion of the theoretical investigation of the FMS scheduling problem. The main emphasis is on the aspects of practical use. So, the formulation of the feedback control law is simpler (but equivalent) than in [1]. Because the goal is to extend the results to multi-section scheduling problems the results are formulated to serve this goal.

In **Section 4** we describe the method developed for single section scheduling. We propose an approach for optimal determination of demand rates. This is important because the basis for the effective solution of the multi-section problem is the effective solution of single-section problems.

The main results of the present paper are given in Section 5 where we generalize the demand rates determination method for systems with multi-section scheduling intervals.

In **Section 6** some idea is given how the proposed in the paper make possible to **contact FMS scheduling and MRP.**

Conclusions are formulated in **Section 7.**

2 Problem Statement

Flexible manufacturing systems for scheduling by the use of HDS theories may be modeled as follows:

- (i) There are P part-types labeled $1; 2; \dots; P$, and a set $M = \{1, 2, \dots, M\}$ of machine-groups which we will also call simply machines, in the following.
- (ii) Parts of type p require processing at the machines $\mu_{p,1}, \mu_{p,2}, \dots, \mu_{p,n_p}$ in that order where $\mu_{p,j} \in 1, 2, \dots, M$. Here n_p is the index of the machine which processes the last operation of the given part (index of final machine-group). So, for example, when $\mu_{p,1}=3, \mu_{p,2}=1, \mu_{p,3}=4$ the part with index p is processed on machine identified with indices 3,1,4, in this order. Because the machine with index 3 is the last $n_p=3$.)
- (iii) Raw parts of type p arrive to the system at the machine $\mu_{p,1}$ at a constant rate $r_p > 0$.

(iv) At the j -th machine they visit, parts of type p enter the buffer labelled $b_{p,j}$ from which they are eventually processed by this machine at a given constant rate $R_{p,j} > 0$. The dimension of $R_{p,j}$ is [part/time unit]. We will use also the value $\tau_{p,j} = \frac{1}{R_{p,j}}$. This is the time of processing one part on the given machine.

(v) We also assume that parts of type p incur a fixed transportation delay $l_{p,j} \geq 0$ when moving from the machine j to the machine $j + 1$.

(vi) The machine m is served from the buffers $B_m := \{b_{p,j} : \mu_{p,j} = m\}$

A minimal set-up time $\delta_m^0 > 0$ is required when the machine with index m switches from processing parts of type p in the buffer b in B_m to processing parts of another type p' in B_m . The machine does not work during such a set-up time. This set-up time can be artificially increased to achieve our control goal. In other words, set-up time $\delta_m(t)$ of the machine m is a control variable. However, condition

$$\delta_m(t) \geq \delta_m^0 \quad (2.1)$$

should be satisfied.

Now we face the task of scheduling the operations to perform the production orders. For that we should know the production capacities which we have assigned to perform the tasks. These capacities are given as the time intervals of available machine-groups devoted to the given operations.

2.1 Scheduling Sections

Single-section case

There is given the scheduling section as

$$0 \leq t \leq T_{sch} \quad (2.2)$$

During this the given numbers of part-types should be produced in the number of items:

$$N_1, N_2, N_3, \dots, \dots, N_p$$

Multi-section case

The scheduling sections are given as

$$re_j \leq t \leq dd_j \quad (2.3)$$

$$j=1, 2, 3, \dots, J$$

Where:

re_j – is the release time; *dd_j* – is the due data for the given section

During the individual scheduling sections the following number of parts should be produced:

$$N_{j(P_{j-1+1})}, N_{j(P_{j-1+2})}, \dots, N_{j(P_j)}$$

As can be recognized, the indexing of the part-types is continuous from 1, (1,2,3.....). In a given section the part-types indices are from $P_{j-1} + 1$ to P_j

3 Scheduling FMS using Hybrid Dynamical Methods

As was mentioned, in the present paper we use the results outlined in [1]. Here only the basic definitions and results are described to give a background for the formulation of the new results concerning the determination of demand rates for multi-section scheduling.

The structure of one layer of the manufacturing system in consideration is given in Fig. 3.1.

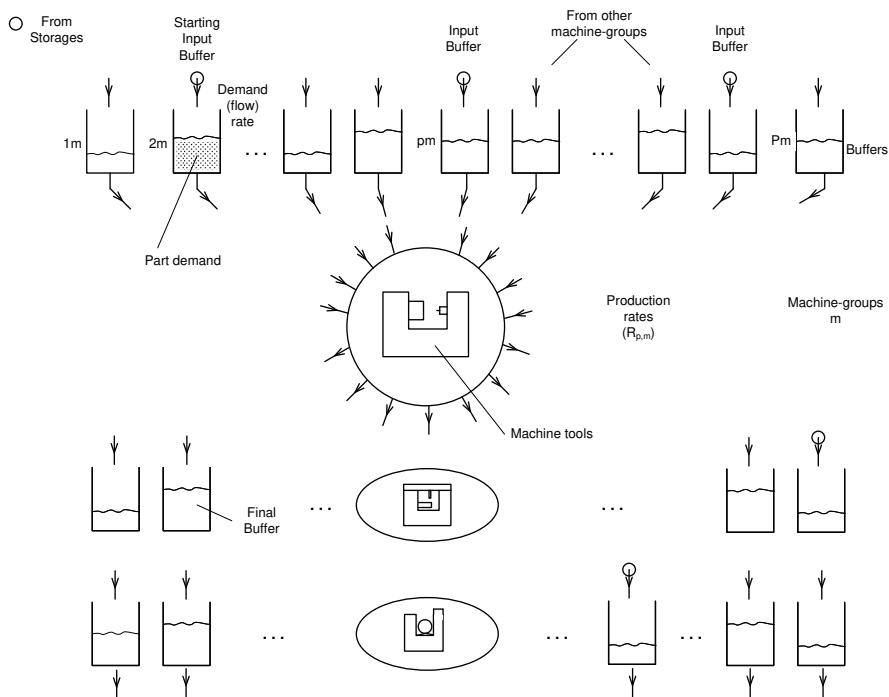


Figure 3.1

One layer of the flexible manufacturing system

This layer represents a machine-group together with the buffers serving the machines in supplying some given parts. Every part-type has its dedicated buffer. Here we remark that the buffers are understood as virtual ones because in reality these buffers may have different physical implementation. The buffers may be individual devices but may be parts of common storages or pallets, etc. Another side of this virtuality is that the numbers of part items are treated as real numbers

and not as integers, as is in real production. The buffers are filled-up from central (or local) storages, or from the output of other machine-groups. We suppose that the delivery among machine-groups is a continuous process. Among the buffers, the most common types are those which are served from some other buffers. But there are initial buffers served from storages. The momentary role of the initial buffers may be different. Some of them may supply parts for immediate processing. We name those as the starting initial buffer. Other buffers are only filled up with no output flow because the given machine (machine-group) is engaged to produce other parts. In the Figure, the final buffers are indicated, too. But they do not have any role in the systems actions. They serve only for the registration of the end of some production action.

We remark that the buffers here have symbolic meaning. In reality these indicate the buffer-machine-part-type items conglomerate. Their actions are equivalent with the actions of the conglomerate. One more remark: there are systems where the systems processes are continuous in reality. An example of these is: chemical systems processing fluid components. Of course, all that are proposed here are fully applicable to those systems.

As was already mentioned, we consider switching feedback control laws. Now, according to that the system, processes may be characterized as follows. At some particular time instant

- A given buffer is filled-up from storage (with r_p flow rate), but the machine-group which is served from this buffer is engaged in making other parts (or set-up is performed). In this case the buffer content is not reduced and its content permanently grows according to the input flow rate (demand rate).
- The same as above but the machine-group is engaged to produce the given parts so the buffer content is reduced according to the production rates.
- The buffer content is supplied from the machine before the given one (from the previous buffer) in the sequence of the production, but its content is not reduced because the given buffer for the time being is not engaged in the production.
- The same but the buffer content is reduced because the part-type items are produced.

In describing the systems work we will use the terminology: **active buffer**. An active buffer is the one which is engaged in production. That is; it receives a command for production from the previous buffer but the conditions to finish this production are not met, yet. (Where to relate the set-up times does not have any importance from the systems actions viewpoint.)

As we mentioned, the systems activities to produce parts are characterized from the point of view of buffers. Accordingly, we will use for the description of processes the vector of buffer levels

$$\mathbf{x}(t) = \{x_{p,m}(t)\} \quad (3.1)$$

$p \in 1, 2, \dots, P$

$m \in 1, 2, \dots, M$

Finally let $y_{p,i}(t)$ denote the cumulative output of part-type p from the buffer $b_{p,i}$ over the time interval $[0, t]$ i.e., the amount of part-type items of type p processed by the machine $\mu_{p,i}$ over $[0, t]$. Then, $y_{p,i}(t)$ is described by initial condition $y_{p,i}(0) = 0$ and equations:

$$\text{if a buffer is active then } \dot{y}_{p,i}(t) = R_{\mu_{p,i}} \quad (3.2)$$

$$\text{if a buffer is not active then } \dot{y}_{p,i}(t) = 0$$

The cumulative output may be characterized by vector

$$\mathbf{y}(t) = \{y_{p,i}(t)\}$$

3.1 Feedback Control Law for Self-Organizing, Distributed, Real-Time Scheduling of FMS

In the system described above the continuous parts are characterized by the relations

$$\dot{x}_{p,m} = u_{p,m}(t) \quad (3.3)$$

$p \in 1, 2, \dots, P$

$m \in 1, 2, \dots, M$

where $u_{p,m}(t)$ are the input flows of the buffers.

In [1] the processes of the given system are given in algorithmic form.

This formulation gives, for example, for a buffer filled-up from the storage and reduced at the same time

$$\dot{x}_{p,1} = r_p - R_{\mu_{p,1}} \quad (3.4)$$

Another example is when a buffer is filled-up from a machine-group before and at the same time its content is reduced according to the present production

$$\dot{x}_{p,i} = R_{\mu_{p,i-1}}(t - l_{p,i-1}) - R_{\mu_{p,i}}(t) \quad (3.5)$$

For the relations describing the other processes in the system, see [1].

In [1] the following goal was formulated:

Let $d_1 > 0$; $d_2 > 0, \dots, d_p > 0$ be given constants. These constants are called production levels. Let $T > 0$ be a given time value. The goal is to determine the part arrival rates r_1, r_2, \dots, r_p and feedback control policy such that for all $p = 1, 2, \dots, P$; $i = 1, 2, \dots, n_p$, the value $y_{p,i}(k+1)T - y_{p,i}(kT)$ (that is the amount of parts of type p processed by the machine $\mu_{p,i}$ over the interval $[kT; (k+1)T]$) is

close, in some sense, to d_p , where $k = 0, 1, 2, \dots$. Furthermore, we wish to find the minimal time T for which this will be possible. Also, the closed-loop system should be stable. (The definition of stability is given below.)

For future use the following will be introduced:

Definition 2.1: (See [4], [5].) The closed-loop system constructed according to Fig. 3.1 and working with the use of switching feedback control is said to be stable if for any solution $[\mathbf{x}(t)]$ with initial conditions $\mathbf{x}(0) = \mathbf{x}_0$ (where \mathbf{x}_0 is a vector with non-negative components) the vector function $\mathbf{x}(t)$ is bounded on $[0, \infty)$, i.e. there exists a constant

$$L(\mathbf{x}_0) > 0$$

such that

$$x_{p,i}(t) \leq L(\mathbf{x}_0) \quad \forall p, i, t. \quad (3.6)$$

Definition 2.2: The closed-loop system discussed above is said to be regular with the production levels d_1, d_2, \dots, d_p and the scheduling period T if it is stable and the following condition holds

$$\lim_{k \rightarrow \infty} (y_{p,i}((k+1)T) - y_{p,i}(kT)) = d_p \quad (3.7)$$

$$p \in 1, 2, \dots, P; \quad i \in 1, 2, \dots, n_p$$

As was mentioned above, regularity with the production levels d_1, d_2, \dots, d_p and the scheduling period T means that for any p the amount of part-type p processed over time intervals $[kT; (k+1)T]$ converges to d_p as k tends to infinity.

Definition 2.3: Assume that $d_1 > 0, d_2 > 0, \dots, d_p > 0$ are given. The minimal time T_0 for which there exist constants $r_1 > 0, r_2 > 0, \dots, r_p > 0$ and a feedback policy such that the closed-loop system is regular with the production levels d_1, d_2, \dots, d_p and the scheduling period T_0 , is called the minimal scheduling period of the system.

For the sake of the simplicity of future discussion, we introduce some more definitions and terminology.

The quantity

$$L_t = \sum_{p=1}^{P} N_p \tau_{p,m} \quad (3.8)$$

$$m \in 1, 2, \dots, M$$

is the net manufacturing time needed for any machine-group to produce the parts.

The quantity

$$D_m = \sum_{p=1}^{P} d_p \tau_{p,m} \quad (3.9)$$

$$p \in 1, 2, \dots, P$$

$$m \in 1, 2, \dots, M$$

is the net manufacturing time when $d_p(p=1,2,\dots,P)$ number of parts is produced from a part-type items in a period of periodic motions.

The quantity

$$ELt_m = [k_m \delta_m^0 + Lt_m] \quad (3.10)$$

$$m \in 1, 2, \dots, M;$$

is named extended load time, where: k_m is the number of set-up events on a machine-group when performing a production order.

We will use also the following quantities

$$Mlt_m = \text{Max} Lt_m \quad (3.11)$$

$$m \in 1, 2, \dots, M;$$

and

$$MELt_m = \text{Max} ELt_m \quad (3.12)$$

$$m \in 1, 2, \dots, M;$$

These quantities belong to the bottleneck machine groups. It very frequently happens that the machine-groups for which the maximums of Lt_m and ELt_m occur are the same. This is because the set-up times usually are that of suitably small value. In the following, we will suppose that the bottleneck machine-group is the same as regards the net and extended load times. In the opposite case, it is very easy to modify the results.

It was proved in [1] that the minimal time T_0 for the closed loop system to be regular is

$$T_0 = \text{Max} [k_m \delta_m^0 + \sum_{p=1}^{p=P} d_p \tau_{p,m}] = \text{Max} [k_m \delta_m^0 + D_m] \quad (3.13)$$

$$m \in 1, 2, \dots, M$$

We introduce for any time value $T \geq T_0$ a quantity, which we name synchronization coefficient, as follows

$$\delta_m^M = \frac{T - D_m}{k_m} \quad (3.14)$$

The machine m works with k_m buffers. Denote the corresponding buffers b_1, b_2, \dots, b_{k_m} in an arbitrary order. Let us form the following cyclic sequence of these buffers

$$b_1 \rightarrow b_2 \rightarrow \dots \rightarrow b_{k_m} \rightarrow b_1 \quad (3.15)$$

Let $b \in B_m$. Then **next**[b] is the next buffer from B_m that is the next to b in the cyclic sequence (3.15).

We consider an active buffer. For the activity period of a buffer the following feedback policy was proposed. Let τ_m be the time instant when after the set-up time the processing of the parts begins. Furthermore, we introduce

$$\Delta_{p,m} = \frac{d_p}{R_{p,m}} = d_p \tau_{p,m} \quad (3.16)$$

This is the net manufacturing time to produce sub-parts of part-type p in number of items d_p in machine-group with index m.

The b_a value indicates which buffer is active at a given time instant. That is just after τ_m ; $b = b_a$.

The following feedback policy is proposed

$$\begin{aligned} &\text{if}\{x_{p,m} = 0 \text{ or } \Delta_t = \Delta_{p,m} - (t - \tau_m) = 0\} \\ &\text{then}\{\delta_m = \delta_m^M + \Delta_t \text{ and } b(t + \delta_m + 0) = \text{next}[b]\} \end{aligned} \quad (3.17)$$

As was mentioned, in Equation (3.17) τ_m is the time instant when the given active buffer began to produce the given part-type items.

Finally, we introduce the demand rates as follow:

$$r_p = \frac{d_p}{T} \quad \forall p = 1, 2, \dots, P \quad (3.18)$$

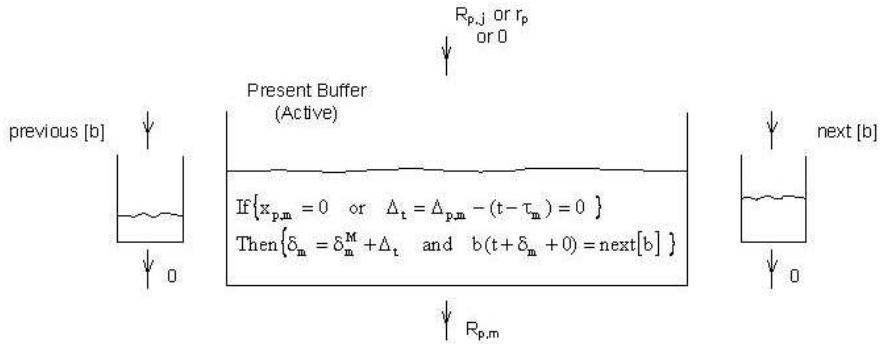
Now, we are can formulate the basic results concerning the problem outlined above:

- 1) The minimal scheduling period T_0 of this system with the production levels $d_1; d_2, \dots, \dots, d_p$ is defined by (3.13).
- 2) For any $T \geq T_0$ the closed-loop system with the part demand (3.18) and the feedback policy defined by relation (3.17) is regular with the production levels $d_1, d_2, \dots, \dots, d_p$ and the scheduling period T .

The above results were formulated and proved in [1] (See: Theorem 1).

The given control solution is named **Enforced-Period** switching law.

In Figure 3.2 we demonstrate the above switching law. In the centre there is the present buffer which is active, that is, which produces the sub-part items p by rate $R_{p,m}$. The buffer is supplied from the previous machine-group by rate $R_{p,j}$, or is not supplied because the previous machine-group is not engaged by the production of this sub-part, or is supplied from storage (if the buffer is an input one). At the time corresponding to the situation in Figure 3.2, only $b = b_a$ is an active buffer in machine-group m. When according to the switching law the conditions for a switch are satisfied, the “activity” is transferred to the next buffer.



3.2

The switching law

4 Determination of the Demand Rates for Single-Sections

The orders for production are determined on the MRP (Material Requirement Planning) level of systems. As was mentioned, there are two cases for this:

1. single section scheduling
2. multi-section scheduling

First we deal with the single section case.

The task is to produce during the scheduling time:

$$0 \leq t \leq T_{sch} \tag{4.1}$$

the given number of items of the part-types

$$N = N_1, N_2, \dots, N_p, \dots, N_P \tag{4.2}$$

As was mentioned, in the classic formulation of tasks, the part numbers are given for the whole scheduling period. It is not specified when exactly in this time window the part items should be produced. The only important point is to have them at the final time instant (due date). Using hybrid dynamical approaches there is a change in this respect. We distribute the part requirement equally along the time axis. We name **demand rate** the rate at which the parts are required by the system. The part **demands** are the integral in time of the demand rates. We also use for this the terminology **arrival rate**. This is the rate the parts arrive into the buffers. Clearly, the demand rate and the arrival rate represent different ideas but are characterized by the same quantities.

Now, let us consider the manufacturing capacities necessary to perform an order. As was mentioned, the machines loads (necessary net manufacturing capacities) are:

$$Lt_m = \sum_{p=1}^{p=P} N_p \tau_{p,m} \quad (4.3)$$

$$m \in 1, 2, \dots, M$$

The global minimum of net production time is determined by the maximum of this quantity. The machine-group for which we have this maximum is the bottleneck machine-group considering the net manufacturing times. As we mentioned, we suppose that the given machine is the bottleneck, taking into consideration the set-up times, too. We identify this machine group by index

$$m_{bt} \in 1, 2, \dots, M \quad (4.4)$$

In the following, for the maximum of loading time we will use (see: (3.11))

$$Mtl = \text{Max} Lt_m \quad (4.5)$$

$$m = 1, 2, \dots, M$$

In [10] it was proposed to determine the demand rates as

$$r_p = \frac{N_p}{Mtl} k \quad (4.6)$$

$$p = 1, 2, \dots, P$$

The coefficient k was named **demand rate coefficient**.

It was proposed to choose the k coefficient having a value slightly less than one. Now we discuss the reasons of this proposal. According to the description of system processes above, the part demands appear as contents in the buffers at the first machine-groups processing given part-types. So, there is an input buffer, the content of which characterizes the momentary for a part-type requirement. The demand rate choice according to Equation (4.6) is illustrated in Figure 4.1. Clearly, because Mtl is the maximum of net manufacturing time and at the same time the global minimum of production time, it is impossible to finish the overall task, for any part-type, for less time than Mtl . So, if we use equal distribution of demands along the time axis the $\frac{N_p}{Mtl}$ value, will give the slope of the upper border of the “demand sector”. Similarly, the $\frac{N_p}{T_{sch}}$ value will provide the lower border because for any value less, the due date requirement may not be satisfied. (There may exist some technological restrictions (see: [10, 11, 12]) which in most of the practical cases do not affect the results.) It is expedient to choose the demand rates as big as possible for decreasing the production time. A k value slightly less than one, which provides some reserve for set-up times, can give a suitable solution for the above goal. The upper and lower borders determine the so-called “demand sector”. The mentioned will be discussed later in more detail.

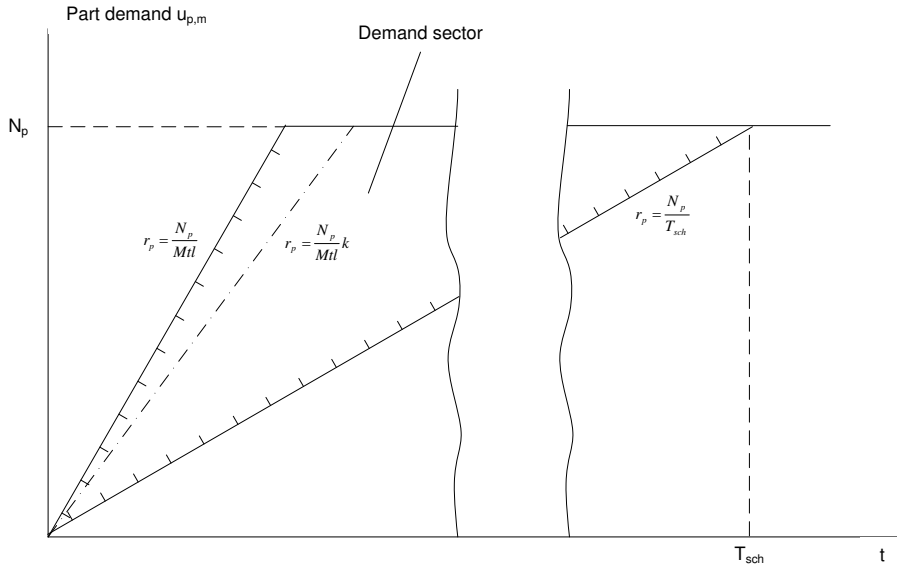


Figure 4.1
The demand sector

Returning to analyze the system processes, the demands appear at the first machine-group processing a given part-type. As was proved, the processes in the systems converge to regular. The processes at the output of this first machine-group will converge to periodic ones, too. At the beginning of the system actions, some starting procedure should be realized. (We will discuss later how to start the systems processes.) If the system actions are properly planned, the processes in every buffer will have some starting, transient, then periodic parts, and at the end, some final sections. Accordingly, the production time can be described as

$$t_{pr} = t_{start} + t_{periodic} + t_{end} \quad (4.7)$$

We are most interested in the $t_{periodic}$ part of the motions.

It has been shown by a number of simulation studies (see: [10, 11, 12]) that the starting transient parts may be made very short. The final section has no significant effect on system performance. So, the system goodness may be characterized quite well considering the processes of the periodic part of the motions.

So, let us suppose that the planning of system processes may be performed based on periodic motion.

We assume that the scheduling task is performed during “W” period of periodic motions where W is a properly chosen integer value.

Then

$$d_p = \frac{N_p}{W} \quad p=1,2,\dots,P \quad (4.10)$$

According to Equations (3.13) and (3.18) the arrival rate can be determined as

$$r_p = \frac{N_p}{W \left(k_m \delta_m^o + \sum_{b(p,i) \in B_m} \frac{N_p}{W} \tau_{p,i} \right)} \quad (4.11)$$

Considering Relation (4.5) and (4.6) we get

$$k = \frac{Mtl}{Wk_m \delta_m^o + Mtl} \quad (4.12)$$

The only free parameter in the above expression is the W value.

We remark that the low values of W exclude the use of hybrid dynamical methods, because, for example, $W=1$ corresponds to the classic scheduling problem. Its solution has well-known results and difficulties. The other small values of W would indicate the necessity to use classic (or modern) lot-streaming technologies (see e.g.: [20]) which, as far as we know, do not have significant, general results. The development of computational technology makes it possible to solve very sophisticated problems. But the computation difficulties and, what is even more important, the complicated realization makes the use of these approaches not very attractive. The proposed self-organizing approach is free from these difficulties.

Now, we will try to analyze the problem of the proper selection of the W (or k) value.

4.1 Optimal Demand Rate Selection

The production time (t_{pr}) when using HDS methods can be represented as

$$t_{pr} = Mtl + W * k_m \delta_m^o + \Delta\Gamma \quad (4.13)$$

where $\Delta\Gamma$ is the time of finishing all of the operations on other than the bottleneck machine-group. The task is to choose the W value minimizing the last two terms of (4.13). It depends on the task and may be solved by simulation. To gain some general idea we may have some supposition. In Savkin, Somlo (2009) it was supposed that

$$\Delta\Gamma = T_0 \quad (4.14)$$

By that, the optimal W is (see: Savkin, Somlo (2009)):

$$W_{opt} = \sqrt{\frac{Mtl}{k_m \delta_m^o}} \quad (4.15)$$

According to some new idea about the effect of lot-streaming (see: [21, 22]) it seems that a better estimation of production time may be provided by

$$\Delta\Gamma = \frac{H * Mtl}{W} \quad (4.16)$$

where the H coefficient value is

$$H=0,2 \div 0,5$$

The above supposition was concerned with the investigation of the solution of the scheduling problems with full load of bottleneck machines. It was supposed that for “full load” problems, scheduling the production times may be characterized as

$$t_{pr} = Mtl(1+H) + k_m \delta_m^0 \quad (4.17)$$

where H is about the above given values.

We remark that, depending on the task, H may have, in some cases, less value than the above. But these cases are trivial from scheduling points of views. The obtained schedules should be realized in the most usual way. (Lot-streaming should not be used.)

In general, substituting (4.16) into (4.17) we get:

$$W_{opt} = \sqrt{H} \sqrt{\frac{Mtl}{k_m \delta_m^0}} \quad (4.17)$$

The proper H value depends on the tasks. A rather defensive choice is H=0,5. By this

$$W_{opt} = \frac{\sqrt{2}}{2} \sqrt{\frac{Mtl}{k_m \delta_m^0}} \quad (4.18)$$

As the simulation experiments show, the system performance is not very sensitive to W value. So, wide variety “close” to the optimal value may be used.

So,

$$W_{opt} = (0,5 \div 1,0) \sqrt{\frac{Mtl}{k_m \delta_m^0}} \quad (4.19)$$

value seems a reasonable choice.

Buffer size aspects

Because (see: Equation. (4.10))

$$d_p = \frac{N_p}{W} \quad p=1,2,\dots,P \quad (4.20)$$

if at the chosen W, at all of the machine groups, the d_p values are below the physical buffer sizes, then the successful working regimes can be realized. In the

other case W should be increased (or buffer sizes increased). The planning issues are straightforward from the mentioned.

4.2 How to Start the System

Now, let us deal with the problem of how to start the system work. The rough parts come into the system from storages. We have given the way how the part demands are formulated. Clearly, at every machine-group it should be determined which part-type processing should begin first because the feedback control algorithm do not give any information about that at time instant $t=0$. (There is no previous machine which would give the command “next”.) The work starting strategy also affects how the demands are fulfilled because they determine the transient processes. It is very difficult to say anything about the selection of starting input buffers from among the input buffers because the transient processes are highly nonlinear, dynamic ones, and so their parameters are very difficult to estimate. But, according to our simulation experiments (see: [11, 12]), it is not necessary. The transient processes, usually, are very short. Another point in this line is that (as the simulations have shown) the transient parts of the motions can be used for automatic scheduling, as well, without losing anything in quality. Different rules for starting buffers selection may be developed. For example, they may be chosen in decreasing order of demand rates.

Now, let us suppose we have chosen the starting input buffers. We propose the following starting strategy. Let us introduce some starting waiting time value $t_{p,start}$. The parts arrivals begins at time $t=0$. Then, at

$$t = t_{p,start} + \delta_m^0 \quad (4.21)$$

we propose to begin the processing of the chosen part-type item on all of the machine-groups where it is possible. It is a strategically important decision how to determine the starting waiting time value. With the proper determination of these values, the time of the transient processes may be decreased. It is easy to recognize that if we want to process part-type items in number d_p in the first sub-lot (in the bottleneck machine-group, machining the part-type with label p), the following waiting time value should be applied (see: [10, 11, 12])

$$t_{p,start} = \frac{d_p(1-\tau_{p,m}r_p)}{r_p} \delta_m^0 \quad (4.22)$$

This is obtained from the relation

$$(t_{p,start} + \delta_m^0 + d_p \tau_{p,m}) r_p = d_p \quad (4.23)$$

Then, the output of the first machine-group producing the given part-type will be exactly as at the periodic regime. But because of the dynamic processes in the system, in the following the situation will change. Hopefully, the processes will converge quickly to periodic ones. It seems to us that slightly smaller values than obtained according to (4.22) would result in favorable performance. Concerning

other machine-groups than the bottleneck, the same strategy can be used. A similar Equation to (4.22) can be used but actualized for the given machine-group.

5 Demand Rates Determination in Multi-Section Case

Now, let us consider the general formulation of the FMS scheduling tasks. The order for the production is formulated at the MRP (Material Requirement Planning) level. There are given: the time sections (time windows) of production and, for every section, the types of parts and the corresponding numbers of items to be produced.

That is:

$$re_j \leq t \leq dd_j \tag{5.1}$$

$$j = 1, 2, \dots, J$$

where:

re_j – is the release time from which the production may begin,

dd_j – is the due date,

J – is the number of scheduling sections.

We will identify the part-types as follows:

for $j=1$ we have the identification index $p=1, 2, \dots, P_1$

for $j=2$ we have $p=P_1+1, P_1+2, \dots, P_2$ (5.2)

•

for $j=J$ we have $p=P_{J-1}+1, P_{J-1}+2, \dots, P_J$.

For all of the part-types, the number of part-items to be produced is given.

They are:

$$N_1, N_2, N_3, \dots, N_P \tag{5.3}$$

The scheduling sections are overlapping. This is because otherwise the tasks could be solved as outlined above for single (common) scheduling sections problems.

Let us first deal with a simple example, when there are only two sections. In the first section let be produced 2, in the second 3 part-types.

Let $re_1=0; re_2 < dd_1 < dd_2$

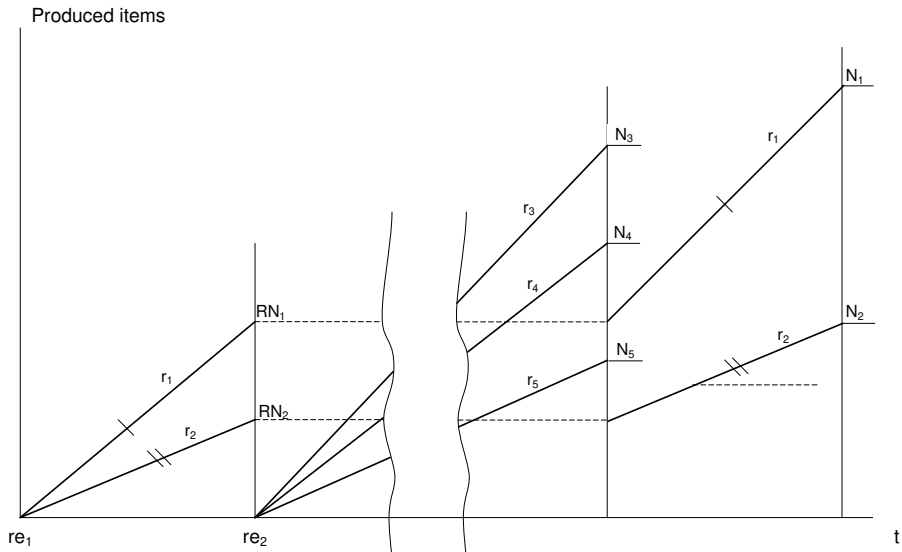


Figure 5.1

Demand rates for the example

We apply the following heuristic approach for demand rate determination. At any production period which begins at time instant re_j we produce first the part-type items scheduled for $re_j \leq t \leq dd_j$. When we arrive to a new release time instant (re_{j+1}), we interrupt to produce the items of the j -th period and begin to produce the new ones. The not finished part-type items of the j -th period will be produced later.

Now, let us consider the simple example. Let us perform for the first section all the planning steps proposed for single-sections.

We use the following symbols for the planning results:

- W_1 - is the number of sub-lots
- Mtl_1 - is the global minimum of net manufacturing time for the first section
- r_1, r_2 - are the demand rates
- T_1 - is the time-period of the periodic motions

In the case of the example, Mtl_1 is determined as

$$Mtl_1 = \text{Max}\{N_1\tau_{1,m} + N_2\tau_{2,m}\} \quad (5.4)$$

$$m=1,2,\dots,M$$

Let us begin the production in a self-organizing, decentralized, real-time controlled manner. When reaching the time instant re_2 , we interrupt producing the part-type items of the first period and begin to produce the parts of the second section. For the second section, we determine the quantities outlined above exactly

in the same manner as we did for the first section. The expression, we interrupt producing the part-type items of the first period, means that at $t=re_2$ the input flows are not introduced anymore for the input buffers and the buffer contents of part-types produced in the first period are freeze-in. The reason why we acted in this way is that the value of re_2 shows that having the parts of the second section is certainly more important than finishing the production of the part-types of the first section.

Furthermore, we have, certainly, some reserve in the due date of the task for the first section to be able for this kind of interruption. Below we will give some details about how the due dates effect the above.

So, for the first section we had the planning results:

$$W_1, Mtl_1, r_1, r_2, T_1. \quad (5.5)$$

After the interruption we can determine the planning parameters for the second section

$$W_2, Mtl_2, r_3, r_4, r_5, T_2. \quad (5.6)$$

The system actions we begin in self-organizing manner (see: Figure 3.1) for the first section. Then, at $t=re_2$ the processes of the second section begin. When these terminate the first section items are finished. For these finishing operations the best is to use the demand rates determined before (re_1 and re_2). It is advisable, inspite of the fact that the freeze-in values are not exactly those which would exactly match the planning conditions. But it is possible, of course, to recalculate the demand rates having the actual parameters (numbers of produced already sub-part-type items).

Due date aspects

Now, let us consider the opportunity to begin the production at a time instant other than re_2 . In this case we should use some estimation of the production time value for the second section. The simplest is:

$$t_{pr2}=k_2Mtl_2 \quad (5.7)$$

This value can be slightly less than the real.

Or we can use

$$t_{pr2}=(W_2+1)T_2 \quad (5.8)$$

It might be slightly more than the real production time.

A compromise is also possible (like using Equation (4.17)).

Anyway, a not very bad estimation is possible. Then, if we introduce some starting reserve time (indicated as Res_2) we have:

$$Res_2=dd_2-tpr_2 \quad (5.9)$$

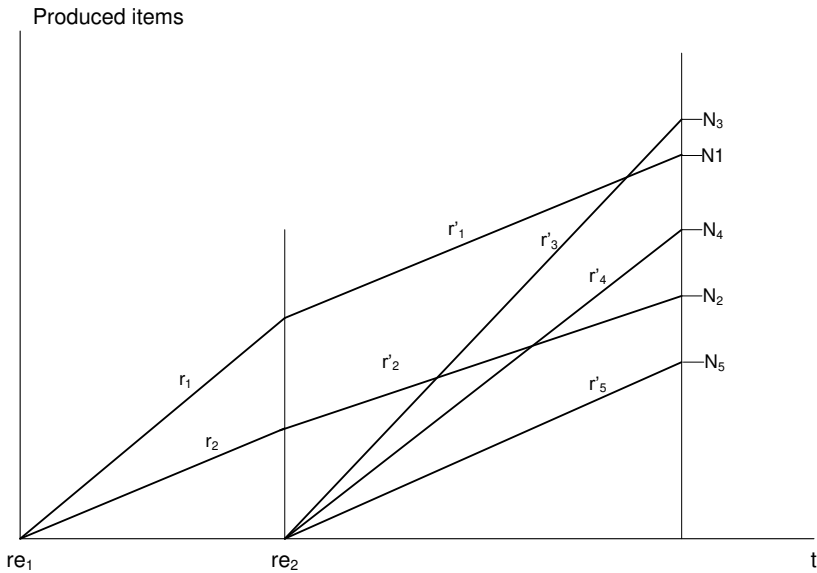


Figure 5.4
Second method of demand rates determination

General solution for demand rates determination

Now let us consider the general case as determined by Relations (5.2), (5.3).

For multi-section scheduling we propose applying the first method described above for demand rates determination.

For the first production section let us take $t=re_1=0$. By this choice we determine:

$$W_1, Mtl_1, r_1, r_2, \dots, r_{P_1}, T_1,$$

Then, for $t=re_2$ we determine

$$W_2, Mtl_2, r_{P_1+1}, r_{P_1+2} \dots r_{P_2}, T_2,$$

Going on we may have

.....
.....

$$W_J, Mtl_J, r_{P_{(J-1)+1}}, \dots, r_{P_{(J-1)+2}}, \dots, r_{P_J}, T_J, \tag{5.15}$$

Having finished the production in every section, we can estimate the number of any part-type items which were not completed and left for future production.

$$LN_i = N_i - r_i \Delta t_i \tag{5.16}$$

$i \in 1, 2, \dots, P_j$

where Δt_j is the time interval a part-type was processed during any section.

These values give the simplest estimations but do not differ too much from real numbers.

If a part-type production is interrupted several times, (5.16) is applied several times in the proper sense.

This rather simple approach described above can be used for planning of the processes. In fact, as self-organizing, distributed, real-time control is used, the processes will be determined by the nonlinear dynamics of the systems. The inputs are the demand rates and the starting time values at the starting input buffers. At system level, of course, the data should be up-dated for the different scheduling sections. To understand the nature of the problems, the inter-connection of MRP and scheduling should be analyzed.

6 MRP and Scheduling Interconnections

The production orders come from the MRP systems. MRP is product oriented. By the time a product is assembled, all of the components should be available. MRP allocates the time intervals for production and at the same time checks whether the production capacities are available or not. Every time a new part-type series comes into consideration, MRP assigns the necessary production times to all of the homogeneous capacities (machine-groups). If any production capacity is overloaded (it happens at the bottleneck machine-group), the given task is rejected. Scheduling is production oriented. It allocates the loads necessary to perform the tasks (corresponding to the given orders) to the production capacities.

There is a contradiction among MRP and scheduling. The practical scheduling problems (frequently) may not have an exact solution. So, it may happen that the capacities estimated by MRP are not enough. (Practical scheduling problems (usually) may only be solved exactly with full enumeration (see, for example, French [13]) which is in most of the cases impossible).

To eliminate the above difficulty, unnecessarily big reserves should be provided at MRP level. All this constrains significantly the MRP-scheduling system efficiency.

This difficulty is eliminated when the approach proposed in the present paper is used. The production control provides that the production time is close to the global minimum. This is caused by the automatic lot streaming and overlapping production. This means that a full load strategy may be applied at MRP level.

In Section 5 of the present paper, we analyzed the question of the estimation of the production time. The global minimum of the net manufacturing time is a good basis for this estimation. If a scheduling may be produced resulting close to the

global minimum production times, it fulfils all the expectations. The proposed control solution gives close to the above goal results. In the classical approaches, there is no direct contact between scheduling and MRP level. So, on the MRP level, the production times should be highly overestimated. This leads to the low effective utilization of devices. The hybrid dynamical approach may totally improve this situation.

It is possible to give a formal description of the proposed direct connection of scheduling and MRP, but because of the lack of space we will not give it here.

Conclusions

In the paper we outlined a **self-organizing, distributed, real-time scheduling method for Flexible Manufacturing Systems**. This method provides production times very close to the global minimum as the result of automatic lot-streaming and overlapping production. Our earlier investigations have shown that the condition of usability is to have a suitably large number of parts (as minimum 300÷ 400) in the series, and small set-up times. It seems to us that the sum of the maximum set-up times should be 300÷ 400 times less than the global minimum of net manufacturing time to produce all of the part-types in the given number. The above, is based on analytical investigations and simulation studies. **The proposed Enforced-Period-Switching-Law** and by that the **hybrid dynamical feedback control provides stability and regularity**. The first means that for every task it is possible to find buffers with given capacity which will be able to serve the stable work of machine tools (will not overflow). The second means that the processes converge to periodic ones which automatically realize lot streaming and overlapping production. The above results and the proposed control law make it possible to realize self-organizing, distributed, real-time control of flexible manufacturing systems. This is a significant achievement, not only in the respect of quality improvement but also in bringing dramatic simplification in the organization of processes control, too.

The most important achievement of the paper is the proposal for multi-section problems demand rates determination method. For the practical application, only a single planning parameter for every scheduling section should be properly chosen (the number of sub-lots or the demand rates coefficient). The paper details, also, the demand rates determination method for single-section case which is the basis for solving the multi-section problem.

The outlined makes it possible to contact directly FMS scheduling and MRP.

Acknowledgement

The research reported in the present paper was stimulated by the outstanding theoretical results of professor A. V. Savkin (UNSW, Sydney). Authors express sincere thanks for the opportunity of cooperation with him. Authors are grateful to Olesya Ogorodnikova and Akos Antal for the help in formulation of the results and the preparation of the paper.

References

- [1] Savkin A. V., Somlo J. Optimal Distributed Real-Time Scheduling of Flexible Manufacturing Networks Modeled as Hybrid Dynamical Systems. *Robotics and Computer- Integrated Manufacturing*. V. 25, Issue 3, June 2009, pp. 597-609
- [2] VanderSchaftA,SchumacherH.An Introduction to Hybrid Dynamical Systems. London: Springer; 1999
- [3] Matveev A. S., Savkin A. V. Qualitative Theoryof Hybrid Dynamical Systems. Boston: Birkhauser; 2000
- [4] Perkins J. R. Kumar P. R. Stable, Distributed, Real-Time Scheduling of Flexible Manufacturing/Assembly/Disassembly Systems. *IEEE Trans Automat Control* 1989; 34(2):139-48
- [5] PerkinsJR,Humes C. J. , Kumar P. R. Distributed Scheduling of Flexible Manufacturing Systems: Stability and Performance. *IEEE Trans Robotics Automat*1994;10(4):133-41
- [6] Savkin A. V. Regularizability of Complex Switched Server Queueing Networks Modelled as Hybrid Dynamical Systems. *Systems Control Letters* 1998;35(5):291-300
- [7] Savkin A. V., Matveev A. S. Cyclic Linear Differential Automata: A Simple Class of Hybrid Dynamical Systems. *Automatica*2000; 36(5):727-34
- [8] Savkin A. V. , Matveev A. S. A Switched Single Server System of Order n with All Its Trajectories Converging to $(n-1)!$ Limit Cycles. *Automatica* 2001; 37(2):303-6
- [9] Savkin A. V. Evans R. J. Hybrid Dynamical Systems. Controller and Sensor Switching Problems. Boston. Birkhauser, 2002
- [10] Somlo J. Hybrid Dynamical Approach Makes FMS Scheduling More Effective. *PeriodicaPolitechnica Ser. Mech. Eng.* 2001;45(2):175-200
- [11] Somlo J., Savkin A. V., Anufriev A., Koncz T. Pragmatic Aspects of the Solution of FMS Scheduling Problems Using Hybrid Dynamical Approach. *Robotics and Computer Integrated Manufacturing* 2004;20:35-47
- [12] Somlo J. Savkin A. V. Periodic and Transient Switched Server Schedules for FMS. *Robotics and Computer Integrated Manufacturing*. 2006. 22;93-112
- [13] Castillo I., Smith J. S. Formal Modeling Methodologies for Control of Manufacturing Cells: Survey and Comparison. *J. Manuf. Systems* 2002;21(1):40-57
- [14] .Coffman E. G. Computer and Job-Shop Scheduling Theory. NewYork:Wiley, 1976

- [15] French S. Sequencing and Scheduling: an Introduction to the Mathematics of the Job-Shop. NewYork:Wiley;1982
- [16] Dai J. G., Weiss G. A Fluid Heuristic for Minimizing Make Job Shops. *Oper. Res.* 2002;50(4):692-707
- [17] Kumar P. R., Seidman T. I. Dynamic Instabilities and Stabilization Methods in Distributed Real-Time Scheduling of Manufacturing Systems. *IEEE Trans. Automat. Control.*1990;35(3):289-98
- [18] Rybko A. N. ,Stolyar A.L. Ergodicity of Stochastic Processes Describing the Operations of Open Queueing Networks. *ProblemyPeredachi Inf.* 1992;28:2-26
- [19] Dai J. G., Hasenbein J. J., VandeVate J. H. Stability of a Three-Station Fluid Network. *Queueing Systems.*1999;33:293-325
- [20] Dauzere-Peres S, Lasserre J. B. An Iterative Procedure for Lot Streaming in Job-Shop scheduling.*Comput. Ind .Eng.* 1993;25(1-4):231-4
- [21] Somlo J, Kodeekha E. Optimal Lot Streaming for a Class of FMS Scheduling Problems – Joinable Schedule Approach. *Proc. IFAC CEFIS'07 Symposium.* Oct. 9-11, 2007, Istambul, Turkey
- [22] Somlo J., Kodeekha E. Improving FMS Scheduling by Lot Streaming. *Journal PeriodicaPolytechnika. Ser. Mechanical Engineering.* 2007, 51/1, 3-14, Budapest, Hungary

Correcting Fine Structure of Surfaces by Genetic Algorithm

György Gyurecz¹, Gábor Renner²

¹ Institute of Machine Design and Safety Engineering, Óbuda University
Népszínház u. 8, H-1081 Budapest, Hungary, gyurecz.gyorgy@bgk.uni-obuda.hu

² Computer and Automation Research Institute, Hungarian Academy of Sciences
Kende u. 13-17, H-1111 Budapest, Hungary, renner@sztaki.hu

Abstract: Highlight lines are powerful in quality evaluation and disclosing errors of high quality surfaces. We propose a method that enables the designer to correct surfaces by adjusting their highlight lines. The adjustment of highlight line curves is carried out by replacing the defective parts with curves of the designer's intent. The corrected surface, which corresponds to the highlight line adjustment, is determined by a genetic algorithm (GA). The paper discusses genetic representation and fitness function developed for the specific problem and gives a usability analysis. The advantage of the method is its robustness and applicability to surfaces regardless of shape, and CAD representation. The method is meant to be applied in the final phase of shape modeling; its effectiveness is demonstrated by several industrial examples.

Keywords: surface errors; highlight lines; genetic algorithm

1 Introduction

The class of “high quality surfaces” is attributed to their smoothness, evenness and aesthetic appeal. The most important high quality surfaces in industry are those representing car, airplane and ship hulls, household appliances, etc. Their design involves not only functional criteria but also subjective ones, related to style and appearance. Creating methods and tools that support the work of a stylist is a challenging task in the areas in CAD and CAGD (Computer Aided Geometric Design).

Various visual display methods are available for the quality evaluation of surfaces. Some of these are also suitable for visualizing different representations of reflection status of the surfaces [8, 9, 15, 16]. In this way, designers can determine surface quality in accordance with their own aesthetic demands. One of the most sensitive indicators of surface quality is the highlight line display method. The

method is well applicable in disclosing minor errors and in fine tuning of surface shape that other methods fail to achieve.

Related work. The highlight-line display method was first suggested by Klaus-Peter Beier and Yifan Chen [1] but they didn't address surface modification. A method for smoothing free form surfaces by the adjustment of highlight lines was first developed by Klass and Kaufmann [13, 14]. The correlation between highlight lines and the defining parameters of the surfaces i.e. control points (CP) is established by a non-linear equation system, which is too time consuming to solve, and the results are not always good enough. The method developed by Zhang and Cheng [17] introduces a great number of simplifications to obtain a linear system of equation to modify control points through highlight lines. However, the highlight line cannot accurately follow the points specified by the designer and the method yields adequate results only in a small range of the errors.

The above methods try to handle the complex mathematic relation between the adjusted highlight line and the defining parameters of the corresponding surface. We propose a method that solves this problem by genetic algorithms (GA), which can find modified control points even in the absence of direct mathematical relations.

The proposed method of surface correction starts with the computation of highlight lines (Figure 1). Inspection of the surface quality is carried out by several light-source settings and surface orientations. Then the designer selects and corrects the defective highlight lines using the facilities of a CAD system [2]. This is followed by the automatic determination of the affected surface region and corresponding control points. Adjustment of the control points is carried out by a genetic algorithm.

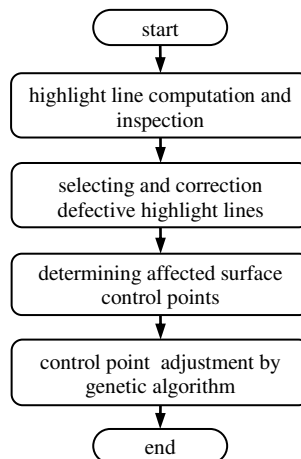


Figure 1

Block diagram of the surface correction method

2 Representation of Surfaces and Highlight Line Computation

Parametric representation of the free form surfaces in Bézier, B-spline or NURBS form [12] are widely used in CAD applications. In surface design they are used for the interactive creation and modification of shapes as well for converting physical prototypes, such as automotive clay models, into CAD models. Parametric representation defines the shape of the surface $\mathbf{S}(u, v)$ by an array of control points \mathbf{P}_{ij} and the Bézier, B-spline or NURBS basis functions N_{ik} and N_{jl} of order k as

$$\mathbf{S}(u, v) = \sum_{i=0}^m \sum_{j=0}^n \mathbf{P}_{ij} N_{ik}(u) N_{jl}(v) \quad (1)$$

The shape of the surface is mainly defined by the control points, knots and weights of the basis functions provide additional degree of freedom in design.

A highlight line is created on the surface by the reflection of a linear light-source of infinite length. The highlight line consists of a set of highlight points. They are points on the surface where the corresponding surface normal and the light-source intersect each other; that is, the perpendicular distance between them is zero.

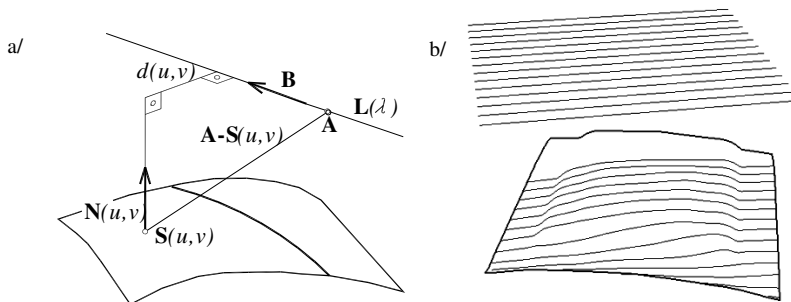


Figure 2

Distance interpreted between surface normal and the light-source (a) Highlight lines of a surface (b)

The line of the light-source can be described as $\mathbf{L}(\lambda) = \mathbf{A} + \mathbf{B}\lambda$ where \mathbf{A} is a point on $\mathbf{L}(\lambda)$, and \mathbf{B} is a vector defining the direction of the line (Figure 2a). The signed perpendicular distance $d(u, v)$ between the normal $\mathbf{N}(u, v)$ at a surface point $\mathbf{S}(u, v)$ and the linear light-source is:

$$d(u, v) = \frac{[\mathbf{B} \times \mathbf{N}(u, v)] \cdot [\mathbf{A} - \mathbf{S}(u, v)]}{\|\mathbf{B} \times \mathbf{N}(u, v)\|} \quad (2)$$

For a point on the highlight line $d(u, v) = 0$ holds, which must be solved for the control points of $\mathbf{S}(u, v)$. To calculate highlight lines, this relation must be computed with high accuracy. We have developed a robust method for computing highlight lines, which is described in detail in [6].

For the detailed investigation of surfaces, an appropriate set of coplanar parallel linear light-sources is necessary (See Figure 2b). As a result, a corresponding set of highlight lines is obtained; their distribution density and shape is a firm and sensitive indicator of surface quality.

3 Fundamentals of Genetic Algorithm

Genetic algorithms were introduced by J. H. Holland [11]. The basic idea is to apply the Darwinian mechanism of evolution in finding optimal solution to complex or non-linear problems. Solutions are represented by chromosomes, composed of genes that contain variable parameters of the solution. The chromosomes form a population and they are evaluated according to predefined criteria called fitness, which quantifies the optimality of the solution they represent. Chromosomes of the next generations are created by genetic operators. The basic operators include selection, crossover and mutation. The algorithm runs until stop criteria is met; that is, until an acceptable solution is found, or a maximal number of generations is reached. A number of articles have been published dealing with the design of GA [3, 4, 5, 10].

The parameters of effective GA including the applied operator types depend on the particular problem. Their selection and adjustment must be analyzed and tested carefully. Special attention must be made to the fitness function. It should be composed of terms closely related to the objective of the search. The effectiveness of GAs is often characterized by achieving precise results quickly and reliably in a wide parameter range of the particular problem.

4 Genetic Algorithm in Surface Correction

Our goal is to correct the shape of surfaces by means of their reflection characteristics through the shape and distribution of their highlight lines. The objective of GA is to adjust the parameters of the surfaces, resulting in a new surface shape that produces the desired highlight lines.

The efficiency of the proposed method was tested on several industrial surfaces that greatly differ from each other in size, shape and degree of detected shape irregularity. This latter is defined in terms of magnitude, extent and complexity of the shape error. Special attention was paid to tuning the genetic process, in order to arrive at a fast and stable process that at the same time reveals the desirable technical solution.

In this paper we outline the GA we developed by providing its main characteristics and give insight into the construction of three, problem specific elements – the genetic representation, the fitness function and the stop condition. A more detailed description of our GA can be found in [7].

4.1 Structure of Genes and Chromosomes

Free form surfaces are determined by a number of parameters. However, the most effective parameter for surface modification is the control point $\mathbf{P}_{i,j}$. In genetic representation those control points are included that have influence on the surface region that the designer wants to optimize. They can be computed from the basis functions corresponding to particular control points. Their strength of influence is represented by the constant $b_{i,j}$, which is calculated by integrating the basis functions over the region of interest. A gene g_γ consist of control point modification $\Delta\mathbf{P}_{i,j}$ and the constant $b_{i,j}$ applied to the corresponding $\mathbf{P}_{i,j}$:

$$g_\gamma = \Delta\mathbf{P}_{i,j}(x, y, z), b_{i,j}. \quad (3)$$

where x , y and z are Cartesian co-ordinates of $\Delta\mathbf{P}_{i,j}$, while γ is the identifier of genes within a chromosome. The chromosome of a surface has the following structure: $c_\beta = (g_1 \dots g_\gamma \dots g_J)$, where β identifies the chromosome in the population and J is the number of genes in the chromosomes.

4.2 Search Space

The search space of the GA is the region in the space where the control points may vary. It is the union of search spaces of chromosomes r_β , and is defined by

$$r_\beta = s \cdot b_{i,j}. \quad (4)$$

The scaling factor s is estimated from the maximal necessary improvement of the highlight lines. The search space limits the change of control point positions in the generation of initial population and in mutation.

4.3 Fitness Function

The developed fitness function contains geometric deviation between actual and desired highlight lines. It consists of two components: accuracy and shape similarity. Accuracy is based on the distance, while shape similarity on the angle difference of tangent vectors between corresponding highlight points. Denote h_i^{des} the desired, and h_i^{cur} the highlight line, created during the search and $d_i(t_k)$ the deviation between corresponding highlight points at different t parameters of highlight lines. Then, the distance error component of the fitness function is:

$$f_{\text{dist}} = \sum_{i=1}^l \left(\sum_{k=1}^{n_i} \left(d_i(t_k) - \frac{1}{n_i} \cdot \sum_{k=1}^{n_i} d_i(t_k) \right)^2 \cdot \frac{1}{n_i} \right) \quad (5)$$

where $d_i(t_k) = |h_i^{cur}(t_k) - h_i^{des}(t_k)|$ while n_i denotes the number of examined highlight points. Variable l indicates the number of highlight lines. The angle

difference of the error component f_{ang} is calculated in same manner, except the deviation is composed as follows:

$$d_i(t_k) = \arccos \left(\frac{\mathbf{h}_i^{\text{des}}(t_k) \cdot \mathbf{h}_i^{\text{cur}}(t_k)}{\|\mathbf{h}_i^{\text{des}}(t_k)\| \|\mathbf{h}_i^{\text{cur}}(t_k)\|} \right) \quad (6)$$

We evaluated the fitness components regarding their efficiency of correcting highlight lines. We found that the distance error component promotes the creation of accurate highlight lines, but their shape similarity is often poor. The tangency error component behaves in the opposite way; it promotes producing highlight lines with good shape similarity, but at the expense of their accuracy. We eliminated the disadvantages by weighting so that the distance component dominates in the beginning, while the tangency component is prevalent in the latter phase of the search. This is realized by the following fitness function:

$$f = f_{\text{dist}}(w_{\text{dist}}^0 - \Delta w) + f_{\text{ang}}(1 - w_{\text{dist}}^0 + \Delta w) \quad (7)$$

where w_{dist}^0 is the weight of distance error component of the initial population, and Δw is the weight value change during the search.

Fine adjustment of fitness function was performed by choosing an appropriate weighting strategy. They were applied to several test surfaces with different shape errors. In each case a rank concerning the number of generations to reach the stop condition was established.

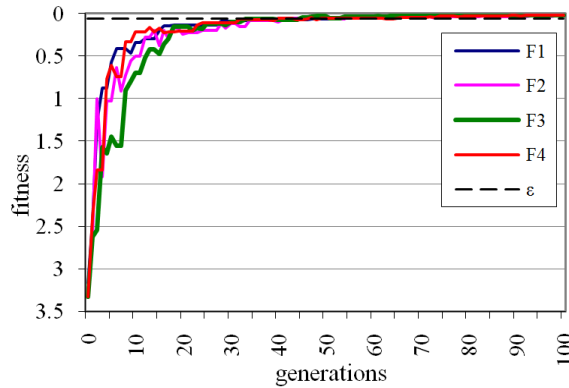


Figure 3

Weight change strategies tracked in fitness development

In Figure 3, comparison of four strategies applied to a particular case is seen. The final rank of a weighting strategy is determined by the average rank calculated concerning all test surfaces. In Table 1 the parameters and the calculation rules of the best performing strategies are shown. It can be seen that the best rank – the best weighting strategy – is obtained by strategy F3.

Table 1
Best performing weighting strategies

Id.	parameter(s)	calculation rule	rank
F1	$w_{dist}^0 = 0.75$	$\Delta w = 0$	4.25
F2	$w_{dist}^0 = 0.8, a = 0.75$	$\Delta w = 0$ if $\tau < a\tau_{max}$ else $\Delta w = 2w_{dist}^0 - 1$	2.625
F3	$w_{dist}^0 = 0.75$	$\Delta w = (2w_{dist}^0 - 1) \cdot (1 - (c_{var}^0 - c_{var}^{\tau-1}))$	1.25
F4	$w_{dist}^0 = 1, a = 0.15$	$\Delta w = 0$ if $c_{var}^0 - c_{var}^{\tau-1} < a$ else $\Delta w = 2w_{dist}^0 - 1$	2.375

Where a coefficient that defines the swap point of component weights
 τ index of the current generation
 τ_{max} allowed maximal number of generations
 c_{var}^0 chromosome variability of the initial population
 $c_{var}^{\tau-1}$ chromosome variability of the previous generation

4.4 Stop Condition

The source of the search stop condition is the allowable residual error, which is based on the comparison of the original and the redesigned highlight lines. Let μ_{stop} denote the stop condition

$$\mu_{stop} = \begin{cases} \text{true} & \text{if } f^\tau / f^0 \leq \varepsilon \text{ or } \tau = \tau_{max} \\ \text{false} & \text{otherwise} \end{cases} \quad (8)$$

Where ε is the allowable residual error.

f^τ fitness of the best chromosome at generation number τ

f^0 fitness of the initial chromosome.

In case the search fails to meet the stop condition, it is stopped at the maximum number of generations τ_{max} . During the analysis, we used the following stop conditions: $\varepsilon = 0.05$, $\tau_{max} = 100$.

5 Analysis and Results

In practice, different sizes, extents and complexity of shape errors occur in different design conditions that may have influence on the quality and preciseness of the resulting surface. We investigated this relation extensively. In this paper we give details of one investigation; we prove that the same final surface is achieved regardless of the size of the necessary corrections.

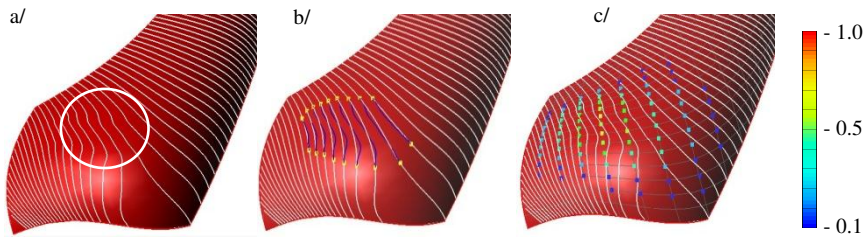


Figure 4

Disclosing defective highlight lines (a) Redesign of highlight lines (b) Affected CP-s (c)

Figure 4a displays the defective highlight lines of a car body part. Irregularities occur in the indicated region. The domain of highlight lines to be redesigned is marked by the designer (parts between bullets in Figure 4b). The affected control points are selected automatically. The different colors of control points in Figure 4c indicate the values of b_{ij} . Genetic search is performed with the above genetic operators and the fitness function. GA runs until the user-defined stop criterion is fulfilled. The same surfaces with different quality, i.e. different error sizes in the highlight lines were taken into consideration. The results of the analysis are presented in Table 2.

Table 2

Data to measure the efficiency and robustness of the algorithm

	size_1	size_2
average distance between desired and the defective highlight lines [mm]	0.57	1.54
average distance between desired and the corrected highlight lines [mm]	0.028	0.031
improvement [%]	95	98
average distance between highlight lines of corrected surfaces [mm]	0.017	
iterations (number of generations past)	72	84

The initial error defined as the average distance between the desired and the defective highlight lines are highly different (more than 100%). The average distance between the desired and the corrected highlight lines shows how the initial error was eliminated by an improvement of 95% and 98% respectively. The average distance between the highlight lines of the corrected surfaces (0.017 mm) indicates that the algorithm converged to the same resulting surface in both case. This can be also verified by the distance map defined between the corrected surfaces (Figure 5). It can be easily recognized that the difference between them is insignificant.

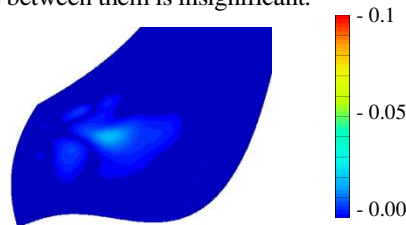


Figure 5

Difference map between resulting surfaces

To measure the computational costs of solving the problem, we used the required number of generations. In the case of bigger error it took 84 generations, while in case of smaller error 72 generations, to reach the stop criteria. This means that the algorithm needed only 17% more computation for a surface error that caused 170% growth in the error of highlight lines.

In the following we give practical examples visually demonstrating the efficiency of our method in Figures 6, 7 and 8. The rendered pictures of the surfaces (a. in figures) seem to be free of errors. The fine structure of the surface is disclosed by highlight lines, and the effective regions are indicated by circles (b. in figures). The highlight lines of the corrected surfaces are shown in c. figures. Their shape, smoothness, coherence and distribution show that the surfaces are smooth and error free.

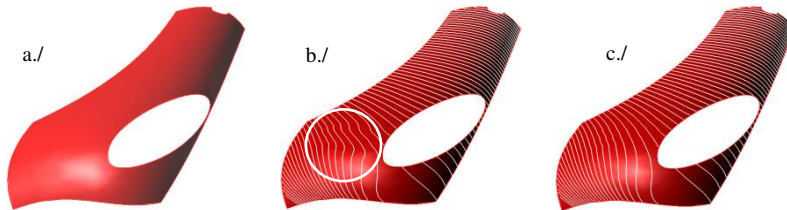


Figure 6

Surface of a car-body element before (a. and b.) and after correction (c.)

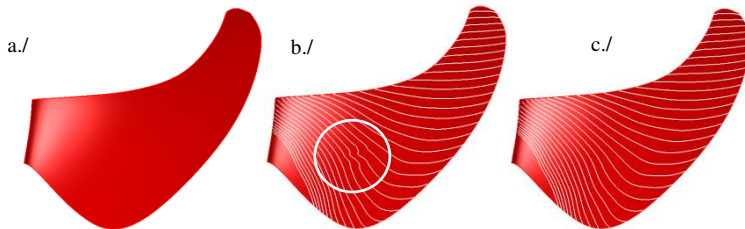


Figure 7

Surface of a propeller shovel before (a. and b.) and after correction (c.)

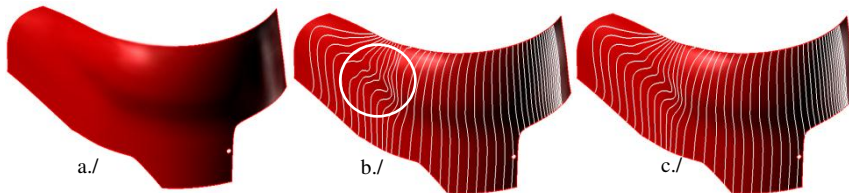


Figure 8

Surface of a car-body element before (a., b.) and after correction (c.)

Conclusion

A robust and intuitive method for correcting surface errors by highlight lines was presented. Control point modification is achieved through genetic algorithm, circumventing the computation of highly non-linear relations between control

points and highlight lines. Our method is applicable to surfaces of any shape and any kind of CAD representations. It can be successfully applied to a wide range of highlight line and surface errors. The increase of computational cost is much smaller than the corresponding error size growth.

References

- [1] Beier K. P., Chen Y., Highlight-Line Algorithm for Real Time Surface Quality Assessment, *Computer Aided Design*, 1994, 26(4), pp. 268-277
- [2] Catalano C. E., Falcidieno B., Giannini F., Monti M., A Survey of Computer-Aided Modeling Tools for Aesthetic Design, *J. Comput. Inf. Sci. Eng.*, 2002, 2(1) pp. 11-21
- [3] Deb K., Anand A., Josh D., A Computationally Efficient Evolutionary Algorithm for Real-Parameter Optimization, 2002, Kanpur, Genetic Algorithms Laboratory
- [4] Deb K., *Multi-objective Optimization using Evolutionary Algorithms*, 2001, Chichester, Wiley
- [5] Goldberg D. E., *Genetic Algorithms for Search, Optimization, and Machine Learning*, 1989, Reading, MA: Addison-Wesley
- [6] Gyurecz Gy., Renner G., Robusztus módszer reflexiós vonalak számítására. *Gépgyártás*, 2009, 49(1), pp. 8-11
- [7] Gyurecz Gy., Renner G., Improving Quality of Freeform Surfaces Using Genetic Algorithm and Highlight Lines, *TMCE*, 2010, pp. 317-331
- [8] Hagen H., Hahmann S., Schreiber T., Nakajima Y., Würdenweber B., Hollemann-Grundstedt P., Surface interrogation algorithms, *IEEE Computer Graphics and Applications*, 1992, 12(5), pp. 53-60
- [9] Hahmann S., Belyaev A., Buse L., Elber G., Mourrain B., Rössl, C., *Mathematics and Visualization, Shape Interrogation*, 1998 Springer, Berlin
- [10] Herrera F., Lozano M., Verdegay J. L., Tackling Real-coded Genetic Algorithms, *Artificial Intelligence Review*, 1998, 12(4), pp. 265-319
- [11] Holland J. H., *Adoption in Natural and Artificial Systems*, 1998, MIT Press Edition
- [12] Hoschek J., Lasser D., *Fundamentals of Computer Aided Geometric Design*, AK Peters, Wellesley, MA 1993
- [13] Klass R., Correction of Local Surface Irregularities Using Reflection Lines. *Computer Aided Design*, 1980, 12(2), pp. 73-78
- [14] Kaufmann E., Klass R., Smoothing Surfaces Using Reflection Lines for Families of Splines, *Computer Aided Design*, 1988, 20(6), pp. 312-316
- [15] Patrikalakis N. M., Maekawa T., *Shape Interrogation for Computer Aided Design and Manufacturing*, 2002, Heidelberg, Springer-Verlag
- [16] Pottmann H., Visualizing Curvature Discontinuities of Free-Form Surfaces. *Eurographics' 89*, 1989, pp. 529-36
- [17] Zhang C., Cheng F., Removing Local Irregularities of NURBS Surfaces by Modifying Highlight Lines, *Computer Aided Design*, 1998, 30(12), pp. 923-930

Secure Unicast Position-based Routing Protocols for Ad-Hoc Networks

Liana Khamis Qabajeh, Miss Laiha Mat Kiah

Faculty of Computer Science and Information Technology
University of Malaya
58200 Kuala Lumpur, Malaysia
liana_tamimi@ppu.edu; misslaiha@um.edu.my

Mohammad Moustafa Qabajeh

Department of Electrical and Computer Engineering
International Islamic University Malaysia
58200 Kuala Lumpur, Malaysia
m_qabajeh@yahoo.com

Abstract: Ad-Hoc networks are decentralized wireless networks. A fundamental problem in Ad-Hoc networks is finding a secure and correct route between a source and a destination efficiently. The need for scalable and energy efficient routing protocols, along with the availability of small, inexpensive and low power positioning instruments, results in making position-based routing protocols a promising choice for mobile Ad-Hoc networks. This paper presents an extensive overview of the existing Ad-Hoc unicast routing protocols that make forwarding decisions based on the geographical position of the destination of a packet, while keeping security issues in mind. We outline the main problems for this class of routing protocols and a qualitative comparison of the existing protocols is done in regards to both security and performance issues. We conclude our work by investigating some future research opportunities.

Keywords: secure, unicast, position-based routing, location-aware routing, ad-hoc networks, wireless networks, routing protocols

1 Introduction

An Ad-Hoc network is considered as a very particular network since it is a self-organizing network with no pre-deployed infrastructure and no centralized control; instead, nodes carry out basic networking functions like routing. With this flexibility, Ad-Hoc networks have the ability to be formed anywhere and at any

time. In addition to traditional uses such as for military battlefields, these networks are being increasingly used in every-day applications, such as in conferences, personal area networking and meetings.

Routing protocol in Ad-Hoc networks is a fundamental part of the network infrastructure that supports the delivery of packets. It is a challenging task, as it has to face the challenge of link instability, frequently changing topology, the absence of a fixed infrastructure and low transmission power. Also, owing to differences in transmission capacity, some of the links may be unidirectional, which leads to the existence of asymmetric links.

All nodes in the network act as routers; hence security in routing protocols is necessary to guard against attacks, such as eavesdropping, spoofing, misdirection and the generating of deceptive routing messages. Moreover, wireless networks are generally more susceptible to physical security risks than wired networks. Therefore, routing in Ad-Hoc networks is a difficult task to accomplish efficiently, robustly and securely.

Several routing protocols have been proposed for Ad-Hoc networks. In general, they can be divided into two main categories: *topology-based* and *position-based*. Topology-based routing protocols use information about links that exist in the network to perform packet forwarding. However, position-based routing protocols use the nodes' geographical positions to make routing decisions, which improves performance and efficiency.

Although topology-based routing protocols (such as *DSR* [8] and *AODV* [7]) represent important steps in Ad-Hoc routing research area, some of these are not scalable and still exhibit security vulnerabilities. Even secure ones (such as *SAODV* [12], *ARIADNE* [37] and *ARAN* [22]) have some problems, such as single point of attack and failure, increased packet and processing overhead, as well as delays in the route discovery process. These problems become worse if these protocols are implemented in large networks since any request packet is flooded to the entire network.

Position-based Ad-Hoc routing protocols have proved to have better performance than traditional topology-based ones in end-to-end throughput and network scalability. Many position-based routing protocols have been proposed for Ad-Hoc networks such as *MFR* [16], *DIR* [11], *GPSR* [5], *ARP* [32], *I-PBBLR* [34] *DREAM* [28], *LAR* [38], *LARWB* [30], *LABAR* [13], *GRID* [33] and *TERMINODES* [23]. Although each of these protocols employs different techniques the basic goal is the same: only nodes making forward progress toward the destination are supposed to be involved in the route discovery process in an attempt to decrease the overall routing overhead.

These protocols require that a node be able to obtain its own, as well as the destination's geographical position. Generally, this information is obtained via Global Positioning System (GPS) and location services. The routing decision at

each node is then based on the destination's position contained in the packet and the position of the forwarding node's neighbors. So packets are delivered to the nodes in a particular geographic region in a natural way. There are different kinds of position-based protocols, which can be categorized into three main groups: *Restricted Directional Flooding (RDF)*, *greedy* and *hierarchical* protocols [27] (to be discussed in Section 2).

All the aforementioned position-based routing protocols are exposed to some attacks as they focus on improving performance while disregarding security issues [31]. Recently some secure unicast position-based routing protocols have been proposed for mobile Ad-Hoc networks; *SPAAR* [29], *AODPR* [31] and *SGF* [21].

This survey is a continuation of our work in [24] and [26]. Our previous works have discussed position-based routing in general. In this paper, however, we have concentrated mainly on security issues by providing an extensive overview of the existing *secure* position-based routing protocols for Ad-Hoc networks. We outline the main problems that need to be solved for this class of routing protocols and present the solutions that are currently available. The discussed protocols are also compared with respect to the security level they achieve, the used location service, the used forwarding strategy, tolerability to position inaccuracy, robustness, implementation complexity, scalability, packet and processing overhead, guaranteeing loop-freedom, probability of finding the shortest path as well as the suitable network density for deployment.

The rest of the paper is organized as follows. Section 2 presents the basic idea and principles of position-based routing. Section 3 tackles security issues and requirements in Ad-Hoc networks routing protocols. Section 4 gives an overview of the selected secure position-based routing protocols. Sections 5 and 6 contain a qualitative comparison as well as analysis and discussion of the presented protocols. Future research directions are outlined in Section 7. Finally, we conclude the paper in Section 8.

2 Basic Principles of Position-based Routing

An important requirement of position-based routing is for the source node to be able to obtain the current position of the destination node. Usually a location service is responsible for this task. Existing location services are classified according to how many nodes host the service. This can be either some specific nodes or all nodes of the network. Additionally, each location server may maintain the position of some specific or all nodes in the network. The four possible combinations can be summarized as some-for-some, some-for-all, all-for-some and all-for-all [27].

Three main packet-forwarding strategies are used for position-based protocols: *greedy forwarding*, *Restricted Directional Flooding (RDF)* and *hierarchical* approaches. While their main objective is to utilize available position information in the Ad-Hoc routing, their means to achieve it are quite different. Most position-based protocols (such as *MFR*, *DIR*, *GPSR*, *ARP* and *I-PBBLR*) use *greedy forwarding* to route packets from a source to the destination. Greedy protocols do not establish and maintain paths between sources and their destinations; instead, a source node includes the position of the data packet's destination and selects the next hop depending on the optimization criteria of the algorithm, the nearest neighbor to the destination for example. Each intermediate node selects a next hop node until the packet reaches the destination. In order for the nodes to be able to do so, they periodically broadcast small packets (called beacons) to announce their position and enable other nodes to maintain a 1-hop neighbor table.

Some greedy position-based routing protocols, such as *MFR*, try to minimize the number of hops by selecting the node with the largest progress; i.e., the projection of the distance of the next hop from the sender on the straight line between the sender and the destination. Compass routing algorithms, such as *DIR*, try to minimize the spatial distance that a packet travels and base on forwarding the packet to the neighboring node that minimizes the angle between itself, the previous node and the destination. Whatever the used optimization criteria is, greedy forwarding is efficient, scalable and resilient to topology changes since it does not need routing discovery and maintenance. Greedy forwarding robustness is medium since the failure of an individual node may cause the loss of a packet in transit, but it does not require setting up a new route, as would be the case in topology-based Ad-Hoc routing.

On the other hand, periodic beaconing creates lot of congestion in the network and consumes the nodes' energy [32]. While the beaconing frequency can be adapted to the degree of mobility, a fundamental problem of inaccurate (outdated) position information is always present; a neighbor selected as a next hop may no longer be in transmission range. This leads to a significant decrease in the packet delivery rate with increasing node mobility. To reduce the inaccuracy of position information, it is possible to increase the beaconing frequency. However, this increases the load on the network, creates lot of congestion, increases the probability of collision with data packets and consumes the nodes' energy [34].

Unfortunately, greedy routing may not always find the optimum route, and it may even fail to find a path between source and destination when one exists [21]. An example of this problem is shown in Fig. 1. The problem here is that *S* is closer to the destination *D* than any of the nodes in its transmission range; greedy forwarding will reach a local maximum even if there is a valid path from *S* to *D*. Generally, greedy forwarding works well in dense networks, but in sparse networks it fails due to voids; i.e., regions without nodes [11].

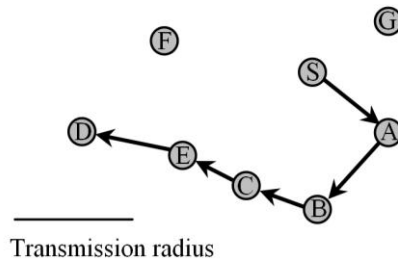


Figure 1
Greedy routing failure example

Finally, *DIR* and any other method that includes forwarding a message to a neighbor with closest direction are not loop-free as shown in [17] using the counterexample in Fig. 2. In *DIR* the source or intermediate node *A* uses the location information of the destination *D* to calculate its direction. Then the message *m* is forwarded to the neighbor *C*, such that the direction *AC* is closest to the direction *AD*. Referring to Fig. 2 the loop consists of four nodes denoted *S*, *B*, *C* and *A*. The transmission radius is as indicated in the figure. Let the source be any node in the loop, e.g. *S*. Node *S* selects node *B* to forward the message, because the direction of *B* is closer to destination *D* than the direction of its other neighbor *A*. Similarly node *B* selects *C*, node *C* selects *A*, and node *A* selects *S*.

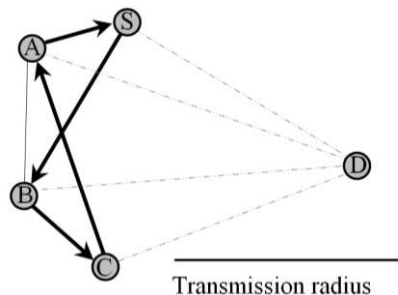


Figure 2
A loop in the directional routing

In *RDF*, such as *DREAM*, *LAR*, *LARWB* and *MLAR*, the sender will broadcast the packet to all 1-hop neighbors towards the destination. The node which receives the packet checks whether it is within the set of nodes that should forward the packet (according to the used criteria). If yes, it will retransmit the packet. Otherwise, the packet will be dropped. In *RDF*, instead of selecting a single node as the next hop, several nodes participate in forwarding the packet in order to increase the probability of finding the shortest path and the robustness against a failure of individual nodes and position inaccuracy. On the other hand, they have higher communication complexity than greedy ones and, therefore, have less scalability to large networks.

The last forwarding strategy is to form a *hierarchy* in order to scale to a large number of mobile nodes. Some strategies combine nodes' locations and hierarchical network structures by using zone based routing such as *LABAR*. Others use dominating set routing such as *GRID*. Some others, such as *TERMINODES*, present a two level hierarchy within them; if the destination is close to the sender (in number of hops), packets will be routed base on a proactive distance vector. Greedy routing is used in long distance routing; as a result, they inherit some characteristics of greedy forwarding.

We note that none of the above mentioned position-based routing protocols defined their security requirements and that they inherently trust all participants. Obviously, this could result in security vulnerabilities and exposures that could easily allow routing attacks. Recently, a limited work has been done to introduce some security issues to position-based routing protocols. Examples of these are *Secure Position Aided Ad-Hoc Routing (SPAAR)* [29], *Anonymous On-Demand Position-based Routing in Mobile Ad-Hoc Networks (AODPR)* [31] and *Secure Geographic Forwarding (SGF)* [21]. These protocols are discussed in details in Section 4.

3 Security Issues in Ad-Hoc Routing Protocols

Ad-Hoc network security, in particular routing protocols security, has attracted more attention recently. Securing Ad-Hoc routing faces many challenges, especially that each user brings to the network his/her own mobile unit, without any centralized control such as is found in a traditional network. In Ad-Hoc routing protocols, nodes exchange information with each other about the network topology, constructing a virtual view of the network topology to allow the routing of the data packet. This information allows them to create, delete and update routes between the nodes of the network. On the other hand, this capability can pose a security weak point in Ad-Hoc networks because a compromised node could give bad information to redirect traffic or simply stop it. Thus, this information must be protected to avoid malicious nodes disrupting the network [15].

Securing Ad-Hoc routing faces difficulties which do not exist in wired networks, nor in infrastructure-based wireless networks. These difficulties make trust establishment among nodes virtually impossible [4]. Among these difficulties are the wireless medium itself and its physical vulnerability, the lack of centralized control and permanent trust infrastructure, the cooperation of nodes, restricted power and resources, highly dynamic topology and short-lived connectivity and availability, implicit trust relationship between neighbors and other problems associated with wireless communication [4] [15].

To ensure the security of Ad-Hoc networks, a number of requirements need to be satisfied. These requirements are availability, confidentiality, integrity, authentication and non-repudiation [2] [6] [25]:

- **Availability:** the network should remain operational and available to send and receive messages at any time. It is supposed to be robust enough to tolerate link failure and survive despite attacks.
- **Confidentiality:** provides secrecy to sensitive data being sent over the network; the contents of every message can be understood only by its source and destination. Although an intruder might get hold of the data being sent, he should not be able to derive any useful information.
- **Integrity:** ensures that messages being sent over the network are not corrupted by intentional or accidental modification.
- **Authentication:** ensures the identity of the nodes in the network, to assure that they are who they claim to be.
- **Non-repudiation:** guarantees that neither sender nor receiver can deny that he has sent or received the message.

Recently, as privacy has emerged as an important security issue, plenty of work on anonymous routing has been done (such as *ANODR* [18], *SDAR* [1], *ASRP* [35], *ODAR* [9] and *A3RP* [20]). Anonymity in an Ad-Hoc routing means that the identity of node, route path information, and location information should be veiled from not only an adversary, but also other valid nodes.

4 Secure Position-based Ad-Hoc Routing Protocols

In this section the selected protocols are described. For each protocol, we tried to summarize its main objectives, the basic security mechanisms used, how it works and its advantages and disadvantages compared to other protocols. Additionally, a performance analysis is conducted, taking into consideration the following evaluation criteria:

- **Location service type:** indicates the type of the location service used with the given protocol, i.e., shows how many nodes participate in providing location information and for how many other nodes each of these nodes maintains location information.
- **Location service robustness:** it is considered to be low, medium or high depending on whether the position of a given node will be inaccessible upon the failure of a single node, the failure of a small subset of the nodes or the failure of all nodes, respectively.

- Approach: describes the fundamental strategy used for packet forwarding.
- Tolerable position inaccuracy: forwarding strategies tolerate different degrees of inaccuracy of the position of the destination. This is reflected by the tolerable position inaccuracy criterion.
- Robustness: the robustness of a particular protocol is considered as high if the failure (or absence due to mobility) of a single intermediate node does not prevent the packet from reaching its destination. It is medium if the failure of a single node might lead to the loss of the packet but does not require the set up of a new route. Finally, it is low if the failure of an individual node might result in packet loss and the setting up of a new route. Thus, the routing protocols that start data transmission immediately without routing setup have at least medium robustness.
- Implementation complexity: describes how complex it is to implement and test a given forwarding strategy. This measure is highly subjective and we will explain our opinion while discussing each protocol.
- Scalability: describes the performance of the protocol with an increasing number of nodes in the network.
- Packet overhead: refers to bandwidth consumption due to larger packets and/or a higher number of signaling packets. The protocols can be classified as follows: Low overhead is used to describe protocols which have small packets and reduce the number of packets sent using unicast for example. Medium overhead is used to classify the protocols that have small packets but require large number of signaling packets, or if they require larger packets but use unicast to send the data. High overhead means that an approach requires larger packets as well as an increased number of signaling packets. Note that all position-based routing protocols have lower packet overhead compared to other types, but this criterion is defined to compare the discussed protocols together.
- Processing overhead: is used to associate each protocol with the processing requirements. Low processing refers to approaches that require a low CPU processing.
- Loop-freedom: any routing protocol should be inherently loop-free to preserve the network resources and guarantee the correct operation of the protocol. Therefore, the discussed protocols are classified as having or not having loop-freedom property.
- Optimal path: is used to indicate the protocol probability of finding and using the shortest path for data packet relay.
- Density: indicates whether the protocol is more suitable to be implemented in dense or sparse networks.

4.1 SPAAR

SPAAR uses position information in order to improve the efficiency and security of mobile Ad-Hoc networks. It was designed for protecting position information in managed-hostile environments where security is a primary concern and uses geographical information to make forwarding decisions, resulting in a significant reduction in the number of routing messages. SPAAR provides the necessary requirements to secure routing in a high-risk environment: authentication, non-repudiation, confidentiality, and integrity. It uses asymmetric cryptography to protect against malicious nodes, which are unauthorized nodes that attempt to disrupt the network. Also it attempts to minimize the potential for damage of attacks from compromised nodes which are authorized nodes which have been overtaken by an adversary.

Two of the well-known attacks are the invisible node attack and the wormhole attack. In the invisible node attack, a malicious node may forward a packet without appending its address to the address field of that packet. The wormhole attack involves the cooperation between two malicious nodes sharing a private communication. One attacker captures routing packets at one point of the network and tunnels them to another point in the network. The new attacker then selectively injects tunneled traffic back into the network. SPAAR prevents both the invisible node attack and the wormhole attack by allowing the nodes to accept routing messages only from 1-hop neighbors.

To participate in SPAAR, each node requires a public/private key pair, a certificate binding its identity to its public key (signed by a Certificate Authority (CA) server), and the public key of that CA. Additionally, each node maintains two keys for each neighbor. The first is the neighbor's public key, which is obtained from its certificate and used to encrypt some routing messages such as Route REPLY (RREP). The second is the neighbor's group decryption key, which is used to decrypt some routing messages such as Route REQuest (RREQ) to verify that the sender is a 1-hop neighbor.

Each node periodically broadcasts a "table update" message to inform the neighbors about its new position coordinates and transmission range. Each node maintains a neighbor table that contains the identity and position information of each verified neighbor, as well as the cryptographic keys required for secure communication with each neighbor; the used location service is all-for-some.

Additionally, each node maintains another table for the recent destinations it has communicated with. This table is similar to the neighbor table, except that the destination table also contains information about the speed of the node, making it possible to predict the node's next position. If this is the source node's first attempt at communication with a particular destination, the source may not have the destination's position. In this situation, a location service may be used. If no location service is available, a selective flooding algorithm may be used to reach the destination and receive its position information.

Route instantiation is triggered by the source through broadcasting a RREQ that is encrypted with its group encryption key. SPAAR uses a RREQ sequence number which is incremented each time a node initiates a RREQ and used to prevent replays of RREPs. RREQ recipients decrypt it with the appropriate group decryption key to verify that the sender of the RREQ is a 1-hop neighbor. The intermediate node checks if it or any of its neighbors is closer to destination; if so, it will encrypt the RREQ with its group encryption key, forward the RREQ and record the address of the predecessor neighbor; otherwise the RREQ is discarded. This process is repeated until the destination is reached. Upon receiving a RREQ, the destination constructs a RREP signed with its private key and encrypted with the public key of the neighbor it received the RREQ from. The RREP propagates along the reverse path of the RREQ, being verified at each hop.

Intermediate nodes, upon receiving a RREP, decrypt it with their private key and verify the signature with the public key of the neighbor node they received it from. Then they sign the RREP and encrypt it with the public key of the next node in the reverse route. Upon receiving the RREP, the successful decryption and the signature verification, the source begins sending data.

In SPAAR, each node maintains a neighbor table that contains the identity and position information of each verified neighbor; the used location service type is all-for-some. The source node can calculate the approximate geographic location of the destination from the most recent location and most recent velocity information stored in the source node's destination table. On the first attempt at communication with a particular destination, the source may use a location service or a selective flooding algorithm to reach the destination and receive its position information. The general robustness of this approach is medium, since the position of a node will become unavailable if a significant number of nodes fail.

SPAAR uses the *RDF*, so it exhibits properties such as the high probability of using the optimal path. Moreover it is loop free since it forwards packets to nodes towards the destination and uses a sequence number. SPAAR tolerates position inaccuracy by the expected region; each node forwards the RREQ only if it, or any of its neighbors, is closer to the destination. Its robustness is low since the failure of an individual node might result in packet loss and the setting up of a new route. SPAAR has high implementation complexity since messages must be verified, signed with the private key and encrypted with the public key of a neighbor. But it is still less complex than SGF since there is no reputation system.

SPAAR assumes the existence of one certificate server, which may be the operation bottleneck especially in large networks. Also, increasing the number of nodes in the network with using *RDF* will increase the packet overhead. Additionally, in large area networks the probability of having long routes is increased, and since each node spends time in signing and encrypting the messages, the probability of nodes movement and routes breakage are also increased. For these three reasons, SPAAR's scalability is considered as medium.

Moreover, SPAAR has a high packet overhead due to large-size packets resulting from the security techniques used along with the increased number of packets compared to greedy forwarding. These security techniques lead also to high processing overhead.

Finally, SPAAR can be implemented in both sparse and dense networks. It is suitable for sparse networks since it uses *RDF*, not greedy. Also, it is suitable for dense networks since increasing the number of neighbors will cause a larger neighbor table, but the computational overhead for the encryption of messages remains constant [29].

4.2 AODPR

Due to the dynamic, infrastructure-less and broadcast nature of MANETs, communications in these networks are susceptible to malicious traffic analysis. As a following step, an attacker may determine a target node and conduct an intensive attack against it, called a target-oriented attack. AODPR keeps routing nodes anonymous, thereby preventing possible traffic analysis. A time variant temporary identifier is computed from the time and position of a node in an attempt to keep the node anonymous. Moreover, it uses the concept of Virtual Home Regions (VHR), which is a geographical region around a fixed center. In this scheme each node stays in one of the VHRs, and nodes within a VHR obtain their own geographic position through GPS and report their position information to Position Servers (PSs).

When a node joins the network, it registers to the PS and gets a Common Key (CK) and a public/private key pair from the PS. When a node wants to get position information of other nodes, it first sends a signed request and authenticates itself to the PS; accordingly the PS provides it with the required position information, the public key of the destination and other needed information. Then the source estimates the minimum Number of Hop (NH) which the route request packet travels to find a route from the source to the destination. Each intermediate node decrements NH by 1 and compares the updated NH with the minimum number of hop which the route request packet travels to find a route from this node to the destination (NH'). If NH' is less than or equal to NH, then the intermediate node forwards the packet to its neighbors and keeps the needed route information; otherwise it discards the packet. Both NH' and NH are calculated depending on the distance from the node to the destination and the radius of the maximum radio range coverage of each node.

To improve the security of their protocol, the position of the destination is encrypted with CK in the route request phase; hence there is no position information exposure to nodes outside the intended network. After authenticating the sources, the destination replies by a route reply and keeps the route information to itself. Upon receiving the route reply and authenticating the

destination, the source begins sending the data encrypted by the destination's public key. If source receives a fail packet, then it tries again with a new, larger estimated NH.

AODPR is robust against the wormhole attack in which an attacker records a packet in one location of the network and sends it to another location, making a tunnel; later it is retransmitted to the network under its control. Therefore, a packet might travel a long distance before finding the route from the source to the destination. In AODPR source nodes as well as intermediate nodes wait for a limited time to get a response. If the attacker response exceeds the limited time then it cannot be a forwarder within a routing path. So the effect of the wormhole attack is not effective in AODPR.

Although the AODPR is applicable to any node density in a network, ensures the anonymity of both route and nodes, and is robust against the target-oriented attack [31], it suffers from many problems. Many fields such as NH and destination position are encrypted using the CK; if this key is compromised, a large percentage of the communication in the whole network will be compromised. Moreover, AODPR suffers from two problems inherited from the VHR approach. First, nodes may be hashed to a VHR distant from the one they are currently residing in, leading to increased communication and time complexity, as well as to problems if the VHR of a node cannot be reached. Second, since an Ad-Hoc network is dynamic, it might be difficult to guarantee that at least one position server will be present in a given VHR due to regions not including nodes.

In AODPR each PS keeps the position information of the nodes that hashed into its VHR; hence, the used location service type is some-for-some. Accordingly, a given node will be inaccessible upon the failure of the PSs of its VHR; i.e., its location service has medium robustness. AODPR uses the *RDF*, so its probability of using the optimal path is high. Moreover it is loop-free since it depends on forwarding the packets to the nodes towards the destination and uses a sequence number. AODPR tolerates to position inaccuracy by using the expected region. Its robustness is low since the failure of an individual node might result in packet loss and the setting up of a new route. AODPR's implementation complexity is considered to be medium since messages are signed only with the private key of each node. So its complexity is less than SPAAR and SGF since it does not use neighbor public key or reputation system.

AODPR has a medium scalability since increasing the number of nodes in the network with the usage of *RDF* will increase the packet overhead. However, it still has a higher scalability than SPAAR due to the reasons mentioned in the discussion of SRAAR scalability. AODPR also has less packet overhead compared to SRAAR. Even though the number of sent packets in AODPR is large, its packet size is smaller than that in SPAAR due to the later security techniques; AODPR is considered to have a medium packet overhead and processing overhead. Finally, AODPR is applicable to any node density in a network [31]. It

is suitable for sparse networks, since it uses *RDF*, as well as dense networks, since increasing the number of nodes will cause larger position information tables in the PSs without affecting computational overhead for encrypting messages.

4.3 SGF

In [21] the SGF mechanism was proposed. It provides source authentication, neighbor authentication and message integrity by using both the shared key and the Instant Key disclosure (TIK) protocol [36]. By combining SGF with the Grid Location Service (GLS) [19], they proposed the Secure Grid Location Service (SGLS) where any receiver can verify the correctness of location messages. In this paper also a Local Reputation System (LRS) is proposed to detect and isolate compromised as well as selfish users.

The SGF mechanism incorporates both the hashed Message Authentication Code (MAC) [14] and the Timed Efficient Stream Loss-tolerant Authentication (TESLA) [3] with TIK protocol. The MAC is computed over the non-mutable part (e.g., the location information of a destination) of unicast messages with the pairwise shared secret key between the source and destination.

Instead of introducing overhead by signing the destination's location information of all data and control messages, they proposed the use of a reputation system, LRS, to classify nodes as good or bad and to detect as well as isolate message tampering and dropping attackers. In LRS, each node only needs to manage the reputation information of its local neighbors and periodically send the reputation information report to its neighbors by using the HELLO messages. The TIK protocol with tight time synchronization is used to authenticate a previous forwarding node in order to prevent malicious users from joining a path and to avoid a message replay attack, re-sending recorded old valid control messages. Finally, when the destination receives a message, it can verify the authenticity of the message by comparing the received MAC to the MAC value that is computed over the received message with the secret key it shares with the source node.

In combination with SGF, the secure location service, SGLS, was proposed by combining SGF with the GLS so that any receiver can verify the correctness of location messages. The original GLS is a distributed location service in which each node maintains information about the locations of specific subsets of the nodes based on the node's identifiers. GLS divides the area that contains a MANET into a hierarchy of squares. Each node periodically broadcasts the list of neighbors it has. Consequently, each node can maintain a table of immediate neighbors as well as each neighbor's neighbors. Each node enlists nodes with IDs "close" to its own ID to serve as its Location Servers (LSs) by sending location update messages.

The general concept of the proposed SGF can generally be applied to any unicast message of GLS such as location query and location reply. So the 1-hop

neighbor's location information can be verified by using a location verification technique, and the TIK protocol can be used for neighbor authentication. The TESLA broadcast authentication method is used to verify the location information of 2-hop neighboring nodes. Unlike other messages, the location update message has no assigned destination address field in it. Thus, it is unfeasible to provide source authentication with a symmetric secret key. Hence, a public key infrastructure is assumed in the MANET under consideration. Each node stores the trusted CA's public key and signs the location update message with its private key.

The simulation results in [21] showed that SGLS can operate efficiently by using effective cryptographic mechanisms. Results also showed that LRS effectively detects and isolates message dropping attackers from the network. On the other hand, the simulations showed that the average end-to-end delay for SGLS is slightly higher than that of GLS, and that SGLS's routing overhead is significantly higher than that of GLS. This is obviously due to the increase in size of routing control messages with digital signatures and MACs in SGLS.

Generally, systems using a reputation system along with a cryptography scheme in order to defend against both compromised and malicious nodes do not scale well since they have to track the reputation of all nodes, which might require huge tables of information that are difficult to manage and to keep up to date [10]. Moreover, SGF assumes the existence of pair-wise shared secret keys between the nodes, which is difficult to implement in large area networks. Another drawback is that SGF assumes all nodes have tightly synchronized clocks, which is somewhat impractical for Ad-Hoc networks. Finally, it uses the greedy forwarding, which is not guaranteed to find the optimal path.

In SGF, each node should maintain a table of its immediate neighbors as well as each neighbor's neighbors [21]. So the used location service type is all-for-some. Accordingly, a given node will be inaccessible upon the failure of a subset of the nodes; the robustness of its location service is medium. SGF uses the greedy forwarding, so it exhibits some greedy properties such as uncertainty of using the optimal path. SGF robustness is medium since the failure of an individual node may cause the loss of a packet in transit, but it does not require setting up a new route.

SGF tolerates to position inaccuracy by the list of neighbors HELLO messages that each node periodically broadcasts; each node knows the exact position of nodes in its transmission range and neighbors' transmission ranges.

It is clear that it is very complex to implement SGF since it uses many securing techniques whether with the location service or the forwarding strategy. SGF assumes the existence of pair-wise shared secret keys between the nodes, which is difficult to implement in large area networks; so it has medium scalability. Moreover it has a high packet overhead due to the periodically sent reputation information report and the list of neighbors HELLO messages, in addition to the

large-size packets due to the security techniques used. These security techniques lead also to high processing overhead. SGF loop freedom depends on the used optimization criteria (directional or other). Finally, SGF is preferably implemented in moderate density networks, since greedy forwarding may have problems in sparse networks. On the other hand, implementing it in a dense network will increase the size of the periodic list of neighbors and reputation information HELLO messages, which may consume the network bandwidth and the nodes' memory.

5 Comparison of Discussed Protocols

Table 1 summarizes the discussed secure position-based protocols together with the security and performance evaluation criteria used. The three discussed protocols utilize position-based routing to achieve better performance than other topology-based ones while considering security issues and requirements.

SPAAR provides the necessary requirements to secure routing in hostile environments by assuring authentication, non-repudiation, confidentiality and integrity. It uses asymmetric cryptography to protect against malicious and compromised nodes. *SPAAR* uses the *RDF* resulting in high probability of using optimal paths. Furthermore *SPAAR* is loop free due to forwarding packets to nodes towards the destination and using sequence numbers. It tolerates to position inaccuracy via the expected region; i.e., each node forwards the *RREQ* only if it or any of its neighbors is closer to the destination. Its robustness is considered as low since the failure of an individual node might result in packet loss and the setting up of a new route. The implementation complexity of *SPAAR* is high since messages must be verified, signed with the private key and encrypted with the public key of a neighbor.

SPAAR is considered to have a medium scalability due to three reasons. *SPAAR* assumes the existence of a certificate server resulting in a system operation bottleneck, especially in large area networks. Moreover, increasing number of nodes, along with the use of *RDF*, results in high packet overhead. Finally, in large area networks, the probability of having long routes is high, and since each node spends time signing and encrypting routing messages, the probability of node movement and route breakage is increased. *SPAAR* has a high packet overhead due to large-size packets resulting from the security techniques used and an increased packets number compared to greedy forwarding. These security techniques result also in increased processing overhead. Lastly, *SPAAR* is suitable for implementing in both sparse and dense networks. It is suitable for sparse networks due to the usage of *RDF*. It is also suitable for dense networks since the increased number of neighbors causes a larger neighbor table but does not affect the computational overhead for message encryption.

Table 1
 Characteristics of the presented secured position-based routing protocols

Criterion	SPAAR [29]	AODPR [31]	SGF [21]
Security mechanism	Certificates and timestamps	Symmetric and asymmetric cryptography and hash functions	Symmetric and asymmetric cryptography and hashed MAC algorithm
Synchronization	No	Yes	Yes
Central trust	Certificate Authority	Key Distribution Center	Certificate Authority
Main idea/contribution	Uses cryptographic certificates to protect routing packets in managed-hostile environments	Keeps routing nodes anonymous to prevent possible traffic analysis and target-oriented attack	Provides source authentication, neighbor authentication and message integrity
Proposal	<ul style="list-style-type: none"> • Intermediate node checks if it or any of its neighbors is closer to destination it encrypts RREQ with its group encryption key so that recipients can decrypt it with the appropriate group decryption key and verify that the sender is a 1-hop neighbor. • Intermediate nodes sign the RREP with its private key and encrypt it with the public key of the neighbor it received the RREQ from and verify the signature with the public key of the neighbor node it received the RREP from. 	<ul style="list-style-type: none"> • Uses VHRs; nodes' positions are reported to PSs. • Each intermediate node decides to broadcast the route request packet or not depending on the distance from the node to the destination and the radius of the maximum radio range coverage of each node. • Destination's position is encrypting with CK on the route request phase. • After authenticating the sources, the destination replies by a route reply. • Upon authenticating the route reply sender, source begins sending data encrypted by destination's public key. 	<ul style="list-style-type: none"> • Uses a reputation system to detect and isolate message tampering and dropping attackers as well as a secure location service to verify the correctness of location messages. • The MAC is computed over the destination's location with the pairwise shared secret key between source and destination to enable the destination to verify authenticity of message. • The TIK protocol is used to authenticate the predecessor and TESLA is used to verify the location information of 2-hop neighboring nodes.
Location service type	All-for-Some	Some-for-Some	All-for-Some
Location service robustness	Medium	Medium	Medium
Approach	Restricted directional flooding	Restricted directional flooding	Greedy

AODPR uses the *RDF*, resulting in a high probability of using the optimal path. Moreover, it is guaranteed to be loop-free since it depends on forwarding the packets to the nodes towards the destination and uses sequence numbers. *AODPR* tolerates to position inaccuracy by using the expected region. *AODPR* is robust against the wormhole attack and target-oriented attack. It is applicable to any node density and ensures routes and nodes anonymity. On the other hand, it suffers from numerous problems. For example, a large percentage of communication is done using the CK; hence it is a big concern to keep this key uncompromised.

AODPR's robustness is low since the failure of an individual node might result in packet loss and setting up a new route. In AODPR, messages are signed only with the private key of each node. Accordingly, its implementation complexity is less than SPAAR and SGF since it does not use neighbor public keys or a reputation system. AODPR has a medium scalability since increasing the number of nodes in the network with the usage of *RDF* increases the packet overhead. Even though the number of sent packets in AODPR is large, its packet size is smaller than that in SPAAR due to the later security techniques; AODPR is considered to have a medium packet overhead and processing overhead.

SGF provides source authentication, neighbor authentication and message integrity by using both the shared key and the Instant Key disclosure. *SGF* tolerates to position inaccuracy by the list of neighbors HELLO messages that each node periodically broadcasts; hence each node knows the exact position of nodes in its transmission range and its neighbors' transmission ranges.

It is clear that it is complex to implement *SGF* since it uses many securing techniques whether during the location service or the forwarding process. *SGF* assumes the existence of pair-wise shared secret keys among nodes, which is difficult to implement in large area networks; i.e., it has medium scalability. Moreover, it has high packet overhead due to the reputation reports and list of neighbors HELLO messages that are sent periodically, as well as to large-size packets due to the security techniques used. These security techniques result also in high processing overhead. *SGF* loop freedom depends on the used optimization criteria (directional or other). Finally, it is preferable to implement *SGF* in moderate density networks since greedy forwarding may have problems in sparse networks. On the other hand, implementing it in a dense network increases the size of the periodic list of neighbors and reputation information messages, which may consume the network's bandwidth and the nodes' memory.

Table 1
Characteristics of the presented secured position-based routing protocols (Continued)

Criterion	SPAAR [29]	AODPR [31]	SGF [21]
Tolerable position inaccuracy	Expected Region	Expected Region	Transmission range and neighbors' transmission range
Robustness	Low	Low	Medium
Implementation complexity	High	Medium	High
Scalability	Medium	Medium	Medium
Packet overhead	High	Medium	High
Processing overhead	High	Medium	High
Loop freedom	Yes	Yes	Depends on optimization criteria
Optimal path	High	High	Medium

Density	Both	Both	Moderate
Advantages	<ul style="list-style-type: none"> • Provides authentication, confidentiality, integrity and non-repudiation. • Provides high security level against malicious and compromised nodes as well as being robust against invisible node and wormhole attacks 	<ul style="list-style-type: none"> • Provides authentication, confidentiality and Anonymity. • Ensures the anonymity of both route and nodes and robust against the target-oriented and wormhole attacks 	<ul style="list-style-type: none"> • Provides authentication and integrity. • Effectively detects and isolates message dropping attackers from the network and robust against the replay attack
Disadvantages	<ul style="list-style-type: none"> • Requires the double of processing time, since it uses asymmetric cryptography, not only for end to end communication, but also for hop-to-hop communications 	<ul style="list-style-type: none"> • Suffers serious security problem if the CK is compromised. • Nodes may be hashed to a distant VHR leading to increased communication and time complexity and unreachable VHRs. 	<ul style="list-style-type: none"> • Has scalability problem due to assuming pair-wise shared secret keys, assuming tightly synchronized nodes' clocks and tracking reputation of all nodes

6 Analysis and Discussion

The three presented protocols depend on position-based routing to achieve better performance compared to traditional topology-based ones while taking security issues into consideration. They aim to provide the necessary requirements to secure routing; however, they suffer from some problems limiting their scalability. SPAAR, for example, requires high processing time, since it uses asymmetric cryptography, not only for end to end communication, but also for hop-to-hop communications. SPAAR also has a centralized trust and so suffers from the compromised server problem and the single point of failure.

AODPR uses a common key; if this key is compromised a large percentage of the communication in the whole network will be compromised. Moreover, it suffers from increased communication and time complexity if the nodes are hashed to a distant VHR, as well as if the VHR of a node cannot be reached. Additionally, due to nodes' movement, it might be difficult to guarantee that at least one position server will be present in a given Ad-Hoc network. SGF on the other hand suffers from high average end-to-end delay and packet overhead. Moreover, SGF assumes the existence of pair-wise shared secret keys between the nodes, which is difficult to implement in large area networks. Another drawback is that SGF assumes all nodes have tightly synchronized clocks, which is somewhat impractical for Ad-Hoc networks. Finally, it uses the greedy forwarding, which is not guaranteed to find the optimal path.

As a summary, even though the three discussed protocols try to improve performance and security, they suffer from several problems, such as single point

of failure and attack, along with high packet and processing overhead as in SPAAR and SGF; and sharing single key among all nodes as in AODPR, as well as assuming pair-wise shared secret keys and tightly synchronized nodes' clocks as in SGF. Consequently, these problems result in limiting the scalability of the discussed protocols.

7 Directions of Future Research

This paper has demonstrated that there are many approaches to be considered for position-based packet forwarding. Even so, there still exist a number of issues that need to be addressed. Position-based protocols make it possible to have larger networks without scalability problems. However, geographical routing also introduces new opportunities for attackers, especially given that most protocols broadcast position information in a clear form, which allows anyone within range to receive it. Hence, node position can be altered, making other nodes believe that it is in a different position. This could make other nodes believe that the attacker is the closest node to the destination and choose it as the best candidate for the next hop.

Consequently, the attacker might be able to alter or drop the received packets. Thus, it is imperative that more intensive works be done for secure position-based routing protocols to defend against several attacks, not only from malicious nodes, but also from the compromised ones. Additionally, location privacy is one of the most major issues that needs to be addressed, since location privacy is hard to achieve when a node identifier can be immediately associated with its position.

Alternative security schemes that are not based on infrastructure for key distribution should be considered, especially given that they suffer from high processing requirement (due to signing and signature verification of every packet) and may be a perfect target for Denial of Service (DoS), where attackers try to exhaust a node's processing time and battery through forcing them to spend time doing cryptographic calculations that are not required. Moreover, approaches that suggest the usage of symmetric cryptography suffer from a scalability problem since every pair of nodes would require a unique shared key.

Geographical routing protocols depend heavily on the existence of secure distributed scalable location services which are able to provide the location of any host at any time throughout the entire network. Hence, researches should consider the security and scalability points upon developing a new location service. Finally, the most common way to enable nodes to know their locations is by equipping them with GPS. To decrease the cost and power consumption of small mobile nodes other techniques for finding relative coordinates should be discussed.

Summary and Conclusions

Efficient routing protocol is one of the most important issues in mobile Ad-Hoc wireless networks. Many points should be considered when developing a routing protocol, such as a high delivery rate, a short path, a small flooding ratio, a small end-to-end delay, low power consumption, a high level of security and avoiding single point of failure. This study has presented the current state of secure position-based Ad-Hoc routing and provided a qualitative evaluation of the presented approaches. Lastly, we identified a number of research opportunities which could lead to further improvements in this field.

Position-based routing protocols use the geographical position of nodes to make routing decisions, which results in improving efficiency and performance. Forwarding techniques based on position information was classified into three distinct categories. *Greedy* routing does not require the maintenance of explicit routes; however, it works by forwarding a single copy of data packet towards the destination. Greedy packet forwarding is an efficient approach that scales well even with highly dynamic networks, and it is a promising strategy for general purpose position-based routing. However, it is not guaranteed to find the optimal path or it may not find a path at all. In *RDF* packets are broadcasted in the general direction of the destination. It was found that RDF protocols have better performance than greedy ones in term of finding the shortest path. Using *hierarchical* approaches increases the scalability of a routing protocol. This may be done through the usage of zone based routing, dominating sets or by means of a position-independent protocol at the local level and a greedy variant at the long-distance level.

Recently, security has gained attention in topology-based routing protocols and many attempts at proposing end-to-end security schemes have been made. However, it is clear that few research efforts have addressed position-based security issues. Even secure ones suffer from many problems. Some of these problems are single point of failure and attack, along with some problems regarding packet and processing overhead, as in SPAAR and SGF, sharing single key among all nodes as in AODPR as well as assuming pair-wise shared secret keys and tightly synchronized nodes' clocks as in SGF. Consequently, these problems result in limiting the scalability of the discussed protocols.

Without online trusted servers, it is difficult to be aware of the trustworthiness of each node, thus to exclude malicious nodes from the routes. Furthermore, the approach in which one centralized server is used in the Ad-Hoc network is not practical as the server may be mobile, and result in operation bottlenecks as well as system single point of failure and attack. In order to address this problem, the position service system and the certificate authority should be distributed among multiple servers. Hence, it is an important issue to develop a scalable, distributed, secure and position-based routing protocol for Ad-Hoc networks.

Acknowledgement

We want to thank the editors and the anonymous reviewers for their valuable effort and time. This work was done under the VotF University Malaya fund no. FS132/2008C and PPP University Malaya funds no. PS091/2009A and PS410/2010B.

References

- [1] A. Boukerche, K. El-Khatib, L. Xu, L. Korba: SDAR: a Secure Distributed Anonymous Routing Protocol for Wireless and Mobile Ad Hoc Networks, in Proceedings of International Conference on Local Computer Networks (LCN '04), 2004, pp. 618-624
- [2] A. Mahmoud: Reputed Authenticated Routing for Ad Hoc Networks Protocol (Reputed-ARAN), Master thesis, Computer Science Department, The American University in Cairo, 2005
<http://www.mbifoundation.com/media/18949/Abdalla%20Mahmoud%20-%20Thesis%20Defense.pdf>
- [3] A. Perrig, R. Canetti, D. Song, D. Tygar, B. Briscoe: TESLA: Multicast Source Authentication Transform Introduction, Internet Engineering Task Force, Internet Draft of Multicast Security Working Group, 2004
<http://tools.ietf.org/html/draft-ietf-msec-tesla-intro-04.txt>
- [4] A. Pirzada, C. McDonald: Reliable Routing in Ad Hoc Networks Using Direct Trust Mechanisms. In M. Cheng, D. Li: Advances in Wireless Ad Hoc and Sensor Networks, 2008, pp. 133-159
- [5] B. Karp, H. Kung: GPSR: Greedy Perimeter Stateless Routing for Wireless Networks, in Proceedings of 6th Annual ACM/IEEE International Conference on Mobile Computing and Networking (MOBICOM 2000), Boston, Massachusetts, USA, 2000, pp. 243-254
- [6] C. Murthy, B. Manoj: Ad Hoc Wireless Networks: Architectures and Protocols, ISBN:013147023X, Prentice Hall Communications Engineering and Emerging Technologies Series, Upper Saddle River, NJ, USA, 2004, pp. 213-214 & 475-490
- [7] C. Perkins, E. Royer: Ad Hoc On-Demand Distance Vector Routing, in Proceedings of 2nd IEEE Workshop on Mobile Computing Systems and Applications, New Orleans, LA, 1999, pp. 90-100
- [8] D. Johnson, D. Maltz: Dynamic Source Routing in Ad Hoc Wireless Networks, Mobile Computing, Vol. 353, Kluwer Academic Publishers, 1996, pp. 153-181
- [9] D. Sy, R. Chen, L. Bao: ODAR: On-Demand Anonymous Routing in Ad Hoc Networks, in Proceedings of IEEE International Conference on Mobile Adhoc and Sensor Systems (MASS), Oct, 2006, pp. 267-276

- [10] E. Fonseca, A. Festag: A Survey of Existing Approaches for Secure Ad Hoc Routing and Their Applicability to VANETS, NEC Technical Report NLE-PR-2006-19, NEC Network Laboratories, 2006
<http://www.network-on-wheels.de>
- [11] E. Kranakis, H. Singh, J. Urrutia: Compass Routing on Geometric Networks, in Proceedings of 11th Canadian Conference on Computational Geometry, Vancouver, 1999, pp. 51-54
- [12] G. Zapata: Secure Ad hoc On-Demand Distance Vector Routing, ACM Mobile Computing and Communications Review, Vol. 6, No. 3, 2002, pp. 106-107
- [13] G. Zaruba, V. Chaluvadi, A. Suleman: LABAR: Location Area-based Ad Hoc Routing for GPS-Scarce Wide-Area Ad Hoc Networks, in Proceedings of 1st IEEE International Conference on Pervasive Computing and Communications (PerCom'03), 2003, pp. 509-513
- [14] H. Krawczyk, M. Bellare, R. Canetti: HMAC: Keyedhashing for Message Authentication, Internet Engineering Task Force, Request for Comment RFC 2104, 1997
<http://www.ietf.org/rfc/rfc2104.txt>
- [15] H. Rifa-Pous, J. Herrera-Joancomarti: Secure Dynamic MANET On-demand (SEDYMO) Routing Protocol, in Proceedings of 5th Annual Conference on Communication Networks and Services Research(CNSR '07), Fredericton, NB, Canada, 2007, pp. 372-380
- [16] H. Takagi, L. Kleinrock: Optimal Transmission Ranges for Randomly Distributed Packet Radio Terminals, IEEE Transactions on Communications, Vol. 32, No. 3, 1984, pp. 246-257
- [17] I. Stojmenovic, X. Lin: Loop-Free Hybrid Single-Path/Flooding Routing Algorithms with Guaranteed Delivery for Wireless Networks, IEEE Transactions on Parallel and Distributed Systems, Vol. 12, No. 10, 2001, pp. 1023-1032
- [18] J. Kong, X. Hong: ANODR: Anonymous on Demand Routing with Untraceable Routes for Mobile Ad-Hoc Networks, in Proceedings of MOBIHOC '03, June 1-3, Annapolis, Maryland, USA, 2003, pp. 291-302
- [19] J. Li, J. Jannotti, D. De Couto, D. Karger, R. Morris: A Scalable Location Service for Geographic Ad Hoc Routing, in Proceedings of 6th Annual ACM/IEEE International Conference on Mobile Computing and Networking (MOBICOM 2000), Boston, Massachusetts, USA, 2000, pp. 120-130
- [20] J. Paik, B. Kim, D. Lee: A3RP: Anonymous and Authenticated Ad Hoc Routing Protocol, in Proceedings of International Conference on Information Security and Assurance, 2008, pp. 67-72

-
- [21] J. Song, V. Wong, V. Leung: Secure Position-based Routing Protocol for Mobile Ad Hoc Networks, Elsevier Ad Hoc Networks Journal, Elsevier, Vol. 5, 2007, pp. 76-86
- [22] K. Sanzgiri, D. LaFlamme, B. Dahill, B. Levine, C. Shields, E. Belding-Royer: Authenticated Routing for Ad Hoc Networks, IEEE Journal on Selected Areas in Communications, Vol. 23, 2005, pp. 598-610
- [23] L. Blazevic, L. Buttyan, S. Capkun, S. Giordano, J. Hubaux, J. Le Boudec: Self-Organization in Mobile Ad-Hoc Networks: the Approach of Terminodes, IEEE Communication Magazine, Vol. 39, No. 6, 2001, pp. 166-174
- [24] L. Qabajeh, M. L. Mat Kiah, M. Qabajeh: A Qualitative Comparison of Position-based Routing Protocols for Ad-Hoc Networks, International Journal of Computer Science and Network, Vol. 9, No. 2, 2009, pp.131-140
- [25] L. Zhou, Z. Haas: Securing Ad Hoc Networks, IEEE Networks Special Issue on Network Security, Vol. 13, 1999, pp. 24-30
- [26] M. L. Mat Kiah, L. Qabajeh, M. Qabajeh: Unicast Position-based Routing Protocols for Ad-Hoc Networks, Acta Polytechnica Hungarica, Vol. 7, No. 5, 2010, pp. 19-46
- [27] M. Mauve, J. Widmer, H. Hartenstein: A Survey on Position-based Routing in Mobile Ad-Hoc Networks, IEEE Network, Vol. 15, No. 6, 2001, pp. 30-39
- [28] S. Basagni, I. Chlamtac, V. Syrotiuk, B. Woodward: A Distance Routing Effect Algorithm for Mobility (DREAM), in Proceedings of 4th Annual ACM/IEEE International Conference on Mobile Computing and Networking (MOBICOM), Dallas, TX, USA, 1998, pp. 76-84
- [29] S. Carter, A. Yasinsac: Secure Position Aided Ad Hoc Routing, in Proceedings of IASTED International Conference on Communications and Computer Networks (CCN02), Cambridge, 2002, pp. 329-334
- [30] S. Kalhor, M. Anisi, A. Haghighat: A New Position-based Routing Protocol for Reducing the Number of Exchanged Route Request Messages in Mobile Ad-hoc Networks, in Proceedings of 2nd International Conference on Systems and Networks Communications (ICSNC 2007), 2007, p. 13
- [31] Sk. Mizanur Rahman, M. Mambo, A. Inomata, E. Okamoto: An Anonymous On-Demand Position-based Routing in Mobile Ad Hoc Networks, in Proceedings of International Symposium on Applications and the Internet, Mesa/Phoenix, Arizona, USA, IEEE, 2006, pp. 300-306
- [32] V. Giruka, M. Singhal: Angular Routing Protocol for Mobile Ad-hoc Networks, in Proceedings of 25th IEEE International Conference on Distributed Computing Systems Workshops, 2005, pp. 551-557

- [33] W. Liao, Y. Tseng, J. Sheu: GRID: A Fully Location-Aware Routing Protocols for Mobile Ad Hoc Networks, *Telecommunication Systems*, Vol. 18, 2001, pp. 61-84
- [34] Y. Cao, S. Xie: A Position-based Beaconless Routing Algorithm for Mobile Ad Hoc Networks, in *Proceedings of International Conference on Communications, Circuits and Systems*, Vol. 1, IEEE, 2005, pp. 303-307
- [35] Y. Cheng, D. Agrawal: Distributed Anonymous Secure Routing Protocol in Wireless Mobile Ad Hoc Networks, *OPNETWORK*, Aug. 2005, pp. 22-26
- [36] Y. Hu, A. Perrig, D. Johnson: Packet Leashes: a Defense against Wormhole Attacks in Wireless Network, in *Proceedings of 22nd Annual Joint Conference of the IEEE Computer and Communications Societies (INFOCOM 2003)*, San Francisco, CA, Vol. 3, 2003, pp. 1976-1986
- [37] Y. Hu, A. Perrig, D. Johnson: ARIADNE: A Secure On-Demand Routing Protocol for Ad Hoc Networks, in *Proceedings of ACM International Conference on Mobile Computing and Networking (MOBICOM'02)*, Atlanta, Georgia, USA, 2002, pp. 12-23
- [38] Y. Ko, N. Vaidya: Location-aided Routing (LAR) in Mobile Ad Hoc Networks, *Wireless Network (WINET)*, Vol. 6, No. 4, ACM, 2000, pp. 307-321

2011 Reviewers

Bede, Barnabás
Bessenyei, Lajos
Borbély, Ákos
Borsányi, János
Chaudhry, Amit
Czap, László
Czifra, Árpád
Czigler, István
Csink, László
Dobos, László
Dunai, László
Erdélyi, Ferenc
Fehér, Gyula
Felhősi, Ilona
Fodor, János
Fullér, Róbert
Goda, Tibor
Gonda, Viktor
Gyurecz, György
Henk, Tamás
Jobbágy, Ákos
Kádár, Péter
Kersner, Róbert
Kovács, Szilveszter
Lovassy, Rita
Madarász, Tamás
Nagy, Lóránt
Nagy, Péter
Ormos, Mihály
Orosz, Tamás

Pap, Endre
Precup, Radu-Emil
Preitl, István
Rácz, Pál
Roska, Tamás
Rövid, András
Ruszinkó, Endre
Sergyán, Szabolcs
Sík-Lányi, Cecília
Siklósi, Ágnes
Strauss, Matthew
Tar, József K.
Vámosy, Zoltán
Váradi, Károly
Várlaki, Péter